

University of Sydney



0000000609654786

INVESTIGATIONS OF DIHYDRODIPICOLINATE
SYNTHASE AND DIHYDRODIPICOLINATE REDUCTASE

J. J. TURNER

This thesis is a report of original research undertaken by the author and is submitted for admission to the degree of Doctor of Philosophy at the University of Sydney. The work was completed in the School of Chemistry at the University of Sydney and in the School of Biological Sciences at the University of Canterbury, Christchurch, New Zealand during the period of March 2000 to November 2003. The work and results presented in this thesis are those of the author, unless otherwise stated.

Sections of this work have been published:

Stereochemical and Conformational Consequences of the Oxidation of 1,4-Dihydropyridin-3,5-dicarboxylates, Craig A. Hutton, Rania Jaber, Michelle Otaregui, Jennifer J. Turner, Peter Turner, Jonathan M. White and George B. Backus, *Journal of the Chemical Society, Perkin Transactions 2*, 2002, 1066-1071.

Inhibitors of Lysine Biosynthesis as Antibacterial Agents, Craig A. Hutton, Timothy J. Southwood, Jennifer J. Turner, *Mini Reviews in Medicinal Chemistry*, 2003, 3, 115-127.

to my mum & dad

This thesis is a report of original research undertaken by the author and is submitted for admission to the degree of Doctor of Philosophy at the University of Sydney. The work was completed in the School of Chemistry at the University of Sydney and in the School of Biological Sciences at the University of Canterbury, Christchurch, New Zealand during the period of March 2000 to November 2003. The work and results presented in this thesis are those of the author, unless otherwise stated.

Sections of this work have been published:

Stereochemical and Conformational Consequences of the Oxidation of 1,4-Thiazane-3,5-dicarboxylates, Craig A. Hutton, Rania Jaber, Michelle Otaegui, Jennifer J. Turner, Peter Turner, Jonathan M. White and George B. Bacskay, *Journal of the Chemical Society, Perkin Transactions 2*, **2002**, 1066–1071.

Inhibitors of Lysine Biosynthesis as Antibacterial Agents, Craig A. Hutton, Timothy J. Southwood, Jennifer J. Turner, *Mini Reviews in Medicinal Chemistry*, **2003**, 3, 115–127.

The L-lysine biosynthetic pathway provides a unique and exciting target for the design of novel antibacterial agents through inhibition of the synthesis of *meso*-DAP or L-lysine, crucial components of the bacterial peptidoglycan cell wall. The first two enzymes in this pathway—dihydrodipicolinate synthase (DHDPS) and dihydrodipicolinate reductase (DHDPR)—were targeted for inhibition. DHDPS catalyses the first committed step to L-lysine biosynthesis, the condensation of pyruvate and (*S*)-aspartate β -semialdehyde to give DHDP. DHDPR, the next enzyme in the pathway, then reduces DHDP in an NAD(P)H dependent reaction to give THDP.

A suite of inhibitors were designed and synthesised to act as product- or substrate-based analogues of DHDPS and DHDPR, respectively. Heterocyclic compounds based on chelidamic acid or thiazane-3,5-dicarboxylates were synthesised as potential inhibitors of DHDPS. Stereoselective procedures for the oxidation of thiazane-3,5-dicarboxylates were developed. It was found that when direct oxidants were used (such as sodium periodate, peroxides and peracids) the axial sulfur lone-pair reacts preferentially, providing the axial *S*-oxide. Oxidation *via* a two step mechanism using bromine/water gives the epimeric equatorial *S*-oxide. Acyclic analogues of the heterocyclic compounds were also synthesised as potential inhibitors of the intermediate in the DHDPS reaction pathway.

Two methods of synthesising the DHDPS substrate aspartate β -semialdehyde (ASA) were investigated. The first four step procedure beginning from racemic allylglycine, installed the aldehyde moiety through an osmium tetroxide/sodium periodate reaction. The ASA produced by this procedure was of variable yield and purity. The second method of synthesising ASA was achieved by reduction of a Weinreb amide derivative of aspartic acid. This procedure gave ASA in excellent yield and purity and was the method of choice for preparing ASA for use in kinetic studies. Additionally the required enzymes, DHDPS and DHDPR were purified to homogeneity as judged by SDS-PAGE visualised by Coomassie brilliant blue staining and specific activity tables.

The inhibitors synthesised were tested for inhibition of DHDPS and DHDPR. The heterocyclic compounds were not found to be potent inhibitors of DHDPS. Furthermore, chelidamic acid and its dimethyl ester were shown NOT to be competitive inhibitors of

DHDPS. Unfortunately, none of the analogous acyclic compounds proved to be potent DHDPS inhibitors either.

Two potent acyclic irreversible inhibitors synthesised *en route* to other target inhibitors of DHDPS were discovered, possessing micromolar–millimolar activity. These compounds provide a new lead in the design of more potent DHDPS inhibitors.

From the DHDPS inhibitory results obtained in this study the mechanism of DHDPS was revised. It was postulated that the DHDPS-catalysed reaction proceeds *via* a protonated aldehyde intermediate that is consistent with the inhibitory data obtained herein.

None of the synthesised inhibitors evaluated against DHDPR were found to be more potent than the known inhibitor dipicolinic acid. Consistent with the literature results dipicolinic acid was found to be a competitive inhibitor of DHDPR, however dimethyl chelidamate was found to be an uncompetitive inhibitor of DHDPR.

To my closest friends and family: Mum & Dad for always being there for me; Dad for being a great dad and a great friend; Mum for being a great mum and a great friend; David Barker for teaching me the tricks of the trade all those years ago (you're a synthetic guru); Phillip Chan for being a walking encyclopedia of organic reactions but more importantly for a being a great laugh, friend and funchood buddy (Bexa2 belongs to you); Edward Humphries for all the chichi tips and nines that I have wanted run so urgently; Andrew Scott for teaching Ed how to cook as well as your friendship; Timothy Southwood & Alex Yuen for general amusement, shenanigans and laughs.

From the Christchurch massive thanks must go to: Renwick Dobson (Dogroll) for the patience to teach me all things biochemical and tolerating my turns, it was a pleasure to work with you and a good laugh (go ren time); Michael Griffin (mysterious mokey nuke) for your help and yummy cooking; Jackie Healy for all the wondrous technical advice; Antonia Miller (tones) for all the laughs YOU ROCK! (danger, danger, high voltage!); Susie, Sarah & Lawrence for making the lab a fun and sometimes crazy place to work. I must also thank my surrogate family in NZ the Webbers, especially Caroline and Hugh for always making sure I was OK and for being such wonderful company.

Many thanks are expressed to all the technical staff (past and present) in the school whose work often goes unnoticed and is taken for granted, specifically: NMR department, Ming, Ian, Suz, Ed and & Jon; The Mass Spec department, Xiao Ming & Keith; X-ray

ACKNOWLEDGMENTS

- IV -

There are many people to thank who made this thesis possible.

Many, many thanks must go to my supervisor Craig Hutton for introducing me to DHDPS and for providing me with a project that enabled me to learn many new skills and meet new people. Your encouragement throughout the years has made this experience an unforgettable one.

Kudos goes to Juliet Gerrard whose help, assistance and pizzazz has helped keep me both motivated and sane. Jules, your enthusiasm for all things in life is truly amazing. It was a privilege to work in your lab - thanks!

I would also like to thank the lovely George Bacskay for his wondrous help with the theoretical calculations.

To my Usyd lab mates past and present it's been fun but I am glad it's over. Thanks go to: David Barker for teaching me the tricks of the trade all those years ago (you're a synthetic guru); Philip Chan for being a walking encyclopedia of organic reactions but more importantly for a being a great laugh, friend and fumehood buddy (Bexta2 belongs to you); Edward Humphries for all the chem tips and nmrs that I have wanted run so urgently; Andrew Scott for teaching Ed how to cook as well as your friendship; Timothy Southwood & Alex Yuen for general amusement, shenanigans and laughs.

From the Christchurch massive thanks must go to: Renwick Dobson (Dogroll) for the patience to teach me all things biochemical and tolerating my turns, it was a pleasure to work with you and a good laugh (go ren time); Michael Griffin (mysterious mikey mike) for your help and yummy cooking; Jackie Healy for all the wondrous technical advice; Antonia Miller (tones) for all the laughs YOU ROCK! (danger, danger, high voltage!); Susie, Sarah & Laurence for making the lab a fun and sometimes crazy place to work. I must also thank my surrogate family in NZ the Webbers, especially Caroline and Hugh for always making sure I was OK and for being such wonderful company.

Many thanks are expressed to all the technical staff (past and present) in the school whose work often goes unnoticed and is taken for granted, specifically: NMR department, Ming, Ian, Suz, Ed and & Jen; The Mass Spec department, Xiao Ming & Keith; X-ray

crystallography lab, Peter Turner; Service room staff on level 5 Bruce, Cliff and Carlo; Main store staff, especially Arthur. I would also like to thank Athol Turner for his help and patience in teaching me HPLC.

To those of you who assisted in the preparation of this manuscript, thank you: Craig, Juliet, Margaret, Edward, Joseph, Jen & Alex.

To my many friends I cannot express enough thanks for all your support whilst I have been studying (both here and overseas) I promise to catch up with you soon. A few particular people stand out though - they have bought me coffee when it was needed most, helped me out with computer problems & have been keen for a beer most Friday nights they are (in no particular order): Vesna, Edward, Joseph, Adam & Gen.

I will be forever indebted to my mum and dad for all their unconditional love and support during my many years of study (no one else would pick me up from uni at 1am in the morning). You will never realise what an inspiration you have been (and continue to be). To my cute Grummy - THANKS ! To the rest of my family—this is what I have been up to—now I can say I am no longer a student and yes I have FINISHED!

Finally, I would like to thank my soulmate Edward, for everything.

ABBREVIATIONS

Å	Angstrom
A ₃₄₀	absorbance at 340 nm
(R)-ASA	(R)-aspartate β-semialdehyde
ASA	aspartate β-semialdehyde
(S)-ASA	(S)-aspartate β-semialdehyde
amp ^R	ampicillin resistance gene
Ar	aryl
Boc ₂ O	di- <i>tert</i> -butyldicarbonate
BOP.PF ₆	(benzotriazol-1-yloxy) tris (dimethylamino) phosphonium hexafluorophosphate
bp	base pair(s)
bs	broad singlet
BSA	bovine serum albumin
°C	degrees Celsius
δ	chemical shift in parts per million
Da	dalton
DAP	diaminopimelate
<i>dap</i>	gene encoding for an enzyme in the <i>dap</i> pathway
<i>dapA</i>	gene encoding dihydrodipicolinate synthase
<i>dapB</i>	gene encoding dihydrodipicolinate reductase
DHDPR	dihydrodipicolinate reductase
DHDPS	dihydrodipicolinate synthase
DMSO	dimethyl sulfoxide
DMF	dimethylformamide
DNA	deoxyribonucleic acid
ε	molar extinction coefficient
<i>E. coli</i>	<i>Escherichia coli</i>
<i>EcoR</i> I	DNA restriction enzyme from <i>Escherichia coli</i> RY13
EDTA	ethylenediaminetetraacetic acid
Et ₃ N	triethylamine
FMN	Flavin mononucleotide
GlcNAc	<i>N</i> -acetylglucosamine
HEPES	<i>N</i> -2-hydroxymethylpiperazine- <i>N'</i> -2-ethane sulphonic acid
<i>Hind</i> III	DNA restriction enzyme from <i>Haemophilus influenzae</i>
HPLC	high performance liquid chromatography
HTHDP	4-hydroxytetrahydrodipicolinate
Hz	Hertz
IC ₅₀	inhibitor concentration resulting in 50% enzyme inhibition
ID	Internal Diameter
kb	kilobase
kDa	kilodalton
K _i	inhibition constant
K _m	Michaelis-Menten constant
LB	Luria-Bertani

m	multiplet	1
mCPBA	<i>meta</i> -chloroperbenzoic acid	2
mesoDAP	<i>meso</i> -diaminopimelate	17
M_r	relative molecular mass	18
m.p.	melting point	21
MurNAc	<i>N</i> -acetylmuramic acid	21
MRSA	methicillin resistant <i>Staphylococcus aureus</i>	21
NAD ⁺	nicotinamide adenine dinucleotide	21
NADH	nicotinamide adenine dinucleotide, reduced form	21
NADP ⁺	nicotinamide adenine dinucleotide phosphate	21
NADPH	nicotinamide adenine dinucleotide phosphate, reduced form	21
NaIO ₄	sodium periodate	21
nm	nanometer	21
n.m.r.	nuclear magnetic resonance	21
OsO ₄	osmium tetroxide	21
PMB-Cl	<i>para</i> -methoxybenzyl chloride	21
PAGE	polyacrylamide gel electrophoresis	21
pJG001	Bluescript plasmid containing the <i>dap A</i> gene	21
pJK001	Bluescript plasmid containing the <i>dap B</i> gene	21
PLP	pyridoxal phosphate	21
ppm	parts per million	21
PyBOP	benzotriazole-1-yl-oxy-tris-pyrrolidino-phosphonium hexafluorophosphate	21
RNA	ribonucleic acid	21
Rxn	reaction	21
s	singlet	21
SDS	sodium dodecyl sulfate	21
SDS PAGE	sodium dodecyl sulphate polyacrylamide gel electrophoresis	21
SMCS	(<i>S</i>)-methylcysteine sulfoxide	21
<i>Sp.</i>	Species	21
t	triplet	21
TBE	Tris borate EDTA electrophoresis buffer	21
TEMED	N,N,N',N'-tetramethylethylenediamine	21
<i>tet</i> ^R	tetracycline resistance gene	21
TFA	trifluoroacetic acid	21
THF	tetrahydrofuran	21
TMS	tetramethylsilane	21
Tris	Tris(hydroxymethyl)methylamine	21
UDP	undecaprenyl	21
UV	ultra-violet	21
VISA	vancomycin intermediate resistant <i>Staphylococcus aureus</i>	21
V_{max}	maximum rate	21
VRE	vancomycin resistant <i>Enterococci</i>	21
%	percentage	21

TABLE OF CONTENTS

- VIII -

PREFACE	I
ABSTRACT	II
ACKNOWLEDGMENTS	IV
ABBREVIATIONS	VI
LIST OF FIGURES	XII

Chapter 1 - Introduction

1.1	HISTORY OF ANTIBIOTIC RESISTANCE	1
1.2	THE BASIS OF MICROBIAL RESISTANCE TO ANTIBIOTICS	2
1.3	MECHANISTIC ACTION OF ANTIMICROBIAL DRUGS	2
1.3.1	INHIBITION OF PROTEIN SYNTHESIS	2
1.3.2	INHIBITION OF NUCLEIC ACID SYNTHESIS	3
1.3.3	CELL MEMBRANE DISRUPTION	3
1.3.4	METABOLIC ANTAGONISTS	3
1.3.5	INHIBITION OF BACTERIAL CELL WALL SYNTHESIS	4
1.4	STRUCTURE AND ASSEMBLY OF PEPTIDOGLYCAN CELL WALL	5
1.5	BIOSYNTHESIS OF LYSINE AND <i>MESO</i> -DAP	7
1.6	THE FIRST STEP IN THE BIOSYNTHESIS OF LYSINE	9
1.7	DIHYDRODIPICOLINATE SYNTHASE	10
1.8	INHIBITORS OF DIHYDRODIPICOLINATE SYNTHASE	13
1.8.1	SUBSTRATE ANALOGUE DHDPS INHIBITORS	13
1.8.2	HETEROOCYCLIC DHDPS INHIBITORS	15
1.9	THE SECOND STEP IN THE BIOSYNTHESIS OF LYSINE	17
1.10	DIHYDRODIPICOLINATE REDUCTASE	17
1.11	INHIBITORS OF DHDPR	19
1.12	INHIBITING THE LYSINE BIOSYNTHETIC PATHWAY	20
1.13	REFERENCES	22

Chapter 2 - Synthesis of Inhibitors

2.1	DESIGN OF CYCLIC INHIBITORS OF DHDPS	25
2.2	SYNTHESIS OF ALCOHOLS 51 AND 52	27
2.3	STEREOSELECTIVE PREPARATION OF THE 1,4-THIAZANE-1-OXIDE (THIAMORPHOLINE- <i>S</i> -OXIDE) DERIVATIVES 53, 54, 71.	32
2.3.1	OXIDATION OF THE (R,R)-THIAZANE 60	34
2.3.2	OXIDATION OF THE <i>MESO</i> -THIAZANE 6	38
2.3.3	PREPARATION OF SULFONES 54-76	42

2.3.3	PREPARATION OF DILITHIUM SALTS 77-82	43
2.4	DESIGN OF ACYCLIC INHIBITORS	44
2.5	SYNTHESIS OF ACYCLIC ALCOHOL 83	44
2.6	SYNTHESIS OF ACYCLIC SULFOXIDES 84 AND 85	48
2.7	SUMMARY	49
2.8	REFERENCES	50

Chapter 3 - Synthesis of ASA & Purification of DHDPS and DHDPR

3.1	PREPARATION OF (S)-ASPARTATE β -SEMIALDEHYDE	52
3.1.1	INTRODUCTION	52
3.1.2	PREVIOUS SYNTHESSES OF (S)-ASPARTATE β -SEMIALDEHYDE	53
3.2	SYNTHESIS OF ASPARTATE β -SEMIALDEHYDE	54
3.3	PURIFICATION OF DHDPS AND DHDPR	57
3.3.1	INTRODUCTION	57
3.3.2	PLASMID EXTRACTION	57
3.4	OVER-EXPRESSION OF THE <i>DAPA</i> GENE AND PURIFICATION OF DHDPS	59
3.5	OVER-EXPRESSION OF THE <i>DAPB</i> GENE AND PURIFICATION OF DHDPR	61
3.6	SUMMARY	63
3.7	REFERENCES	64

Chapter 4 - Kinetic & Inhibition Studies of DHDPS and DHDPR

4.1	INTRODUCTION	66
4.2	<i>O</i> -AMINOBENZALDEHYDE ASSAY	66
4.3	IMIDAZOLE BUFFER ASSAY	67
4.4	COUPLED ASSAY	68
4.5	MODIFICATIONS TO THE COUPLED ASSAY	68
4.6	ENZYME KINETICS OF <i>E. COLI</i> DHDPS	68
4.7	ENZYME KINETICS OF <i>E. COLI</i> DHDPR	69
4.8	SUMMARY	74
4.9	PRELIMINARY COMPOUND SCREENING OF DHDPS INHIBITORS	78
4.9.1	DHDPS INHIBITOR SCREEN OF NITROGEN CONTAINING HETEROCYCLIC COMPOUNDS	78
4.9.2	DHDPS INHIBITOR SCREEN OF SULFUR CONTAINING HETEROCYCLIC COMPOUNDS	78
4.10	INHIBITION KINETICS	80
4.10.1	INTRODUCTION	82
4.10.2	COMPETITIVE INHIBITION	82
4.10.3	NON-COMPETITIVE INHIBITION	82

4.10.4	UNCOMPETITIVE INHIBITION	83
4.10.5	MIXED INHIBITION	83
4.11	INHIBITION OF DHDPS BY DIMETHYL CHELIDAMATE HYDROCHLORIDE 52	84
4.12	INHIBITION OF DHDPS BY CHELIDAMIC ACID 55	88
4.13	ACYCLIC INHIBITORS OF DHDPS	92
4.13.1	REVERSIBLE ACYCLIC DHDPS INHIBITORS	92
4.13.2	IRREVERSIBLE ACYCLIC DHDPS INHIBITORS	93
4.14	MECHANISTIC REVISION OF DHDPS BASED ON INHIBITOR RESULTS	96
4.15	PRELIMINARY COMPOUND SCREENING OF DHDPR INHIBITORS	99
4.15.1	DHDPR INHIBITOR SCREEN OF NITROGEN CONTAINING HETEROCYCLES	99
4.15.2	DHDPR INHIBITOR SCREEN OF SULFUR CONTAINING HETEROCYCLES	100
4.16	INHIBITION OF DHDPR BY DIPICOLINIC ACID 18	101
4.17	INHIBITION OF DHDPR BY DIMETHYL CHELIDAMATE HYDROCHLORIDE 52	104
4.18	SUMMARY	106
4.17	REFERENCES	107

Chapter 5 - Experimental

5.1	GENERAL PROCEDURES FOR SYNTHESIS	109
5.2	SYNTHESIS OF CYCLIC INHIBITORS	111
5.3	OXIDATION OF SULFIDES	115
5.4	PREPARATION OF LITHIUM SALTS	119
5.5	SYNTHESIS OF ACYCLIC INHIBITORS	122
5.6	SYNTHESIS OF ASPARTATE β-SEMIALDEHYDE TRIFLUOROACETATE SALT	130
5.7	GENERAL PROCEDURES FOR ENZYMOLOGY AND KINETICS	135
5.8	BACTERIAL CULTURES	136
5.8.1	MEDIA	136
5.8.2	ANTIBIOTICS	136
5.9	BACTERIAL STRAINS	136
5.9.1	PREPARATION OF GLYCEROL FREEZES	137
5.9.2	PLATE PREPARATION	137
5.9.3	INCUBATION OF COLONIES	137
5.9.4	STANDARD PLASMID PREPARATION BY ALKALINE LYSIS	138
5.9.5	RESTRICTION DIGESTS	139
5.9.6	AGAROSE GEL ELECTROPHORESIS	140
5.9.7	SODIUM DODECYL SULFATE POLYACRYLAMIDE GEL ELECTROPHORESIS (SDS-PAGE)	141
5.9.8	PREPARATION OF DIALYSIS TUBING	142
5.10	ISOLATION AND PURIFICATION OF DHDPS	142

5.10.1	DHDPS OVEREXPRESSION	142
5.10.2	DHDPS PURIFICATION	143
5.10.3	THE O-AMINOBENZALDEHYDE ASSAY FOR QUALITATIVE ASSESSMENT OF THE PRESENCE OF DHDPS ACTIVITY.	144
5.11	ISOLATION AND PURIFICATION OF DHDPR	145
5.11.1	DHDPR OVEREXPRESSION	145
5.11.2	DHDPR PURIFICATION	145
5.11.3	THE QUALITATIVE COUPLED ASSAY TO TEST FRACTIONS FOR DHDPR ACTIVITY	147
5.11.4	ENZYME PURITY	148
5.11.5	BRADFORD ASSAY (DETERMINATION OF PROTEIN CONCENTRATION)	148
5.12	ENZYME KINETICS OF DHDPS	149
5.12.1	KINETICS OF DHDPS WITH RESPECT TO (<i>S</i>)-ASA	149
5.12.2	KINETICS OF DHDPS WITH RESPECT TO PYRUVATE	149
5.13	ENZYME KINETICS OF DHDPR	150
5.13.1	KINETICS OF DHDPR WITH RESPECT TO DHD	150
5.13.2	KINETICS OF DHDPR WITH RESPECT TO THE COFACTOR NADPH	151
5.14	IRREVERSIBLE INHIBITION STUDIES OF 56 AND 84 WITH RESPECT TO DHDPS	151
5.15	INHIBITION OF DHDPS AND DHDPR BY HTHDP MIMICS	152
5.15.1	INHIBITION SCREENING ASSAY FOR DHDPS	152
5.15.2	INHIBITION SCREENING ASSAY FOR DHDPR	152
5.16	INHIBITION KINETICS OF DHDPS BY HTHDP MIMICS	153
5.16.1	KINETICS OF INHIBITOR WITH RESPECT TO (<i>S</i>)-ASA	153
5.16.2	KINETICS OF INHIBITOR WITH RESPECT TO PYRUVATE	153
5.17	INHIBITION KINETICS OF DHDPR BY HTHDP MIMICS	154
5.17.1	KINETICS OF INHIBITION WITH RESPECT TO DHD	154
5.18	REFERENCES	155

APPENDIX		i
A1 CRYSTALLOGRAPHIC DATA FOR COMPOUND 71		i
A2 KINETIC EQUATIONS		xi
A3 REFERENCES		xiii

Chapter 4 - Kinetic & Inhibition Studies of DHDPS and DHDPR

FIGURE 4.2.1: O-AMINOBENZALDEHYDE ASSAY	36
FIGURE 4.3.1: IMIDAZOLE BUFFER ASSAY	57
FIGURE 4.4.1: COUPLED ASSAY TO TEST FOR DHDPS ACTIVITY	60
FIGURE 4.4.2: COUPLED ASSAY TO TEST FOR DHDPR ACTIVITY	60
FIGURE 4.6.1: MODIFIED REACTION MECHANISM OF <i>E. COLI</i> DHDPS	70
FIGURE 4.6.2: DHDPS KINETICS WITH RESPECT TO PYRUVATE AT DIFFERENT ASA CONCENTRATIONS	72

Chapter 1 - Introduction

FIGURE 1.3.5: STRUCTURE OF VARIOUS ANTIBIOTICS THAT INHIBIT BACTERIAL CELL WALL SYNTHESIS	4
FIGURE 1.4.1: STRUCTURE OF THE PEPTIDOGLYCAN LAYER	5
FIGURE 1.4.2: SCHEMATIC OF BACTERIAL CELL WALL STRUCTURE	7
FIGURE 1.5.1: LYSINE BIOSYNTHETIC PATHWAY	8
FIGURE 1.6.1: PRODUCTION OF DHDP FROM ASA AND PYRUVATE	9
FIGURE 1.7.1: THE STRUCTURE OF <i>E. COLI</i> DHDPS TETRAMER	11
FIGURE 1.8.1: ASA BASED INHIBITORS OF DHDPS	14
FIGURE 1.8.2: PYRUVATE AND LYSINE ANALOGUE INHIBITORS	14
FIGURE 1.8.3: HETEROCYCLIC INHIBITORS OF DHDPS	15
FIGURE 1.9.1: PRODUCTION OF L-THDP FROM DHDP	17
FIGURE 1.10.1: THE STRUCTURE OF <i>E. COLI</i> DHDPR TETRAMER	18
FIGURE 1.11.1: HETEROCYCLIC DHDPR INHIBITORS	19
FIGURE 1.11.2: DHDPR INHIBITORS	20

Chapter 2 - Synthesis of Inhibitors

FIGURE 2.1.1: PROPOSED DHDPS INHIBITORS	25
FIGURE 2.1.2: 3D IMAGE OF DHDP 10 SUPERIMPOSED WITH 39 AND 40	26
FIGURE 2.3.1: CHAIR CONFORMATIONS OF (R,R)-THIAZANE S-OXIDE 71	34
FIGURE 2.3.2: 400 MHZ ¹ H N.M.R. SPECTRUM OF (R,R)-THIAZANE S-OXIDE 71 IN CDCl ₃	35
FIGURE 2.3.3: X-RAY STRUCTURE OF SULFOXIDE 71	36
FIGURE 2.3.5: 300 MHZ ¹ H N.M.R. SPECTRUM OF A MIXTURE OF SULFOXIDES 53 AND 74 IN CDCl ₃	40
FIGURE 2.3.6: DILITHIUM DICARBOXYLATES 77–82	43
FIGURE 2.4.1: PROPOSED ACYCLIC INHIBITORS OF DHDPS 83–85	44

Chapter 3 - Preparation of ASA & Purification of DHDPS and DHDPR

FIGURE 3.3.1: AGAROSE GEL SHOWING DNA RESTRICTION FRAGMENTS OF pJG001 AND pJK001	59
FIGURE 3.4.1: SDS-PAGE COMPARISON OF SAMPLE SOLUTIONS AFTER EACH DHDPS PURIFICATION STEP	60
FIGURE 3.5.1: SDS-PAGE COMPARISON OF SAMPLE SOLUTIONS AFTER EACH DHDPR PURIFICATION STEP	62

Chapter 4 - Kinetic & Inhibition Studies of DHDPS and DHDPR

FIGURE 4.2.1: O-AMINOBENZALDEHYDE ASSAY	66
FIGURE 4.3.1: IMIDAZOLE BUFFER ASSAY	67
FIGURE 4.4.1: COUPLED ASSAY TO TEST FOR DHDPS ACTIVITY	68
FIGURE 4.4.2: COUPLED ASSAY TO TEST FOR DHDPR ACTIVITY	68
FIGURE 4.6.1: MODIFIED REACTION MECHANISM OF <i>E. COLI</i> DHDPS	70
FIGURE 4.6.2: DHDPS KINETICS WITH RESPECT TO PYRUVATE AT DIFFERENT ASA CONCENTRATIONS	72

FIGURE 4.6.3: DHDPS KINETICS WITH RESPECT TO ASA AT DIFFERENT PYRUVATE CONCENTRATIONS	73
FIGURE 4.7.1: REACTION MECHANISM FOR DHDPR	74
FIGURE 4.7.2: DHDPR KINETICS WITH RESPECT TO DHDP AT DIFFERENT NADPH CONCENTRATIONS	76
FIGURE 4.7.3: DHDPR KINETICS WITH RESPECT TO NADPH AT DIFFERENT DHDP CONCENTRATIONS	77
FIGURE 4.9.1: NITROGEN CONTAINING HETEROCYCLIC INHIBITORS OF DHDPS	80
FIGURE 4.9.2: SULFUR CONTAINING HETEROCYCLIC INHIBITORS OF DHDPS	81
FIGURE 4.10.1: COMPETITIVE INHIBITION	82
FIGURE 4.10.2: NON-COMPETITIVE INHIBITION	83
FIGURE 4.10.3: UNCOMPETITIVE INHIBITION	83
FIGURE 4.10.4: MIXED INHIBITION	84
FIGURE 4.11.1: DHDPS KINETICS WITH RESPECT TO PYRUVATE AT DIFFERENT CONCENTRATIONS OF DIMETHYL CHELIDAMATE HYDROCHLORIDE	86
FIGURE 4.11.2: DHDPS KINETICS WITH RESPECT TO ASA AT DIFFERENT CONCENTRATIONS OF DIMETHYL CHELIDAMATE HYDROCHLORIDE	87
FIGURE 4.12.1: DHDPS KINETICS WITH RESPECT TO PYRUVATE AT DIFFERENT CONCENTRATIONS OF CHELIDAMIC ACID	90
FIGURE 4.12.2: DHDPS KINETICS WITH RESPECT TO ASA AT DIFFERENT CONCENTRATIONS OF CHELIDAMIC ACID	91
FIGURE 4.13.1: ACYCLIC INHIBITORS OF DHDPS	92
FIGURE 4.13.2: EFFECT OF DIENE 56 ON DHDPS ACTIVITY	94
FIGURE 4.13.3: SDS-PAGE OF DHDPS INCUBATED WITH DIENE 56	94
FIGURE 4.13.4: EFFECT OF ALKENE 87 ON THE ACTIVITY OF DHDPS	96
FIGURE 4.14.1: DHDPS MECHANISM VIA THE ALDEHYDE 8	96
FIGURE 4.14.2: DHDPS MECHANISM VIA THE HYDRATE 19	97
FIGURE 4.15.1: NITROGEN CONTAINING HETEROCYCLIC INHIBITORS OF DHDPR	100
FIGURE 4.15.2: SULFUR CONTAINING HETEROCYCLIC INHIBITORS OF DHDPR	101
FIGURE 4.16.1: DHDPR KINETICS WITH RESPECT TO DHDP AT DIFFERENT CONCENTRATIONS OF DIPICOLINIC ACID	103
FIGURE 4.17.1: DHDPR KINETICS WITH RESPECT TO DHDP AT DIFFERENT CONCENTRATIONS OF DIMETHYL CHELIDAMATE HYDROCHLORIDE	105

1.1 History of Antibiotic Resistance

Antibiotics are undoubtedly one of the great legacies of medicine. The success of many life-saving antibiotics is, however, being undermined by the emergence of antibiotic resistance. In the United States of America some 14,000 individuals die each year as a result of antibiotic resistant bacterial infections. This alarming figure also highlights the need for the development of new broad-spectrum antibiotics.

In 1941, just over half a century ago, virtually all strains of *Staphylococcus aureus* world-wide were susceptible to penicillin.¹ A few years later, in 1944, a penicillin-resistant strain of *S. aureus* emerged.² Today, in excess of 95% of *S. aureus* strains are resistant to penicillin, ampicillin, and the antipseudomonas-penicillins.³ Since that first case of resistant staphylococcus, the problem of antibiotic resistant bacteria has been of growing concern. Currently, there exists a variety of bacteria which possess resistance to even the most potent antibiotics in our arsenal.² Of increasing alarm is the emergence of vancomycin resistant *Enterococci* (VRE), vancomycin intermediate resistant *S. aureus* (VISA) and methicillin resistant *S. aureus* (MRSA). VRE was first found in France in 1986.⁴ It has since been isolated in the United States of America, Britain, Japan and many other countries, including Australia. The first isolate in Australia occurred in a Melbourne hospital in 1994.⁴ *Enterococcus* is a Gram-positive organism normally found in the lower gastrointestinal and genital tract of healthy individuals. However, this organism can be pathogenic, causing urinary tract infections, wound infections, septicaemia and endocarditis.⁵ Furthermore, the emergence of VISA strains suggest it will only be a matter of time before fully resistant VRSA emerges.⁵ These infections will then be effectively untreatable. Although MRSA is part of the natural human flora found on the skin, it can also be the cause of a number of diseases.^{1,4} In hospital settings, the risk of post-surgical *S. aureus* infections is high.⁶ These infections can cause stitch abscesses, septic phlebitis, chronic osteomyelitis, pneumonia, meningitis, endocarditis and sepsis.⁴ Approximately 85-95% of isolates are antibiotic resistant *S. aureus*, which have developed resistance to penicillin, methicillin and aminoglycosides such as gentamicin.⁴

CHAPTER 1

INTRODUCTION

1.1 History of Antibiotic Resistance

Antibiotics are undoubtedly one of the great legacies of medical research. The effectiveness of many life-saving antibiotics is, however, being undermined by the emergence of antibiotic resistance. In the United States of America some 14,000 individuals die each year as a result of antibiotic resistant bacterial infections.¹ This alarming figure alone highlights the need for the development of new broad-spectrum antibiotics.

In 1941, just over half a century ago, virtually all strains of *Staphylococcus aureus* world-wide were susceptible to penicillin.² A few years later, in 1944, a penicillin-resistant strain of *S. aureus* emerged.² Today, in excess of 95% of *S. aureus* strains are resistant to penicillin, ampicillin, and the antipseudomonas-penicillins.² Since that first case of resistant staphylococcus, the problem of antibiotic resistant bacteria has been of growing concern. Currently, there exists a variety of bacteria which possess resistance to even the most potent antibiotics in our arsenal.² Of increasing alarm is the emergence of vancomycin resistant *Enterococci* (VRE), vancomycin intermediate resistant *S. aureus* (VISA) and methicillin resistant *S. aureus* (MRSA). VRE was first found in France in 1986.³ It has since been isolated in the United States of America, Britain, Japan and many other countries, including Australia. The first isolate in Australia occurred in a Melbourne hospital in 1994.⁴ *Enterococcus* is a Gram-positive organism normally found in the lower gastrointestinal and genital tract of healthy individuals. However, this organism can be pathogenic, causing urinary tract infections, wound infections, septicaemia and endocarditis.¹ Furthermore, the emergence of VISA strains suggest it will only be a matter of time before fully resistant VRSA emerges.⁵ These infections will then be effectively untreatable. Although MRSA is part of the natural human flora found on the skin, it can also be the cause of a number of diseases.^{1,4} In hospital settings, the risk of post-surgical *S. aureus* infections is high.⁴ These infections can cause stitch abscesses, septic phlebitis, chronic osteomyelitis, pneumonia, meningitis, endocarditis and sepsis.⁴ Approximately 85–95% of isolates are antibiotic resistant *S. aureus*, which have developed resistance to penicillin, methicillin and aminoglycosides such as gentamicin.⁶

1.2 The Basis of Microbial Resistance to Antibiotics

The problem of resistance has arisen due to several factors. Firstly, many antimicrobial drugs are derived from natural sources, such as bacteria and fungi, wherein resistance mechanisms are necessary to protect the producing organism. That is, bacteria and/or fungi may be inherently resistant to an antibiotic, or become so by activating the appropriate enzymes. Secondly, bacteria can acquire resistance to antibiotics through changes in the bacterial genome. Acquired resistance is driven by two genetic processes in bacteria: (1) mutation and selection, and; (2) exchange of genes between strains and species.⁷ Finally, due to the immense success of commercial antibiotics, research into novel antimicrobial compounds was not considered to be of primary importance during the 1970s and 1980s, so very few new effective drugs have emerged.^{8,9} If medicine is to remain ahead of the evolution of drug resistant bacterial strains, then the development of new antibiotics is imperative and urgent.

1.3 Mechanistic Action of Antimicrobial Drugs

There are several mechanisms of action of antimicrobial drugs, including the inhibition of protein synthesis, inhibition of nucleic acid synthesis, cell membrane disruption, metabolic antagonism and inhibition of bacterial cell wall synthesis.^{7,10,11}

1.3.1 Inhibition of Protein Synthesis

Antibacterial agents that impair protein synthesis can act either against RNA or against ribosomes. Rifampicin is a semisynthetic derivative of rifamycin B.⁷ It binds non-covalently to RNA polymerase and inhibits RNA synthesis in Gram-positive bacteria.¹⁰ The DNA-dependent RNA polymerases in mammalian cells are unaffected, since the drug binds to a peptide chain not present in eukaryotic RNA polymerase.¹⁰ Streptomycin, an important example of the aminoglycoside class of antibiotics, inhibits protein synthesis by binding to the 30S bacterial ribosomal subunit, thereby preventing the growth of the protein chain by preventing the recognition of the triplet code on mRNA.¹¹ Other classes of drugs that interfere with protein synthesis include tetracyclines, chloramphenicol and macrolides.^{7,10,11}

1.3.2 Inhibition of Nucleic Acid Synthesis

Inhibition of nucleic acid function prevents cell division and/or the synthesis of essential enzymes. The quinolones and fluoroquinolones are two classes of antibiotics that are believed to act on the bacterial enzyme DNA-topoisomerase.⁷ This enzyme catalyses the supercoiling of chromosomal DNA into its tertiary structure. A consequence of DNA-topoisomerase inhibition is the loss of replication and transcription, leaving the bacterial cell's genetic code unread.¹⁰ Specific examples of these drugs include nalidixic acid and enoxacin.^{7,10,11}

1.3.3 Cell Membrane Disruption

Cell membrane inhibitors disorganize the structure, and inhibit the function, of bacterial membranes. The integrity of the cytoplasmic and outer membranes is vital to bacteria, and compounds that disorganize the membranes rapidly kill the cells. However, due to similarities in phospholipids in eubacterial and eukaryotic membranes, this action is rarely selective enough for compounds of this class to be clinically useful.¹¹ There are only a few antibiotics of clinical importance that work by this mechanism: these include polymyxin B1, gramicidin S and tyrocidin A.¹¹

1.3.4 Metabolic Antagonists

Antibacterial agents that inhibit cell metabolism are called antimetabolites.¹² These compounds inhibit the metabolism of a micro-organism, but not the metabolism of the host. Such compounds work by inhibiting an enzyme-catalysed reaction which is present in the bacterial cell, but not in animal cells.⁷ The sulfonamides are a class of antimetabolic drugs that act as competitive enzyme inhibitors and block the biosynthesis of folic acid in bacterial cells. They inhibit dihydropteroate synthase, the enzyme that is responsible for linking together the component parts of folic acid.^{7,10,12}

Figure 1.3.1: Structure of Various Antibiotics that Inhibit Bacterial Cell Wall Synthesis

1.3.5 Inhibition of Bacterial Cell Wall Synthesis

Many currently used antibiotics are known to inhibit the synthesis of the bacterial cell wall in a variety of ways (Table 1.3.5).¹⁰ Each of these antibiotics inhibits a step(s) in the biosynthesis of peptidoglycan, the main constituent of the bacterial cell wall.

Table 1.3.5: Antibiotics that Inhibit Cell Wall Synthesis¹⁰

Target	Antibiotic
Alanine racemase	D-Cycloserine 3
D-Ala-D-Ala ligase	D-Cycloserine 3
Translocation across membrane	Bactracin
Transpeptidation of peptidoglycan	β -lactams (e.g. penicillin G) 4
Binding of peptidyl D-Ala-D-Ala	Vancomycin 5

The integrity of the bacterial cell wall, including the unique peptidoglycan structure found therein, must be preserved or cell death will occur.¹⁰ Any defects or disruptions to the peptidoglycan layer leads to cell lysis as a result of high internal osmotic pressure.⁸

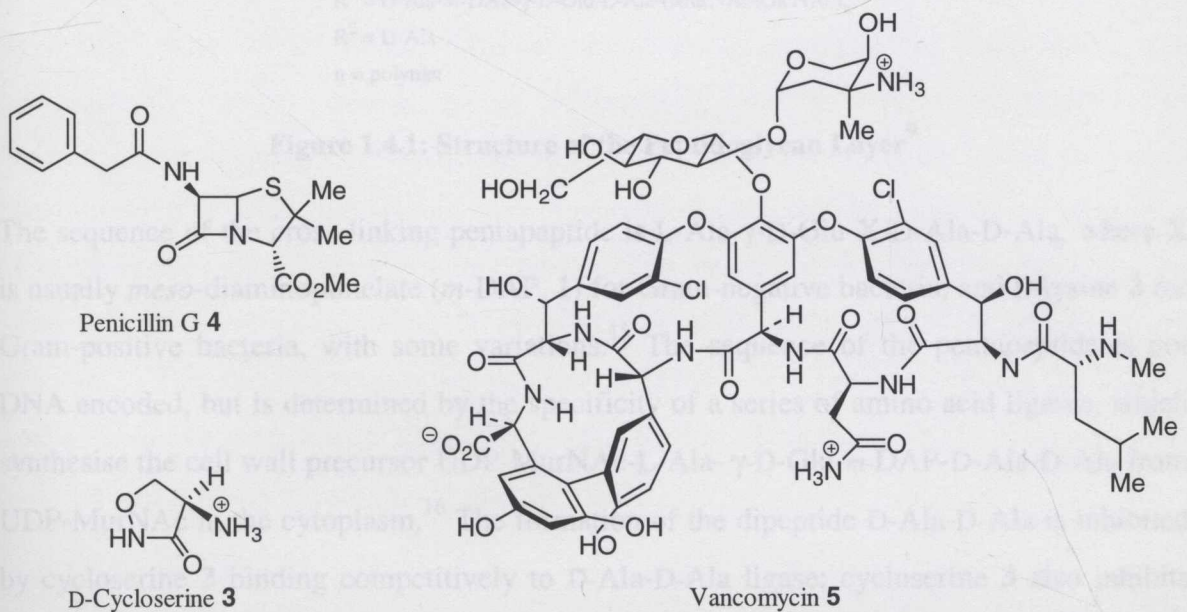


Figure 1.3.1: Structure of Various Antibiotics that Inhibit Bacterial Cell Wall Synthesis

1.4 Structure and Assembly of Peptidoglycan Cell Wall

The peptidoglycan layer consists of a matrix of polysaccharide chains, composed of alternating *N*-acetylmuramic acid (MurNAc) and *N*-acetylglucosamine (GlcNAc) sugar residues, cross-linked through peptide sidechains attached to the MurNAc residues (Figure 1.4.1).^{13,14}

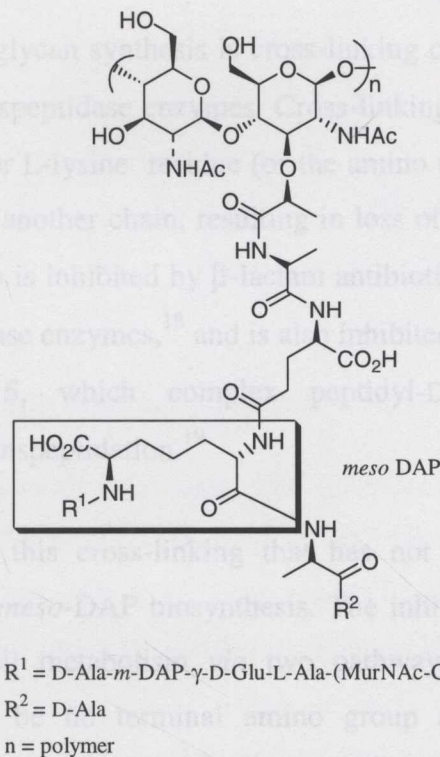


Figure 1.4.1: Structure of the Peptidoglycan Layer⁹

The sequence of the cross-linking pentapeptide is L-Ala- γ -D-Glu-X-D-Ala-D-Ala, where X is usually *meso*-diaminopimelate (*m*-DAP, **1**) for Gram-negative bacteria, and L-lysine **2** for Gram-positive bacteria, with some variations.¹⁵ The sequence of the pentapeptide is not DNA encoded, but is determined by the specificity of a series of amino acid ligases, which synthesise the cell wall precursor UDP-MurNAc-L-Ala- γ -D-Glu-*m*-DAP-D-Ala-D-Ala from UDP-MurNAc in the cytoplasm.¹⁶ The formation of the dipeptide D-Ala-D-Ala is inhibited by cycloserine **3** binding competitively to D-Ala-D-Ala ligase; cycloserine **3** also inhibits alanine racemase.¹² The MurNAc-pentapeptide is attached to an undecaprenyl (UDP) lipid carrier, to which is then attached a GlcNAc residue. At this point in many Gram-positive bacteria, 1–5 amino acid residues, activated as their aminoacyl-tRNAs, may be successively attached to the ϵ -amino group of the L-lysine residue.¹⁷ These additional amino acids are

usually glycine residues, although L-serine, L-threonine and other amino-acids are sometimes found.¹⁵ The free α -amino terminus at the end of this additional peptide chain is then used for transpeptidation. The lipid-linked disaccharide-pentapeptide is translocated across the cytoplasmic membrane, exposing the pentapeptide side-chains to the cell surface. Transglycosylation of the sugar residues leads to polymerisation of the backbone sugar residues.

The final step of peptidoglycan synthesis is cross-linking of the pentapeptide sidechains, a process catalysed by transpeptidase enzymes. Cross-linking involves attack at the ϵ -amino group of the *meso*-DAP or L-lysine residue (or the amino terminus of the linker unit) onto the penultimate D-Ala of another chain, resulting in loss of the terminal D-Ala and peptide bond formation. This step is inhibited by β -lactam antibiotics such as penicillin G **4**, which inactivate the transpeptidase enzymes,¹⁸ and is also inhibited by the glycopeptide antibiotics such as vancomycin **5**, which complex peptidyl-D-Ala-D-Ala, preventing both transglycosylation and transpeptidation.¹⁹

One way of preventing this cross-linking that has not been fully investigated is the inhibition of L-lysine or *meso*-DAP biosynthesis. The inhibition of L-lysine or *meso*-DAP biosynthesis prevents cell metabolism *via* two pathways. Firstly, without L-lysine or *meso*-DAP there would be no terminal amino group available for cross-linking the polysaccharide chains, leading to an inferior cell wall in both Gram-positive and Gram-negative bacteria, eventually resulting in cell lysis. Secondly, disruption to protein biosynthesis will occur, as L-lysine is a component of most cellular proteins and inhibition of its biosynthesis debilitates protein synthesis. The disruption of L-lysine biosynthesis has already been shown to be lethal, presumably due to the instability of the peptidoglycan structure.²⁰ The *dapA*⁻ *E. coli* auxotroph, strain AT997, will not grow unless the growth media is supplemented with diaminopimelate, thereby demonstrating the importance of L-lysine biosynthesis in cell growth and survival.²⁰

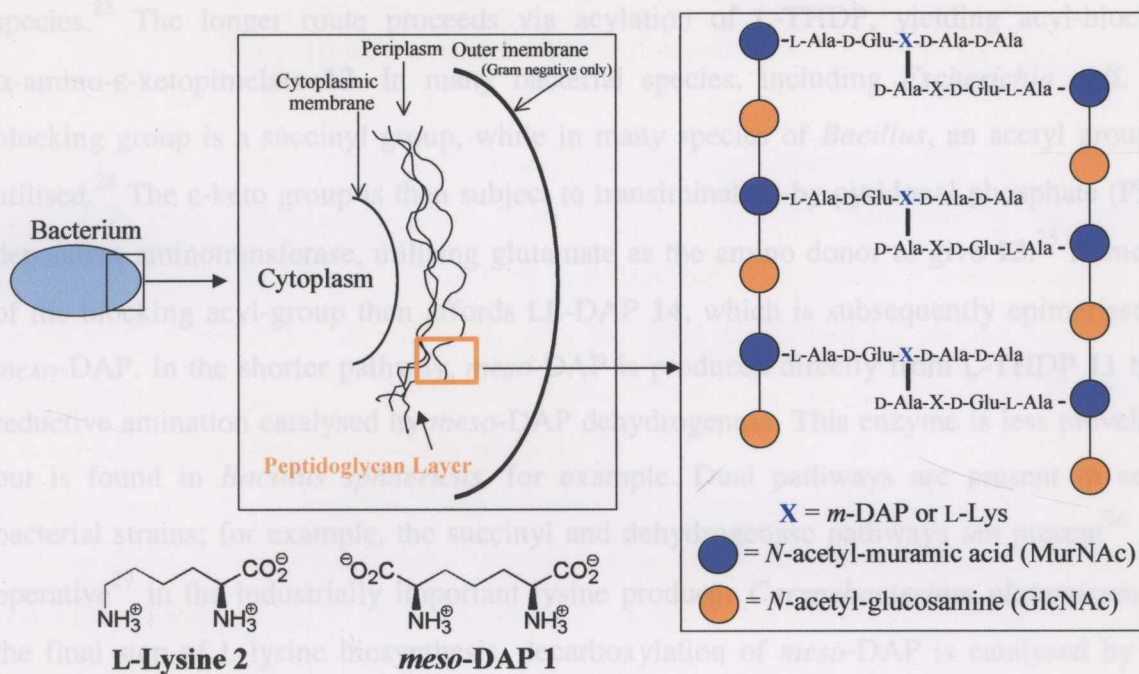


Figure 1.4.2: Schematic of Bacterial Cell Wall Structure⁸

Inhibitors of the biosynthesis of L-lysine should therefore provide potent new antibiotics through their ability to inhibit both protein and cell-wall biosynthesis. Furthermore, L-lysine is one of the essential amino-acids for humans which must be provided through a dietary source. This is because the L-lysine biosynthetic pathway (Figure 1.5.1) occurs in plants and micro-organisms, but not in mammals, which suggests that specific inhibitors of this pathway may display novel antibacterial and herbicidal activity with low mammalian toxicity.

1.5 Biosynthesis of Lysine and *meso*-DAP

The biosynthetic pathway leading to *meso*-DAP and lysine production in bacteria is known as the diaminopimelate (DAP) pathway (Figure 1.5.1). The initial steps toward the L-lysine pathway involve the conversion of aspartate **6** to aspartyl phosphate **7**, with subsequent reduction to aspartate semi-aldehyde (ASA, **8**). These steps are common to L-lysine, L-threonine, L-isoleucine and L-methionine biosynthesis.²¹ The first committed step in the DAP pathway is the conversion of ASA **8** and pyruvate **9** to dihydrodipicolinate (DHDP, **10**), catalysed by dihydrodipicolinate synthase (DHDPS).^{9,22} Reduction of DHDP to tetrahydrodipicolinate (THDP, **11**) by dihydrodipicolinate reductase (DHDPR) then occurs. At this point the pathway splits, and three routes have been identified in different bacterial

species.²³ The longer route proceeds via acylation of L-THDP, yielding acyl-blocked α -amino- ϵ -ketopimelate **12**. In many bacterial species, including *Escherichia coli*, the blocking group is a succinyl group, while in many species of *Bacillus*, an acetyl group is utilised.²⁴ The ϵ -keto group is then subject to transimination by pyridoxal phosphate (PLP) dependent aminotransferase, utilising glutamate as the amino donor to give **13**.²⁵ Removal of the blocking acyl-group then affords LL-DAP **14**, which is subsequently epimerised to *meso*-DAP. In the shorter pathway, *meso*-DAP is produced directly from L-THDP **11** by a reductive amination catalysed by *meso*-DAP dehydrogenase. This enzyme is less prevalent, but is found in *Bacillus sphaericus*, for example. Dual pathways are present in some bacterial strains; for example, the succinyl and dehydrogenase pathways are present²⁶ and operative²⁷ in the industrially important lysine producer *Corynebacterium glutamicum*. In the final step of L-lysine biosynthesis, decarboxylation of *meso*-DAP is catalysed by the PLP-dependent *meso*-DAP decarboxylase produces L-lysine.²⁸ As DHDPS and DHDPR are common to all three routes leading to the synthesis of *meso*-DAP and L-lysine, attention was focused on designing potential inhibitors of these enzymes.

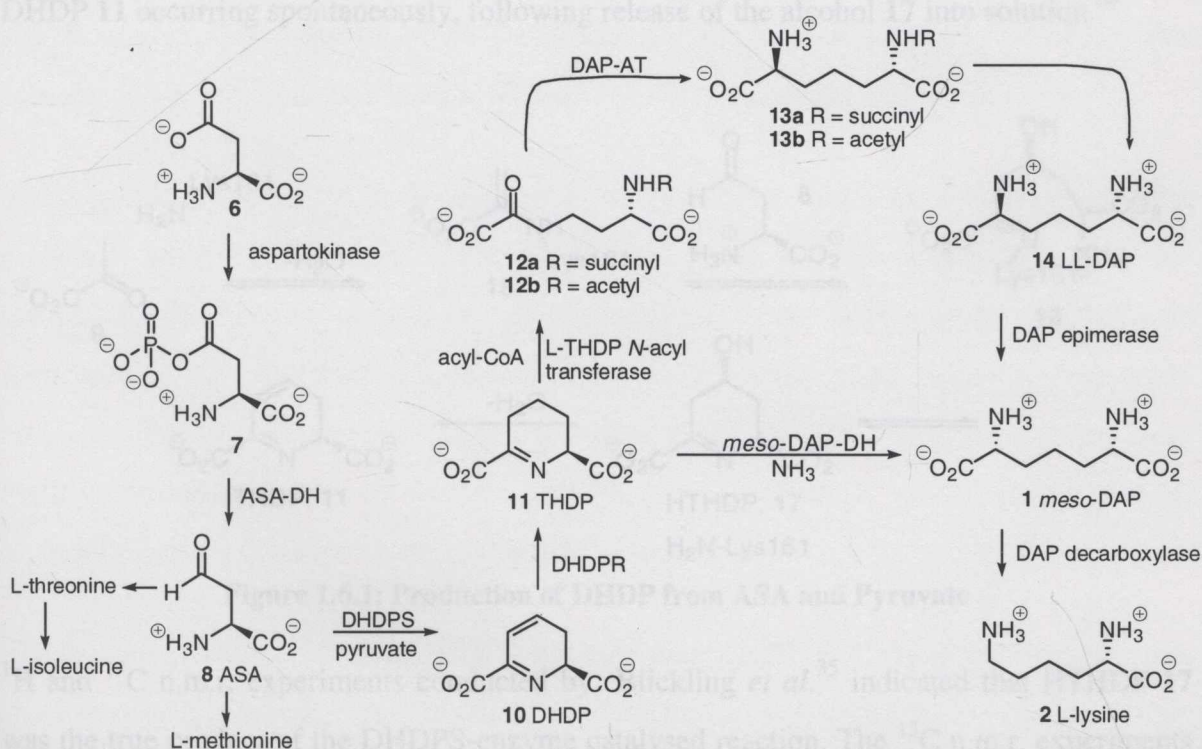


Figure 1.5.1: Lysine Biosynthetic Pathway: ASA-DH = Aspartate Semi-Aldehyde Dehydrogenase, DHDPS = Dihydrodipicolinate Synthase, DHDPR = Dihydrodipicolinate Reductase, L-THDP = L-Tetrahydrodipicolinate, AT = Aminotransferase, DAP = Diaminopimelate.

1.6 The First Step in the Biosynthesis of Lysine

The first unique step in lysine biosynthesis involves the condensation of pyruvate **9** and ASA **8** to give dihydrodipicolinate (DHDP, **10**), a reaction catalysed by the enzyme DHDPS.²⁹⁻³⁴ The reaction is initiated by condensation of pyruvate **9** with an active site lysine residue forming a Schiff base. This has been confirmed by sodium borohydride trapping experiments.^{29,32,35} Subsequent tautomerisation gives the enamine **15** (Figure 1.6.1). Aldol-type reaction of the enamine **15** with (*S*)-ASA **8** then gives the acyclic enzyme-bound intermediate **16**. Transimination of the acyclic intermediate **16** is thought to give the cyclic alcohol **17** with simultaneous release of the active site lysine residue. Loss of water then provides DHDP **11**. As the name suggests, it was originally believed that DHDP **11** was the enzymatic product formed in this reaction. However, recent work by Blickling and co-workers³⁵ has suggested that the actual product is 4-hydroxytetrahydrodipicolinate (HTHDP, **17**), which was observed as a discrete species in solution. It was postulated that this species is the true product of the enzyme-catalysed reaction, with dehydration to give DHDP **11** occurring spontaneously, following release of the alcohol **17** into solution.³⁵

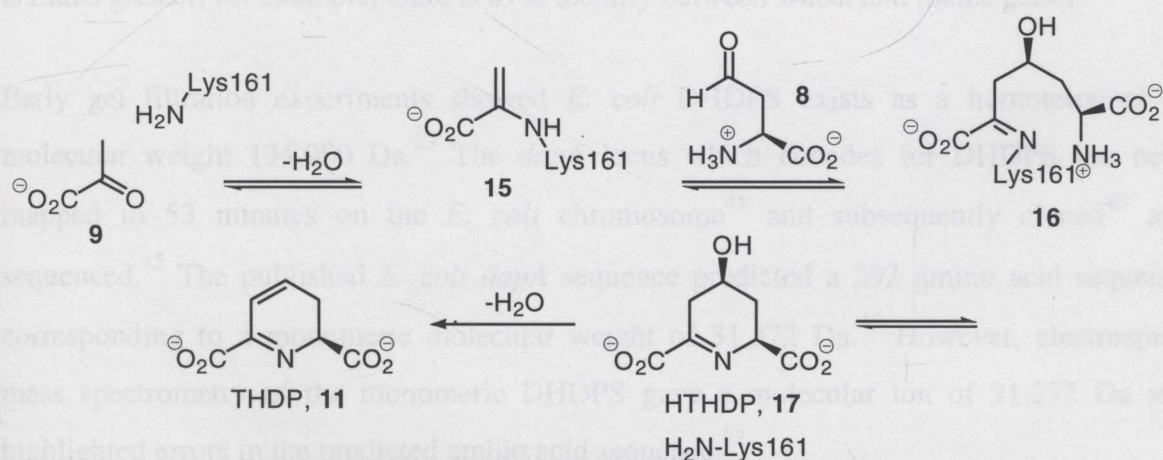


Figure 1.6.1: Production of DHDP from ASA and Pyruvate

¹H and ¹³C n.m.r. experiments conducted by Blickling *et al.*³⁵ indicated that HTHDP **17** was the true product of the DHDPS-enzyme catalysed reaction. The ¹³C n.m.r. experiments using labelled pyruvate showed that when using [3-¹³C]pyruvate a triplet at 34 ppm developed as the DHDPS reaction proceeded. Employing [2,3-¹³C]pyruvate lead to the appearance of two signals, a triplet of doublets at 34 ppm and a doublet at 166.5 ppm. These

resonances were assigned to C5 (formation of a methylene group originating from C-3 of pyruvate) and C6 of the cyclic imine **17**. The possibility of an open chain amino ketone was ruled out as the chemical shift of the ketone carbon would be higher. ^1H n.m.r. studies using labelled pyruvate were also consistent with the product being HTHDP **17**. The appearance of the axial C-4 proton at 3.9 ppm along with the signal at 1.28 ppm attributed to the C-3 proton together with the C-2 proton assigned at 4.0 ppm and the C-5 axial proton at 2.8 ppm indicated that the actual product is HTHDP **17**.³⁵

1.7 Dihydrodipicolinate Synthase

Dihydrodipicolinate synthase has been isolated from a variety of bacterial^{29,36,37} and plant³⁸⁻⁴² sources. All characterised DHDPS enzymes thus far are reported to be tetrameric, with one exception: a single, uncorroborated, gel filtration experiment suggested that pea DHDPS was trimeric.⁴² A high level of homology exists at the amino acid level between DHDPS obtained from different species. For example, the *E. coli* DHDPS shows 30% identity to wheat,⁴³ 35% identity to *Nicotiana sylvestris*³³ and 33% identity to *Brevibacterium lactofermentum*⁴⁴ DHDPS enzymes. The level of homology between plants is much greater, for example, there is 87% identity between wheat and maize genes.²⁰

Early gel filtration experiments showed *E. coli* DHDPS exists as a homotetramer of molecular weight 134,000 Da.²⁹ The *dapA* locus which encodes for DHDPS has been mapped to 53 minutes on the *E. coli* chromosome⁴⁵ and subsequently cloned⁴⁵ and sequenced.⁴⁵ The published *E. coli* *dapA* sequence predicted a 292 amino acid sequence corresponding to a monomeric molecular weight of 31,372 Da.⁴⁵ However, electrospray mass spectrometry of the monomeric DHDPS gave a molecular ion of 31,272 Da and highlighted errors in the predicted amino acid sequence.³²

The crystal structure of *E. coli* DHDPS has been determined by X-ray crystallography to a resolution of 2.5 Å.³¹ The data obtained confirm that *E. coli* DHDPS is a homotetramer, revealing a dimer of dimers with approximate 222 symmetry (Figure 1.7.1). Each *E. coli* DHDPS monomer is composed of two domains: The amino-terminal domain (residues 1–224) assumes an eight-stranded parallel α/β -barrel similar to that observed in triose phosphate isomerase.⁴⁶ The α/β -barrel consists of a hydrophobic core formed by an

irregular layer of mainly hydrophobic residues. The carboxy-terminal domain (residues 224–292) is composed predominately of α -helices. The catalytic site, as defined by the position of lysine-161, is located at the carboxy-terminal end of the barrel, inside a 10 Å deep by 30 Å long cleft. This is similar in structure to class I aldolases, including *N*-acetylneuraminate lyase⁴⁷ and several other enzymes^{48–52} which are mechanistically related to DHDPS.^{53,54}

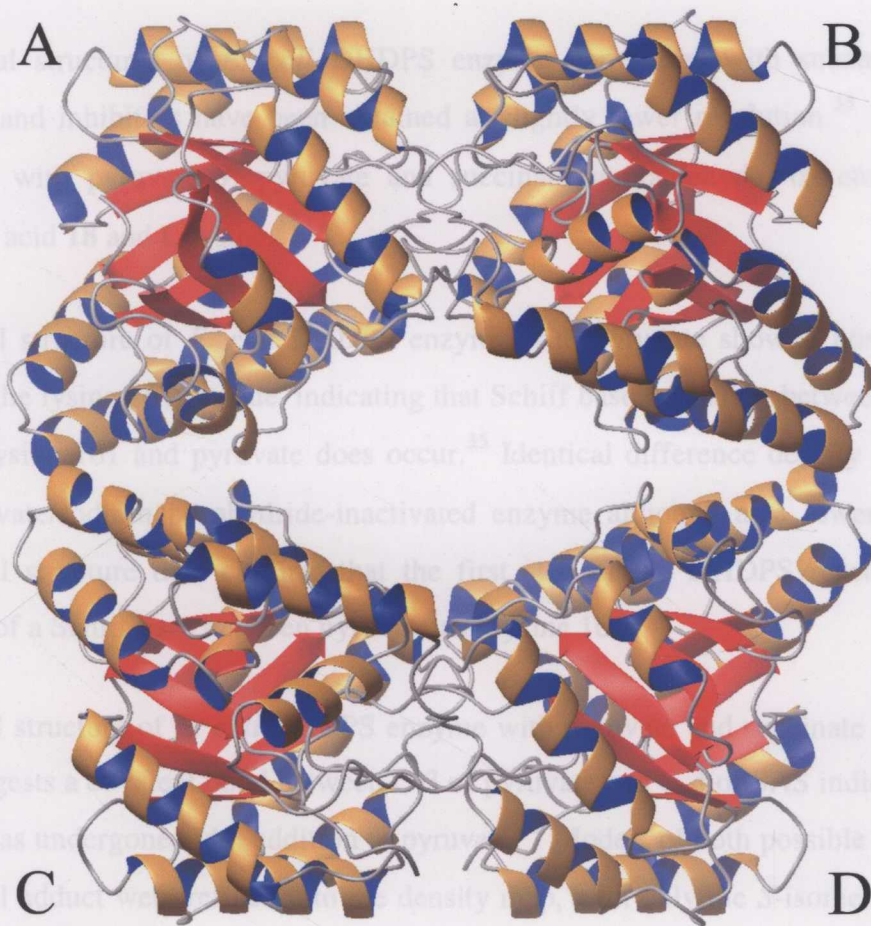


Figure 1.7.1: The Structure of *E. coli* DHDPS Tetramer: Monomers A and B, and C and D associate tightly to form dimers, which loosely associate to form the tetrameric structure of native DHDPS. β -Sheets are coloured red and α -helices are detailed in gold and blue.

The dimers of DHDPS associate loosely to form the native tetrameric enzyme. The contacts occur between monomers A and C and monomers B and D via three α -helices (Figure 1.7.1). It is interesting to note that just three residues from each monomer make contact between dimers. This association is rather weak and less than 5% of the total surface area of each monomer is buried in the loose dimer interface.^{31,35}

In contrast to the loose association *between* dimers, the subunits associate quite tightly into dimers. Residues tyrosine-106 and tyrosine-107 occur at the interface between subunits and, are conserved in all DHDPS protein sequences. The side chains of these conserved tyrosines interdigitate with those of the adjacent subunit, causing a hydrophobic, sandwich-like stack, resulting in a 12.4% burial of the total surface area of each subunit, almost blocking the amino terminus end of the active site. The binding site of lysine, the feedback inhibitor of DHDPS, is also formed at the monomer-monomer interface.

Five crystal structures of *E. coli* DHDPS enzyme complexes with substrate, substrate analogues and inhibitors have been obtained at slightly lower resolution.³⁵ These include complexes with pyruvate **9**, pyruvate and succinate semialdehyde, α -ketopimelic acid, dipicolinic acid **18** and L-lysine.³⁵

The crystal structure of *E. coli* DHDPS enzyme with pyruvate showed positive electron density at the lysine 161 residue, indicating that Schiff base formation between the ϵ -amino group of lysine 161 and pyruvate does occur.³⁵ Identical difference density was observed from pyruvate/sodium borohydride-inactivated enzyme although at a lower resolution.⁵⁵ The crystal structure data confirm that the first step of the DHDPS reaction is indeed formation of a Schiff base between pyruvate and lysine 161.

The crystal structure of *E. coli* DHDPS enzyme with pyruvate and succinate semialdehyde (SAS) suggests a covalent bond between C-3 of pyruvate and C-4 of SAS indicating that the aldehyde has undergone aldol addition to pyruvate.³⁵ Models of both possible stereoisomers of the aldol adduct were refined into the density map, with only the *S*-isomer in agreement with experimental results, suggesting that the stereochemistry at the C4 position is *S*.³⁵ Additional ¹H n.m.r studies of the reaction of DHDPS with pyruvate **9** and ASA **8** by Blickling *et al.*³⁵ showed the formation of only one product, confirming no racemisation occurred during the aldol addition.

The crystal structure of *E. coli* DHDPS enzyme with dipicolinic acid did display some positive electron density at the active site. However, there was no significant overlap with the electron density obtained from the pyruvate/succinate β -semialdehyde soak. These results suggest that dipicolinic acid **18** does not act as a simple product analogue.³⁵

The crystal structure of *E. coli* DHDPS enzyme with L-lysine displayed positive electron density at the interface of two monomer subunits, indicating that two lysine molecules bind causing a rotation of one subunit of the dimer onto the other. Each of the two lysines is in contact with both subunits and each other.³⁵

1.8 Inhibitors of Dihydrodipicolinate Synthase

As DHDPS is the branchpoint enzyme in the biosynthesis of lysine it has attracted much attention by various groups. Despite this, no potent inhibitors of DHDPS based on either substrate analogy or product analogy have yet been developed.

1.8.1 Substrate Analogue DHDPS Inhibitors

Studies of the solution structure of ASA **8** have revealed that it exists predominantly as the hydrate **19**, with only minor amounts of the aldehyde **8** present (Figure 1.8.1).^{56,57} The cyclic lactol **20** has been proposed as another possible form of ASA in solution.⁵⁷ Analogues of the different forms of ASA have been prepared and their inhibition of DHDPS analysed in an attempt to define the form of ASA that binds to DHDPS. Homoserine lactone **21**, (*S*)-3-aminopyrrolidin-2-one **22** and 2-aminocyclopentanone **23** were prepared as analogues of the cyclic lactol form of ASA **20**. Homoserine lactone **21** was found to be a non-competitive inhibitor of DHDPS with respect to both ASA **8** and pyruvate **9**. Pyrrolidinone **22** failed to inhibit DHDPS, whereas ketone **23** showed reversible non-competitive inhibition with respect to ASA. These results suggest that the biologically relevant form of ASA is not the cyclic lactol **20**. If the biologically relevant form was the cyclic lactol **20**, the corresponding analogues would be expected to show competitive inhibition.

Analogues of ASA hydrate **19** including aspartic acid **6** and compounds **24–26** were designed and assayed as inhibitors of DHDPS. Both cysteine sulfinic acid **24** and glutamic acid **25** were found to be non-competitive inhibitors of DHDPS with respect to ASA, and aspartic acid **6** was a mixed inhibitor, indicating that these compounds also act at an allosteric site, rather than the active site of the enzyme. Another analogue of the hydrate **19**, *S*-methylcysteine sulfone **26**, did not inhibit DHDPS. (*S*)-Methylcysteine sulfoxide (SMCS, **27**), an analogue of the aldehyde form of ASA **8**, did not inhibit DHDPS either, so no

conclusive information about the form of ASA **8** recognised by DHDPS could be ascertained from these results, but the most likely form appears to be the hydrate **19** based on the ^1H n.m.r. solution studies.

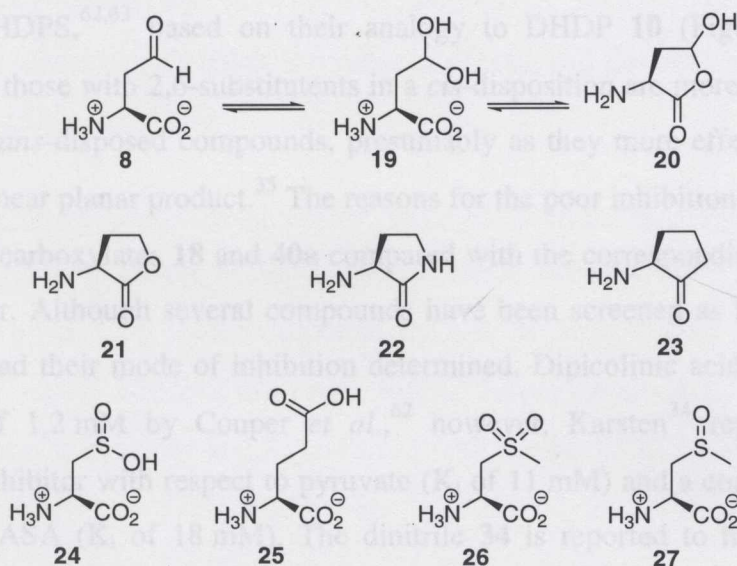


Figure 1.8.1: ASA Based Inhibitors of DHDPS

The pyruvate analogue 3-bromopyruvate **28** has been shown to irreversibly inactivate DHDPS^{32,58} by direct alkylation. 3-Bromopyruvate **28** (Figure 1.8.2) was first introduced by Meloche⁵⁹ as an active site-directed alkylating reagent and has proven to be quite versatile in labelling pyruvate-binding sites of many enzymes.^{60,61} Other pyruvate analogues such as **29–31** (Figure 1.8.2) exhibit competitive inhibition against pyruvate but uncompetitive inhibition against ASA, however the specificity of these compounds in biological systems would be limited as pyruvate is recognised by many enzymes in all cells. L-lysine analogues **32** and **33** have also been tested as potential inhibitors of DHDPS but have also proven to be quite poor.³⁰ DHDPS is feedback inhibited by L-lysine (IC_{50} of 1.0 mM) but it is not a competitive inhibitor of either pyruvate or ASA.³⁰

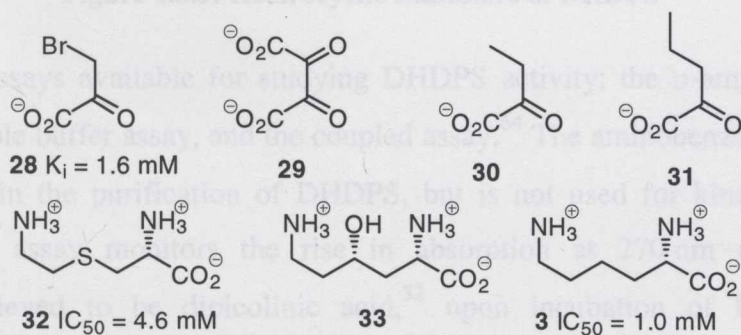


Figure 1.8.2: Pyruvate and Lysine Analogue Inhibitors

1.8.2 Heterocyclic DHDPS Inhibitors

Several heterocyclic compounds (**34–40** and **18**) have been synthesised as potential inhibitors of DHDPS,^{62,63} based on their analogy to DHDP **10** (Figure 1.8.3). Planar compounds, and those with 2,6-substituents in a *cis*-disposition are more effective than the corresponding *trans*-disposed compounds, presumably as they more effectively mimic the geometry of the near planar product.³⁵ The reasons for the poor inhibition of DHDPS by the piperidine-2,6-dicarboxylates **18** and **40a** compared with the corresponding diesters **35** and **40b** are not clear. Although several compounds have been screened as DHDPS inhibitors very few have had their mode of inhibition determined. Dipicolinic acid **18** is reported to have an IC_{50} of 1.2 mM by Couper *et al.*,⁶² however, Karsten³⁴ reports it to be an uncompetitive inhibitor with respect to pyruvate (K_i of 11 mM) and a competitive inhibitor with respect to ASA (K_i of 18 mM). The dinitrile **34** is reported to have IC_{50} value of 0.3 mM, and although K_i values are reported in a review by Cox *et al.*,⁹ no information about the mode of inhibition or by which assay it was determined is given and thus it is unclear whether this inhibitor binds at the active site.

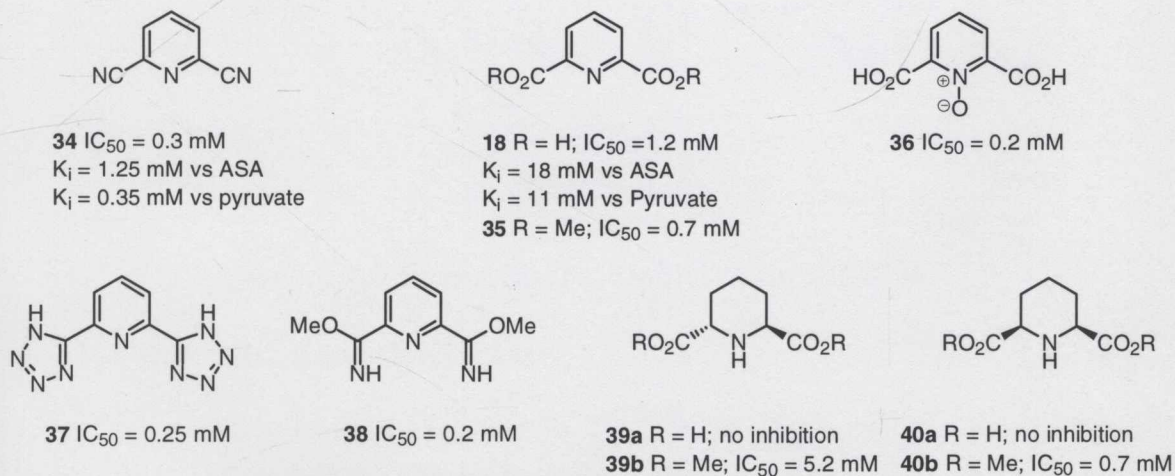


Figure 1.8.3: Heterocyclic Inhibitors of DHDPS

There are three assays available for studying DHDPS activity; the *o*-aminobenzaldehyde assay, the imidazole buffer assay, and the coupled assay.⁶⁴ The aminobenzaldehyde assay is used extensively in the purification of DHDPS, but is not used for kinetic studies. The imidazole buffer assay monitors the rise in absorption at 270 nm of an unknown chromophore believed to be dipicolinic acid,³² upon incubation of DHDPS and its substrates in imidazole buffer. However, a lag phase of more than ten seconds is present

before the absorbance at 270 nm increases, thereby making the results provided by this assay questionable. The coupled assay involves determination of DHDPS activity by monitoring the conversion of DHDP **10** to THDP **11** in the presence of excess DHDPR, with the utilisation of NADPH by DHDPR detected at 340 nm. This assay is able to measure DHDPS kinetics, if DHDPR is present in excess, and DHDPS kinetics, if DHDPS is present in excess.

It may be that the discrepancies in inhibitory values obtained for dipicolinic acid **18** are due to deficiencies of the imidazole buffer assay, compared with the more kinetically precise coupled assay. The IC_{50} of 1.2 mM reported by Couper *et al.*⁶² was obtained using the imidazole buffer assay, whereas the much higher values obtained by Karsten³⁴ (K_i of 11 mM with respect to pyruvate and K_i of 18mM with respect to ASA) were obtained using the coupled assay.

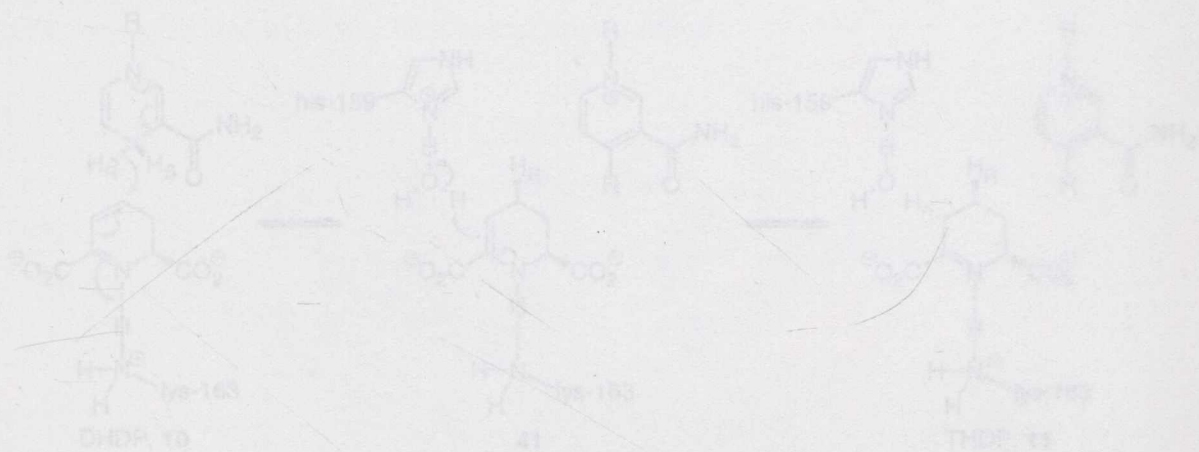


Figure 1.9.1: Production of L-THDP **11** from DHDP **10**

1.10 Dihydrodipicolinate Reductase

Dihydrodipicolinate reductase has been isolated from a variety of plant and bacterial sources. *E. coli* DHDPR is encoded by the *dapB* gene and was first reported in 1984 by Bouvier.⁶³ DHDPR has also been cloned and sequenced from *B. subtilis*,⁶⁴ *A. lactofermentum*,⁴⁶ *C. glutamicum*,⁷⁰ *Mycobacterium leprae*,⁴⁹ *Haemophilus influenzae*,⁷¹ *Pseudomonas syringae*,⁷² *Mycobacterium tuberculosis*⁷³ and *Synechocystis sp.*⁷⁴ which all encode reductases between 246–286 residues. The *E. coli* *dapB* gene encodes a 273 amino acid polypeptide of molecular weight 35,758 Da, confirmed by electrospray mass spectrometry,⁶⁵ and has been expressed and purified to homogeneity by Reddy *et al.*⁶⁶

1.9 The Second Step in the Biosynthesis of Lysine

The second step in the biosynthesis of lysine is the reduction of dihydrodipicolinate (**10**) to tetrahydrodipicolinate (THDP, **11**), a process catalysed by the NADPH-dependent enzyme dihydrodipicolinate reductase (DHDPR). DHDPR is quite unusual as it can utilise NADPH or NADH, but does possess a six-fold higher affinity for NADH.⁶⁵ The reaction is initiated by hydride transfer from the 4-*pro-R* position of NAD(P)H to the C-4 position of DHDP, resulting in the formation of an intermediate enamine **41**. Subsequent tautomerisation yields the product THDP **11** (Figure 1.9.1).^{66,67} The proton added at C3 is most likely derived from a water molecule hydrogen-bonded to the conserved His-159 residue.⁶⁶ Kinetic analysis suggests that the enzyme binds the cofactor and the substrate sequentially before reaction and release of product and oxidised cofactor.⁶⁶

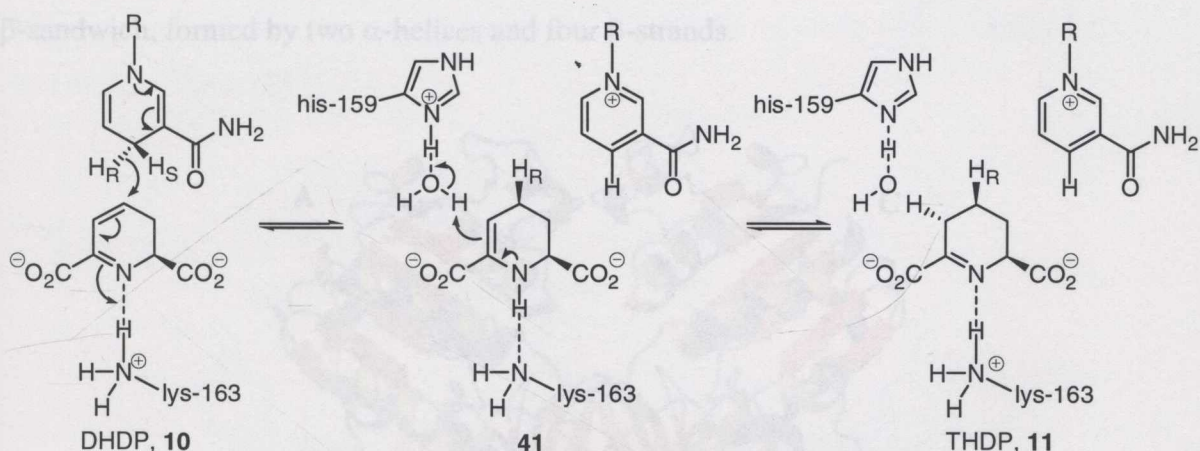


Figure 1.9.1: Production of L-THDP **11** from DHDP **10**

1.10 Dihydrodipicolinate Reductase

Dihydrodipicolinate reductase has been isolated from a variety of plant and bacterial sources. *E. coli* DHDPR is encoded by the *dapB* gene and was first reported in 1984 by Bouvier.⁶⁸ DHDPR has also been cloned and sequenced from *B. subtilis*,⁶⁹ *B. lactofermentum*,⁴⁴ *C. glutamicum*,⁷⁰ *Mycobacterium leprae*,⁴⁹ *Haemophilus influenzae*,⁷¹ *Pseudomonas syringae*,⁷² *Mycobacterium tuberculosis*⁷³ and *Synechocystis sp.*⁷⁴ which all encode reductases between 246–286 residues. The *E. coli* *dapB* gene encodes a 273 amino acid polypeptide of molecular weight 28,758 Da, confirmed by electrospray mass spectrometry,⁶⁶ and has been expressed and purified to homogeneity by Reddy *et al.*⁶⁶

Currently there are no published gene sequences of plant DHDPR. This reflects the lesser importance of DHDPR relative to that of DHDPS, as the DHDPS-catalysed step is feedback inhibited by L-lysine and therefore regulates the production of L-lysine.⁷⁵

Gel filtration experiments conducted on *E. coli* DHDPR revealed a molecular weight of 110 KDa and it was deduced that the enzyme is homotetrameric (Figure 1.10.1).^{66,67} The crystal structure of *E. coli* DHDPR bound with NADPH (determined by X-ray crystallography to a resolution of 2.2 Å⁷⁶) showed that the tetramer possesses crystallographic 222 symmetry.⁷⁶

Each *E. coli* DHDPR monomer is composed of two domains: the amino-terminal dinucleotide-binding domain, which contains four α -helices and seven β -strands making up a Rossman fold; and the carboxy-terminal substrate domain, which contains an open mixed β -sandwich, formed by two α -helices and four β -strands.



Figure 1.10.1: The Structure of *E. coli* DHDPR Tetramer: Monomers A, B, C and D associate tightly via 4 β -strands from their C-terminal domains to form a 16-stranded mixed, flattened β -barrel. β -Sheets are coloured red and α -helices are detailed in gold and blue.

1.11 Inhibitors of DHDPR

Several DHDPR inhibitors have been developed based on substrate analogy (Figure 1.11.1). More potent DHDPR inhibitors have been found than is the case for DHDPS presumably because the substrate is well defined, in contrast to the substrates and product of DHDPS. Dipicolinic acid (**18**) is a competitive inhibitor with respect to the substrate ($K_i = 26 \pm 6 \mu\text{M}$), and an uncompetitive inhibitor with respect to NADPH ($K_i = 330 \pm 50 \mu\text{M}$) consistent with an ordered, sequential mechanism.⁶⁶ Much weaker inhibition has been observed for other substrate analogues, such as *iso*-phthalic acid **42**⁶⁷ ($\text{IC}_{50} = 2 \text{ mM}$) and pipercolic **43** and picolinic acids **44**,⁶⁶ which are both very poor inhibitors ($\text{IC}_{50} > 20 \text{ mM}$). Piperidine dicarboxylates showed no inhibition whatsoever.^{9,22,77} The vinylogous amide **45** has been shown to be a competitive inhibitor of DHDPR, with a $K_i = 32 \mu\text{M}$ with respect to DHDP **10**, and is one of the most potent inhibitors of DHDPR reported, with a similar activity to that of dipicolinate **18**.⁷⁷

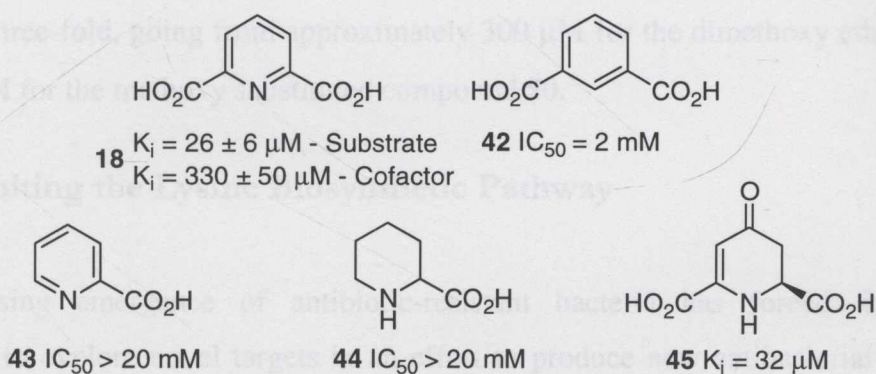


Figure 1.11.1: Heterocyclic DHDPR Inhibitors

Recently Paiva *et al.*⁷⁸ combined molecular modelling and conventional drug screening strategies to identify novel inhibitors **46–50** of DHDPR (Figure 1.11.2). Through this work a variety of compounds were found to be competitive inhibitors of DHDPR with K_i values ranging from 10–90 μM . A number of sulfonamide compounds (**46**, **47** and **49**) were identified through molecular modelling and were found to be inhibitory towards DHDPR. Although the sulfonamides were shown to be good inhibitors of DHDPR they lacked good antimicrobial activity.⁷⁸

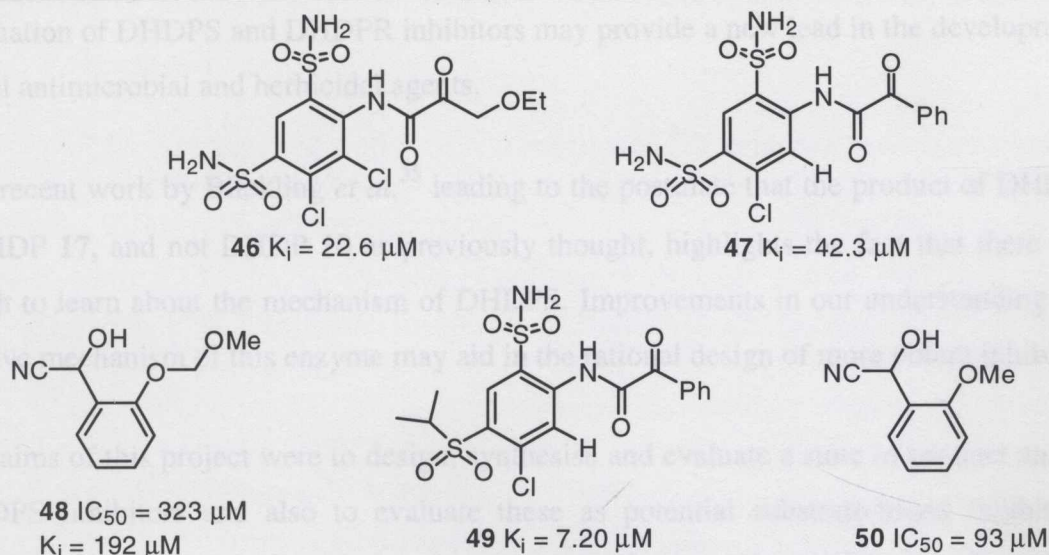


Figure 1.11.2: DHDPR Inhibitors

General structure screening by Paiva *et al.*⁷⁸ identified a number of compounds not predicted by the molecular modelling approach. These compounds generally possessed more hydrophobic moieties and heterocyclic components. Two compounds that are interesting to note are the relatively simple structures **48** and **50**. The IC_{50} value decreases more than three-fold, going from approximately 300 μM for the dimethoxy ether **48** to less than 100 μM for the methoxy substituted compound **50**.

1.12 Inhibiting the Lysine Biosynthetic Pathway

The increasing emergence of antibiotic-resistant bacteria has forced the scientific community to explore novel targets in an effort to produce new antibacterial agents. The lysine biosynthetic pathway is one such target and has attracted much attention, however no commercial product has been developed to date which inhibits this pathway.

The inhibition of lysine and (*meso*-DAP) biosynthesis could inhibit bacterial growth *via* two mechanisms. Firstly by disrupting protein synthesis and secondly by inhibiting bacterial cell wall formation. Additionally, mammals lack the ability to biosynthesise lysine and hence it is one of the amino acids which must be provided through a dietary source. The occurrence of the lysine biosynthetic pathway in microorganisms and plants but not in mammals suggests that specific inhibitors of this pathway may display novel antibacterial or herbicidal activity with low mammalian toxicity. Therefore, the design, synthesis and

evaluation of DHDPS and DHDPR inhibitors may provide a new lead in the development of novel antimicrobial and herbicidal agents.

The recent work by Blickling *et al.*³⁵ leading to the postulate that the product of DHDPS is HTHDP **17**, and not DHDP **10** as previously thought, highlights the fact that there is still much to learn about the mechanism of DHDPS. Improvements in our understanding of the elusive mechanism of this enzyme may aid in the rational design of more potent inhibitors.

The aims of this project were to design, synthesise and evaluate a suite of product analogue DHDPS inhibitors and also to evaluate these as potential substrate-based inhibitors of DHDPR. Chapter 2 describes the work towards the design and synthesis of both cyclic and acyclic DHDPS/DHDPR inhibitors. Chapter 3 describes the preparation of one of the required substrates ASA, along with the purification of DHDPS and DHDPR necessary to evaluate the proposed inhibitors. Chapter 4 describes the kinetic analysis of DHDPS and DHDPR as well as the inhibition assays and kinetics of inhibitors conducted on both enzymes and furthermore a mechanistic interpretation of the results obtained. Chapter 5 contains all the experimental work pertaining to chapters 2–4.

- (13) Dezelic, P.; Bricas, S. *Biochemistry* 1970, 9, 823.
- (14) Begg, T. D. H.; Bradish, P. S. *FEMS Microbiol. Lett.* 1994, 119, 255.
- (15) Schleifer, K.; Kandler, O. *Bact. Rev.* 1972, 36, 407.
- (16) Cirillo, J. D.; Weiskrod, T. R.; Banerjee, A.; Bloom, B. R.; Jacobs, W. B. J. *J. Bacteriol.* 1994, 176, 4424.
- (17) Kamryo, T.; Matsuyashi, M. *J. Biol. Chem.* 1972, 247, 6306.
- (18) Waxman, D. J.; Strominger, J. L. *Ann. Rev. Biochem.* 1983, 52, 825.
- (19) Barna, J. C. J.; Williams, D. H. *Ann. Rev. Microbiol.* 1984, 34, 339.
- (20) Silk, G. W.; Matthews, B. F.; Somers, D. A.; Gengenbach, B. G. *Plant Molecular Biology* 1994, 26, 989.
- (21) Chen, N.; Jiang, S.; Klien, D. A.; Paulus, H. *J. Biol. Chem.* 1993, 268, 9448.
- (22) Cox, R. J. *Nat. Prod. Rep.* 1996, 20.
- (23) Schrumpf, B.; Schwarzer, A.; Kalinowski, J.; Puhler, A.; Eggeling, L.; Stein, H. *J. Bacteriol.* 1991, 173, 4510.
- (24) Bartlett, A. T.; White, P. J. *J. Gen. Microbiol.* 1985, 131, 2145.
- (25) Peterkofsky, B. *Meth. Enzymol.* 1962, 3, 853.
- (26) Ishino, S.; Yamaguchi, K.; Shirahata, K.; Anki, K. *Agric. Biol. Chem.* 1984, 48, 2557.
- (27) Sonntag, K.; Eggeling, L.; De Graff, A. A.; Sahn, H. *Eur. J. Biochem.* 1993, 213, 1325.

1.13 References

- (1) W.H.O. "Overcoming Antimicrobial Resistance.," World Health Organization Report on Infectious Diseases, 2000.
- (2) Neu, C. H. *Science* **1992**, 257, 1064.
- (3) Leclerq, R.; Derlot, E.; Duval, J.; Courvalin, P. *N. Engl. J. Med.* **1988**, 319, 157.
- (4) Division, P. H. "Antibiotic Resistance," Commonwealth Department of Health and Aged Care, Australia, 1998.
- (5) C.D.C. "VISA/VRSA - Vancomycin-Intermediate/Resistant Staphylococcus aureus," Centre for Disease Control, United States of America, 2003.
- (6) Lyon, B. R.; Skurray, R. *Microbiol. Rev.* **1987**, 51, 88.
- (7) Hayes, J. D.; Wolf, C. R. *Biochem. J.* **1990**, 272, 281.
- (8) Bugg, T. D. H.; Walsh, C. T. *Nat. Prod. Rep.* **1992**, 199.
- (9) Cox, R. J.; Sutherland, A.; Vederas, J. C. *Bioorg. Med. Chem. Lett.* **2000**, 8, 843.
- (10) Gale, E. F.; Cundliffe, E.; Renyolds, P. E.; Richmond, M. H.; Waring, M. J. *The Molecular Basis of Antibiotic Action*; 2nd ed.; Wiley-Interscience: New York, 1981.
- (11) Patrick, G. L. *An Introduction to Medicinal Chemistry*; 1st ed.; Oxford University Press Inc., New York, 1997.
- (12) Franklin, T. J.; Snow, G. A. *Biochemistry and Molecular Biology of Antimicrobial Drug Action*; 5th ed.; The Kluwer Academic Publishers: Dordrecht, The Netherlands, 1998.
- (13) Dezelee, P.; Bricas, E. *Biochemistry* **1970**, 9, 823.
- (14) Bugg, T. D. H.; Brandish, P. E. *FEMS Microbiol. Lett.* **1994**, 119, 255.
- (15) Schleifer, K.; Kandler, O. *Bact. Rev.* **1972**, 36, 407.
- (16) Cirillo, J. D.; Weisbrod, T. R.; Banerjee, A.; Bloom, B. R.; Jacobs, W. R. J. *J. Bacteriol.* **1994**, 176, 4424.
- (17) Kamiryo, T.; Matsuashi, M. *J. Biol. Chem.* **1972**, 247, 6306.
- (18) Waxman, D. J.; Strominger, J. L. *Ann. Rev. Biochem.* **1983**, 52, 825.
- (19) Barna, J. C. J.; Williams, D. H. *Ann. Rev. Microbiol.* **1984**, 38, 339.
- (20) Silk, G. W.; Matthews, B. F.; Somers, D. A.; Gengenbach, B. G. *Plant Molecular Biology* **1994**, 26, 989.
- (21) Chen, N.; Jiang, S.; Klien, D. A.; Paulus, H. *J. Biol. Chem.* **1993**, 268, 9448.
- (22) Cox, R. J. *Nat. Prod. Rep.* **1996**, 29.
- (23) Schrupf, B.; Schwarzer, A.; Kalinowski, J.; Puhler, A.; Eggeling, L.; Sahm, H. *J. Bacteriol.* **1991**, 173, 4510.
- (24) Bartlett, A. T.; White, P. J. *J. Gen. Microbiol.* **1985**, 131, 2145.
- (25) Peterofsky, B. *Meth. Enzymol.* **1962**, 5, 853.
- (26) Ishino, S.; Yamaguchi, K.; Shirahata, K.; Araki, K. *Agric. Biol. Chem.* **1984**, 48, 2557.
- (27) Sonntag, K.; Eggeling, L.; De Graff, A. A.; Sahm, H. *Eur. J. Biochem.* **1993**, 213, 1325.

- (28) Work, E. *Meth. Enzymol.* **1962**, 5, 864.
- (29) Shedlarski, J. G.; Gilvarg, C. *J. Biol. Chem.* **1970**, 245, 1362.
- (30) Laber, B.; Gomis-Ruth, F. X.; Romao, M. J.; Huber, R. *Biochem. J.* **1992**, 288, 691.
- (31) Mirwaldt, C.; Korndorfer, I.; Huber, R. *J. Mol. Biol.* **1995**, 246, 227.
- (32) Borthwick, E. B.; Connell, S. J.; Tudor, D. W.; Robins, D. J.; Shneier, A.; Abell, C.; Coggins, J. R. *Biochem. J.* **1995**, 305, 521.
- (33) Blickling, S.; Beisel, H.; Bozic, D.; Knablein, J.; Laber, B.; Huber, R. *J. Mol. Biol.* **1997**, 274, 608.
- (34) Karsten, W. *Biochemistry* **1997**, 36, 1730.
- (35) Blickling, S.; Renner, C.; Laber, B.; Pohlenz, H.; Holak, T. A.; Huber, R. *Biochemistry* **1997**, 36, 24.
- (36) Stahly, D. P. *Biochim. Biophys. Acta* **1969**, 191, 439.
- (37) Cremer, J.; Treptoe, C.; Eggeling, L.; Sahm, H. *J. Gen. Microbiol.* **1988**, 134, 3221.
- (38) Yamakura, F.; Ikeda, Y.; Kimura, K.; Sasakawa, T. *J. Biochem. (Tokyo)* **1974**, 76, 611.
- (39) Frisch, D. A.; Gengenbach, B. G.; Tommey, A. M.; Sellner, J. M.; Somers, D. A.; Myers, D. E. *Plant Physiol.* **1991**, 96, 444.
- (40) Gishlain, M.; Frankard, V.; Jacobs, M. *Planta* **1990**, 180, 480.
- (41) Kumpaisal, R.; Hashimoto, T.; Yamada, Y. *Plant Physiol.* **1987**, 85, 145.
- (42) Dereppe, C.; Bold, G.; Ghisalba, O.; Edbert, E.; Schar, H. *Plant Physiol.* **1992**, 98, 813.
- (43) Kaneko, T.; Hashimoto, T.; Kumpaisal, R.; Yamada, Y. *J. Biol. Chem.* **1990**, 265, 17451.
- (44) Pisabarro, A.; Malumbres, M.; Mateos, L. M.; Oguiza, J. A.; Martin, J. F. *J. Bacteriol.* **1993**, 175, 2743.
- (45) Richaud, F.; Richaud, C.; Ratet, P.; Patte, J. *J. Bacteriol.* **1986**, 166, 297.
- (46) Banner, D. W.; Bloomer, A. C.; Petsko, G. A.; Phillips, D. C.; Pogson, C. I.; Wilson, I. A.; Corran, P. H.; Furth, A. J.; Milman, J. D.; Offord, R. E.; Priddle, J. D.; Waley, S. G. *Nature* **1975**, 255, 609.
- (47) Izard, T.; Lawrence, M. C.; Malby, R. L.; Lilley, G. G.; Colman, P. M. *Structure* **1994**, 2, 361.
- (48) Jeffcoat, R.; Hassall, H.; Dagley, S. *Biochem. J.* **1969**, 115, 969.
- (49) Jeffcoat, R.; Hassall, H.; Dagley, S. *Biochem. J.* **1969**, 115, 977.
- (50) Eaton, R. W. *J. Bacteriol.* **1992**, 174, 7542.
- (51) Iwabuchi, T.; Harayama, S. *J. Bacteriol.* **1998**, 180, 945.
- (52) Buchanan, C. L.; Connaris, H.; Danson, M. J.; Reeve, C. D.; Hough, D. W. *Biochem. J.* **1999**, 343, 563.
- (53) Barbosa, J. A. R. G.; Smith, B. J.; DeGori, R.; Ooi, H. C.; Marcuccio, S. M.; Campi, E. M.; Jackson, W. R.; Brossmer, R.; Sommer, M.; Lawrence, M. C. *J. Mol. Biol.* **2000**, 303, 405.
- (54) Lawrence, M. C.; Barbosa, J. A. R. G.; Smith, B. J.; Hall, N. E.; Pilling, P. A.; Ooi, H. C.; Marcuccio, S. M. *J. Mol. Biol.* **1997**, 266, 381.

- (55) Laber, B.; Gomis-Ruth, F.; Romao, M. J.; Huber, R. *Biochem. J.* **1992**, 288, 691.
- (56) Tudor, D. W.; Lewis, T.; Robins, D. J. *Synthesis* **1993**, 1061.
- (57) Coulter, C. V.; Gerrard, J. A.; Kraunsoe, J. A. E.; Pratt, A. J. *Pest. Sci.* **1999**, 55, 887.
- (58) Webster, F. H.; Lechowich, R. V. *J. Bacteriol.* **1970**, 101, 118.
- (59) Meloche, H. P. *Biochem. Biophys. Res. Comm.* **1965**, 18, 277.
- (60) Apfel, M. A.; Ikeda, B. H.; Speckhard, D. C.; Frey, P. A. *J. Biol. Chem.* **1984**, 259, 2905.
- (61) Froelich, L.; Strauss, M.; Kornhuber, J.; Hoyer, S.; Sorbi, S.; Riederer, P.; Amaducci, L. *J. Neu. Trans.: Parkinsons Disease and Dementia Section* **1990**, 2, 169.
- (62) Couper, L.; McKendrick, J. E.; Robins, D. J. *Bioorg. Med. Chem. Lett.* **1994**, 4, 2267.
- (63) Walters, D. R.; McPherson, A.; Robins, D. J. *Mycol. Res.* **1997**, 101, 329.
- (64) Yugari, Y.; Gilvarg, C. *J. Biol. Chem.* **1965**, 240, 4710.
- (65) Eliel, E. L., Wilen, S. H., Eds.; John Wiley & Sons: New York, 1994, p 665.
- (66) Reddy, S. G.; Sacchettini, J. C.; Blanchard, J. S. *Biochemistry* **1995**, 34, 3492.
- (67) Tamir, H.; Gilvarg, C. *J. Biol. Chem.* **1974**, 249, 3034.
- (68) Bouvier, J.; Richaud, C.; Richaud, F.; Patte, J.; Stragier, P. *J. Biol. Chem.* **1984**, 259, 14829.
- (69) Henner, D.; Gollnick, P.; Moir, A. *Proc. Sixth. Int. Symp. Genet. Ind. Microorg.* **1990**, 6, 657.
- (70) Eikmanns, B. J. *Direct GeneBank Submission* **1992**, Accession Number X67737.
- (71) Fleischmann, R. D.; Adams, M. D.; White, O.; Clayton, R. A.; Kirkness, E. F.; Kerlavage, A. R.; Bult, C. J.; Tomb, J. F.; Dougherty, B. A.; Merrick, J. M. *Science* **1995**, 269, 496.
- (72) Liu, L.; Shaw, P. D. *J. Bacteriol.* **1997**, 179, 507.
- (73) Pavelka, M. S., Jr.; Weisbrod, T. R.; Jacobs, W. R., Jr. *J. Bacteriol.* **1997**, 179, 2777.
- (74) Tabata, S. **1997**, Accession Number D90899.
- (75) Blickling, S.; Knablein, J. *Biol. Chem.* **1997**, 378, 207.
- (76) Scapin, G.; Blanchard, J. S.; Sacchettini, J. C. *Biochemistry* **1995**, 34, 3502.
- (77) Caplan, J. F.; Renjian, Z.; Blanchard, J. S.; Vederas, J. C. *Org. Lett.* **2000**, 24, 3857.
- (78) Paiva, A. M.; Vanderwall, D. E.; Blanchard, J. S.; Kozarich, J. W.; Williamson, J. M.; Kelly, T. M. *Biochim. Biophys. Acta* **2001**, 1545, 67.

2.1 Design of Cyclic Inhibitors of DHDPS

Although several DHDPS inhibitors have been reported, no novel ones have been developed. All previous inhibitors have been designed either as analogues of the enzyme product (Chapter 1, Figures 1.8.1 and 1.8.2) or as products of the enzyme reaction (Chapter 1, Figures 1.8.1 and 1.8.2).

CHAPTER 2

SYNTHESIS OF INHIBITORS

Research by Bliokling and co-workers¹ has suggested that the true product is actually HTDHP 17. As HTDHP contains a hydroxyl group at the C-4 position this inspired the design of several novel analogues containing oxygen functionality at the C-4 position. As compounds incorporating oxygen at the C-4 position mimic the putative product HTDHP 17 more closely than compounds designed to mimic DHDHP 10, there are potentially more binding interactions which could occur at the enzyme active site, thereby providing a lead in the development of more potent inhibitors of DHDPS. Therefore compounds 51–54 were designed as potential inhibitors, all with oxygen functionality at the C-4 position (Figure 2.1.1).

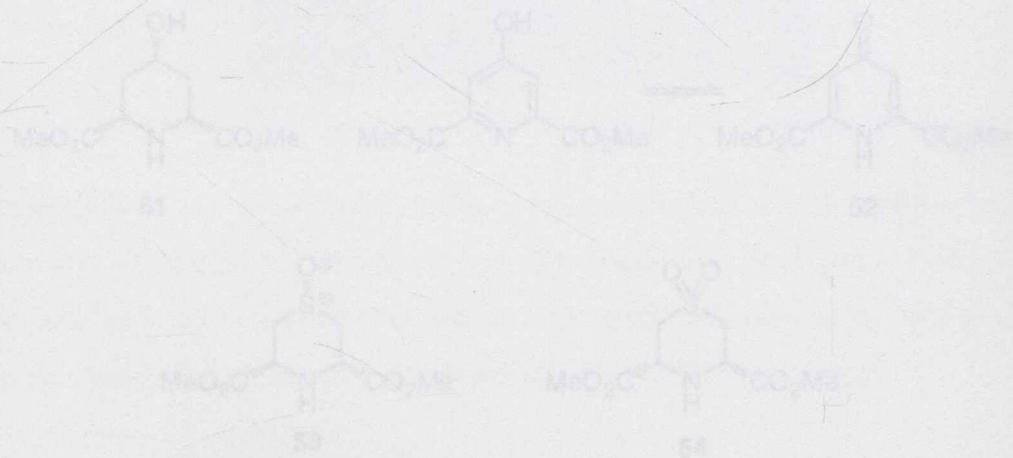


Figure 2.1.1: Proposed DHDPS Inhibitors

The cyclic alcohol 51 (Figure 2.1.1) was designed to closely mimic the enzyme product HTDHP 17. It contains a C-4 hydroxyl group with (5*S*) stereochemistry as given by Bliokling *et al.*¹ for HTDHP 17 (see Figure 1.6.1). One of the differences between 51 and HTDHP 17 is that 51 does not contain the imine functional group and thus should not undergo dehydration or any further enzymatic reaction (specifically it cannot act as a substrate for DHDPS; the next enzyme in the pathway). Couper *et al.*² (see Figure 1.8.3)

2.1 Design of Cyclic Inhibitors of DHDPS

Although several DHDPS inhibitors have been reported, no potent inhibitors have yet been developed. All previous inhibitors have been designed either as substrate analogues (see Chapter 1, Figures 1.8.1 and 1.8.2) or as product analogues (see Chapter 1, Figure 1.8.3) based on the reported product DHDP **10**.

Research by Blickling and co-workers¹ has suggested that the true product is actually HTHDP **17**. As HTHDP contains a hydroxyl group at the C-4 position this prompted the design of several novel analogues containing oxygen functionality at the C-4 position. As compounds incorporating oxygen at the C-4 position mimic the putative product HTHDP **17** more closely than compounds designed to mimic DHDP **10**, there are potentially more binding interactions which could occur at the enzyme active site, thereby providing a lead in the development of more potent inhibitors of DHDPS. Therefore compounds **51–54** were designed as potential inhibitors, all with oxygen functionality at the C-4 position (Figure 2.1.1).

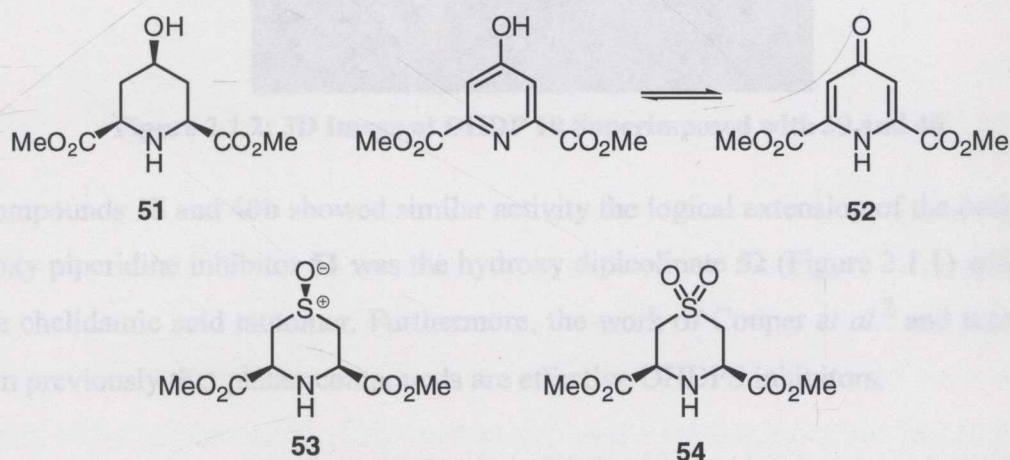


Figure 2.1.1: Proposed DHDPS Inhibitors

The cyclic alcohol **51** (Figure 2.1.1) was designed to closely mimic the putative enzyme product HTHDP **17**. It contains a C-4 hydroxyl group with (*S*)-stereochemistry observed by Blickling *et al.*¹ for HTHDP **17** (see Figure 1.6.1). One of the differences between **51** and HTHDP **17** is that **51** does not contain the imine functional group and thus should not undergo dehydration or any further enzymatic reaction (specifically it cannot act as a substrate for DHDPR, the next enzyme in the pathway). Couper *et al.*² (see Figure 1.8.3)

suggested that compounds with a *cis*-configuration at the C-2 and C-6 positions are more effective inhibitors than the corresponding *trans*-compounds, as exemplified by **40b** possessing an IC_{50} value of 0.7 mM compared with the corresponding value of 5.2 mM for **39b**. Superimposing DHDP **10** or HTHDP **17** with **39** and **40** (Figure 2.1.2) indicates that the all *syn*-configured compound **40** with equatorial $-CO_2R$ groups more closely resembles DHDP **10** or HTHDP **17**. Hence, the combination of 4(*S*)-stereochemistry to match that reported by Blickling *et al.*¹ and the 2(*S*)-stereochemistry to match that derived from (*S*)-ASA, along with the *cis*-2,6 relationship gave the all *syn*-compound **51**. Furthermore, Couper *et al.*² showed that methyl esters were more potent inhibitors than the corresponding acids as seen when comparing the potency of acids **39a** and **40a** against the corresponding methyl esters **39b** and **40b**. The acids showed no inhibitory activity whatsoever. Therefore, methyl esters were incorporated into the design of all new inhibitors.

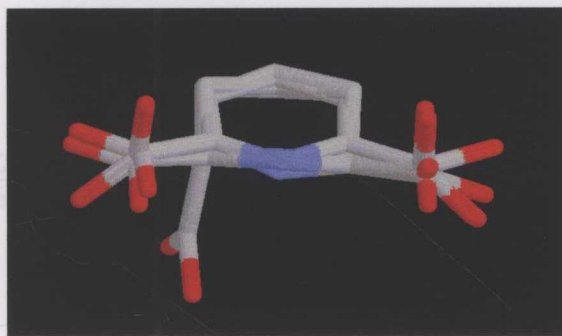


Figure 2.1.2: 3D Image of DHDP **10** Superimposed with **39** and **40**

As compounds **18** and **40b** showed similar activity the logical extension of the design of the hydroxy piperidine inhibitor **51** was the hydroxy dipicolinate **52** (Figure 2.1.1) which exists as the chelidamic acid tautomer. Furthermore, the work of Couper *et al.*² and Karsten³ has shown previously that planar compounds are effective DHDPS inhibitors.

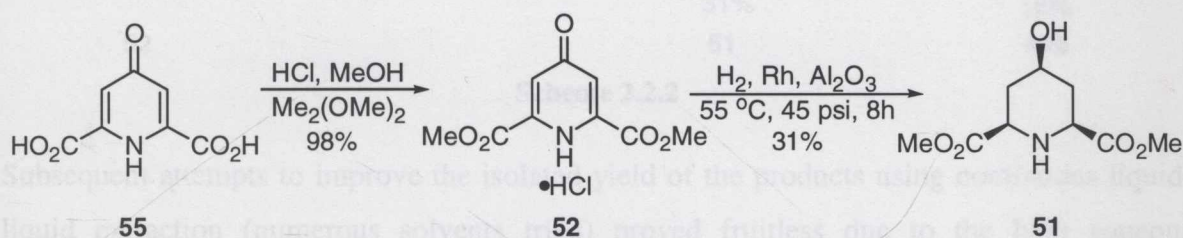
The sulfoxide **53** (Figure 2.1.1) was also proposed as a potential inhibitor of DHDPS. The sulfoxide **53** is similar in structure to that of HTHDP **17**, but was proposed to mimic the transition state of the aldol reaction, rather than the stable intermediate, due to the charge separation inherent in the sulfoxide functional group. Sulfoxides carry a partial negative charge on the oxygen and a partial positive charge on the sulfur atom. This charge separation mimics the developing negative charge on the ASA oxygen in the transition state, as the nucleophilic enamine **15** attacks. Transition state analogues have frequently been proven to be very potent inhibitors of enzymes as they are very tightly bound by the

enzyme in the active site,^{4,5} and consequently, the sulfoxide was predicted to be a potent DHDPS inhibitor.

Finally, the sulfone **54** (Figure 2.1.1) was designed as to mimic the hydrate **19** of ASA by possessing two oxygens at the C-4 position. The hydrate **19** is one of the potentially biologically relevant forms of ASA and thus the sulfone **54** was proposed to be a good active site mimic.

2.2 Synthesis of Alcohols **51** and **52**

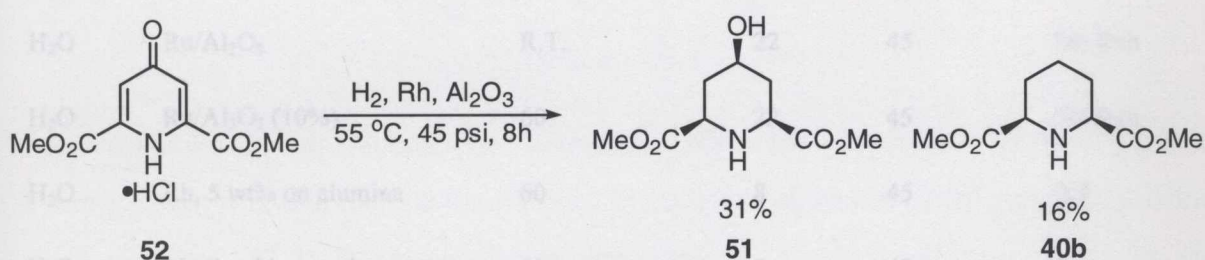
Fortuitously, the synthesis of diesters of chelidamic acid **52** and alcohol **51** was reported by Chênevert *et al.*⁶ Esterification of chelidamic acid **55** using 2,2-dimethoxypropane and hydrochloric acid in methanol gave the desired dimethyl chelidamate hydrochloride **52** in excellent yield (98%).



Scheme 2.2.1

Hermann and Dreiding⁷ reported the hydrogenation of a suspension of dimethyl chelidamate hydrochloride **52** in water using rhodium on alumina as the hydrogenation catalyst at 70 °C and 45 psi for 33 hours gave a ratio of 1.6:1 of desired product **51** to hydrogenolysis product **40b** with an isolated yield of 63% of the desired product (see first entry in blue in Table 2.2.1). Chênevert *et al.*⁶ used a similar procedure but performed the reaction at room temperature and reported a ratio of 2.7:1 of desired product **51** to hydrogenolysis product **40b** with an isolated yield of 74% of the desired product (see second entry in blue in Table 2.2.1). Using the reactions condition of Chênevert *et al.*⁶ no reaction occurred. Heating the reaction to 55 °C (fifteen degrees lower than the temperature used by Hermann *et al.*⁷) and leaving the reaction for 16 hours instead of 33 hours resulted in production of a 1:2 ratio of desired product **51** to hydrogenolysis product **40b**. A multitude of reaction conditions were investigated in an attempt to improve the yield of **51** including different hydrogenation catalysts, temperatures, pressures and solvents (Table

2.2.1). The optimal conditions (see entry in red in Table 2.2.1) were found to be 55 °C and 45 psi for eight hours in water with the products obtained in a ratio of 2:1 in favour of the desired product **51** (Scheme 2.2.2). This procedure still only provided a yield of 31% of the isolated product which is quite poor when compared with the previously reported yields. Although other rhodium catalysts were used none gave better ratios than standard rhodium on alumina and none gave higher isolated yields. The most likely cause for the yield of **51** being lower than those reported in the literature is probably due to variations in the catalyst. Although frustrating, the isolation of the over-hydrogenated product **40b** proved somewhat fortuitous, as the byproduct could be used as a control inhibitor, based on the work of Couper *et al.*²



Scheme 2.2.2

Subsequent attempts to improve the isolated yield of the products using continuous liquid-liquid extraction (numerous solvents tried) proved fruitless due to the high aqueous solubility of the compounds. The two compounds **51** and **40b** were easily separated by refluxing the mixture in hexane for 30 min followed by hot filtration. The ¹H n.m.r. data were in agreement with those reported by Chênevert *et al.*⁶ and Hermann *et al.*⁷

Due to the capricious nature of the hydrogenation reaction, an alternative procedure was attempted to prepare **51**.

Hermann *et al.*⁷ have reported the synthesis of piperidine dicarboxylates by a Michael addition of amines to dienones. Accordingly, the diene **56** was synthesised according to the method of Lemaire-Audouin and Vogel⁸ starting from diethyl 4-oxopimelate **57** (Scheme 2.2.3). Treatment of diethyl 4-oxopimelate **57** with two equivalents of piperidine in dichloromethane at 0 °C for one hour resulted in formation of the dibromide **58** in 31%

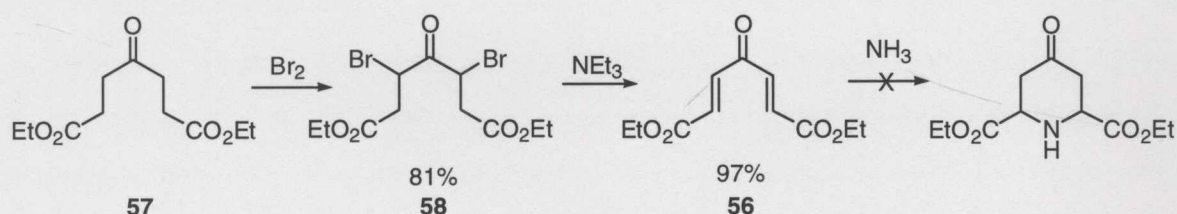
Table 2.2.1: Optimisation of Hydrogenation Conditions for the Synthesis of 51

Solvent	Catalyst (5% unless otherwise stated)	Temperature (°C)	Time (h)	Pressure (psi)	Ratio 51:40b
H ₂ O	Rh/Al ₂ O ₃	R.T.	16	45	2.7:1
H ₂ O	Rh/Al ₂ O ₃	70	33	45	1.6:1
H ₂ O	Rh/Al ₂ O ₃	R.T.	16	45	No Rxn
H ₂ O	Rh/Al ₂ O ₃	50	16	45	1:2
H₂O	Rh/Al₂O₃	55	8	45	2:1
H ₂ O	Ru/Al ₂ O ₃	R.T.	22	45	No Rxn
H ₂ O	Ru/Al ₂ O ₃ (10%)	60	22	45	No Rxn
H ₂ O	Rh, 5 wt% on alumina	60	8	45	2:1
H ₂ O	Rh, 5 wt% on carbon, wet, Degussa type	60	7	45	2:1
H ₂ O	Rh, 5 wt% (dry basis) on carbon, wet, Degussa type	55	4	45	1:1
MeOH	Rh/Al ₂ O ₃	40	17	45	No Rxn
MeOH	Rh/Al ₂ O ₃ Me	Reflux	48	Atmospheric	No Rxn
H ₂ O	Rh/Al ₂ O ₃	Reflux	48	Atmospheric	No Rxn
H ₂ O	Rh/Al ₂ O ₃	R.T.	24	5000 KPa	No Rxn
H ₂ O	RuO	60	8	45	No Rxn

Due to the capricious nature of the hydrogenation reaction, an alternative procedure was attempted to prepare **51**.

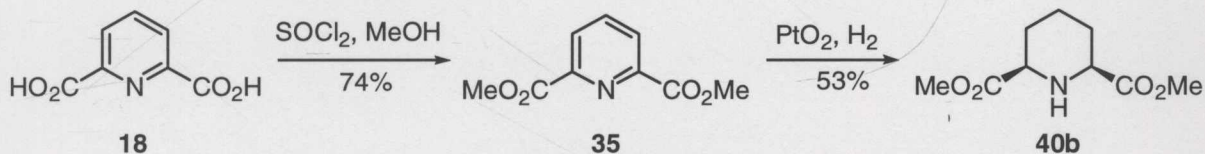
Hermann *et al.*⁷ have reported the syntheses of piperidine dicarboxylates by a Michael addition of amines to dienones. Accordingly, the diene **56** was synthesised according to the method of Lemaire-Audoire and Vogel⁸ starting from diethyl 4-oxopimelate **57** (Scheme 2.2.3). Treatment of diethyl 4-oxopimelate **57** with two equivalents of bromine in dichloromethane at 0 °C for one hour resulted in formation of the dibromide **58** in 81%

yield, which was purified by recrystallisation from hexane at $-15\text{ }^{\circ}\text{C}$. Dibromide **58** was subsequently converted to the diene **56** in excellent yield (97%) upon treatment with two equivalents of triethylamine. The diene **56** was purified by recrystallisation from 96% ethanol. Treatment of the diene **56** with ammonia in ethanol led to decomposition of the starting material, even when performed at low temperature such as $0\text{ }^{\circ}\text{C}$. No further investigations were conducted and the low yielding hydrogenation procedure was used to access the cyclic alcohol **51**.



Scheme 2.2.3

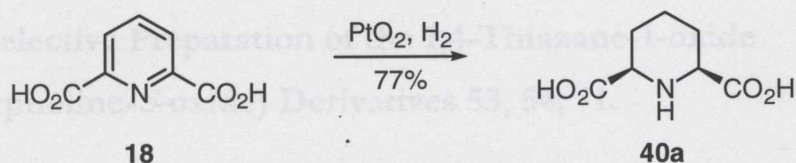
As *meso*-2,6-bis(methoxycarbonyl) piperidine **40b**, the byproduct isolated in the hydrogenation reaction, had previously been investigated as an inhibitor,⁹ another synthetic route (Scheme 2.2.4) to this molecule was used to provide sufficient quantities for biological testing.



Scheme 2.2.4

Esterification of dipicolinic acid **18** with methanolic hydrogen chloride gave diester **35** in good yield (74%). Subsequent hydrogenation of this compound using Adam's catalyst (PtO_2) under an atmosphere of hydrogen afforded according to the method of Chrystal *et al.*⁹ gave the desired compound **40b** in 53% yield (Scheme 2.2.4). The spectral data were identical to those for **40b** isolated from the hydrogenation reaction (Scheme 2.2.2).

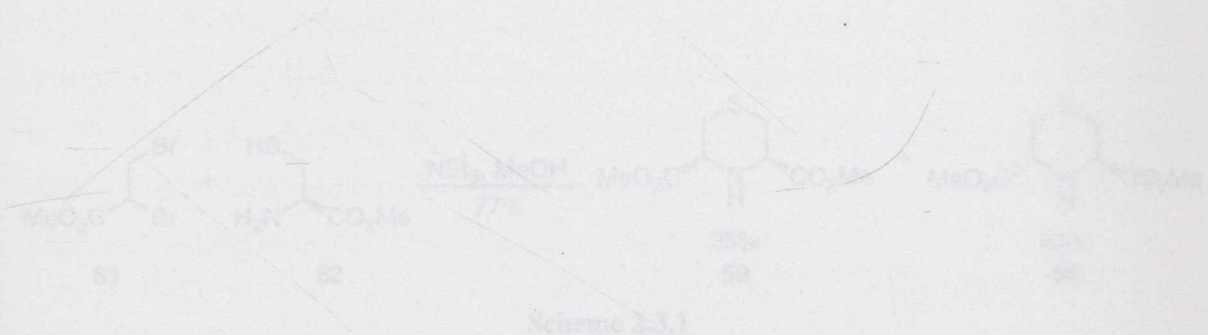
The corresponding acid **40a** was prepared by hydrogenation of dipicolinic acid **18** using Adam's catalyst (PtO_2) under an atmosphere of hydrogen to give the desired dicarboxylate in 77% yield according to the method of Chrystal *et al.*⁹ (Scheme 2.2.5).



Scheme 2.2.5

Having synthesised the desired alcohols **51** and **52** attention was turned to the synthesis of the sulfoxide **53** and sulfone **54** inhibitors.

It was envisaged that the desired sulfoxide and sulfone compounds (**53**, **54**, **71**) could be realised by the oxidation of the corresponding thiathiazane derivatives (**59**, **60**, **70**). The compounds were thus synthesised by treatment of L-cysteine derived ester hydrochloride **61** with 2,3-dibromopropionic **63** in the presence of trimethylsilylacetone (2.3.1). Separation of the diastereomers was accomplished efficiently by flash column chromatography, providing the *meso*-thiazane **59** in 35% yield and the (*R,R*)-thiazane **60** in 42% yield. The structure of these compounds was confirmed by comparison of the ¹H NMR spectral data with that reported by Paradisi *et al.*¹⁰ The H_{3,5} protons of (*R,R*)-thiazane **60** occur at δ 3.96, significantly further downfield than the corresponding H_{3,5} protons of *meso*-thiazane **59** which resonate at δ 3.55, thereby making the diastereomers easily distinguishable.

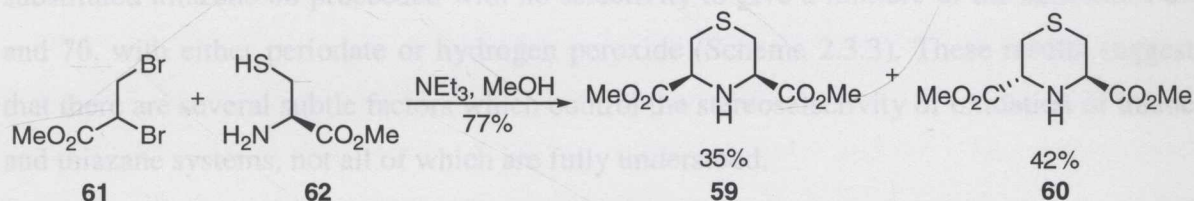


Scheme 2.3.1

The inherent symmetry of these substituted thiazanes, be it planar **59** or axial **60**, renders asymmetric oxidant systems such as those of Brunel *et al.*¹¹ and Komatsu *et al.*¹² of little use in their stereoselective oxidation. However, adoption of a specific chair conformation renders the sulfur lone-pairs non-equivalent, such that preferential reactivity of either the axial or equatorial sulfur lone-pair allows stereoselective oxidation to occur.

2.3 Stereoselective Preparation of the 1,4-Thiazane-1-oxide (thiamorpholine-S-oxide) Derivatives **53**, **54**, **71**.

It was envisaged that the desired sulfoxide compounds (**53**, **54**, **71**) could be obtained through a stereoselective oxidation of the *meso*- and (*R,R*)-thiazanes, **59** and **60**. Conveniently, a synthesis of these compounds had already been developed by Paradisi *et al.*¹⁰ The compounds were thus synthesised by treatment of L-cysteine methyl ester hydrochloride **61** with 2,3-dibromopropionate **62** in the presence of triethylamine (Scheme 2.3.1). Separation of the diastereomers was accomplished efficiently by flash column chromatography, providing the *meso*-thiazane **59** in 35% yield and the (*R,R*)-thiazane **60** in 42% yield. The structure of these compounds was confirmed by comparison of the ¹H n.m.r. spectral data with that reported by Paradisi *et al.*¹⁰ The H_{3/5} protons of (*R,R*)-thiazane **60** occur at δ 3.96, significantly further downfield than the corresponding H_{3/5} protons of *meso*-thiazane **59** which resonate at δ 3.55, thereby making the diastereomers easily distinguishable.

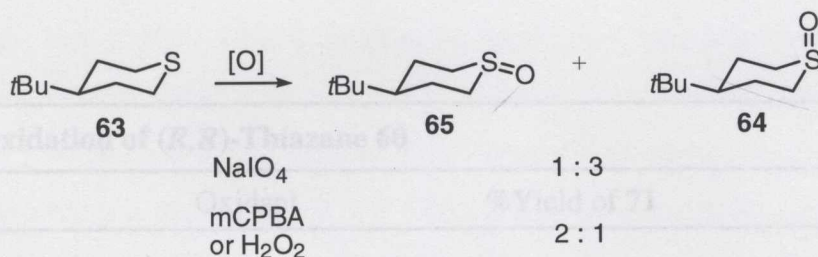


Scheme 2.3.1

The inherent symmetry of these substituted thiazanes, be it planar **59** or axial **60**, renders asymmetric oxidant systems such as those of Brunel *et al.*¹¹ and Komatsu *et al.*¹² of little use in their stereoselective oxidation. However, adoption of a specific chair conformation renders the sulfur lone-pairs non-equivalent, such that preferential reactivity of either the axial or equatorial sulfur lone-pair allows stereoselective oxidation to occur.

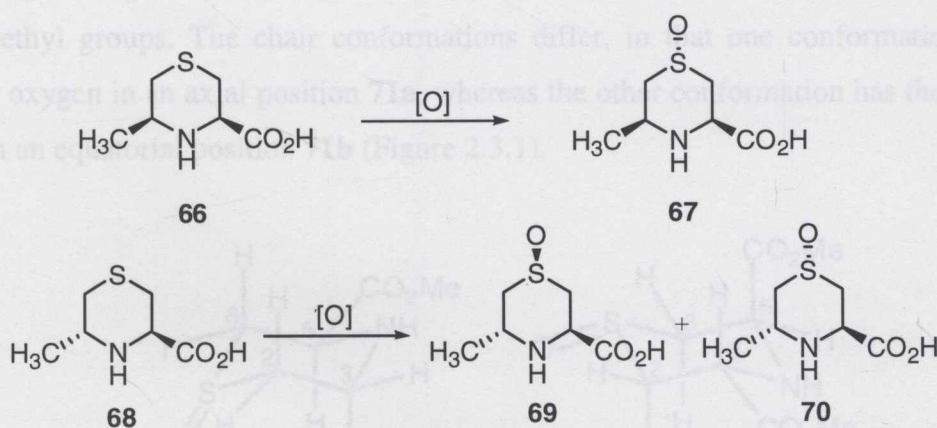
2.3.1 Oxidation of the (R,R)-Thiazane 60

Numerous reports have described the stereoselective oxidation of 1,4-thiazane and thiane ring-systems. Johnson and McCants^{13,14} have reported that selective oxidation of 4-substituted thianes can be achieved through use of an appropriate oxidant. Treatment of 4-*tert*-butylthiane **63** with sodium periodate gave predominantly the *cis*-sulfoxide **64** with the oxygen in the axial position (1:3 ratio of **65**:**64**), whereas treatment with *m*-CPBA gave the equatorial sulfoxide **65** as the major product (2:1 ratio of **65**:**64**, Scheme 2.3.2).



Scheme 2.3.2

Studies of the more closely related cycloalliin systems by Carson *et al.*¹⁵ showed that oxidation of the *cis*-substituted thiazane **66** gave cycloalliin **67** (*S*-oxygen occupying axial position) as the only product, regardless of the oxidant. In contrast, oxidation of the *trans*-substituted thiazane **68** proceeded with no selectivity to give a mixture of the sulfoxides **69** and **70**, with either periodate or hydrogen peroxide (Scheme 2.3.3). These results suggest that there are several subtle factors which control the stereoselectivity of oxidation of thiane and thiazane systems, not all of which are fully understood.



Scheme 2.3.3

Figure 2.3.1: Chair Conformations of (R,R)-Thiazane S-oxide 71

2.3.1 Oxidation of the (*R,R*)-Thiazane 60

Initial investigations of the oxidation of the thiazanes **59** and **60** were conducted with the (*R,R*)-thiazane isomer **60**, as the C_2 axis of symmetry renders the sulfur centre non-chirotopic. Hence, only one sulfoxide stereoisomer is produced upon oxidation of **60**. Various oxidants were trialed, all of which provided the corresponding sulfoxide **71** in good yield (Table 2.3.1). Sodium periodate proved the oxidant of choice, giving the product **71** in 80% yield.

Table 2.3.1: Oxidation of (*R,R*)-Thiazane 60

Oxidant	%Yield of 71
NaIO ₄	80
<i>m</i> -CPBA	77
H ₂ O ₂	78

Although oxidation of the thiazane **60** can yield only one sulfoxide stereoisomer, two non-equivalent chair conformations of **71** are possible (not accounting for configurational isomers at nitrogen, of which interconversion is very rapid and not observable on the n.m.r. timescale). By adopting a chair conformation the molecule loses its symmetry, with one of the methoxycarbonyl substituents occupying an axial position and the other an equatorial position. The ring protons are therefore all in chemically distinct environments, as are the two *O*-methyl groups. The chair conformations differ, in that one conformation has the sulfoxide oxygen in an axial position **71a**, whereas the other conformation has the sulfoxide oxygen in an equatorial position **71b** (Figure 2.3.1).

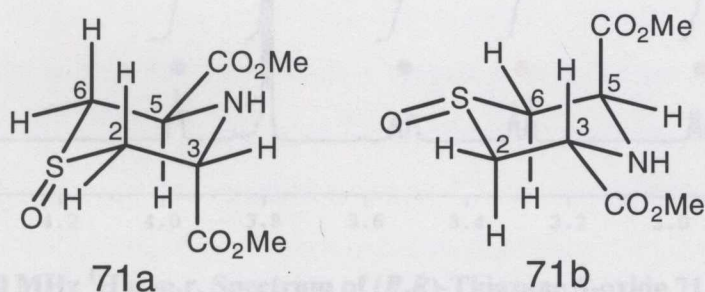


Figure 2.3.1: Chair Conformations of (*R,R*)-Thiazane *S*-oxide 71

The ^1H n.m.r. spectrum of **71** (Figure 2.3.2) exhibited six distinct resonances attributed to the ring protons, the coupling constants were consistent with the adoption of a chair conformation. The doublet of doublets resonance at δ 2.82 exhibits large coupling constants (10.8 and 13.2 Hz), consistent with *trans*-diaxial and geminal couplings, whereas the nearby doublet of doublets resonance at δ 2.94 exhibits medium (5.2 Hz) and large (13.8 Hz) coupling constants, consistent with vicinal gauche and geminal couplings. The resonances at δ 3.29 and δ 3.53 both exhibit large (geminal) and medium (vicinal gauche) couplings, and, interestingly, also exhibit 4-bond coupling to each other, consistent with being in a relative “W”-orientation. These resonances are, therefore, attributed to the H_{2e} and H_{6e} protons.^{15,16} The resonance at δ 3.98 exhibits small-medium couplings, consistent with the equatorial $\text{H}_{3/5}$ proton, and the resonance at δ 4.66 exhibits a *trans*-diaxial coupling of 10.8 Hz, consistent with the axial $\text{H}_{5/3}$ proton. These coupling constants suggest that only one of the chair conformations is adopted to any significant extent. If equilibration between the two conformers was occurring, averaging of the *trans*-diaxial and vicinal gauche couplings would have been observed.

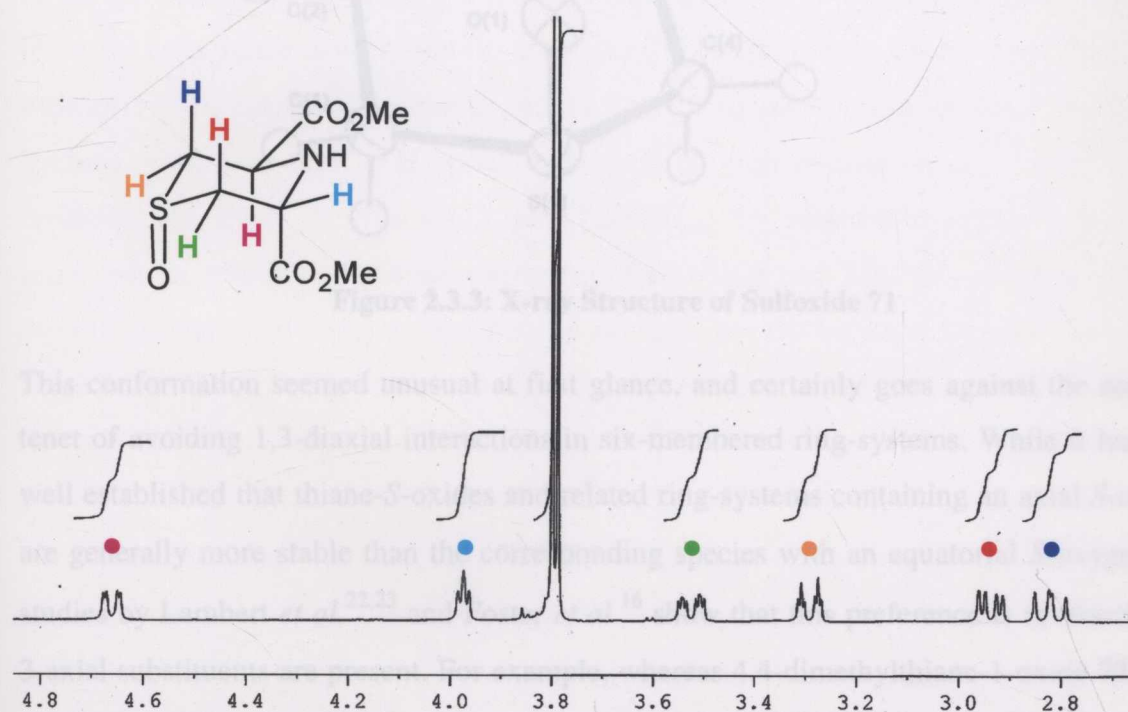


Figure 2.3.2: 400 MHz ^1H n.m.r. Spectrum of (*R,R*)-Thiazane *S*-oxide **71** in CDCl_3

Analysis of the coupling constants, however, does not allow determination of which conformer exists in solution, as the geometry of the ring protons is essentially identical in

each case. In order to confirm the conformational preference of the sulfoxide, the ^1H n.m.r. spectrum was analysed further. It has been shown that the signal for the axial H_3 -proton of thiane-*S*-oxides bearing an axial sulfoxide oxygen occurs significantly downfield with respect to the corresponding signal of thiane-*S*-oxides bearing an equatorial sulfoxide oxygen.¹⁵⁻¹⁷ The significant downfield shift of the axial $\text{H}_{5/3}$ proton signal relative to that of the equatorial $\text{H}_{3/5}$ proton signal in the ^1H n.m.r. spectrum of sulfoxide **71** ($\Delta\delta = 0.68$ ppm) therefore suggests that **71** adopts the axial *S*-oxygen conformation **71a** in solution. The solid-state conformation of **71** was unambiguously determined by X-ray crystallography, which did indeed show that **71** exists in the axial *S*-oxygen conformation (Figure 2.3.3).

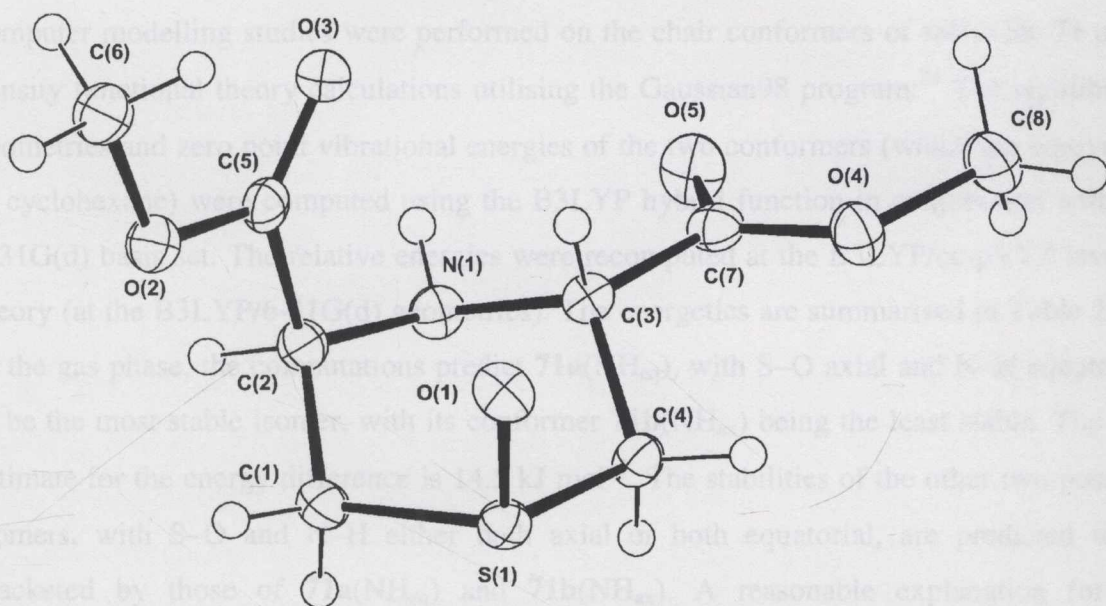
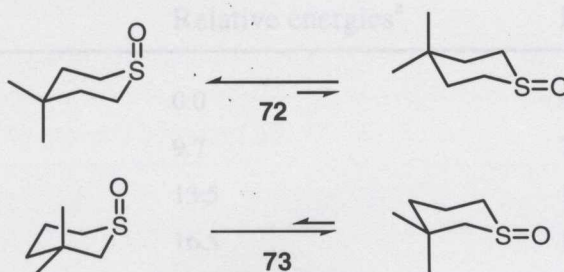


Figure 2.3.3: X-ray Structure of Sulfoxide **71**

This conformation seemed unusual at first glance, and certainly goes against the accepted tenet of avoiding 1,3-diaxial interactions in six-membered ring-systems. While it has been well established that thiane-*S*-oxides and related ring-systems containing an axial *S*-oxygen are generally more stable than the corresponding species with an equatorial *S*-oxygen,¹⁸⁻²² studies by Lambert *et al.*^{22,23} and Foster *et al.*¹⁶ show that this preference is reversed when 3-axial substituents are present. For example, whereas 4,4-dimethylthiane-1-oxide **72** exists predominantly as the axial *S*-oxide conformer, 3,3-dimethylthiane-1-oxide **73** exists nearly exclusively as the equatorial *S*-oxide isomer (Scheme 2.3.4).²³ The greater stability of axial *S*-oxides when no 3-axial substituent is present has been attributed to a combination of attractive Van der Waals interactions between the oxygen and axial 3- and 5-protons and

electrostatic/dipole interactions,¹⁹⁻²¹ whereas the reversal of stability in the presence of 3-axial substituents is attributed to repulsive 1,3-diaxial interactions.



Scheme 2.3.4

In order to rationalise the apparent stability of the axial *S*-oxide conformation of **71**, computer modelling studies were performed on the chair conformers of sulfoxide **71** using density functional theory calculations utilising the Gaussian98 program.²⁴ The equilibrium geometries and zero point vibrational energies of the two conformers (which are equivalent in cyclohexane) were computed using the B3LYP hybrid function in conjunction with the 6-31G(d) basis set. The relative energies were recomputed at the B3LYP/cc-pVTZ level of theory (at the B3LYP/6-31G(d) geometries). The energetics are summarised in Table 2.3.2. In the gas phase, the computations predict **71a**(NH_{eq}), with S–O axial and N–H equatorial, to be the most stable isomer, with its conformer **71b**(NH_{ax}) being the least stable. The best estimate for the energy difference is 14.5 kJ mol⁻¹. The stabilities of the other two possible isomers, with S–O and N–H either both axial or both equatorial, are predicted to be bracketed by those of **71a**(NH_{eq}) and **71b**(NH_{ax}). A reasonable explanation for the difference in stabilities between conformers **71a**(NH_{eq}) and **71b**(NH_{ax}) is that attractive intra-molecular dipolar interactions may be expected to exist between the axial S–O and C–CO₂Me groups. This hypothesis was tested by computing the electrostatic interactions between the atomic charges of the S–O and C–CO₂Me moieties. The atomic charges were obtained by the Merz-Kollman method,²⁵ with calculations predicting an (attractive) interaction energy of –12.0 kJ mol⁻¹ in **71a**(NH_{eq}), to be compared with a repulsion of 1.0 kJ mol⁻¹ in **71b**(NH_{ax}). The total calculated energy difference is thus 13.0 kJ.mol⁻¹, consistent with the quantum chemical values in Table 2.3.2. Accounting for facile inversion of configuration at nitrogen, the low-energy axial S–O isomer is still predicted to be 7.9 kJ.mol⁻¹ more stable than the low-energy equatorial S–O isomer.

Table 2.3.2: Relative Equilibrium Energies of Conformers of 71

Isomer	Relative energies ^a	Relative energies ^b
71a(NH _{eq})	0.0	0.00
71b(NH _{eq})	9.7	7.9
71a(NH _{ax})	13.5	12.7
71b(NH _{ax})	16.5	14.5

^a Geometries and energies determined at B3LYP/6-31G(d) level of the theory.

^b Geometries and energies determined at B3LYP/6-31G(d), energies at B3LYP/cc-pVTZ level of theory.

The computed equilibrium geometry for **71a**(NH_{eq}) is in close agreement with the X-ray data. The difference between theory and experiment for the heavy atom distances is generally within ~ 0.002 Å, the largest difference being for the S–C distances where the computed bond lengths are ~ 0.05 Å longer than the X-ray values. The largest discrepancies in the bond angles are $\sim 2^\circ$, which occur around the heavy atoms of the ring.

Further evidence for the attractive dipolar interaction between the *S*-oxygen and carbonyl carbon is provided by analysis of the solid-state structure of **71**, which indicates that the carbonyl carbon atom of the axial C–CO₂Me group deviates from the plane of its three attached substituents by 0.032 Å towards the transannular axial sulfoxide oxygen. The distance between the axial oxygen and the carbonyl carbon is 3.068 Å, which is slightly shorter than the sum of the Van der Waals radii for O and C (3.15–3.2 Å).²⁵ Dipole–dipole or donor–acceptor interactions of this type have been observed by Dunitz *et al.*,²⁶ together with a corresponding deviation of the carbonyl carbon from a planar arrangement, and are believed to represent the initial stages of the reaction pathway of an attack at the carbonyl group by the nearby nucleophile.

2.3.2 Oxidation of the *meso*-Thiazane 59

Having prepared the sulfoxide **71** from (*R,R*)-thiazane **60** in good yield, attention was turned to the oxidation of the *meso*-thiazane **59** to the corresponding sulfoxides **53** and **74**. In contrast to the oxidation of (*R,R*)-thiazane **60**, oxidation of *meso*-thiazane **59** leads to two diastereomeric sulfoxide products. The sulfur of the *meso*-thiazane **59** is a non-chirotopic

centre, as it lies on a plane of symmetry. However, the *syn*- and *anti*-sulfoxides **53** and **74** generated from the *meso*-thiazane **59** are clearly diastereomeric, indicating the sulfur atoms of **53** and **74** are *pseudo-asymmetric* centres.

Table 2.3.3: Oxidation of *meso*-Thiazane **59**

Oxidant	Ratio 53:74	Yield (%)
<i>m</i> -CPBA	2:3	98
NaIO ₄	1:5	80
Br ₂ -H ₂ O	10:1	61

Oxidation of *meso*-thiazane **59** was conducted with various oxidants as shown in Table 2.3.3. Treatment of **59** with *meta*-chloroperbenzoic (*m*-CPBA) acid at ambient temperature gave the *syn*- and *anti*-sulfoxides **53** and **74** in a 2:3 ratio in 98% overall yield. Oxidation of **59** using sodium periodate produced a 1:5 mixture of the *syn*- and *anti*-sulfoxides **53** and **74** in 80% yield. Diastereomeric ratios were determined by integration of the signals corresponding to the H_{2/6} protons in the ¹H n.m.r. spectrum of the crude product (Figure 2.3.5).

Assignment of the signals corresponding to each of the diastereomers was based on the report of Lambert *et al.*,²² which showed that the H_{2/6} proton signals from thiane-*S*-oxide isomers bearing an equatorial oxygen always have a lower field centrepoint and a larger chemical shift difference than the corresponding signals of the isomers bearing an axial oxygen. The major sulfoxide isomer exhibits resonances at δ 3.30 and δ 2.52, attributed to H_{2e} and H_{2a}, respectively (avg. = δ 2.91, $\Delta\delta$ = 0.78), whereas the minor isomer exhibits the corresponding resonances at δ 3.78 and 2.65 (avg. = 3.22, $\Delta\delta$ = 1.13). The minor isomer therefore exhibits the lower field centrepoint and larger chemical shift difference for the C2 protons, indicating it is the *syn*-isomer with an equatorial *S*-oxygen. Further evidence is provided through the observation that the H₃ signal for the major isomer (δ 4.41) is significantly downfield of that of the minor isomer (δ 3.67), indicative of the major isomer possessing an axial *S*-oxygen, as described earlier. Note that assignment of the signals at δ 3.78 and 3.67, corresponding to the H_{2/6e} and H_{3/5} protons of **53**, was based on the observed

coupling of the upfield resonance to the NH resonance in the spectrum of the purified sulfoxide.

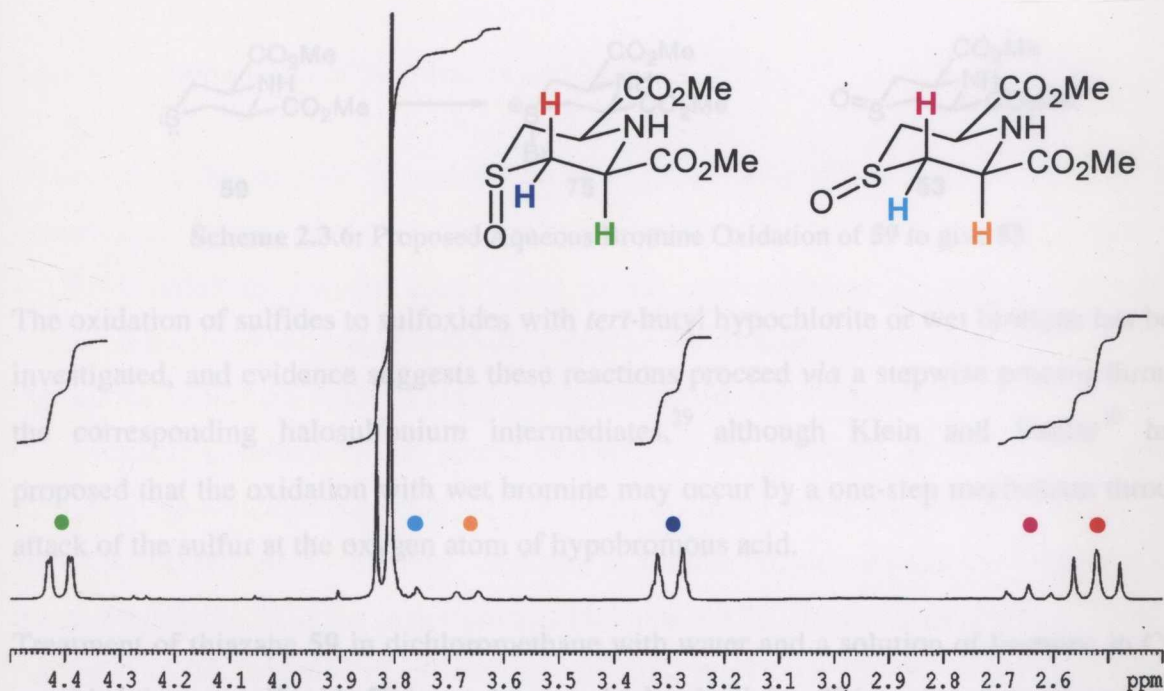
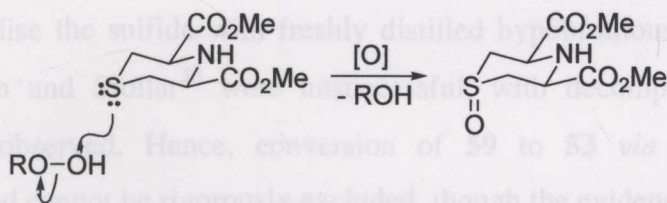


Figure 2.3.4: 300 MHz ^1H n.m.r. Spectrum of a Mixture of Sulfoxides **53** and **74** in CDCl_3

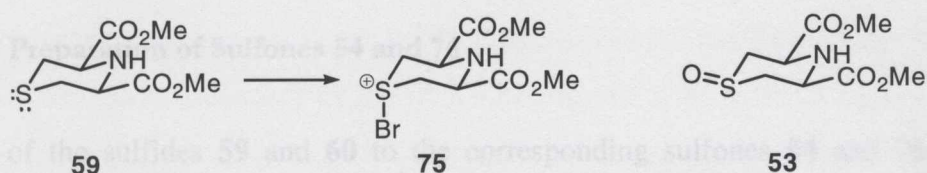
Both peracid and periodate oxidants therefore produce the *anti*-sulfoxide **74** (with an axial *S*-oxygen) selectively, in general agreement with the results observed by Carson *et al.*²⁷ in the selective oxidation of **66** to **67** (Scheme 2.3.3). The greater selectivity for the axial sulfoxide observed upon oxidation with periodate, with respect to the use of *m*-CPBA as the oxidant, is also in general agreement with the observations of Johnson and McCants¹⁴ shown in Scheme 2.3.2.



Scheme 2.3.5: One-step Oxidation of **59** to give Axial Sulfoxide **74**

It seemed plausible, given that these oxidants operate through a direct mechanism in which the sulfur attacks the electrophilic oxygen,²⁸ that the selectivity of these reactions is governed by a preferential attack of the axial sulfur lone pair (Scheme 2.3.5). If this was indeed the case, a stepwise mechanism was surmised, in which initial attack of the sulfur

onto an appropriate electrophile, followed by attack (with inversion) at the sulfur by an oxygen nucleophile, would reverse the observed stereoselectivity and allow for preparation of the *syn*-sulfoxide **53**.



Scheme 2.3.6: Proposed Aqueous Bromine Oxidation of **59** to give **53**

The oxidation of sulfides to sulfoxides with *tert*-butyl hypochlorite or wet bromine has been investigated, and evidence suggests these reactions proceed *via* a stepwise process through the corresponding halosulfonium intermediates,²⁹ although Klein and Stollar³⁰ have proposed that the oxidation with wet bromine may occur by a one-step mechanism through attack of the sulfur at the oxygen atom of hypobromous acid.

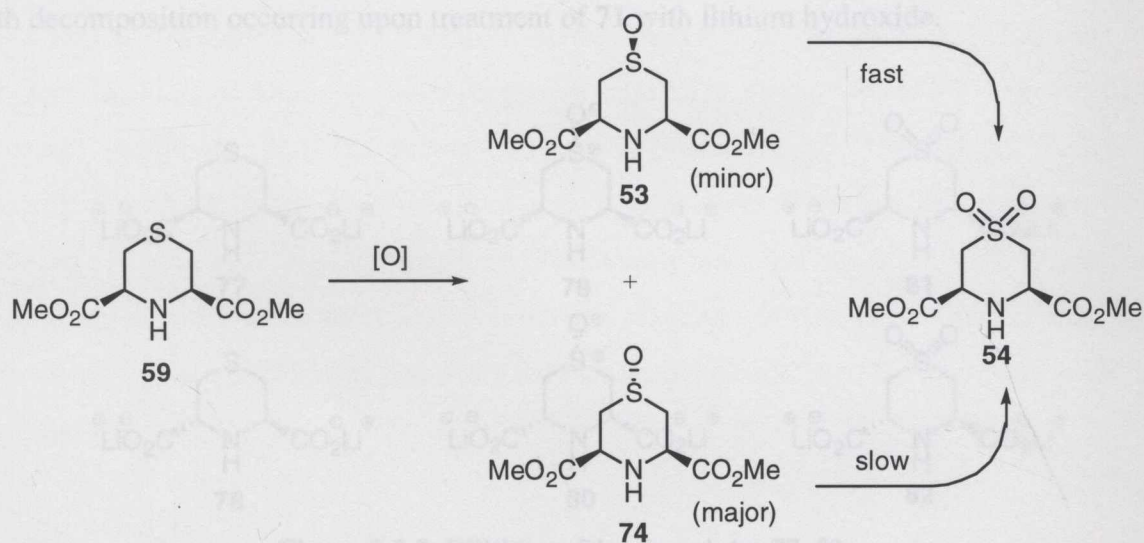
Treatment of thiazane **59** in dichloromethane with water and a solution of bromine in CCl₄ provided the *syn*-sulfoxide **53** in moderate to high selectivity. This reaction was found to be somewhat capricious, with quite variable yields (20–61%) and slight variation in selectivity (5–10:1). In all cases, however, good selectivity for the *syn*-isomer **53** was observed. These results indicate that the bromine/water oxidation system operates through a different mechanism to the direct oxidants, suggesting that initial attack of the axial sulfur lone pair toward molecular bromine, generating the corresponding bromosulfonium intermediate **75** is then followed by displacement of the bromide with water, to ultimately provide the *syn*-sulfoxide **53** (Scheme 2.3.6).

Attempts to oxidise the sulfide with freshly distilled hypobromous acid according to the method of Klein and Stollar³⁰ were unsuccessful, with decomposition of the starting material being observed. Hence, conversion of **59** to **53** *via* direct oxidation with hypobromous acid cannot be rigorously excluded, though the evidence is in favour of a two-step oxidation *via* the corresponding bromosulfonium ion **75**. Although it was not possible to determine the reasons for the capricious nature of the bromine/water oxidation, decomposition of the bromosulfonium ion **75**²⁹ may lead to the complex mixtures occasionally observed.

Both sulfoxide isomers are therefore available in moderate diastereoselectivity by appropriate choice of oxidising agent. Purification of the compounds was achieved by C_{18} reverse phase HPLC to afford the individual diastereomers **53** and **74**.

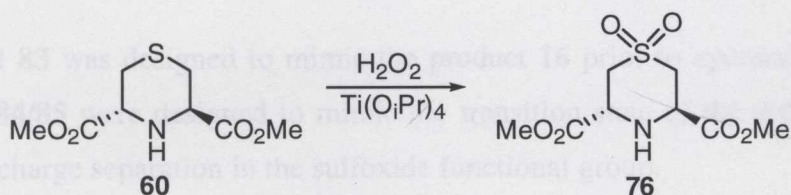
2.3.3 Preparation of Sulfones **54** and **76**

Oxidation of the sulfides **59** and **60** to the corresponding sulfones **54** and **76** was also investigated. It was observed that treatment of the sulfides with excess periodate or *m*-CPBA failed to provide good yields of the corresponding sulfones. Treatment of *meso*-compound **59** with excess sodium periodate for 48 hours gave only a small amount of the sulfone **54** formed, with the major product being the *anti*-sulfoxide **74** (60%). This result is presumably a consequence of kinetic resolution of the sulfoxides **53** and **74**; oxidation of the minor *syn*-sulfoxide **53** to the sulfone **54** occurs much faster than oxidation of the *anti*-sulfoxide **74**, providing a mixture consisting of a minor amount of sulfone **54** together with the *anti*-sulfoxide **74** as the major product (Scheme 2.3.7). The faster oxidation of **53** to **54**, compared to the oxidation of **74** to **54**, is consistent with the reasoning explained above for the stereoselective oxidation of **59**; the *syn*-sulfoxide **53** possesses an axial sulfur lone-pair, which is more reactive toward the oxidant than the equatorial lone-pair of the *anti*-sulfoxide **74**, such that the minor sulfoxide **53** is oxidised more quickly to the sulfone **54**. This observation actually allows for an expedient preparation of pure *anti*-sulfoxide **74**, as it is easily separated from the sulfone **54** by column chromatography.



Scheme 2.3.7

While use of excess oxidant did not provide the sulfone **54** in good yield, an efficient preparation of the *meso*-sulfone **54** was found through the addition of a Lewis acid catalyst to the reaction mixture. Accordingly, treatment of the sulfide **53** with two equivalents of hydrogen peroxide and one equivalent of $\text{Ti}(\text{OiPr})_4$ provided the sulfone **54** in excellent (92%) yield. Similarly, treatment of the (*R,R*)-thiazane **60** with hydrogen peroxide in the presence of $\text{Ti}(\text{OiPr})_4$ provided the (*R,R*)-sulfone **76** in 92% yield (Scheme 2.3.8).



Scheme 2.3.8

2.3.4 Preparation of Dilithium Dicarboxylates 77–82

The dilithium dicarboxylates **77–82** were prepared from the corresponding diesters **59**, **60**, **53**, **74**, **54** and **76** by hydrolysis with lithium hydroxide. The amount of lithium hydroxide was critical to the success of the hydrolysis reactions. The use of two equivalents of lithium hydroxide resulted in incomplete reaction, whereas use of more than four equivalents resulted in epimerisation of the 3,5-*trans* compounds. Three equivalents of lithium hydroxide was found to be optimal, giving quantitative yields of the dilithium dicarboxylates (Figure 2.3.5). Preparation of the dilithium salt of **71** could not be effected, with decomposition occurring upon treatment of **71** with lithium hydroxide.

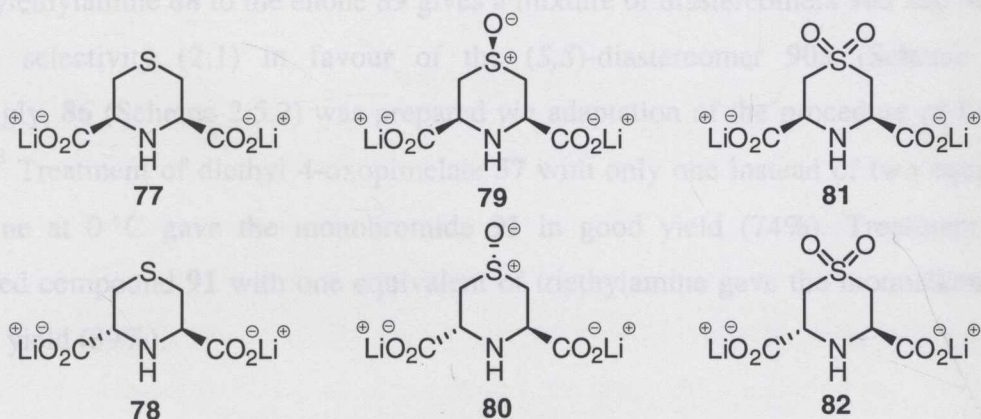


Figure 2.3.5: Dilithium Dicarboxylates 77–82

2.4 Design of Acyclic Inhibitors

A series of acyclic inhibitors **83–85** were also designed, analogous to the cyclic inhibitors. The acyclic inhibitors were designed to mimic the enzyme-bound alcohol **16** prior to cyclisation (see Chapter 1, Figure 1.6.1). No potent acyclic inhibitors based on the reaction intermediate of DHDPS have yet been developed.

The acyclic alcohol **83** was designed to mimic the product **16** prior to cyclisation and the acyclic sulfoxides **84/85** were designed to mimic the transition state of the aldol reaction, due to the inherent charge separation in the sulfoxide functional group.

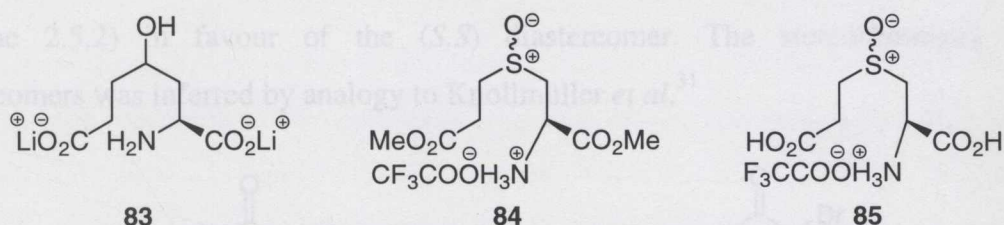
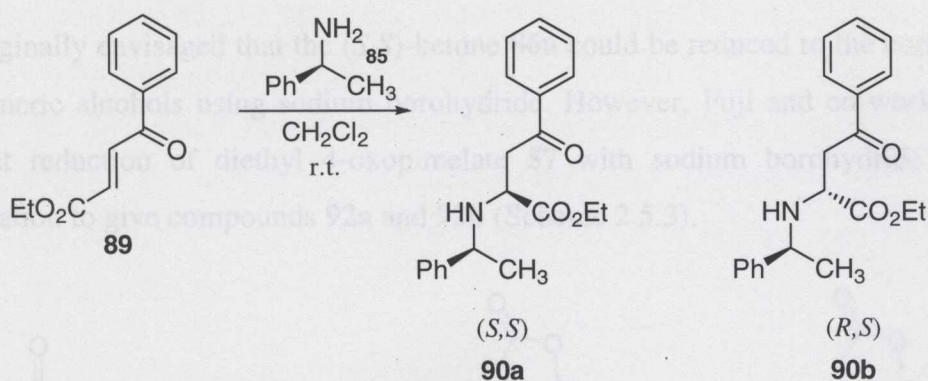


Figure 2.4.1: Proposed Acyclic Inhibitors of DHDPS

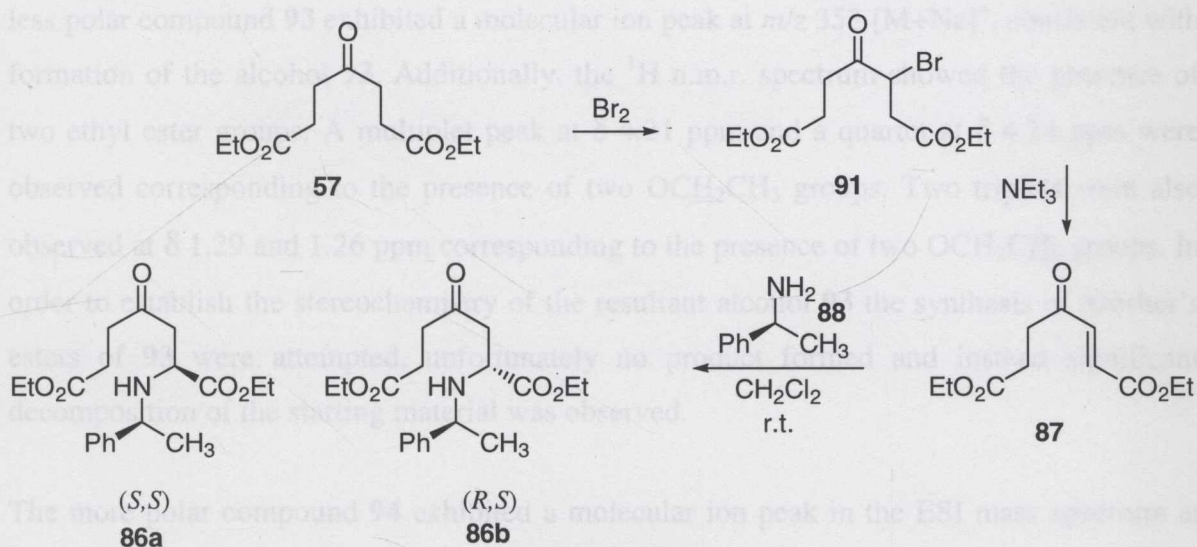
2.5 Synthesis of Acyclic Alcohol 83

It was envisaged that compound **86** could be furnished *via* initial Michael addition of an amine nucleophile to enone **87**. It has already been demonstrated by Knollmüller *et al.*³¹ that the preparation of a β -keto- α -amino esters *via* a Michael addition of (*S*)-phenylethylamine **88** to the enone **89** gives a mixture of diastereomers **90a** and **90b** with moderate selectivity (2:1) in favour of the (*S,S*)-diastereomer **90a** (Scheme 2.5.1). Accordingly, **86** (Scheme 2.5.2) was prepared *via* adaptation of the procedure of Lemaire-Audoire.⁸ Treatment of diethyl 4-oxopimelate **57** with only one instead of two equivalents of bromine at 0 °C gave the monobromide **91** in good yield (74%). Treatment of the brominated compound **91** with one equivalent of triethylamine gave the monoalkene **87** in excellent yield (89%).



Scheme 2.5.1

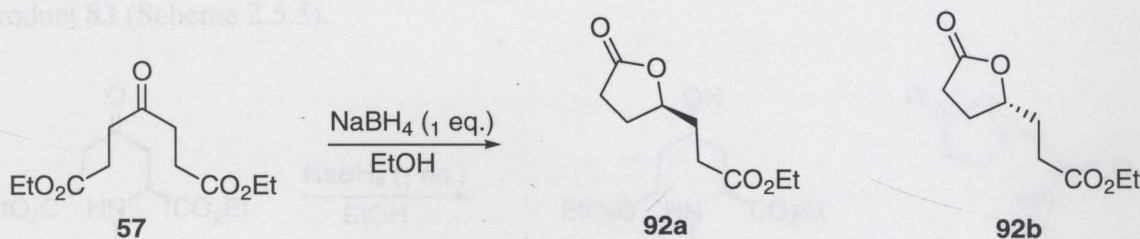
Subsequently, the monoalkene **87** was treated with one equivalent of (*S*)-phenylethylamine **88** in dry ethanol to give the corresponding Michael adducts **86a** and **86b** in a 1.2:1 ratio (Scheme 2.5.2) in favour of the (*S,S*) diastereomer. The stereochemistry of the diastereomers was inferred by analogy to Knollmüller *et al.*³¹



Scheme 2.5.2

The ^1H n.m.r. of the crude reaction mixture displayed a triplet at δ 3.34 ppm, corresponding to the C2 proton of the major isomer **86a**, and a triplet at δ 3.70 ppm, corresponding to the C2 proton of the minor isomer **86b**. Separation of the crude diastereomers was achieved by flash chromatography, providing the major isomer in 42% isolated yield and the minor isomer in 39% isolated yield. No other products were observed, indicating that the Michael addition occurred with high regioselectivity.

It was originally envisaged that the (*S,S*)-ketone **86a** could be reduced to the corresponding diastereomeric alcohols using sodium borohydride. However, Fuji and co-workers³² have noted that reduction of diethyl 4-oxopimelate **57** with sodium borohydride results in γ -lactonisation to give compounds **92a** and **92b** (Scheme 2.5.3).



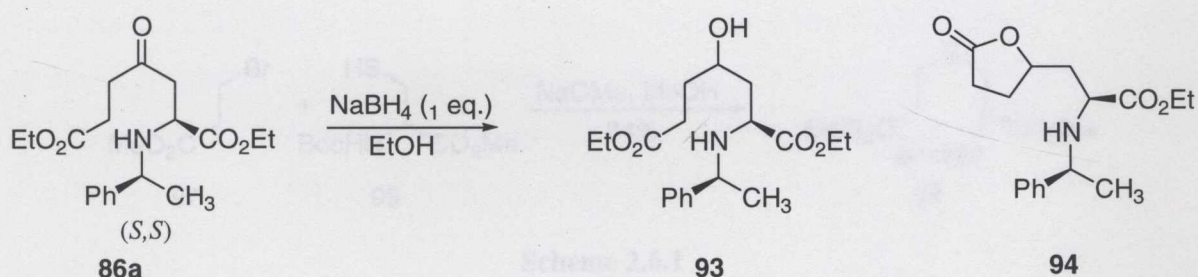
Scheme 2.5.3

Reduction of the (*S,S*)-ketone **86a** in dry ethanol using sodium borohydride as the reductant resulted in the formation of two compounds (Scheme 2.5.4). The mass spectrum data of the less polar compound **93** exhibited a molecular ion peak at m/z 353 $[\text{M}+\text{Na}]^+$, consistent with formation of the alcohol **93**. Additionally, the ^1H n.m.r. spectrum showed the presence of two ethyl ester groups. A multiplet peak at δ 4.21 ppm and a quartet at δ 4.14 ppm were observed corresponding to the presence of two OCH_2CH_3 groups. Two triplets were also observed at δ 1.29 and 1.26 ppm corresponding to the presence of two OCH_2CH_3 groups. In order to establish the stereochemistry of the resultant alcohol **93** the synthesis of Mosher's esters of **93** were attempted, unfortunately no product formed and instead significant decomposition of the starting material was observed.

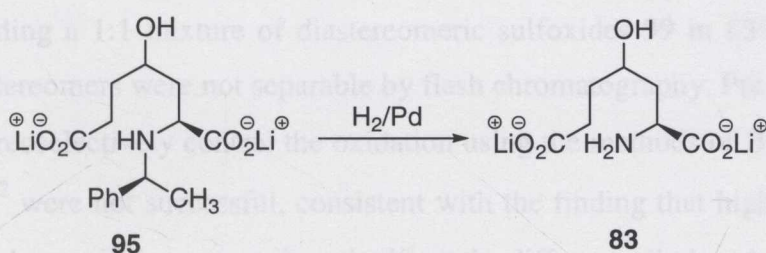
The more polar compound **94** exhibited a molecular ion peak in the ESI mass spectrum at m/z 306 $[\text{M}+\text{H}]^+$ consistent with formation of one lactone **94**. Additionally, the ^1H n.m.r. spectrum showed the presence of only one ethyl ester. The IR spectrum showed a peak at 1770 cm^{-1} indicative of a lactone carbonyl stretch. The ^{13}C n.m.r. exhibited only 17 peaks further supporting the loss of an ethoxy group. The data indicated that reduction to the alcohol **93** occurs followed by spontaneous cyclisation giving rise to one lactone **94** (Scheme 2.5.4). Presumably the cyclisation occurred regioselectively to the less hindered side, giving rise to the γ -lactone ester **94** though this is yet to be rigorously proven.

As it was not possible to ascertain the stereochemistry of the alcohol a mixture of the alcohol **93** and lactone **94** was hydrolysed with two equivalents of lithium hydroxide to

give the dicarboxylate **95** as a mixture of diastereomers. The ^1H n.m.r showed the absence of any ethyl ester groups and the ESI mass spectrum gave an ion at m/z 300 consistent with the product **95**. Subsequent hydrogenolysis of the phenylethylamine group using palladium on charcoal gave the desired acyclic alcohol **83** which showed the absence of the phenylethyl group and the ESI mass spectrum gave an ion at m/z 196 consistent with the product **83** (Scheme 2.5.5).



Scheme 2.5.4

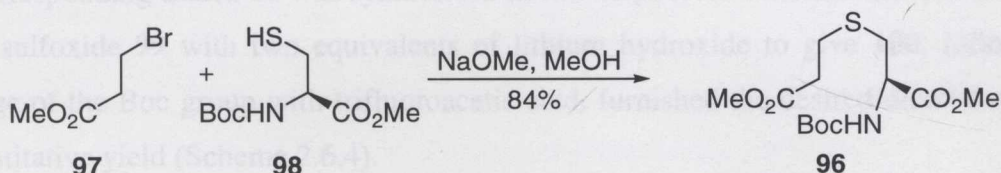


Scheme 2.5.5

Having synthesised the desired acyclic alcohol **83**, attention was turned to the synthesis of the acyclic sulfoxides **84** and **85**.

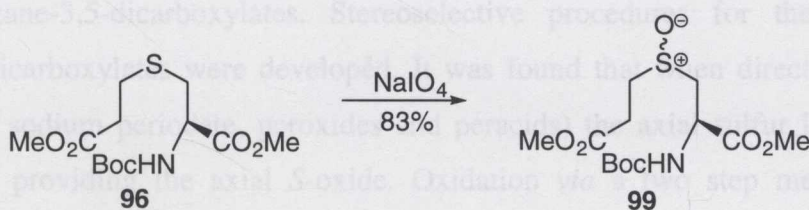
2.6 Synthesis of Acyclic Sulfoxides 84 and 85

It was envisaged that the sulfoxide **84** could be generated by oxidation of the corresponding sulfide **96**. Conveniently, the sulfide **96** could be prepared in one step by coupling methyl 3-bromopropionate **97** with *N*-Boc cysteine methyl ester **98** using sodium methoxide as the base furnishing the product **96** in excellent yield (84%) (Scheme 2.6.1).



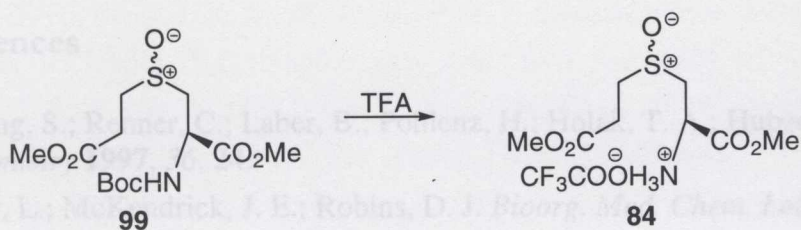
Scheme 2.6.1

The sulfoxide **99** was prepared by oxidising the sulfide **96** with sodium periodate in aqueous methanol, affording a 1:1 mixture of diastereomeric sulfoxides **99** in 83% yield (Scheme 2.6.2). The diastereomers were not separable by flash chromatography. Previous attempts in the group to stereoselectively control the oxidation using the methods of Brunel *et al.*¹¹ and Komatsu *et al.*¹² were not successful, consistent with the finding that high selectivities are obtained only when sulfides possessing significantly different alkyl and aryl substituents either side of the sulfur are employed. For initial biological screening a mixture of diastereomers was deemed to be sufficient.



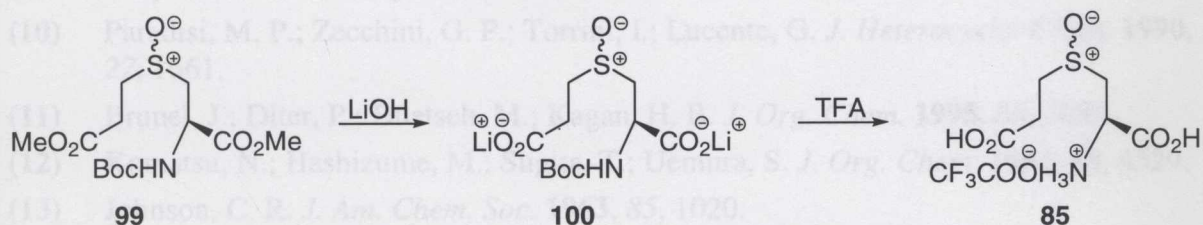
Scheme 2.6.2

Removal of the Boc-group from sulfoxide **99** was effected by treatment with trifluoroacetic acid in dichloromethane to give the corresponding ammonium trifluoroacetate salt **84** (Scheme 2.6.3).



Scheme 2.6.3

The corresponding diacid **85** was synthesised in two steps from the sulfoxide **99**. Treatment of the sulfoxide **99** with two equivalents of lithium hydroxide to give **100**, followed by cleavage of the Boc group with trifluoroacetic acid, furnished the desired dicarboxylate **85** in quantitative yield (Scheme 2.6.4).



Scheme 2.6.4

2.7 Summary

Several heterocyclic inhibitors of DHDPS/DHDPR were synthesised based on chelidamic acid or thiazane-3,5-dicarboxylates. Stereoselective procedures for the oxidation of thiazane-3,5-dicarboxylates were developed. It was found that when direct oxidants were used (such as sodium periodate, peroxides and peracids) the axial sulfur lone pair reacts preferentially, providing the axial *S*-oxide. Oxidation *via* a two step mechanism using bromine/water gives the epimeric equatorial *S*-oxide. Acyclic analogues of the heterocyclic compounds were also synthesised as potential inhibitors of DHDPS/DHDPR. Having prepared the desired inhibitors all in advantageous short synthetic routes, attention was turned to preparing the necessary substrate and enzymes in order to evaluate the proposed inhibitors.

2.8 References

- (1) Blickling, S.; Renner, C.; Laber, B.; Pohlenz, H.; Holak, T. A.; Huber, R. *Biochemistry* **1997**, *36*, 24.
- (2) Couper, L.; McKendrick, J. E.; Robins, D. J. *Bioorg. Med. Chem. Lett.* **1994**, *4*, 2267.
- (3) Karsten, W. *Biochemistry* **1997**, *36*, 1730.
- (4) Leinhard, G. E. *Science* **1973**, *180*, 149.
- (5) Schramm, V. L. *Annu. Rev. Biochem.* **1998**, *67*, 693.
- (6) Chênevert, R.; Dickman, M. *J. Org. Chem.* **1996**, *61*, 3332.
- (7) Hermann, K.; Dreiding, S. A. *Helv. Chem. Acta* **1976**, *59*, 626.
- (8) Lemaire-Audoire, S.; Vogel, P. *Tetrahedron Asymmetry* **1999**, *10*, 1283.
- (9) Chrystal, E. J. T.; Couper, L.; Robins, D. J. *Tetrahedron* **1995**, *51*, 10241.
- (10) Paradisi, M. P.; Zecchini, G. P.; Torrini, I.; Lucente, G. *J. Heterocyclic Chem.* **1990**, *27*, 1661.
- (11) Brunel, J.; Diter, P.; Duetsch, M.; Kagan, H. B. *J. Org. Chem.* **1995**, *60*, 8086.
- (12) Komatsu, N.; Hashizume, M.; Sugita, T.; Uemura, S. *J. Org. Chem.* **1993**, *58*, 4529.
- (13) Johnson, C. R. *J. Am. Chem. Soc.* **1963**, *85*, 1020.
- (14) Johnson, C. R.; McCants, D., Jr. *J. Am. Chem. Soc.* **1965**, *87*, 1109.
- (15) Carson, J. F.; Lundin, R. E. *J. Chem. Soc. Perkin Trans. 1* **1976**, 1195.
- (16) Foster, A. B.; Hasan, Q. H.; Hawkins, D. R.; Webber, J. M. *Chem. Commun.* **1968**, 1084.
- (17) Buck, K. W.; Foster, A. B.; Pardoe, W. D.; Qadir, M. H.; Webber, J. M. *Chem. Commun.* **1966**, 759.
- (18) Martin, J. C.; Ubel, J. J. *J. Am. Chem. Soc.* **1964**, *86*, 2936.
- (19) Allinger, N. L.; Hirsch, J. A.; Miller, M. A.; Tyminski, I. J. *J. Am. Chem. Soc.* **1969**, *91*, 337.
- (20) Frieze, D. M.; Evans, S. A. *J. Org. Chem.* **1975**, *40*, 2690.
- (21) Zefirov, N. S. *Tetrahedron Lett.* **1975**, *16*, 1087.
- (22) Lambert, J. B.; Keske, R. G. *J. Org. Chem.* **1966**, *31*, 3429.
- (23) Lambert, J. B.; Bailey, D. S.; Mixan, C. E. *J. Org. Chem.* **1972**, *37*, 377.
- (24) Frisch, M. J.; Trucks, G. W.; Schlegel, H. B.; Scuseria, G. E.; Robb, M. A.; Cheeseman, J. R.; Zakrzewski, V. G.; Montgomery, J. A.; Stratmann, R. E.; Burant, J. C.; Dapprich, S.; Millam, J. M.; Daniels, A. D.; Kudin, K. N.; Strain, M. C.; Farkas, O.; Tomasi, J.; Barone, V.; Cossi, M.; Cammi, R.; Mennucci, B.; Pomelli, C.; Adamo, C.; Clifford, S.; Ochterski, J.; Petersson, G. A.; Ayala, P. Y.; Cui, Q.; Morokuma, K.; Malik, D. K.; Rabuk, A. D.; Raghavachari, K.; Foresman, J. B.; Cioslowski, J.; Ortiz, J. V.; Stefanov, B. B.; Lui, G.; Liashenko, A.; Piskorz, P.; Koraromi, I.; Gomperts, R.; Martin, R. L.; Fox, D. J.; Keith, T.; Al-Laham, M. A.; Peng, C. Y.; Nanayakkara, A.; Gonzalez, C.; Challacombe, M.; Gill, P. M. W.; Johnson, B. G.; Chen, W.; Wong, M. W.; Andres, J. L.; Head-Gorden, M.; Repogle, E. S.; Pople, J. A.; Revision A.7 ed.; Gaussian Inc.: Pittsburgh, PA, 1998.

- (25) Besler, B. H.; Merz, J. K. M.; Kollman, P. A. *J. Comput. Chem.* **1990**, *11*, 431.
- (26) Burgi, H. B.; Dunitz, J. D.; Shefter, E. *J. Am. Chem. Soc.* **1973**, *95*, 5065.
- (27) Carson, J. F.; Boggs, L. M.; Lundin, R. E. *J. Org. Chem.* **1970**, *35*, 1594.
- (28) Ruff, F.; Kucsman, A. *J. Chem. Soc. Perkin Trans. 2* **1985**, 683.
- (29) Jalsovszky, I.; Ruff, F.; Kajtar-Peredy, M.; Kucsman, A. *Synthesis* **1990**, 1037.
- (30) Klein, J.; Stollar, H. *Tetrahedron* **1974**, *30*, 2541.
- (31) Knollmüller, M.; Ferencic, M.; Gärtner, P.; Girreser, U.; Klinge, M.; Gaischin, L.; Mereiter, K.; Christian, R. N. *Monatshefte für Chemie* **1999**, *130*, 769.
- (32) Fuji, K.; Node, M.; Terada, S.; Murata, M.; Taga, T.; Machida, K. *J. Am. Chem. Soc.* **1985**, *107*, 6404.

3.1 Preparation of (S)-Aspartate β -semialdehyde

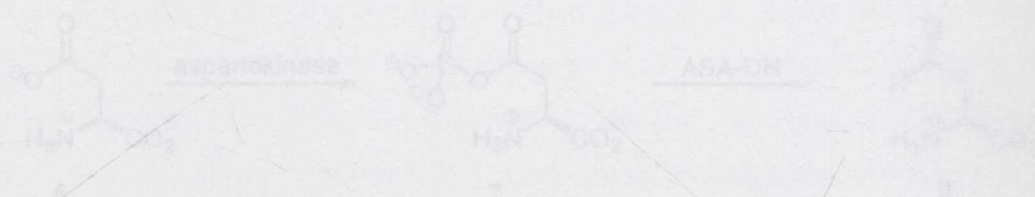
3.1.1 Introduction

CHAPTER 3

SYNTHESIS OF ASA & PURIFICATION OF DHDPS AND DHDPR

needed to perform detailed kinetic analysis of DHDPS and DHDPR and subsequent studies.

(S)-Aspartate β -semialdehyde is a natural non-proteogenic amino acid. It is a key intermediate in the biosynthesis of several essential proteogenic amino acids such as L-lysine, L-methionine, L-isoleucine and L-threonine in higher plants and bacteria. Cellular production of ASA 8 is achieved via the conversion of aspartic acid 6 to aspartyl phosphate 7 and subsequent reduction of 7 in a reaction catalysed by the NADPH-dependent aspartate semi-aldehyde dehydrogenase (ASA-DH) (Scheme 3.1.1)



Scheme 3.1.1: Cellular Synthesis of (S)-ASA

Enantiomerically pure ASA and derivatives are increasingly important synthetic intermediates as the aldehyde moiety of ASA can be functionalised to yield novel complex structures. The potential for access to a variety of polyfunctional non-proteogenic and unnatural amino acids using ASA has already been demonstrated.^{1,2} ASA manipulation has also proved to be important in the synthesis of pharmaceutically, aroma and flavour chemicals, pesticides, herbicides, dyes and pigments.³

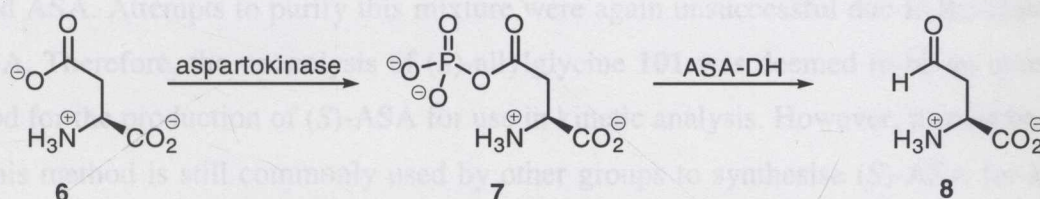
At the outset of these investigations there were three reported methods for synthesising (S)-ASA in common use.⁴⁻⁷ A variety of other methods have been reported in the literature which yield either free ASA or deprotected ASA, however they are often multi-step procedures and/or extremely low-yielding reactions.^{1,2,6,8} The number of methods for synthesising ASA reflects the difficulty in synthesising and characterising ASA since, like

3.1 Preparation of (*S*)-Aspartate β -semialdehyde

3.1.1 Introduction

(*S*)-Aspartate β -semialdehyde (ASA), one of two required substrates for DHDPS, was needed to perform detailed kinetic analysis of DHDPS and DHDPR and inhibition studies.

(*S*)-Aspartate β -semialdehyde is a natural non-proteinogenic amino acid. It is a key intermediate in the biosynthesis of several essential proteinogenic amino acids such as L-lysine, L-methionine, L-isoleucine and L-threonine in higher plants and bacteria.¹ Cellular production of ASA **8** is achieved *via* the conversion of aspartic acid **6** to aspartyl phosphate **7** and subsequent reduction of **7** in a reaction catalysed by the NADPH-dependent aspartate semi-aldehyde dehydrogenase (ASA-DH) (Scheme 3.1.1)



Scheme 3.1.1: Cellular Synthesis of (*S*)-ASA

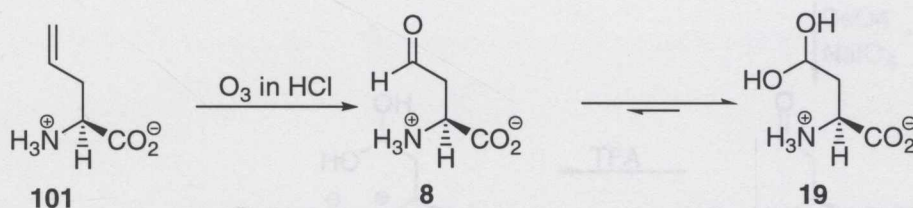
Enantiomerically pure ASA and derivatives are increasingly important synthetic intermediates as the aldehyde moiety of ASA can be functionalised to yield more complex structures. The potential for access to a variety of polyfunctional non-proteinogenic and unnatural amino acids using ASA has already been demonstrated.^{1,2} ASA manipulation has also proved to be important in the synthesis of pharmaceuticals, aroma and flavour chemicals, pesticides, herbicides, dyes and pigments.³

At the outset of these investigations there were three reported methods for synthesising (*S*)-ASA in common use.⁴⁻⁷ A variety of other methods have been reported in the literature which yield either free ASA or diprotected ASA, however they are often multi-step procedures and/or extremely low-yielding reactions.^{1,2,6,8} The number of methods for synthesising ASA reflects the difficulty in synthesising and characterising ASA since, like

many other amino aldehydes, it has a marked tendency to polymerise and is only stable in strong acidic aqueous solutions.^{3,5,9}

3.1.2 Previous Syntheses of (*S*)-Aspartate β -Semialdehyde

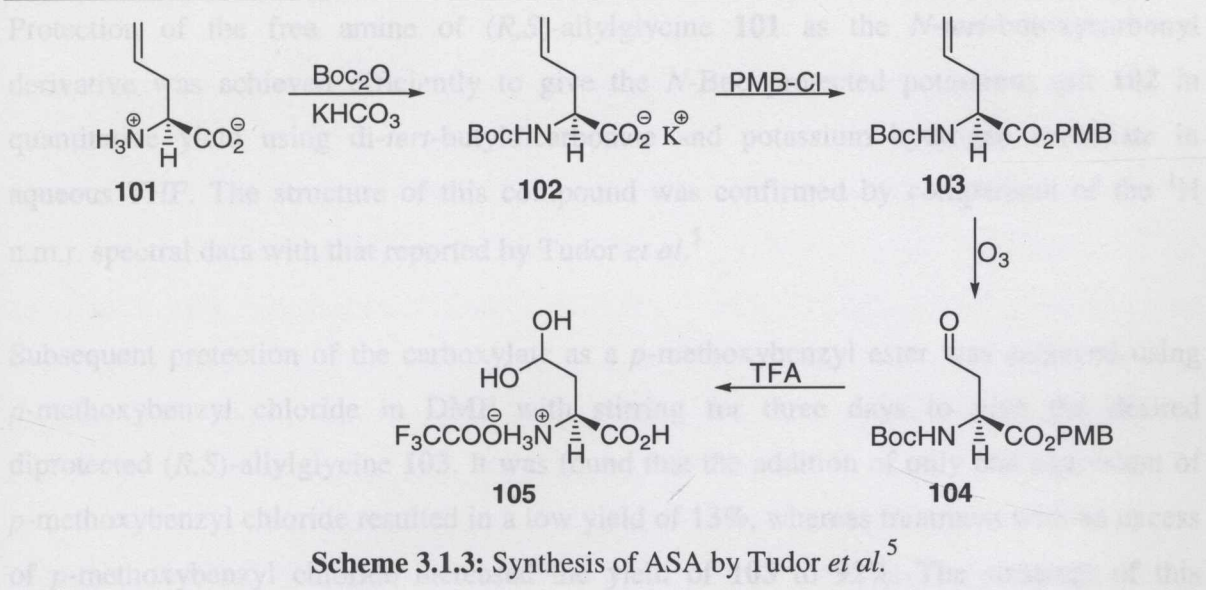
The first synthesis of (*S*)-ASA was reported by Black and Wright⁴ (Scheme 3.1.2). The aldehyde moiety was introduced by oxidative cleavage of the double bond of (*S*)-allylglycine **101** by ozonolysis under acidic conditions. The reported yield of the desired product was 90–100%. This was determined by an enzymatic assay following the conversion of ASA into homoserine by homoserine dehydrogenase. (*S*)-ASA produced by this reaction is known to have variable purity as described by Coulter¹⁰ and Gerrard.⁹ Purification of (*S*)-ASA generated by this reaction also proved difficult due to the instability of (*S*)-ASA.^{9,10} Tudor *et al.*⁵ also attempted the ozonolysis of (*R,S*)-allylglycine **101** but found they got a mixture of products including aspartic acid and formic acid along with the desired ASA. Attempts to purify this mixture were again unsuccessful due to the instability of ASA. Therefore, the ozonolysis of (*S*)-allylglycine **101** was deemed to be an unreliable method for the production of (*S*)-ASA for use in kinetic analysis. However, it must be noted that this method is still commonly used by other groups to synthesise (*S*)-ASA for kinetic studies of the enzymes DHDPS and DHDPR.¹¹⁻¹³



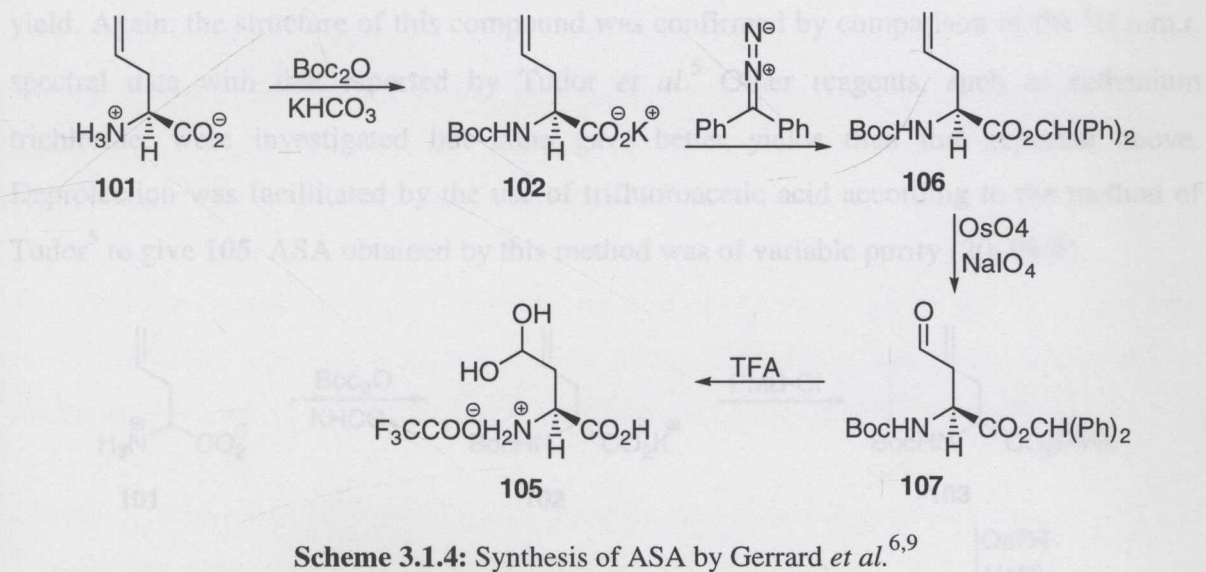
Scheme 3.1.2: Synthesis of ASA by Black and Wright⁴

Tudor *et al.*⁵ devised an alternative synthesis beginning from allylglycine **101**. Protection of both the amine as the *N*-*tert*-butoxycarbonyl derivative **102** and conversion of the carboxylate group to the *p*-methoxybenzyl ester **103** was followed by ozonolysis to give the aldehyde **104**. Subsequent deprotection with TFA gave (*S*)-ASA as the hydrated trifluoroacetate salt **105**, which can be stored at 0 °C as a stable solid (Scheme 3.1.3).

as determined by enzymatic assay.¹⁴ Thus, racemic (*R,S*)-allylglycine **101** was used in the preparation of ASA. A combination of the procedures of Tudor *et al.*⁵ and Gerrard *et al.*⁹ was used in the synthesis of ASA (Scheme 3.2.1).



As an alternative to ozonolysis to install the aldehyde functionality Gerrard^{6,9} oxidised *N*-Boc allylglycine diphenylmethyl ester **106** using catalytic osmium tetroxide with sodium periodate (Lemieux-Johnson reaction, Scheme 3.1.4) to give the desired aldehyde **107** followed by deprotection with trifluoroacetic acid to furnish **105**.



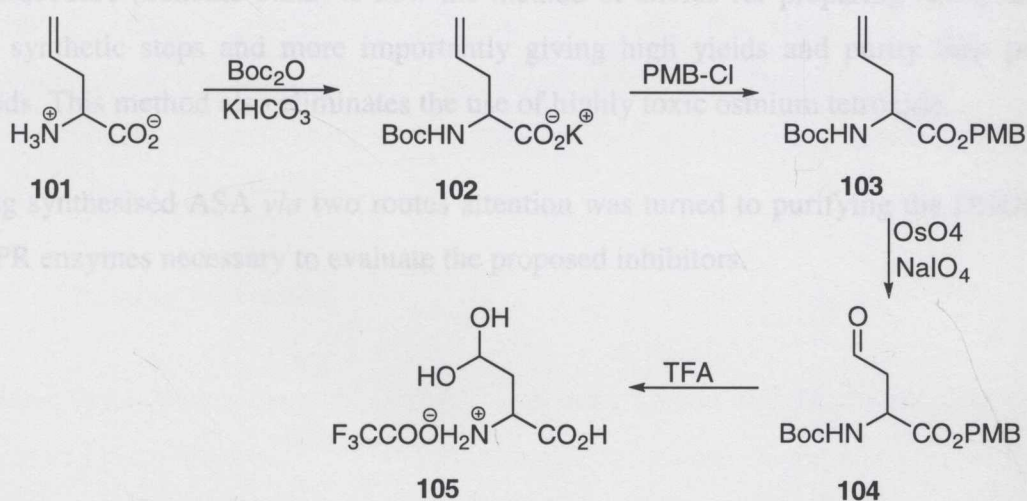
3.2 Synthesis of Aspartate β -Semialdehyde

Previous studies have shown that (*R*)-ASA has no inhibitory effects on the DHDPS enzyme, as determined by enzymatic assay.¹⁴ Thus, racemic (*R,S*)-allylglycine **101** was used in the preparation of ASA. A combination of the procedures of Tudor *et al.*⁵ and Gerrard *et al.*⁹ was used in the synthesis of ASA (Scheme 3.2.1).

Protection of the free amine of (*R,S*)-allylglycine **101** as the *N*-*tert*-butoxycarbonyl derivative was achieved efficiently to give the *N*-Boc protected potassium salt **102** in quantitative yield using di-*tert*-butyldicarbonate and potassium hydrogen carbonate in aqueous THF. The structure of this compound was confirmed by comparison of the ^1H n.m.r. spectral data with that reported by Tudor *et al.*⁵

Subsequent protection of the carboxylate as a *p*-methoxybenzyl ester was achieved using *p*-methoxybenzyl chloride in DMF with stirring for three days to give the desired diprotected (*R,S*)-allylglycine **103**. It was found that the addition of only one equivalent of *p*-methoxybenzyl chloride resulted in a low yield of 13%, whereas treatment with an excess of *p*-methoxybenzyl chloride increased the yield of **103** to 92%. The structure of this compound was confirmed by comparison of the ^1H n.m.r. spectral data with that reported by Tudor *et al.*⁵

Treatment of the diprotected (*R,S*)-allylglycine **103** with sodium periodate and catalytic osmium tetroxide in aqueous acetone provided the aldehyde derivative **104** in 50–60% yield. Again, the structure of this compound was confirmed by comparison of the ^1H n.m.r. spectral data with that reported by Tudor *et al.*⁵ Other reagents, such as ruthenium trichloride, were investigated but none gave better yields than that reported above. Deprotection was facilitated by the use of trifluoroacetic acid according to the method of Tudor⁵ to give **105**. ASA obtained by this method was of variable purity (20–98%).



Scheme 3.2.1: Synthesis of ASA: Using a Combination of Tudor *et al.*⁵ and Gerrard's⁹ Syntheses.

During the course of these studies an alternative procedure for the synthesis of ASA was reported by Roberts *et al.*⁷ which gave consistently high yields and high activity.

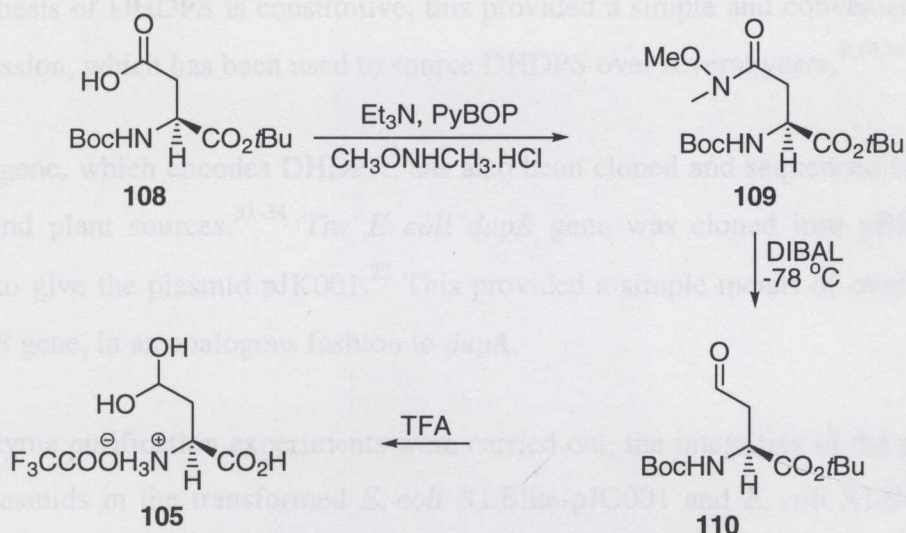
Commerically available α -*tert*-butyl (*S*)-*N*-*tert*-butoxycarbonyl aspartate **108** was converted to its Weinreb amide **109** via a procedure reported by Wernic *et al.*¹⁵ Treatment of the aspartate **108** derivative with BOP.PF₆ or PyBOP, triethylamine and *N,O*-dimethylhydroxylamine hydrochloride gave the desired Weinreb amide **109** in excellent yield (96%). The structure of this compound was confirmed by a comparison of the ¹H n.m.r. data with that reported by Wernic *et al.*¹⁵

Reduction of the Weinreb amide **109** to the aldehyde **110** was achieved using two equivalents of diisobutyl aluminium hydride in THF at -78 °C according to the method of Wernic *et al.*¹⁵ giving the desired product **110** in good yield (86%). The structure of this compound was confirmed by a comparison of the ¹H n.m.r. data with that reported.¹⁵

Deprotection of **110** was achieved using TFA in dichloromethane to give the desired product **105** as a pale yellow solid in excellent yield (96%). The structure of this compound was confirmed by comparison of the ¹H n.m.r data with that reported by Tudor *et al.*⁵ The purity of (*S*)-ASA-trifluoroacetate **105** prepared by this method was analysed using the coupled assay and determined to be consistently between 78–98%.

This procedure (Scheme 3.2.2) is now the method of choice for preparing ASA, requiring fewer synthetic steps and more importantly giving high yields and purity than previous methods. This method also eliminates the use of highly toxic osmium tetroxide.

Having synthesised ASA via two routes attention was turned to purifying the DHDPS and DHDPR enzymes necessary to evaluate the proposed inhibitors.



Scheme 3.2.2: Synthesis of ASA: Using the Method of Roberts *et al.*⁷

3.3 Purification of DHDPS and DHDPR

3.3.1 Introduction

DHDPS and DHDPR from *E. coli* were chosen for study as the *E. coli* enzymes exhibit similar properties and inhibition patterns to analogous enzymes from other bacterial species which also contain the *dap* biosynthetic pathway.¹⁶⁻²¹ In order to study the effects of inhibitors on the properties of *E. coli* DHDPS and DHDPR, large quantities of purified enzyme were required. Strains of *E. coli* were available that had been transformed with pBluescript plasmids pJG001 or pJK001, containing the *dapA*⁹ or *dapB*²² genes respectively. These strains provided a simple and convenient means for over-expression of each of the enzymes, generating several hundred-fold increases in enzyme expression of *E. coli* XL1-Blue.²³

3.3.2 Plasmid Extraction

The *dapA* gene, which encodes DHDPS, has been cloned and sequenced from several bacterial and plant sources.^{16,24-29} The *E. coli* *dapA* gene was cloned into pBluescript high copy number plasmid (500–700) by Gerrard⁹ and transformed into *E. coli* XL1-Blue and successful transformants identified by conferred ampicillin resistance to give pJG001.^{10,23}

Since synthesis of DHDPS is constitutive, this provided a simple and convenient means of over-expression, which has been used to source DHDPS over several years.^{9,10,14,30}

The *dapB* gene, which encodes DHDPR, has also been cloned and sequenced from several bacterial and plant sources.³¹⁻³⁴ The *E. coli* *dapB* gene was cloned into pBluescript by Kraunsoe to give the plasmid pJK001.²² This provided a simple means of over-expression of the *dapB* gene, in an analogous fashion to *dapA*.

Before enzyme purification experiments were carried out, the integrities of the pJG001 and pJK001 plasmids in the transformed *E. coli* XLBlue-pJG001 and *E. coli* XLBlue-pJK001 were confirmed. Standard plasmid preparation methods were used to prepare the pJG001 and pJK001 DNA,³⁵ which each contain restriction sites for both *Hind* III and *Eco*R I restriction enzymes. Following restriction digestion with these enzymes, agarose gel electrophoresis gave a restriction digest consistent with the restriction map predicted for the *dapA* and *dapB* genes within pJG001 and pJK001 plasmids. For plasmid pJG001, each single enzyme restriction digest produced one single-cut linear DNA fragment of approximately 4100 bp, corresponding to the complete linearised pJG001 plasmid. Two linear fragments of approximately 3000 bp and 1100 bp, corresponding to the linearised parent pBluescript and the *dapA* fragment respectively, were observed following the double enzyme digest (Figure 3.3.1).

The pJK001 plasmid single enzyme restriction digest produced one single-cut linear DNA fragment of approximately 5300 bp, corresponding to the complete linearised pJK001 plasmid, while two linear fragments of approximately 3000 bp and 2300 bp, corresponding to the linearised parent pBluescript and the *dapB* fragment respectively, were observed following the double enzyme digest (Figure 3.3.1).

E. coli XL-pJG001 cells over-expressing DHDPS were cultured overnight, harvested by centrifugation, washed and resuspended in buffer. Disruption of the cell, by a series of freeze-thaw cycles, allowed the release of the cell contents, including DHDPS. A few cycles resulted in optimal specific activity of the isolated DHDPS. After centrifugation, the pellet was discarded and the supernatant containing the crude extract was collected. The crude extract contained DHDPS, observed as a monomer in the SDS-PAGE gel after Coomassie Blue staining as the most abundant protein in the extract, with a M_r of approximately 31 kDa (Figure 3.4.1).

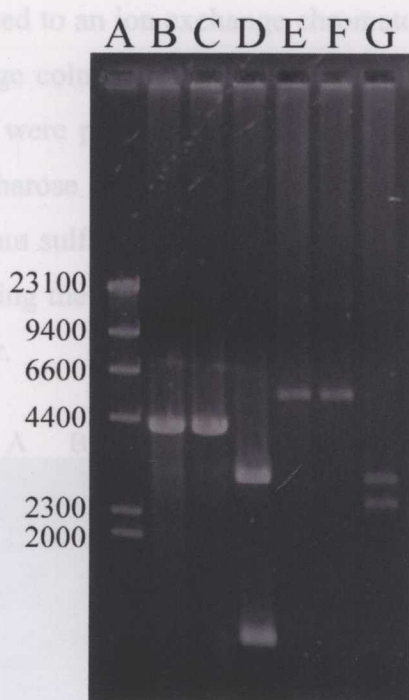


Figure 3.3.1: Agarose Gel Showing DNA Restriction Fragments of pJG001 and pJK001. LANE A: Lambda (23010 bp, 9400 bp, 6600 bp, 4400 bp, 2300 bp); LANE B: pJG001 single digest (*Hind* III) 4100 bp linear fragment; LANE C: pJG001 single digest (*Eco*R I) 4100 bp linear fragment; LANE D: double digest (*Hind* III and *Eco*R I) 3000 bp and 1100 bp linear fragments; LANE E: pJK001 single digest (*Hind* III) 5300 bp linear fragment; LANE F: pJK001 single digest (*Eco*R I) 5300 bp linear fragment; LANE G: pJK001 double digest (*Hind* III and *Eco*R I) 3000 bp and 2300 bp linear fragments.

3.4 Over-expression of the *dapA* Gene and Purification of DHDPS

The purification of DHDPS from *E. coli* XL-1 Blue-pJG001 was based on a modified version¹⁰ of the methods of Yugari and Gilvarg.²⁴ Purification steps were monitored by detection of DHDPS activity using the qualitative *o*-aminobenzaldehyde assay.^{10,30} This method is simple, rapid and sensitive to very low levels of enzyme activity, and is ideal for qualitative measurements to monitor for the presence of the enzyme.^{10,25}

E. coli XL-pJG001 cells over-expressing DHDPS were cultured overnight, harvested by centrifugation, washed and resuspended in buffer. Disruption of the cell, by a series of freeze-thaw cycles, allowed the release of the cell contents, including DHDPS. Seven cycles resulted in optimal specific activity of the isolated DHDPS. After centrifugation, the pellet was discarded and the supernatant containing the crude extract was collected. The crude extract contained DHDPS, observed as a monomer in the SDS-PAGE gel after Coomassie Blue staining as the most abundant protein in the extract, with a M_r of approximately 31 kDa (Figure 3.4.1).

The crude extract was subjected to an ion exchange chromatography purification step using a Q-Sepharose anion exchange column. The proteins were eluted with a sodium chloride gradient and active fractions were pooled. DHDPS from the pooled fractions was further purified using a Phenyl Sepharose column (based on surface hydrophobicity). Fractions were eluted with an ammonium sulfate gradient. Fractions that gave a positive result when tested for DHDPS activity using the *o*-aminobenzaldehyde assay were pooled and dialysed overnight against dilute buffer.



Figure 3.4.1: SDS-PAGE comparison of sample solutions after each DHDPS purification step. LANE A: Sigmamarker, wide molecular weight range, molecular weights of the bands are (from top) 205, 116, 97, 84, 66, 55, 45, 36, 29, 24, 20, 10.2 and 6.5 kDa; LANE B & C: Hi-Trap Q-Sepharose ion exchange fractions; LANES D & E: Phenyl Sepharose; LANE F: Q-Sepharose ion exchange fraction; LANES G & H: Crude cell extract. *N.B.* duplicate lanes contained different loads.

The enzyme was homogenous as judged by denaturing SDS-PAGE stained with Coomassie brilliant blue, which revealed a clean band with an electrophoretic mobility corresponding to a monomer of around 31 kDa (Figure 3.4.1). The increase in purity was reflected in an increase in the specific enzyme activity (Table 3.4.1).

DHDPR displays unusual heat tolerance, as shown by Parkay and Gilvarg.⁶ Heat shock treatment of the crude preparation at 70 °C for three minutes results in no significant loss of DHDPR activity, as shown by the purification table (Table 3.5.1). This step is thought to destroy any contaminating NADPH-utilising enzymes, which might interfere with the coupled assay and is carried out early in the purification process.

The crude extract was then subjected to Q-Sepharose anion exchange chromatography. Fractions were eluted with a sodium chloride gradient and assayed for DHDPR activity

Table 3.4.1: Purification of DHDPS

	[Protein] ^a (mg)	Total Activity ^b (Δ_{NADPH} $\mu\text{mol/s/ml}$)	Specific Activity ^c (Δ_{NADPH} $\mu\text{M/s/mg}$)	Yield (%)	Purification ^c (-fold)
Crude	2883	898	0.31		
Ion Exchange	440	687	1.56	77	5.0
Phenyl Sepharose	193	351	1.81	39	5.8

a Protein concentrations determined using the Bradford assay, section 5.11.5.

b Activity determined using the quantitative coupled assay for DHDPS activity, section 5.15.1.

c Crude preparations of DHDPR contain other enzymes that consume NADPH, or inhibitors, both of which interfere with the coupled assay, consequently the numbers in these columns are not necessarily an accurate measure of purification.

3.5 Over-expression of the *dapB* Gene and Purification of DHDPR

The purification of DHDPR from *E. coli* XL-1 Blue pJK001 was based on a modified¹⁰ version of the methods of Tamir and Gilvarg.³¹ Although Scapin *et al.*³² reported another method for DHDPR purification that yields enzyme of a higher purity suitable for crystallisation, the method of Tamir and Gilvarg³¹ is both simple and efficient, providing enzyme of suitable purity for kinetic studies.

E. coli XL-1 Blue pJK001 cells over-expressing DHDPR were cultured overnight, harvested by centrifugation, washed and resuspended in buffer. Ultrasonication, was used to release the cell contents, including DHDPR.³⁸

DHDPR displays unusual heat tolerance, as shown by Farkas and Gilvarg.⁶ Heat shock treatment of the crude preparation at 70 °C for three minutes results in no significant loss of DHDPR activity, as shown by the purification table (Table 3.5.1). This step is thought to destroy any contaminating NADPH-utilising enzymes, which might interfere with the coupled assay and is carried out early in the purification process.

The crude extract was then subjected to Q-Sepharose anion exchange chromatography. Fractions were eluted with a sodium chloride gradient and assayed for DHDPR activity

using the qualitative coupled assay. Following dialysis, the active fractions were purified and concentrated further by affinity chromatography using a HiTrap Blue nucleotide exchange column. The fractions were eluted with a sodium chloride gradient and assayed again for DHDPR activity using the qualitative coupled assay.

The pooled active fractions contained DHDPR with a specific activity of $1.50 \mu\text{mol NADPH.s}^{-1}.\text{mg protein}^{-1}$, which had been purified to homogeneity, as judged by SDS-PAGE with Coomassie brilliant blue staining (Figure 3.5.1). The gel shows a single band with an electrophoretic mobility corresponding to a protein monomer of approximately 29 kDa. As for DHDPS, the increase in purity was reflected in an increase in the specific enzyme activity (Table 3.5.1).

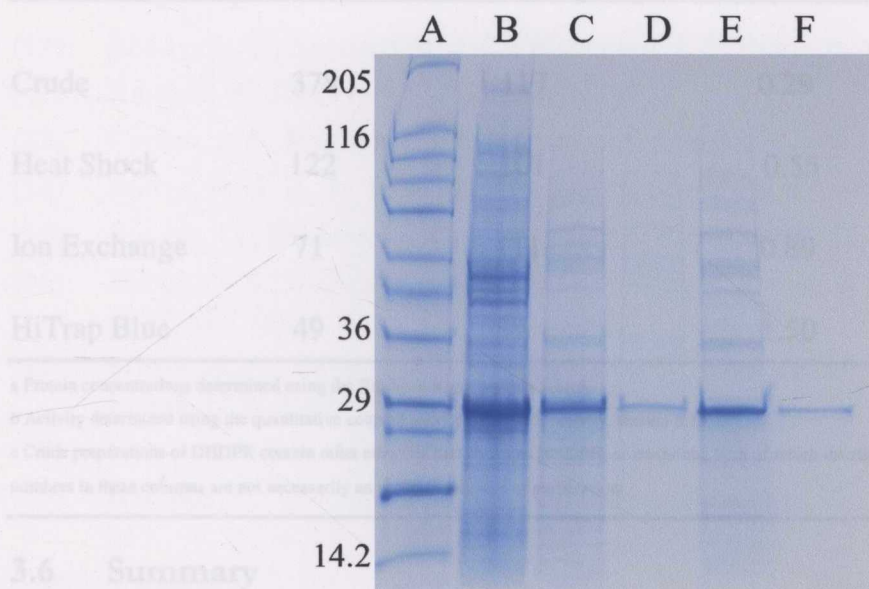


Figure 3.5.1: SDS-PAGE comparison of sample solutions after each DHDPR purification step. LANE A: Sigmamarker, wide molecular weight range, molecular weights of the bands are (from top) 205, 116, 97, 84, 66, 55, 45, 36, 29, 24, 20, 10.2 and 6.5 kDa; LANE B: Crude cell extract ultrasonication; LANE C: Crude cell extract heat shock; LANE D: Q-Sepharose ion exchange fractions; LANE E: Dialysed fractions; LANE F: HiTrap Blue affinity chromatography fractions.

periodate reaction. The ASA produced by this procedure was of variable yield and purity. The second method of synthesising ASA was achieved via reduction of a Weinreb amide derivative of aspartic acid. This procedure gave ASA in excellent yield and high purity and was the method of choice for preparing ASA for use in kinetic studies. Additionally, an established protocol was used to provide sufficient quantities of DHDPS and DHDPR. Having both the necessary substrate and enzymes available, attention was turned to evaluating the proposed inhibitors synthesised in Chapter 2.

The addition of the HiTrap Blue affinity chromatography step has increased the specific activity of the final preparation to $1.50 \mu\text{mol NADPH}\cdot\text{s}^{-1}\cdot\text{mg protein}^{-1}$, a 5.2-fold increase over the crude sample. This is close to the previously reported¹⁰ value of $2.25 \mu\text{mol NADPH}\cdot\text{s}^{-1}\cdot\text{mg protein}^{-1}$, which was also determined using the quantitative coupled assay. The HiTrap Blue affinity chromatography column is extremely selective and only binds NAD(P)H utilising enzymes. Therefore, this step introduces a very specific and selective step for the purification of the DHDPR enzyme.

Table 3.5.1: Purification of DHDPR

	[Protein] ^a (mg)	Total Activity ^b ($\Delta n_{\text{NADPH}} \mu\text{mol/s/ml}$)	Specific Activity ^c ($\Delta n_{\text{NADPH}} \mu\text{M/s/mg}$)	Yield (%)	Purification ^c (-fold)
Crude	378	117	0.29		
Heat Shock	122	101	0.55	60	1.9
Ion Exchange	71	111	0.89	93	3.0
HiTrap Blue	49	89	1.50	61	5.2

a Protein concentrations determined using the Bradford assay, section 5.11.5.

b Activity determined using the quantitative coupled assay for DHDPR activity, section 5.15.2.

c Crude preparations of DHDPR contain other enzymes that consume NADPH, or inhibitors, both of which interfere with the coupled assay, consequently the numbers in these columns are not necessarily an accurate measure of purification.

3.6 Summary

(S)-ASA was synthesised *via* two routes. The first four step procedure beginning from racemic allylglycine, installed the aldehyde moiety through an osmium tetroxide/sodium periodate reaction. The ASA produced by this procedure was of variable yield and purity. The second method of synthesising ASA was achieved *via* reduction of a Weinreb amide derivative of aspartic acid. This procedure gave ASA in excellent yield and high purity and was the method of choice for preparing ASA for use in kinetic studies. Additionally, an established protocol was used to provide sufficient quantities of DHDPS and DHDPR. Having both the necessary substrate and enzymes available, attention was turned to evaluating the proposed inhibitors synthesised in Chapter 2.

3.7 References

- (1) Lusch, H.; Uzar, H. C. *Tetrahedron: Asymmetry* **2000**, *11*, 4965.
- (2) Baldwin, J. E.; Flinn, A. *Tetrahedron Lett.* **1987**, *28*, 3605.
- (3) Meffre, P.; Durand, P.; Le Goffic, F. *Synthesis* **1995**, 1111.
- (4) Black, S.; Wright, N. *J. Biol. Chem.* **1955**, *213*, 27.
- (5) Tudor, D. W.; Lewis, T.; Robins, D. J. *Synthesis* **1993**, 1061.
- (6) Coulter, C. V.; Gerrard, J. A.; Kraunsoe, J. A. E.; Moore, D. J.; Pratt, A. J. *Tetrahedron* **1996**, *52*, 7127.
- (7) Roberts, S. J.; Morris, J. C.; Dobson, R. C. J.; Gerrard, J. A. *Bioorg. Med. Chem. Lett.* **2003**, *13*, 265.
- (8) Ohfuné, Y.; Tomita, M.; Nomoto, K. *J. Am. Chem. Soc.* **1981**, *103*, 2409.
- (9) Gerrard, J. A. D. Phil. Thesis, Oxford University, 1992.
- (10) Coulter, C. V. PhD, University of Canterbury, 1997.
- (11) Reddy, S. G.; Sacchettini, J. C.; Blanchard, J. S. *Biochemistry* **1995**, *34*, 3492.
- (12) Karsten, W. *Biochemistry* **1997**, *36*, 1730.
- (13) Caplan, J. F.; Renjian, Z.; Blanchard, J. S.; Vederas, J. C. *Org. Lett.* **2000**, *24*, 3857.
- (14) Pearce, F. G. B. Sc. Hons. Thesis, University of Canterbury, 1999.
- (15) Wernic, D.; DiMaio, J.; Adams, J. *J. Org. Chem.* **1989**, *54*, 4224.
- (16) Blickling, S.; Beisel, H.; Bozic, D.; Knablein, J.; Laber, B.; Huber, R. *J. Mol. Biol.* **1997**, *274*, 608.
- (17) Frisch, D. A.; Gengenbach, B. G.; Tommey, A. M.; Sellner, J. M.; Somers, D. A.; Myers, D. E. *Plant Physiol.* **1991**, *96*, 444.
- (18) Kumpaisal, R.; Hashimoto, T.; Yamada, Y. *Plant Physiol.* **1987**, *85*, 145.
- (19) Dereppe, C.; Bold, G.; Ghisalba, O.; Edbert, E.; Schar, H. *Plant Physiol.* **1992**, *98*, 813.
- (20) Yamakura, F.; Ikeda, Y.; Kimura, K.; Sasakawa, T. *J. Biochem. (Tokyo)* **1974**, *76*, 611.
- (21) Stahly, D. P. *Biochim. Biophys. Acta* **1969**, *191*, 439.
- (22) Kraunsoe, J. A. E. Part II Thesis, Oxford University, 1992.
- (23) Coulter, C. V.; Gerrard, J. A.; Kraunsoe, J. A. E.; Pratt, A. J. *Pest. Sci.* **1999**, *55*, 887.
- (24) Yugari, Y.; Gilvarg, C. *J. Biol. Chem.* **1965**, *240*, 4710.
- (25) Shedlarski, J. G.; Gilvarg, C. *J. Biol. Chem.* **1970**, *245*, 1362.
- (26) Bonnassie, S.; Oreglia, J.; Sicard, A. M. *Nuc. Acid. Res.* **1990**, *18*, 6421.
- (27) Kaneko, T.; Hashimoto, T.; Kumpaisal, R.; Yamada, Y. *J. Biol. Chem.* **1990**, *265*, 17451.
- (28) Cremer, J.; Treptoe, C.; Eggeling, L.; Sahm, H. *J. Gen. Microbiol.* **1988**, *134*, 3221.
- (29) Bittel, D. C.; Shaver, J. M.; Somers, D. A.; Gengenbach, B. G. *Theor. Appl. Gen.* **1996**, *92*, 70.

- (30) Roberts, S. J. MSc Thesis, University of Canterbury, 2002.
- (31) Tamir, H.; Gilvarg, C. *J. Biol. Chem.* **1974**, *249*, 3034.
- (32) Scapin, G.; Blanchard, J. S.; Sacchettini, J. C. *Biochemistry* **1995**, *34*, 3502.
- (33) Silk, G. W.; Matthews, B. F.; Somers, D. A.; Gengenbach, B. G. *Plant Molecular Biology* **1994**, *26*, 989.
- (34) Pisabarro, A.; Malumbres, M.; Mateos, L. M.; Oguiza, J. A.; Martin, J. F. *J. Bacteriol.* **1993**, *175*, 2743.
- (35) Sambrook, J.; Fritsch, E. F.; Maniatis, T. *Molecular cloning: A laboratory approach*; Oxford University Press: New York, 1989.
- (36) Laber, B.; Gomis-Rueth, F. X.; Romao, M. J.; Huber, R. *Biochem. J.* **1992**, *288*, 691.
- (37) Borthwick, E. B.; Connell, S. J.; Tudor, D. W.; Robins, D. J.; Shneier, A.; Abell, C.; Coggins, J. R. *Biochem. J.* **1995**, *305*, 521.
- (38) Cirillo, J. D.; Weisbrod, T. R.; Banerjee, A.; Bloom, B. R.; Jacobs, W. R. J. *J. Bacteriol.* **1994**, *176*, 4424.

4.1 Introduction

In order to study the kinetics of any enzyme-catalysed reaction, measuring the initial rate of the reaction, either by measuring the formation of a product or the consumption of a substrate, is essential. This requires a study of the initial rate of the reaction to

CHAPTER 4

KINETIC & INHIBITION STUDIES OF DHDPS AND DHDPR

assess the degree and type of inhibition displayed by the compounds synthesised in Chapter 2. This assay had to be capable of accurately measuring the initial rate of the enzyme-catalysed reaction. As described briefly in the introduction (see section 1.8) there are three assays available for the studying the activity of DHDPS: the *o*-aminobenzaldehyde assay, the imidazole buffer assay, and the coupled assay.²

4.2 *o*-Aminobenzaldehyde Assay

The addition of *o*-aminobenzaldehyde to DHDPS and its substrates results in the formation of an unknown purple product, the formation of which can be monitored at 540 nm.^{2,3} It was originally postulated that the product was a dehydroganzolium salt, however this was ruled out due to the formation of a purple product, in comparison to the yellow product observed in assays which utilise *o*-aminobenzaldehyde and similar substrates.² A significant lag time (~30 min) is observed before an increase in purple colouration occurs. The intensity of the purple colour can be increased by the addition of acid after the incubation period. For this assay to be quantitatively useful, the assumption would have to be made that the rate limiting step is the formation of the enzymatic product and not the purple complex; however, this is readily invalidated. Thus, the *o*-aminobenzaldehyde assay was not used as a quantitative assay. However, it was used in the purification of DHDPS due to its high specificity and sensitivity for DHDPS and ease of use.

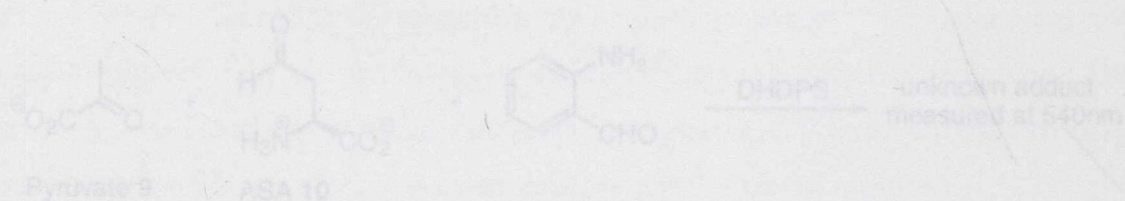


Figure 4.2.I: *o*-Aminobenzaldehyde Assay

4.1 Introduction

In order to study the kinetics of any enzyme-catalysed reaction, a suitable method for measuring the initial rate of the reaction, either by measuring the concentrations of product formation or substrate depletion over time, must be available.¹ A quantitative assay system was required to study the kinetic properties of the enzymes DHDPS and DHDPR, and assess the degree and type of inhibition displayed by the compounds synthesised in Chapter 2. This assay had to be capable of accurately measuring the initial rate of the enzyme catalysed reaction. As described briefly in the introduction (see section 1.8) there are three assays available for the studying the activity of DHDPS: the *o*-aminobenzaldehyde assay, the imidazole buffer assay, and the coupled assay.²

4.2 *o*-Aminobenzaldehyde Assay

The addition of *o*-aminobenzaldehyde to DHDPS and its substrates results in the formation of an unknown purple product, the formation of which can be monitored at 540 nm.^{2,3} It was originally postulated that the product was a dihydroquinazolium salt, however this was ruled out due to the formation of a purple product, in comparison to the yellow product observed in assays which utilise *o*-aminobenzaldehyde and similar substrates.² A significant lag time (≈ 30 min) is observed before an increase in purple colouration occurs. The intensity of the purple colour can be increased by the addition of acid after the incubation period. For this assay to be quantitatively useful, the assumption would have to be made that the rate limiting step is the formation of the enzymatic product and not the purple complex; however, this is readily invalidated. Thus, the *o*-aminobenzaldehyde assay was not used as a quantitative assay. However, it was used in the purification of DHDPS due to its high specificity and sensitivity for DHDPS and ease of use.

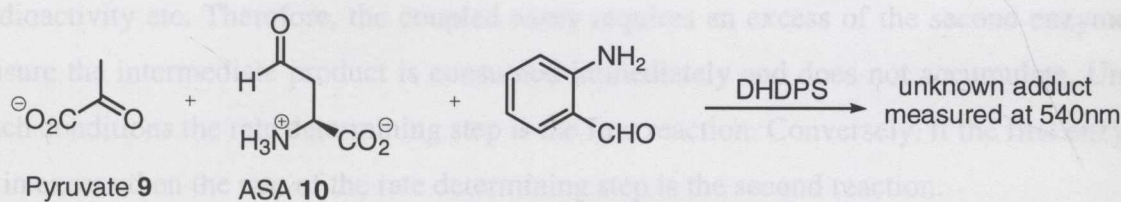


Figure 4.2.1: *o*-Aminobenzaldehyde Assay

DHDPR. The oxidation of NADPH to NADP⁺ by DHDPR is easily monitored and measured. NADPH absorbs strongly at 340 nm (molar extinction coefficient of 6220 M⁻¹cm⁻¹), while the oxidation product exhibits little absorbance at this wavelength. Thus, the rate of this reaction can be measured by the decrease in absorbance at 340 nm, which corresponds to the oxidation of NADPH to NADP⁺ by DHDPR.² This assay is able to measure the kinetics of the DHDPS-catalysed reaction, if DHDPR is present in excess, and conversely the kinetics of the DHDPR-catalysed reaction, if DHDPS is present in excess. This assay was therefore used to investigate the nature of inhibition of compounds synthesised in Chapter 2.

Although the coupled assay was developed in 1965 by Yugari and Gilvarg² it was used rarely until the early nineties, probably due to a lack of availability of DHDPR. As new procedures become available for obtaining sufficient quantities of both DHDPS and DHDPR, with the advent of recombinant DNA technology, the coupled assay is being used more frequently by numerous groups.^{5,9,10}

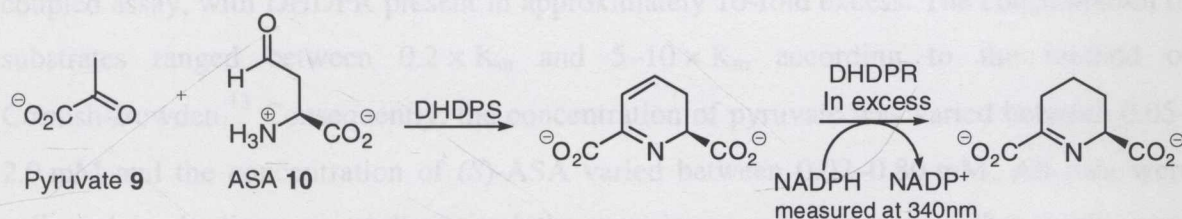


Figure 4.4.1: Coupled Assay to Test for DHDPS Activity

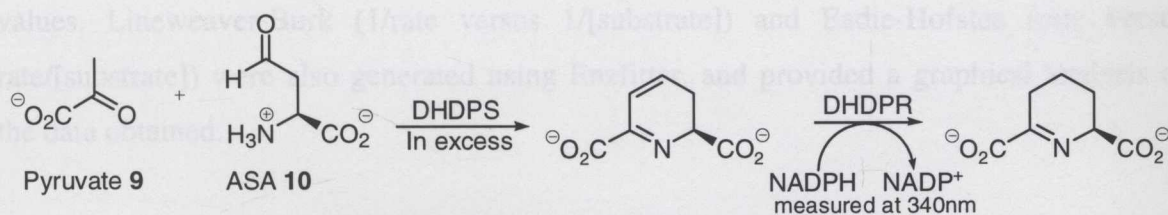


Figure 4.4.2: Coupled Assay to Test for DHDPR Activity

4.5 Modifications to the Coupled Assay

The coupled assay was used to measure the kinetics of DHDPS and DHDPR as it is the only assay which yields reliable kinetic data. This assay has previously been optimised by the Gerrard group to make it more effective for the range of kinetic rates under observation. The pH optimum for DHDPS is 8.4,² but it is advantageous to run the assay at near

physiological pH, to best mimic the true biological situation in the cell. The original coupled assay developed by Yugari and Gilvarg measured DHDPS using Tris buffer at near physiological pH of 7.4.² However, due to the inadequate capacity of Tris buffer at this pH an alternative buffer was used.¹¹ At neutral pH levels inside the cell, formation of a Schiff base between pyruvate and the enzyme is mostly irreversible.⁹ At both pH 8.0 and 7.2 (near physiological pH) the reaction proceeds in the forward direction. It has been shown by Pearce¹² that there is no significant difference between the kinetic parameters at pH 8.0 and pH 7.2 ($P > 0.10$). It was therefore decided to use a buffer that had a buffering capacity around optimum pH for DHDPS. *N*-2-Hydroxyethylpiperazine-*N'*-2-ethane sulphonic acid (HEPES) buffer was chosen as it was found to buffer the assay adequately at pH 8.0 and allow the acquisition of consistent kinetic data, enabling K_m and V_{max} to be calculated.

4.6 Enzyme Kinetics of *E. coli* DHDPS

Enzyme kinetics of DHDPS with respect to pyruvate and (*S*)-ASA were measured using the coupled assay, with DHDPR present in approximately 10-fold excess. The concentration of substrates ranged between $0.2 \times K_m$ and $5-10 \times K_m$ according to the method of Cornish-Bowden.¹³ Consequently, the concentration of pyruvate was varied between 0.05–2.0 mM and the concentration of (*S*)-ASA varied between 0.02–0.80 mM. All data were collected in duplicate or triplicate and the experiment repeated twice. The results were analysed using the Enzfitter computer program¹⁴ in order to determine the K_m and V_{max} values. Lineweaver-Burk (1/rate versus 1/[substrate]) and Eadie-Hofstee (rate versus rate/[substrate]) were also generated using Enzfitter, and provided a graphical analysis of the data obtained.

The Lineweaver-Burk plot is useful for initial analysis of kinetic data, and is by far the most widely used plot in enzyme kinetics. However, it often gives a grossly misleading impression of experimental error, as data points at high substrate concentrations are compressed into a small region of the graph, while data points at low concentrations, when the reaction rate is slowest (highest experimental error) are emphasised.^{13,15}

The Eadie-Hofstee plot provides a more accurate analysis of kinetic data. It has a tendency to make good data look worse, as it makes deviations of the points from the line more

Eadie-Hofstee plots (Figure 4.6.2-c,d), indicating the data were of high quality and fitted the ping-pong kinetic mechanism. The kinetic parameters were calculated using the ping-pong kinetic model and the V_{\max} was found to be $138 \pm 3 \mu\text{mol} \cdot \text{min}^{-1} \cdot \text{mg}^{-1}$. The K_m of DHDPS with respect to pyruvate was found to be $0.38 \pm 0.02 \text{ mM}$. These results yielded a slightly higher K_m than those reported in the literature. Karsten⁹ determined the K_m with respect to pyruvate to be $0.19 \pm 0.03 \text{ mM}$ and similarly Coulter *et al.*⁵ reports a K_m of $0.12 \pm 0.1 \text{ mM}$, Roberts¹³ reports a K_m of $0.18\text{--}0.21 \text{ mM}$ while Yugari and Gilvarg² report a K_m of 0.25 mM . Laber *et al.*²² report a K_m of 0.57 mM which is significantly higher than all other K_m values reported, however this was determined using the imidazole buffer assay, as opposed to the more accurate coupled assay.

The kinetic parameters with respect to (*S*)-ASA were also determined. Again, random scattering in the residual plot was observed (Figure 4.6.3-a). The data clearly fitted the model well (Figure 4.6.3-b) and this is seen in both the Lineweaver-Burk and Eadie-Hofstee plots (Figure 4.6.3-c,d) as a tight grouping of points about the line of best fit, indicating the data were of high quality and fitted the ping-pong kinetic mechanism. The K_m of DHDPS with respect to (*S*)-ASA was found to be $0.14 \pm 0.01 \text{ mM}$. Karsten⁹ determined the K_m with respect to (*S*)-ASA to be 0.12 ± 0.01 . Other values obtained in the literature using the coupled assay are also in good agreement, but it is important to note that data were fitted to a slightly different model (Michaelis-Menten model). Coulter *et al.*⁵ report a K_m range of $0.1 \pm 0.14 \text{ mM}$ at pH 7.2, Yugari and Gilvarg² found the K_m to be 0.13 mM at pH 7.4 while Pearce¹² reports a K_m range of $0.10 \pm 0.46 \text{ mM}$. All these values were obtained by the coupled assay and are notably lower than those obtained using the imidazole buffer assay. For example, Couper *et al.*⁸ report the K_m to be 0.23 mM , while Laber *et al.*²² report the K_m to be 0.55 mM . The difference in values obtained by the coupled assay and the imidazole buffer assay could be due to the shortcomings of the imidazole assay method, as the lags in the reaction time course and the uncharacterised reaction product do not allow the accurate acquisition of quantitative kinetic data.⁹

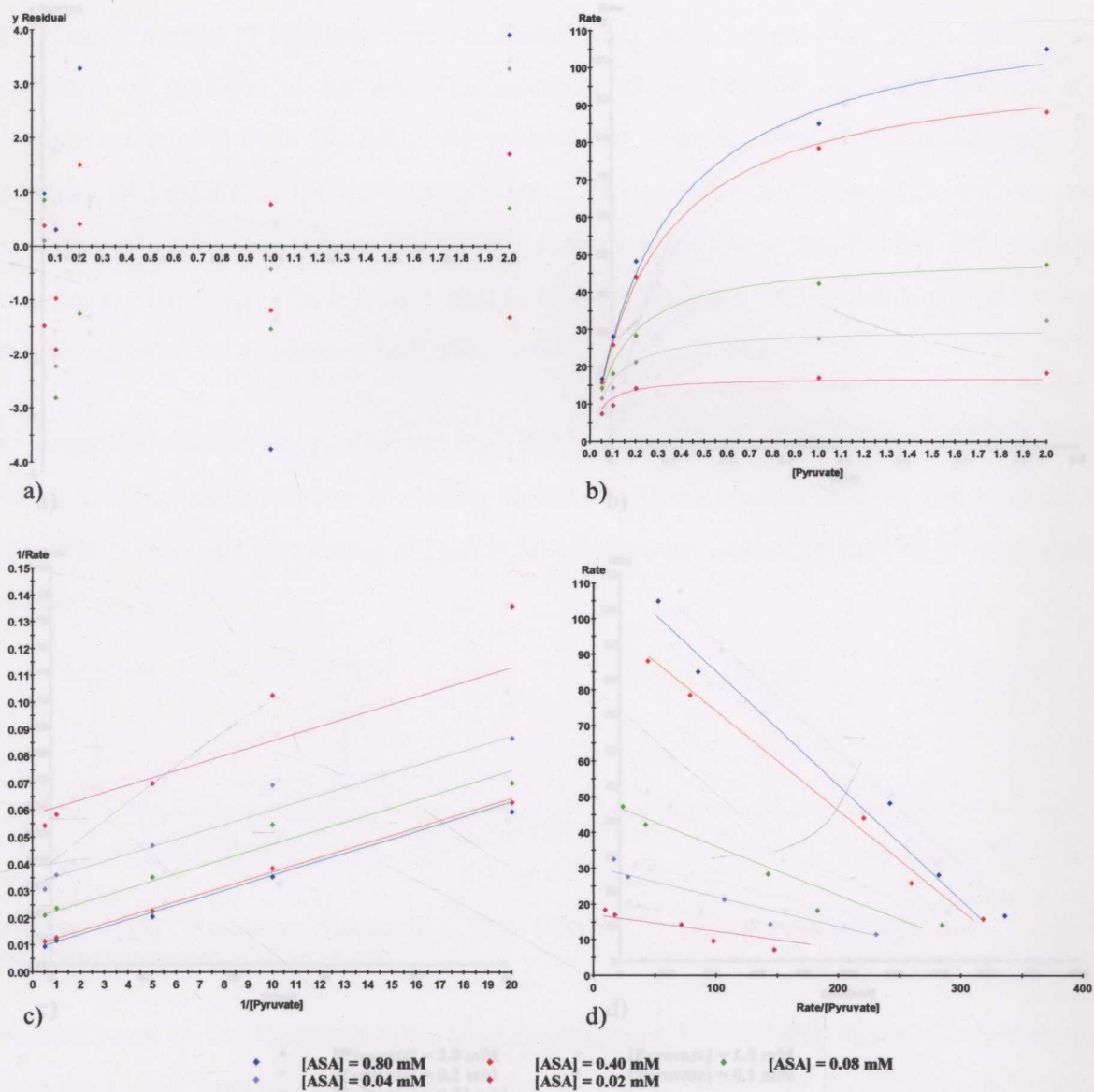


Figure 4.6.2: DHDPS Kinetics with Respect to Pyruvate at Different ASA Concentrations; a) Residuals Plot b) Raw Data with Fitted Model c) Lineweaver-Burk Plot ($R^2 = 0.99$, $P < 0.05$) d) Eadie-Hofstee Plot ($R^2 = 0.99$, $P < 0.05$).

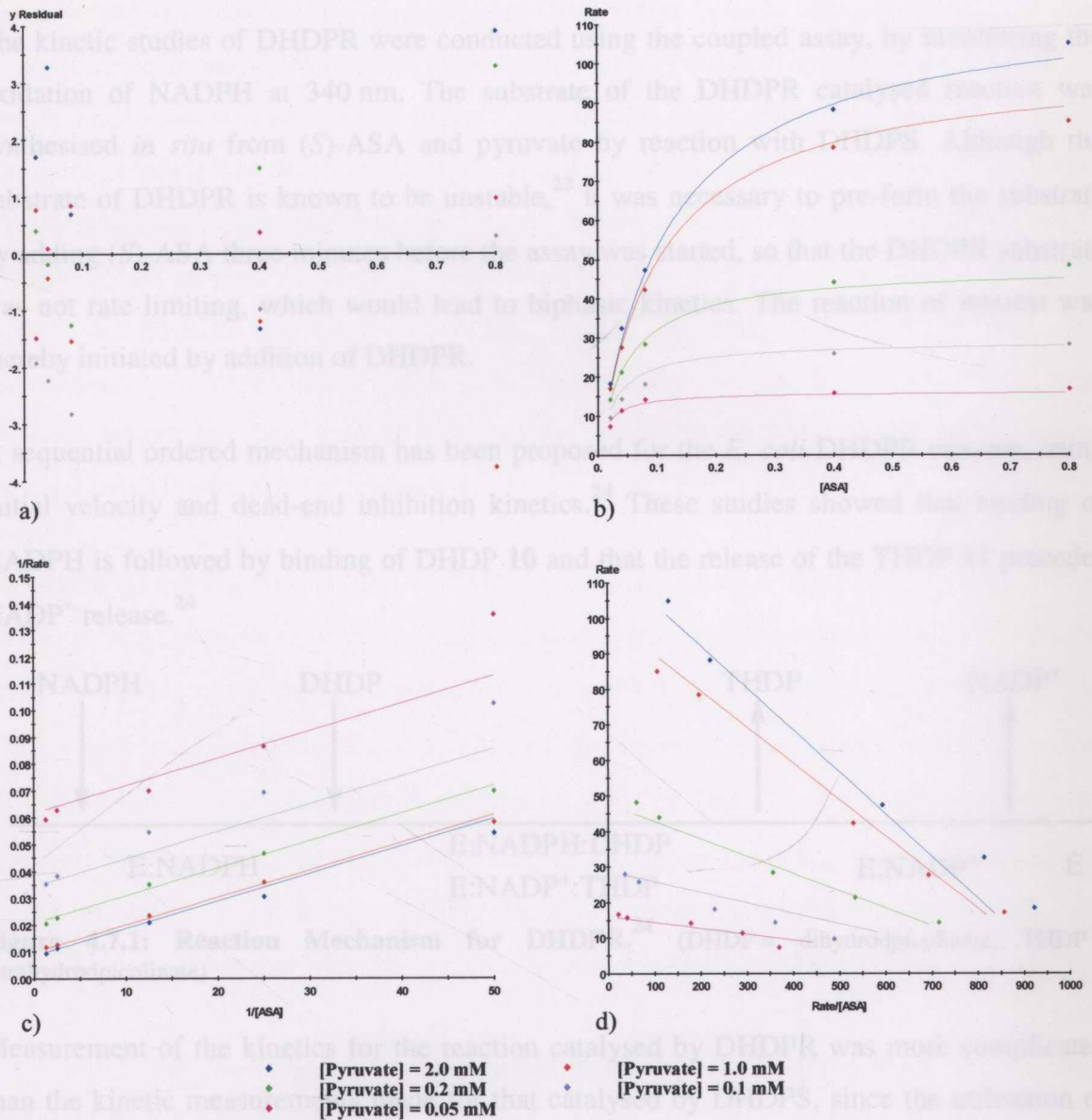
4.7 Enzyme Kinetics of *E. coli* DHDPR

Figure 4.6.3: DHDPS Kinetics with Respect to ASA at Different Pyruvate Concentrations; a) Residuals Plot b) Raw Data with Fitted Model c) Lineweaver-Burk Plot ($R^2 = 0.99$, $P < 0.05$) d) Eadie-Hofstee Plot ($R^2 = 0.99$, $P < 0.05$).

concentrations, experimental errors are introduced when the absorbance of NADPH rises above 1.2 absorbance units, as this coincides with the upper limit of the accurate linear range of the spectrophotometer. Thus, the kinetic measurements were more accurate than those for DHDPS, making the calculated kinetic parameters less reliable.

The K_m and V_{max} values of DHDPR with respect to the substrate and co-factor were measured using the coupled assay, with DHDPS present in approximately 10-fold excess.

4.7 Enzyme Kinetics of *E. coli* DHDPR

The kinetic studies of DHDPR were conducted using the coupled assay, by monitoring the oxidation of NADPH at 340 nm. The substrate of the DHDPR catalysed reaction was synthesised *in situ* from (*S*)-ASA and pyruvate by reaction with DHDPS. Although the substrate of DHDPR is known to be unstable,²³ it was necessary to pre-form the substrate by adding (*S*)-ASA three minutes before the assay was started, so that the DHDPR substrate was not rate limiting, which would lead to biphasic kinetics. The reaction of interest was thereby initiated by addition of DHDPR.

A sequential ordered mechanism has been proposed for the *E. coli* DHDPR enzyme, using initial velocity and dead-end inhibition kinetics.²⁴ These studies showed that binding of NADPH is followed by binding of DHDP **10** and that the release of the THDP **11** precedes NADP⁺ release.²⁴

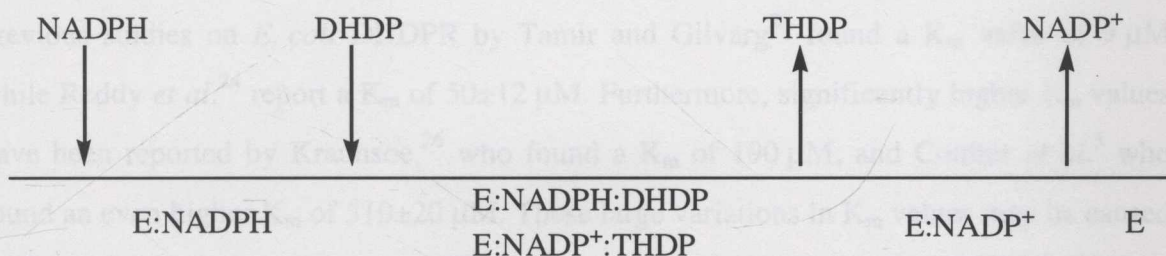


Figure 4.7.1: Reaction Mechanism for DHDPR.²⁴ (DHDP = dihydrodipicolinate, THDP = tetrahydrodipicolinate)

Measurement of the kinetics for the reaction catalysed by DHDPR was more complicated than the kinetic measurements made for that catalysed by DHDPS, since the utilisation of NADPH is the method of measuring the rate of the reaction and NADPH is also a substrate for the reaction. At low concentrations of NADPH in the DHDPR coupled assay, NADPH becomes the rate limiting substrate, decreasing the possible enzymatic rate. At high concentrations, experimental errors are introduced when the absorbance of NADPH rises above 1.2 absorbance units, as this coincides with the upper limit of the accurate linear range of the spectrophotometer. Thus, the kinetic measurements were more limited than those for DHDPS, making the calculated kinetic parameters less reliable.

The K_m and V_{max} values of DHDPR with respect to the substrate and co-factor were measured using the coupled assay, with DHDPS present in approximately 10-fold excess.

The concentration of substrates were varied between $0.2 \times K_m$ and $10 \times K_m$ according to the method of Cornish-Bowden.¹³ Consequently, the concentration of substrate was varied between 0.07–1.0 mM and the co-factor NADPH varied between 0.04–0.12 mM. All data were collected in duplicate and the experiment repeated twice. The data were fitted to the simple Michaelis-Menten kinetic model. The results were analysed using the Enzfitter computer program that determined the K_m and V_{max} values. Lineweaver-Burk (1/rate versus 1/[substrate]) and Eadie-Hofstee (rate versus rate/[substrate]) were also generated using Enzfitter¹⁴ and provided a graphical analysis of the data obtained. Again the residual plots showed a random scattering of points (Figure 4.7.2-a). The Eadie-Hofstee and Lineweaver-Burk plots showed a tight grouping of points about the lines of best fit for these plots, indicating the data were of high quality and fitted the Michaelis-Menten equation appropriately (Figure 4.7.2 and Figure 4.7.3).

For DHDPR, the K_m with respect to DHDP was found to be in the range of $60 \pm 3 \mu\text{M}$. A variety of K_m values have been reported and these values range considerably. For example, previous studies on *E. coli* DHDPR by Tamir and Gilvarg²⁵ found a K_m value of $9 \mu\text{M}$ while Reddy *et al.*²⁴ report a K_m of $50 \pm 12 \mu\text{M}$. Furthermore, significantly higher K_m values have been reported by Kraunsoe,²⁶ who found a K_m of $190 \mu\text{M}$, and Coulter *et al.*⁵ who found an even higher K_m of $510 \pm 20 \mu\text{M}$. These large variations in K_m values may be caused by the instability of the substrate DHDP **10** and its immediate precursor HTHDP **17**, as it has been documented that dihydropyridines are prone to oxidation in air.²³

For DHDPR, the K_m with respect to NADPH was found to be in the range of $30 \pm 2 \mu\text{M}$. Again, as with the K_m values for DHDP the K_m values for NADPH have been found to vary considerably. Previous studies on *E. coli* DHDPR by Tamir and Gilvarg²⁵ found the K_m to be $10 \mu\text{M}$, in close agreement with the value of K_m of $8 \pm 1.2 \mu\text{M}$ reported by Reddy *et al.*²⁴ These low K_m values reflect the high affinity of the DHDPR enzyme for the cofactor NADPH.

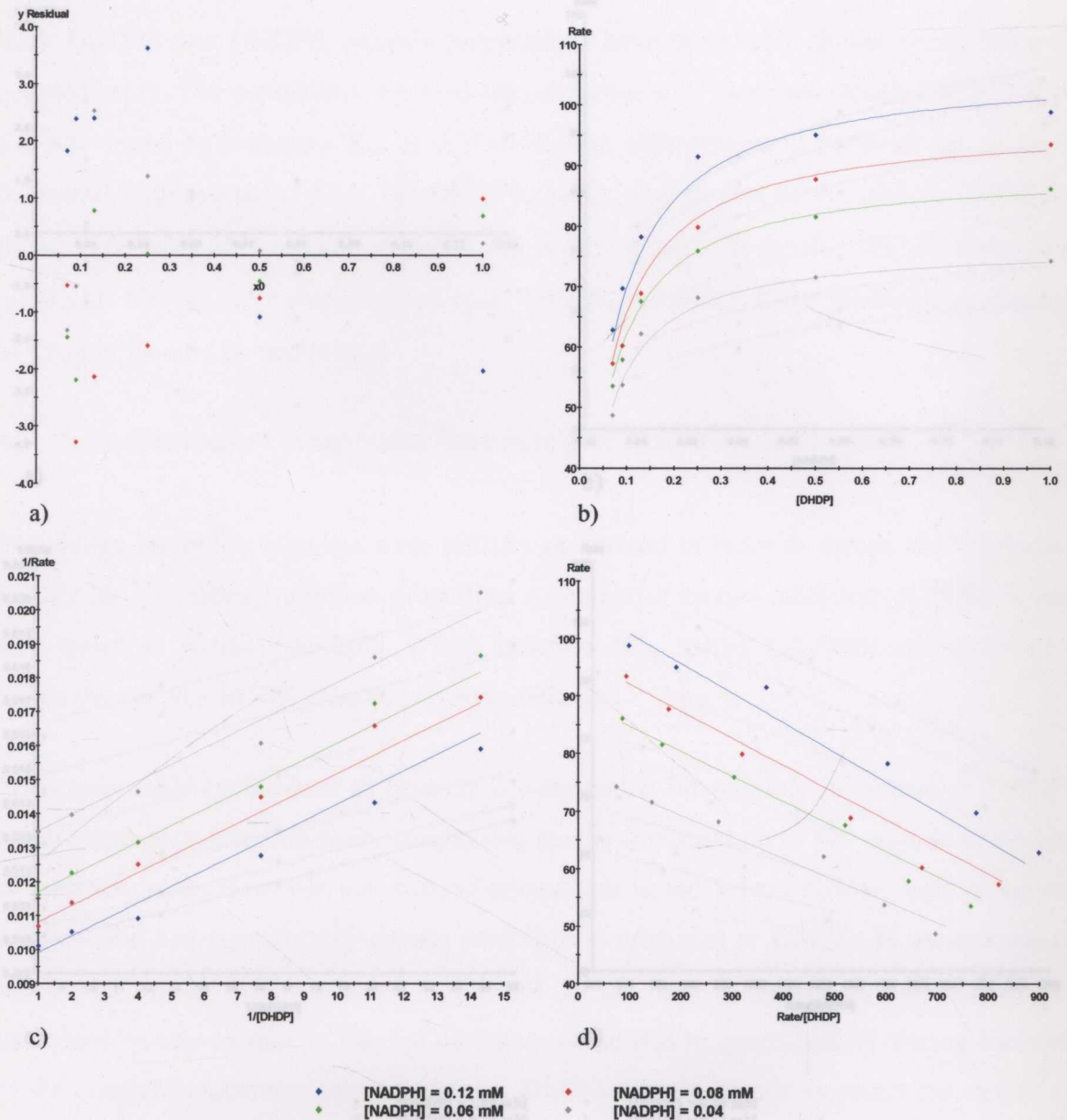


Figure 4.7.2: DHDPR Kinetics with Respect to DHDP at Different NADPH Concentrations; a) Residuals Plot **b)** Raw Data with Fitted Model **c)** Lineweaver-Burk Plot ($R^2 = 0.98$, $P < 0.05$) **d)** Eadie-Hofstee Plot ($R^2 = 0.98$, $P < 0.05$).

4.8 Summary

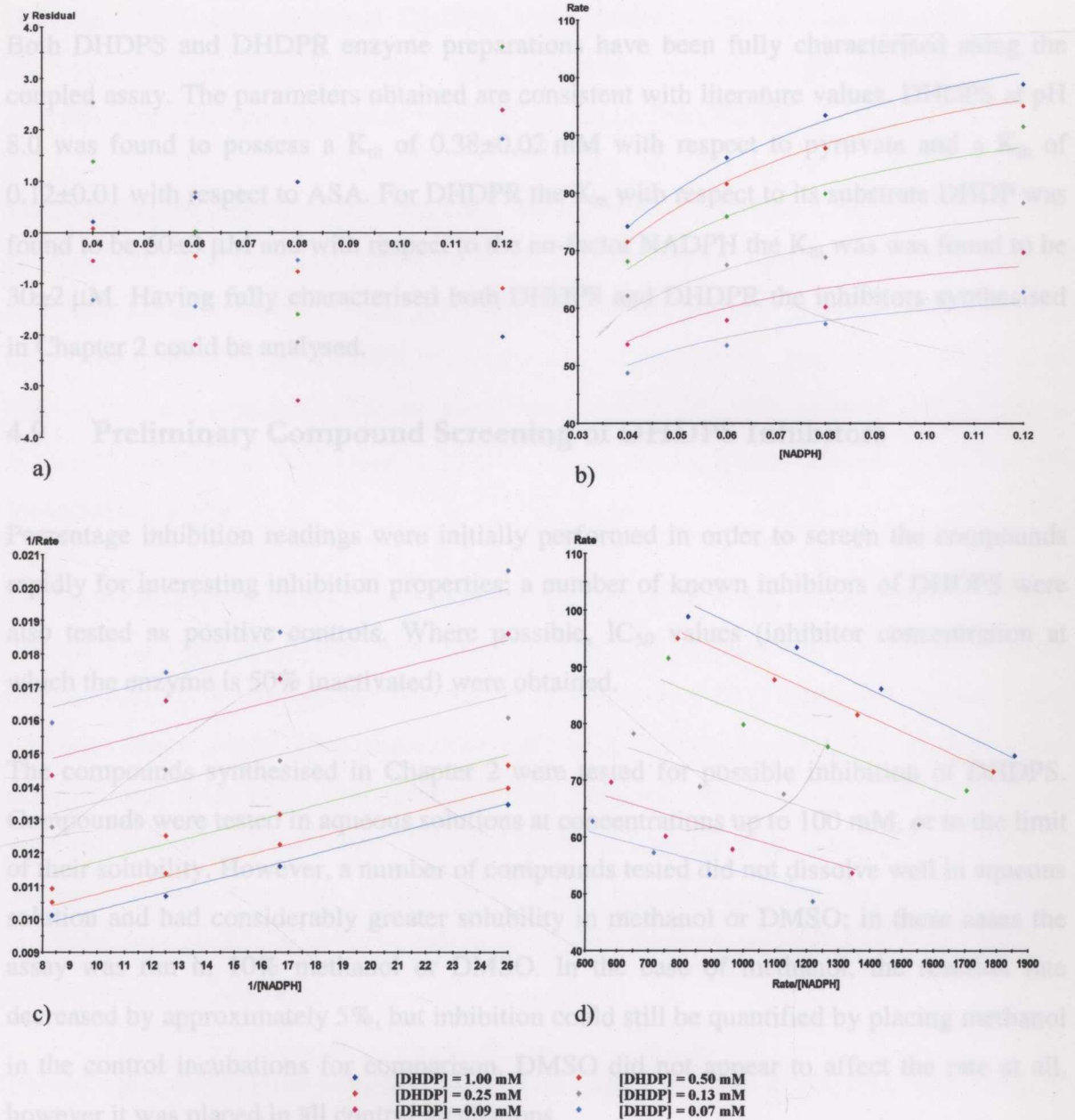


Figure 4.7.3: DHDPR Kinetics with Respect to NADPH at Different DHDP Concentrations; a) Residuals Plot **b)** Raw Data with Fitted Model **c)** Lineweaver-Burk Plot ($R^2 = 0.98$, $P < 0.05$) **d)** Eadie-Hofstee Plot ($R^2 = 0.98$, $P < 0.05$).

4.8 Summary

Both DHDPS and DHDPR enzyme preparations have been fully characterised using the coupled assay. The parameters obtained are consistent with literature values. DHDPS at pH 8.0 was found to possess a K_m of 0.38 ± 0.02 mM with respect to pyruvate and a K_m of 0.12 ± 0.01 with respect to ASA. For DHDPR the K_m with respect to its substrate DHDP was found to be 60 ± 3 μ M and with respect to the co-factor NADPH the K_m was found to be 30 ± 2 μ M. Having fully characterised both DHDPS and DHDPR the inhibitors synthesised in Chapter 2 could be analysed.

4.9 Preliminary Compound Screening of DHDPS Inhibitors

Percentage inhibition readings were initially performed in order to screen the compounds rapidly for interesting inhibition properties; a number of known inhibitors of DHDPS were also tested as positive controls. Where possible, IC_{50} values (inhibitor concentration at which the enzyme is 50% inactivated) were obtained.

The compounds synthesised in Chapter 2 were tested for possible inhibition of DHDPS. Compounds were tested in aqueous solutions at concentrations up to 100 mM, or to the limit of their solubility. However, a number of compounds tested did not dissolve well in aqueous solution and had considerably greater solubility in methanol or DMSO: in these cases the assay was run in 10% methanol or DMSO. In the case of methanol, the reaction rate decreased by approximately 5%, but inhibition could still be quantified by placing methanol in the control incubations for comparison. DMSO did not appear to affect the rate at all, however it was placed in all control incubations.

4.9.1 DHDPS Inhibitor Screen of Nitrogen Containing Heterocyclic Compounds

A preliminary screen of designed and known DHDPS inhibitors yielded some interesting results. Dipicolinic acid **18** is a known inhibitor of DHDPS. Couper *et al.*⁸ report an IC_{50} value of 1.2 mM (imidazole assay) whilst Karsten⁹ reports a K_i of 11 mM versus pyruvate and a K_i of 18 mM versus ASA. The results obtained herein gave an IC_{50} value of 20 mM in close agreement with the results reported by Karsten,⁹ who also used the coupled assay. As

dipicolinic acid **18** is also a competitive inhibitor of DHDPR,¹⁰ increased levels of DHDPR were added to ensure that the DHDPS-catalysed reaction remained the rate limiting step. However, even with additional DHDPR, this inhibitor could not be screened at high concentrations, as biphasic kinetics were observed, consistent with inhibition of both enzymes. The corresponding methyl ester **35** did not inhibit DHDPS.

Furthermore, the piperidine dimethyl ester **40b** has been reported by Couper *et al.*⁸ to have an IC_{50} of 0.7 mM using the imidazole buffer assay, however when **40b** was screened for inhibition using the coupled assay it possessed very little activity: at 50 mM concentration only 10% inhibition of DHDPS was observed. Additionally, the corresponding acid **40a**—which was reported by Couper *et al.*⁸ not to inhibit DHDPS—showed 83% inhibition at 50 mM, yielding an IC_{50} value of 20 mM. Again, this highlights inherent problems with the imidazole assay.

Dimethyl chelidamate **52** was found to inhibit DHDPS by 99% at a concentration of 50 mM and an IC_{50} value of 14 mM was obtained. This was a promising result that required detailed analysis to ascertain the exact nature of inhibition. If **52** is acting as a product-based inhibitor, then it should show competitive inhibition. The corresponding diacid **55** was also screened and at 50 mM, 99% inhibition was observed. An IC_{50} value of 22 mM was obtained, indicating that the acid **55** did not inhibit as strongly as the ester. These results are contrary to those found by Couper *et al.*⁸ who reported that diesters were far better inhibitors than diacids. In order to determine whether **52** or **55** are binding at the active site, further detailed kinetic analyses would be necessary.

Interestingly, the HTHDP mimic **51** showed no inhibition, even at 100 mM concentration. This was an intriguing result as **51** is the closest product mimic designed and was therefore predicted to show the greatest inhibitory activity. This unexpected result poses serious questions as to the true form of the product of the DHDPS-catalysed reaction.

In regard to compounds shown in Figure 4.9.1, no clear inhibitory trends could be ascertained. The pyridine and piperidine diacids appear to be better inhibitors than the corresponding esters as would be expected based on analogy to the reported product, but in contrast to the literature results of Couper *et al.*⁸ However, the chelidamic ester **52** proved to be a better inhibitor than the corresponding acid **55**. Chelidamic acid **55** possesses

approximately the same IC_{50} value as dipicolinic acid **18**, indicating that the introduction of functionality at the C-4 position does not result in increased inhibitory activity. The most striking result from the preliminary screen was that compound **51**, possessing 4-OH functionality in the piperidine ring showed no inhibition of DHDPS whatsoever. However, these results do raise some interesting questions. Firstly, if HTHDP is the true product of the enzyme-catalysed reaction, it seems strange that introducing functionality at the C-4 position diminishes the potency of the inhibition. Secondly, if, as presumed by Couper *et al.*⁸, these so-called product analogues are binding at the active site, why are di-esters often more potent than the corresponding diacids? These questions prompted a detailed investigation as to the mode of inhibition of these compounds, in order to establish whether they were binding at the active site (see section 4.11 and 4.12).

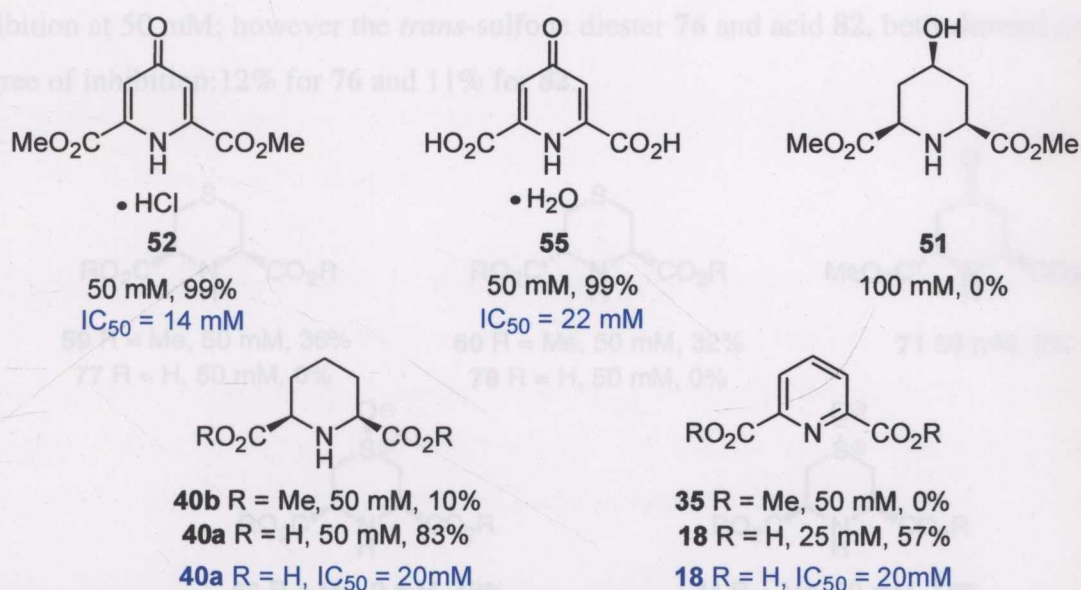


Figure 4.9.1: Nitrogen Containing Heterocyclic Inhibitors of DHDPS: Percent Inhibition of DHDPS Activity at Stated Concentration, [pyruvate]=1.0 mM and [ASA]=1.0 mM.

4.9.2 DHDPS Inhibitor Screen of Sulfur Containing Heterocyclic Compounds

Numerous sulfur-containing heterocyclic compounds were comprehensively screened as potential DHDPS inhibitors. The *cis*-substituted diester **59** is very similar in structure to **40b** and also possessed similar inhibitory activity (36% inhibition at 50 mM). Surprisingly, the diacid **77** showed no inhibition at all, whereas **40a** was a significantly better inhibitor than the ester **40b**. The *trans*-substituted compounds **60** and **78** exhibited similar inhibitory activity to **59** and **77**, in contrast to the reported result that *cis*-compounds are better inhibitors of DHDPS.⁸

The introduction of a C-4 oxygen substituent led to increased inhibition in only one case, the all *syn*-sulfoxide **53**, with 50% inhibition occurring at 9 mM. The epimeric *anti*-sulfoxide **74** showed only 48% inhibition at 30 mM. The corresponding acids **79** and **80** did not display any inhibition.

4.9.2 Inhibition Kinetics

The *trans* sulfoxide **71** did not inhibit DHDPS, even at high concentrations (50 mM). This result is not surprising, as the X-ray crystal structure of **71** (see chapter 2, Figure 2.3.3) shows that both the C-4 oxygen and one of the methoxy carbonyl groups occupy axial positions, whereas the product HTHDP **17** is expected to possess *pseudo*-equatorial substituents at these positions.

Interestingly the *cis*-sulfone diester **54** showed no inhibition but the diacid **81** showed 14% inhibition at 50 mM; however the *trans*-sulfone diester **76** and acid **82**, both showed a small degree of inhibition: 12% for **76** and 11% for **82**.

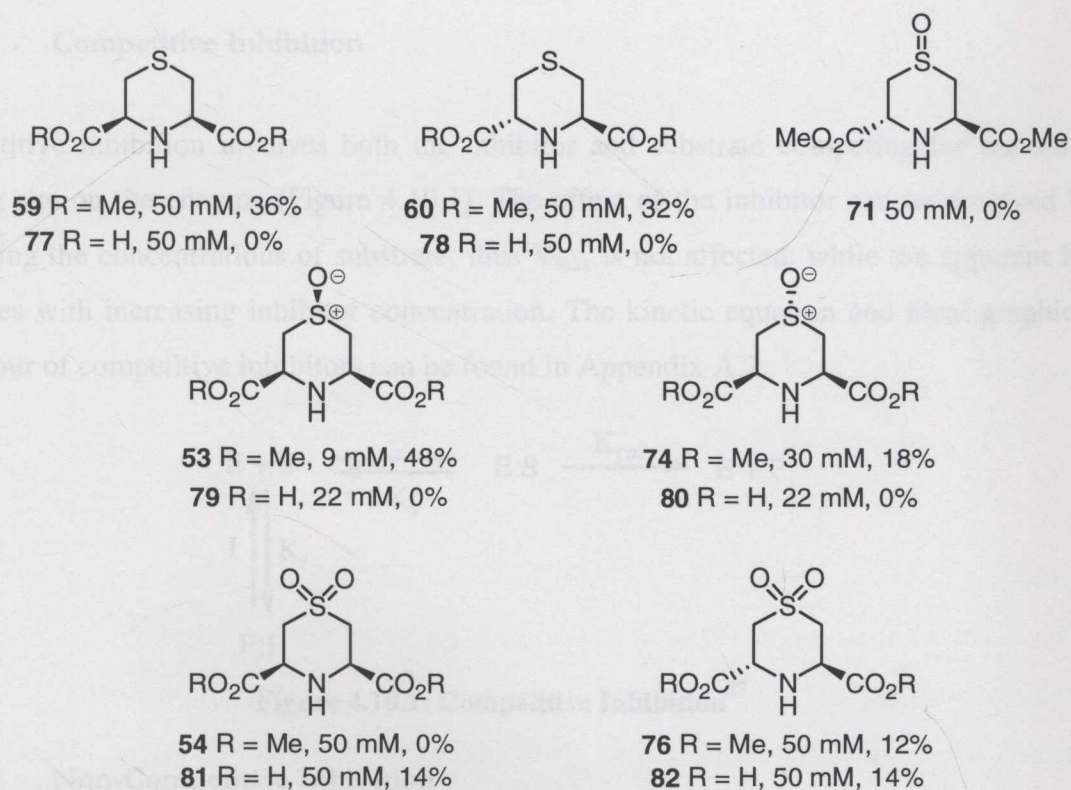


Figure 4.9.2: Sulfur Containing Heterocyclic Inhibitors of DHDPS: Percent Inhibition of DHDPS Activity at Stated Concentration, [pyruvate]=1.0 mM and [ASA]=1.0 mM.

From the preliminary screening results, no trends linking either the stereochemical requirements at the C-2 and C-6 positions, the activity of the acids versus esters, or the level of oxidation at the sulfur to the level of inhibition could be ascertained. Many of the trends

seen by Couper *et al.*⁸ utilising the imidazole buffer assay were not observed when using the coupled assay. It is possible that inherent flaws in the imidazole buffer assay are responsible for the lack of correlation between the two assay systems.

4.10 Inhibition Kinetics

4.10.1 Introduction

In order to establish if any of the inhibitors showed competitive inhibition a more detailed kinetic analysis was necessary. Compounds **52** and **55** were chosen for further analysis for two reasons: firstly, both compounds showed reasonable activity in the preliminary DHDPS screen and were available in sufficient quantities for detailed kinetic analysis; secondly, to ascertain whether compounds containing methyl esters (as in compound **52**) are competitive inhibitors of DHDPS.

4.10.2 Competitive Inhibition

Competitive inhibition involves both the inhibitor and substrate competing for the same binding site on the enzyme (Figure 4.10.1). The effect of the inhibitor can be removed by increasing the concentrations of substrate; thus V_{\max} is not affected, while the apparent K_m increases with increasing inhibitor concentration. The kinetic equation and ideal graphical behaviour of competitive inhibitors can be found in Appendix A.2.

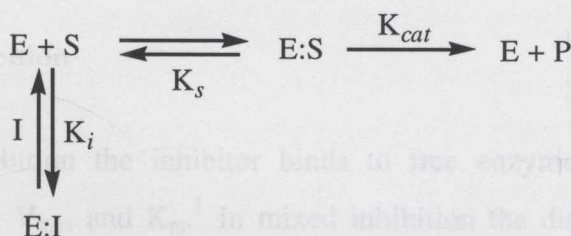


Figure 4.10.1: Competitive Inhibition²⁷

4.10.3 Non-Competitive Inhibition

Non-competitive inhibition involves the inhibitor binding to a site on the enzyme distant from the active site, altering catalysis but not substrate binding (Figure 4.10.2). As such, the V_{\max} is decreased, but the K_m remains constant with increasing inhibitor concentration. In non-competitive inhibition, the dissociation constant of S from ESI is the same as that from

ES. The kinetic equation and ideal graphical behaviour of non-competitive inhibitors can be found in Appendix A.2.

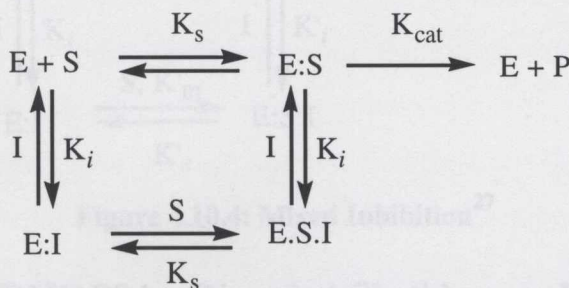


Figure 4.10.2: Non-competitive Inhibition²⁷

4.10.4 Uncompetitive Inhibition

In contrast, in uncompetitive inhibition, the inhibitor only binds to the enzyme-substrate complex, and as such affects both the V_{max} and K_m values by decreasing them with increasing inhibitor concentrations (Figure 4.10.3). The kinetic equation and ideal graphical behaviour of uncompetitive inhibitors can be found in Appendix A.2.

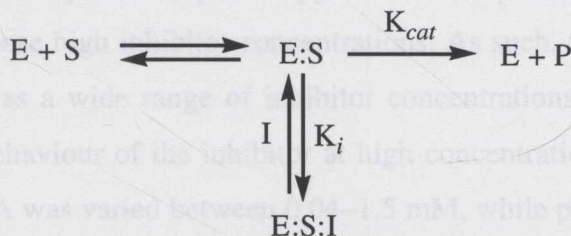
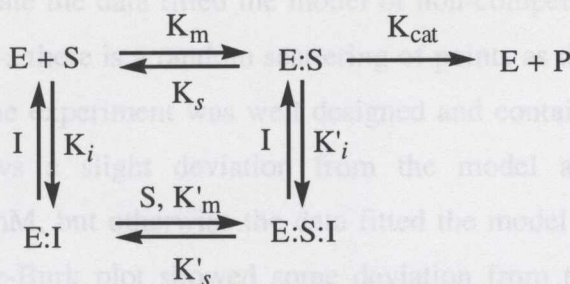


Figure 4.10.3: Uncompetitive Inhibition²⁷

4.10.5 Mixed Inhibition

Finally, in mixed inhibition the inhibitor binds to free enzyme and enzyme-substrate complex affecting both V_{max} and K_m .¹ In mixed inhibition the dissociation constant of S from ESI is different than that from ES (i.e. $K_s \neq K'_s$) (Figure 4.10.4). The kinetic equation of mixed inhibition can be found in Appendix A.2. Graphically, mixed inhibition kinetic behaviour looks like a mixture of competitive and uncompetitive behaviour, and thus may appear as either a mixture of the two (see Appendix A.2).

Figure 4.10.4: Mixed Inhibition²⁷

4.11 Inhibition of DHDPS by Dimethyl Chelidamate Hydrochloride 52

Inhibition kinetics of dimethyl chelidamate hydrochloride **52** with respect to pyruvate and ASA were run at a range of inhibitor and substrate concentrations. Where possible, the inhibitor concentrations were varied by 0.1 and 10 times the IC_{50} value obtained for the individual inhibitor. Dimethyl chelidamate hydrochloride **52** concentrations were varied between 0–7.5 mM with respect to pyruvate, and 0–15 mM with respect to ASA. At very high concentrations of inhibitor, significant absorbance problems and deviations from linear rates were observed, especially with respect to pyruvate. This precluded the acquisition of accurate initial rates at these high inhibitor concentrations. As such, the data obtained must be interpreted carefully, as a wide range of inhibitor concentrations above the IC_{50} value were not taken, so the behaviour of the inhibitor at high concentrations remains unknown. The concentration of ASA was varied between 0.04–1.5 mM, while pyruvate concentrations were varied between 0.05–2.0 mM. The kinetic data were fitted to mathematical models using the Enzfitter¹⁴ computer program that simulated competitive, non-competitive, uncompetitive and mixed inhibition patterns in order to determine the model of best fit and subsequently the inhibition constant K_i . Lineweaver-Burk (1/rate versus 1/[inhibitor]) and Eadie-Hofstee (rate versus rate/[inhibitor]) were also generated using Enzfitter¹⁴ and provided a graphical analysis of the data obtained.

The inhibition was found to be non-competitive with respect to both substrates, pyruvate and ASA. The K_i with respect to pyruvate was found to be 6.90 ± 0.82 mM, while the K_i with respect to ASA was found to be 14.0 ± 1.43 mM. The result that dimethyl chelidamate hydrochloride **52** is a non-competitive inhibitor with respect to both substrates is very significant, in that it demonstrates that the inhibitory effects observed are due to allosteric binding rather than binding at the active site.

With respect to pyruvate the data fitted the model of non-competitive inhibitory behaviour well. In Figure 4.11.1-a there is a random scattering of points as determined by the residual plot, indicating that the experiment was well designed and contained no systematic errors. Figure 4.11.1-b shows a slight deviation from the model at the highest inhibitory concentration of 7.5 mM, but otherwise the data fitted the model well with an R^2 value of 0.97. The Lineweaver-Burk plot showed some deviation from the line of best fit at the highest inhibitor concentration, which is exaggerated in this analysis, as discussed previously (section 4.6). In the Eadie-Hofstee plot (Figure 4.11.-d) some deviations from the line of best fit at high inhibitor concentration were also observed. In general, the data fitted the lines of best fit loosely, but the Eadie-Hofstee plot distinctly showed parallel lines, indicative of a non-competitive inhibitor.

With respect to ASA the data also fitted the model well. In Figure 4.11.2-a there is a random scattering of points as determined by the residual plot confirming the absence of systematic errors. Figure 4.11.2-b shows a slight deviation from the model at the highest inhibitory concentration of 15 mM, but otherwise the data fitted the model well with an R^2 value of 0.96. The Lineweaver-Burk plot (Figure 4.11.2-c) showed some deviation from the line of best fit at the highest inhibitor concentration, as shown in the fitted model; this is further exaggerated in the Lineweaver-Burk plot. In the Eadie-Hofstee plot (Figure 4.11.2-d) some deviations from the line of best fit at high inhibitor concentration were also observed. In general, the data fitted the lines of best fit with the Eadie-Hofstee plot distinctly showing parallel lines, indicative of a non-competitive inhibitor.

Figure 4.11.1: DHDPS Kinetics with Respect to Pyruvate at Different Concentrations of Diamethyl Chelidamate Hydrochloride; a) Residual Plot b) Raw Data with Fitted Model c) Lineweaver-Burk Plot ($R^2 = 0.97$, $P < 0.05$) d) Eadie-Hofstee Plot ($R^2 = 0.97$, $P < 0.05$)

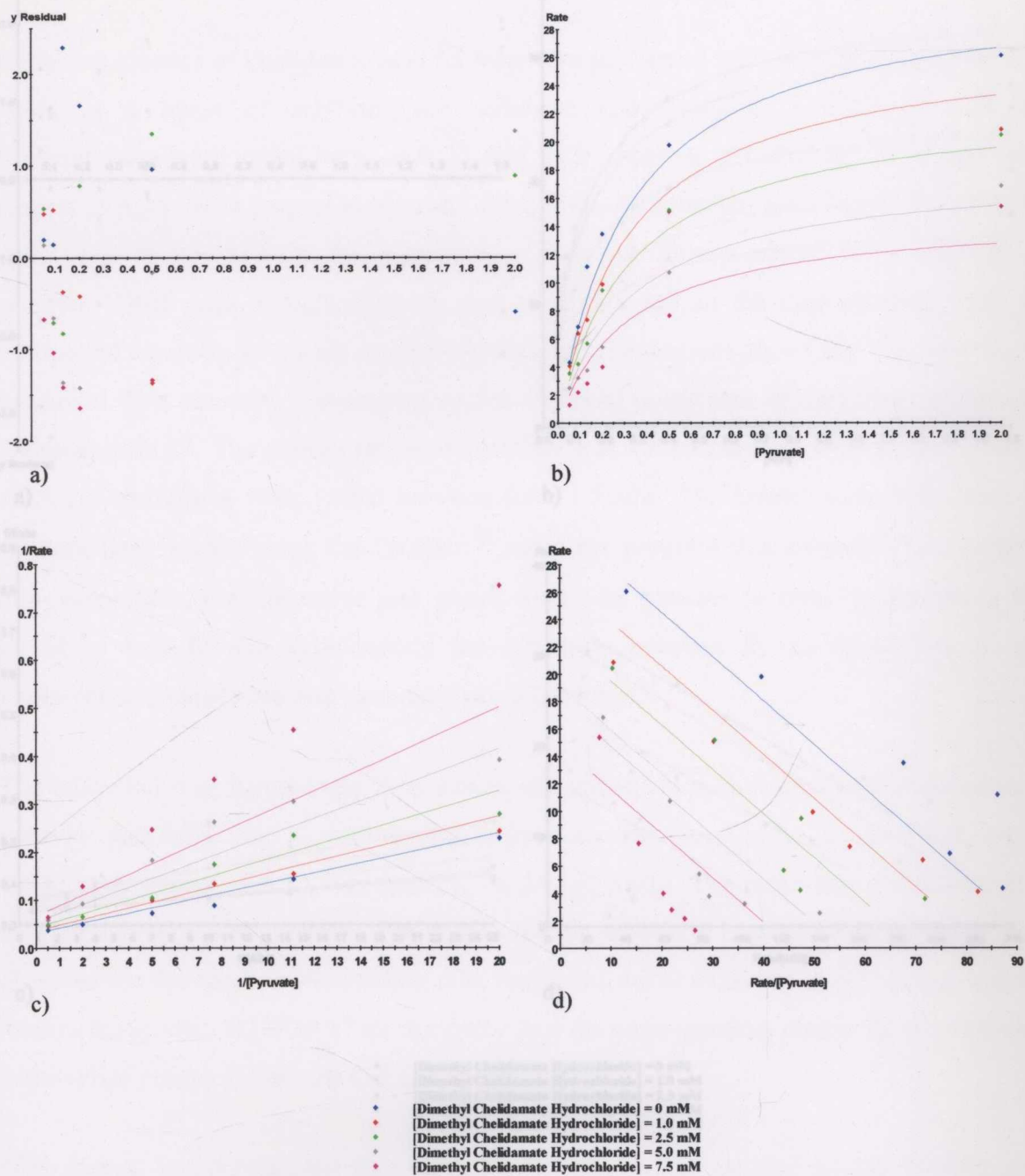


Figure 4.11.2: DHDPS Kinetics with Respect to ASA at Different Concentrations of Dimethyl

Figure 4.11.1: DHDPS Kinetics with Respect to Pyruvate at Different Concentrations of Dimethyl Chelidamate Hydrochloride; a) Residuals Plot b) Raw Data with Fitted Model c) Lineweaver-Burk Plot ($R^2 = 0.97$, $P < 0.05$) d) Eadie-Hofstee Plot ($R^2 = 0.97$, $P < 0.05$).

4.12 Inhibition of DHDPS by Chelidamic Acid 55

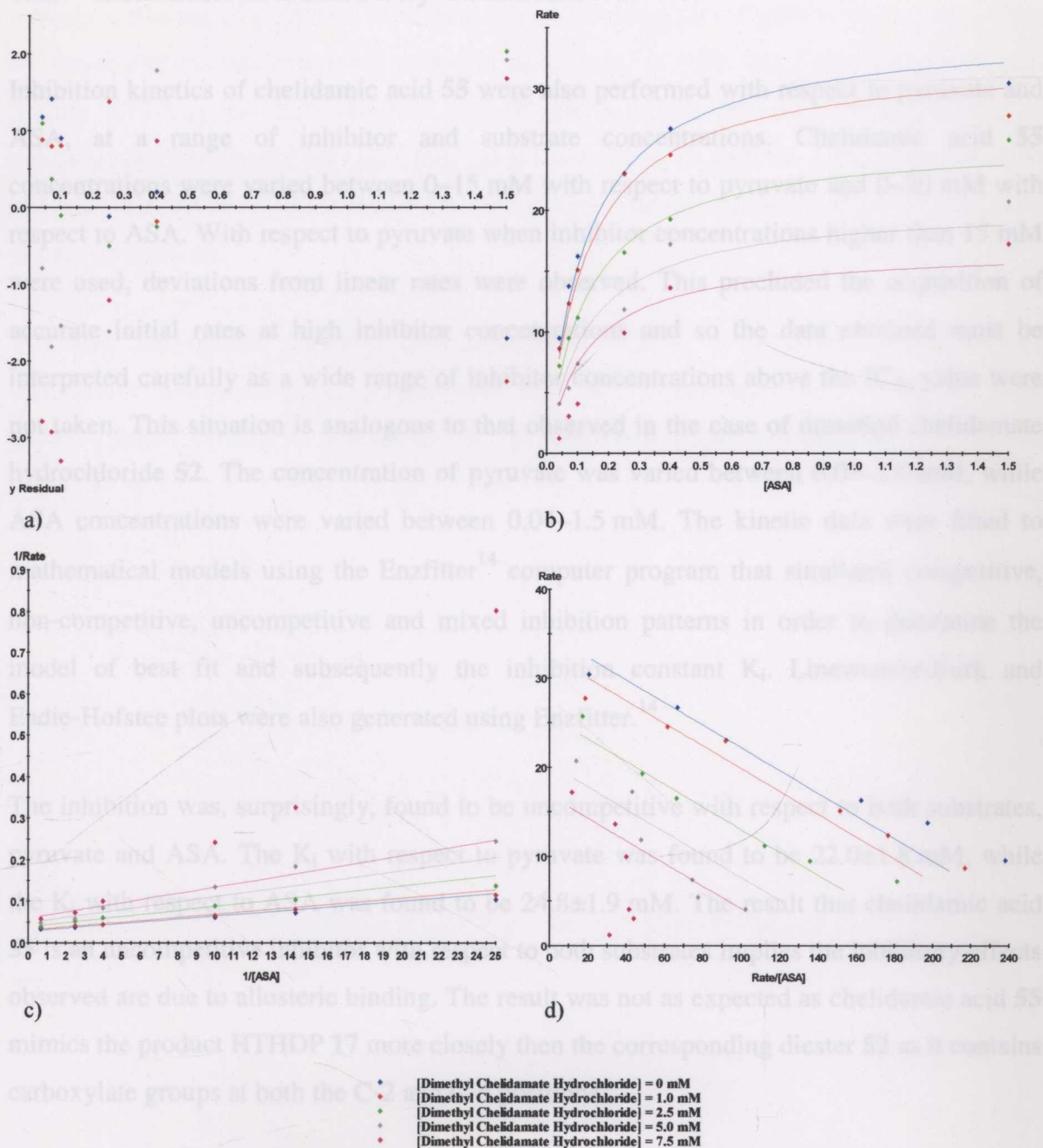


Figure 4.11.2: DHDPS Kinetics with Respect to ASA at Different Concentrations of Dimethyl Chelidamate Hydrochloride; a) Residuals Plot b) Raw Data with Fitted Model c) Lineweaver-Burk Plot ($R^2 = 0.96$, $P < 0.05$) d) Eadie-Hofstee Plot ($R^2 = 0.96$, $P < 0.05$).

4.12 Inhibition of DHDPS by Chelidamic Acid 55

Inhibition kinetics of chelidamic acid **55** were also performed with respect to pyruvate and ASA, at a range of inhibitor and substrate concentrations. Chelidamic acid **55** concentrations were varied between 0–15 mM with respect to pyruvate and 0–20 mM with respect to ASA. With respect to pyruvate when inhibitor concentrations higher than 15 mM were used, deviations from linear rates were observed. This precluded the acquisition of accurate initial rates at high inhibitor concentrations and so the data obtained must be interpreted carefully as a wide range of inhibitor concentrations above the IC_{50} value were not taken. This situation is analogous to that observed in the case of dimethyl chelidamate hydrochloride **52**. The concentration of pyruvate was varied between 0.05–2.0 mM, while ASA concentrations were varied between 0.04–1.5 mM. The kinetic data were fitted to mathematical models using the Enzfitter¹⁴ computer program that simulated competitive, non-competitive, uncompetitive and mixed inhibition patterns in order to determine the model of best fit and subsequently the inhibition constant K_i . Lineweaver-Burk and Eadie-Hofstee plots were also generated using Enzfitter.¹⁴

The inhibition was, surprisingly, found to be uncompetitive with respect to both substrates, pyruvate and ASA. The K_i with respect to pyruvate was found to be 22.0 ± 1.8 mM, while the K_i with respect to ASA was found to be 24.8 ± 1.9 mM. The result that chelidamic acid **55** is an uncompetitive inhibitor with respect to both substrates implies the inhibitory effects observed are due to allosteric binding. The result was not as expected as chelidamic acid **55** mimics the product HTHDP **17** more closely than the corresponding diester **52** as it contains carboxylate groups at both the C-2 and C-6 positions.

With respect to pyruvate, the data fitted the model of uncompetitive inhibitory behaviour well. In Figure 4.12.1-a, there is once again a random scattering of points. Figure 4.12.1-b shows a slight deviation from the model at the highest inhibitory concentration of 15 mM, but otherwise the data fitted the model very well with an R^2 value of 0.98. The Lineweaver-Burk plot (Figure 4.12-c) showed a tight grouping of points around the lines of best fit, as did the more demanding Eadie-Hofstee treatment (Figure 4.12.-d). In general, the data fitted the lines of best fit well, with the Eadie-Hofstee plot distinctly showing convergent lines of best fit with the x-axis, indicative of an uncompetitive inhibitor.

With respect to ASA the data also fitted the model well. In Figure 4.12.2-a there is a random scattering of points as determined by the residual plot. Figure 4.12.2-b shows that the model fits the data extremely well with an R^2 value of 0.99. The Lineweaver-Burk plot (Figure 4.12.2-c) and Eadie-Hofstee plot (Figure 4.12.2-d) showed a tight grouping of points around the lines of best fit. Convergent lines of best fit with the x-axis were obtained in the Eadie-Hofstee plot, indicative of an uncompetitive inhibitor as was the case with respect to pyruvate.

The fact that neither dimethyl ester chelidamate **52** or chelidamic acid **55** showed competitive inhibition poses serious questions as to the nature of binding of these compounds and further, casts doubt on the true form of the product of the DHDPS catalysed reaction.

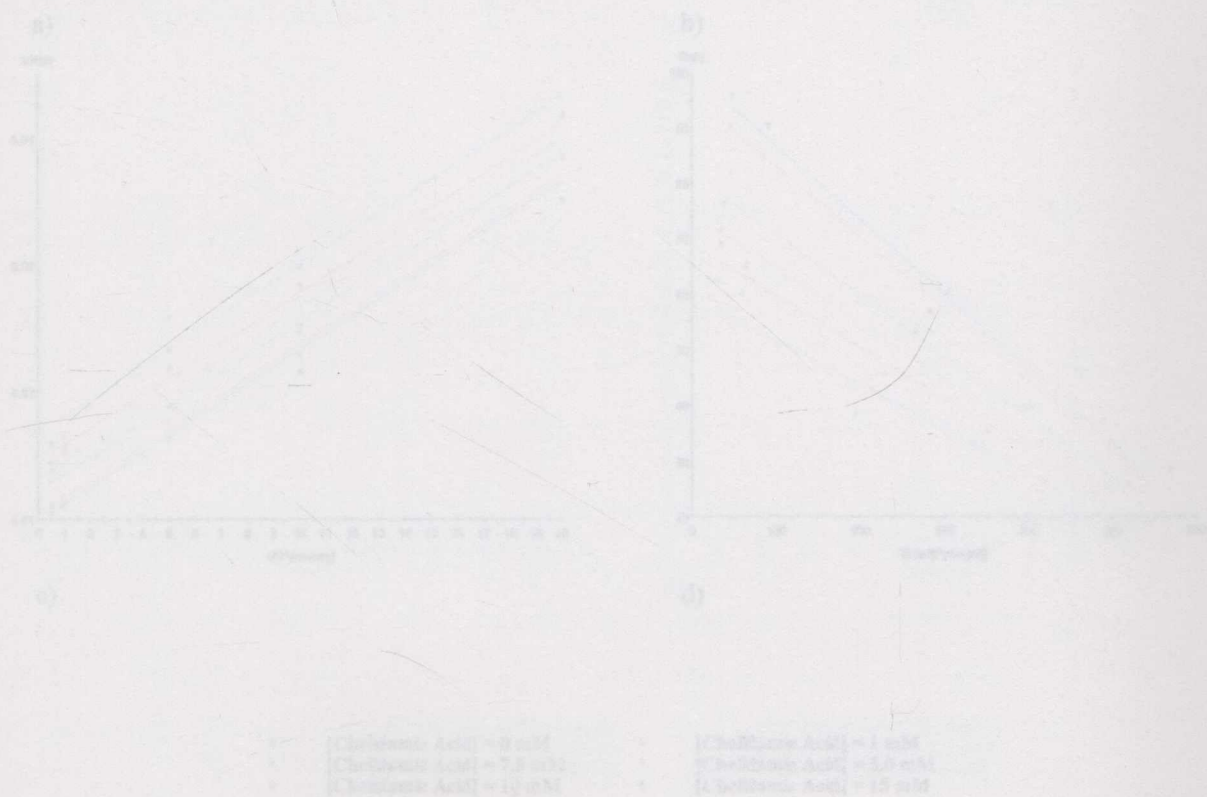


Figure 4.12.1: DHDPS Kinetics with Respect to Pyruvate at Different Concentrations of Chelidamic Acid; a) Residual Plot b) Raw Data with Fitted Model c) Lineweaver-Burk Plot ($R^2 = 0.99$, $P < 0.05$) d) Eadie-Hofstee Plot ($R^2 = 0.99$, $P < 0.05$).

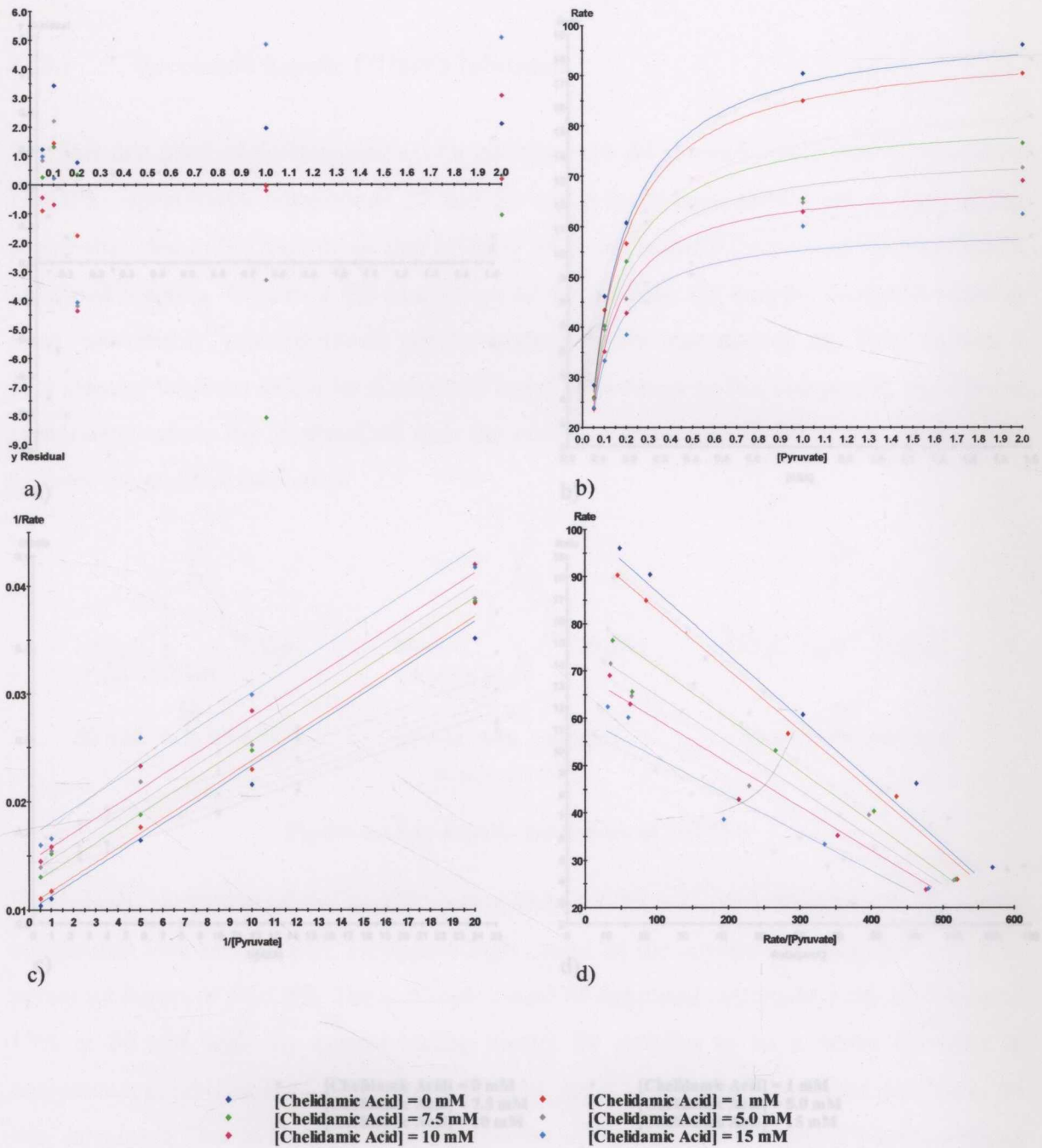


Figure 4.12.1: DHDPS Kinetics with Respect to Pyruvate at Different Concentrations of Chelidamic Acid; a) Residuals Plot b) Raw Data with Fitted Model c) Lineweaver-Burk Plot ($R^2 = 0.98$, $P < 0.05$) d) Eadie-Hofstee Plot ($R^2 = 0.98$, $P < 0.05$).

4.13 Acyclic Inhibitors of DHDPS

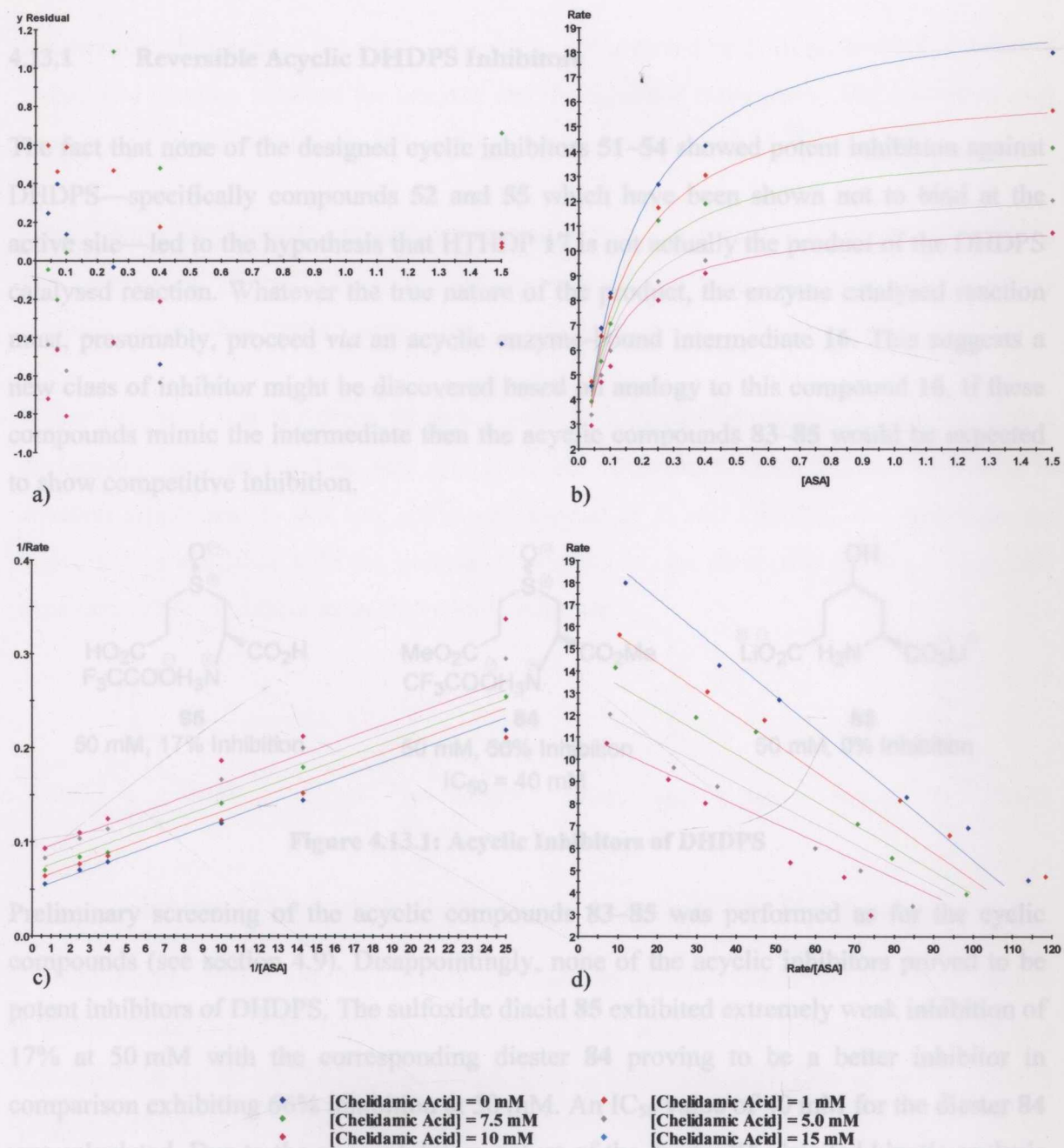


Figure 4.12.2: DHDPS Kinetics with Respect to ASA at Different Concentrations of Chelidamic Acid; a) Residuals Plot b) Raw Data with Fitted Model c) Lineweaver-Burk Plot ($R^2 = 0.99$, $P < 0.05$) d) Eadie-Hofstee Plot ($R^2 = 0.99$, $P < 0.05$).

4.13 Acyclic Inhibitors of DHDPS

4.13.1 Reversible Acyclic DHDPS Inhibitors

The fact that none of the designed cyclic inhibitors **51–54** showed potent inhibition against DHDPS—specifically compounds **52** and **55** which have been shown not to bind at the active site—led to the hypothesis that HTHDP **17** is not actually the product of the DHDPS catalysed reaction. Whatever the true nature of the product, the enzyme catalysed reaction must, presumably, proceed *via* an acyclic enzyme-bound intermediate **16**. This suggests a new class of inhibitor might be discovered based on analogy to this compound **16**. If these compounds mimic the intermediate then the acyclic compounds **83–85** would be expected to show competitive inhibition.

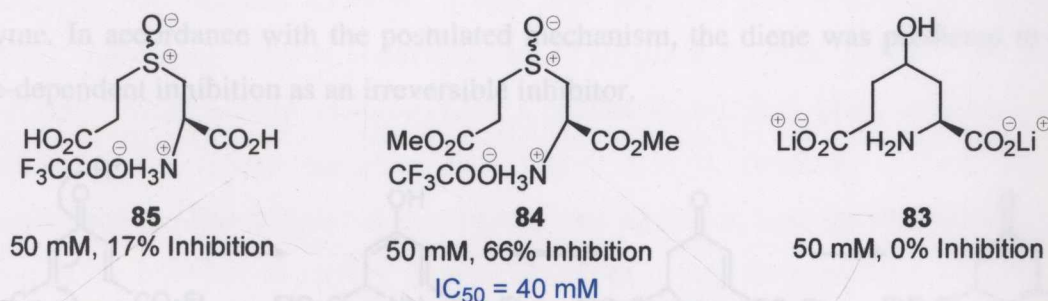


Figure 4.13.1: Acyclic Inhibitors of DHDPS

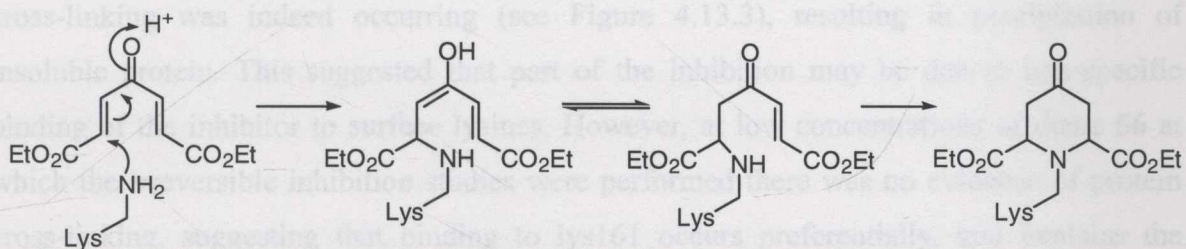
Preliminary screening of the acyclic compounds **83–85** was performed as for the cyclic compounds (see section 4.9). Disappointingly, none of the acyclic inhibitors proved to be potent inhibitors of DHDPS. The sulfoxide diacid **85** exhibited extremely weak inhibition of 17% at 50 mM with the corresponding diester **84** proving to be a better inhibitor in comparison exhibiting 66% inhibition at 50 mM. An IC_{50} value of 40 mM for the diester **84** was calculated. Due to the poor inhibitory nature of the diester **84**, detailed kinetic analysis was precluded, due to the large amount of compound needed and solubility problems at high concentrations. The acyclic alcohol **83** showed no inhibition whatsoever.

4.13.2 Irreversible Acyclic Inhibitors of DHDPS

Irreversible inhibition, as the name suggests, is not reversed by dialysis or dilution because a chemical reaction between the enzyme and the inhibitor takes place. The inhibition may take time to manifest itself, because a chemical reaction is involved.²⁸

Concurrent with the study of potential reversible cyclic and acyclic inhibitors of DHDPS, two compounds **56** and **87** synthesised *en route* to designed inhibitors were tested as potential irreversible DHDPS inhibitors.

It was proposed that the diene **56** could undergo a double Michael-type addition with a nucleophile such as the lone pair on lysine-161 (Scheme 4.13.1). This would result in covalent attachment to this key active site residue of *E. coli* DHDPS, and inactivate the enzyme. In accordance with the postulated mechanism, the diene was predicted to exhibit time-dependent inhibition as an irreversible inhibitor.



Scheme 4.13.1: Proposed Double Michael Addition of Diene **56** with Lysine

Pre-incubation studies with the DHDPS and diene **56** in buffer confirmed that diene **56** was a potent inhibitor of DHDPS. After four minutes the activity was diminished by 50% at a concentration of 50 μM and by ten minutes the activity was only 15% of native DHDPS (Figure 4.13.2).

To confirm whether the inhibition was irreversible, DHDPS was incubated with diene **56** in buffer for 30 minutes followed by dialysis for 16 hours against Tris buffer (20 mM, pH 8.0 at 4 °C). No recovery of activity was observed. Controls in which DHDPS was incubated and dialysed, in the absence of inhibitor showed DHDPS retained its activity under these conditions. Thus diene **56** was shown to be an irreversible inhibitor of DHDPS.

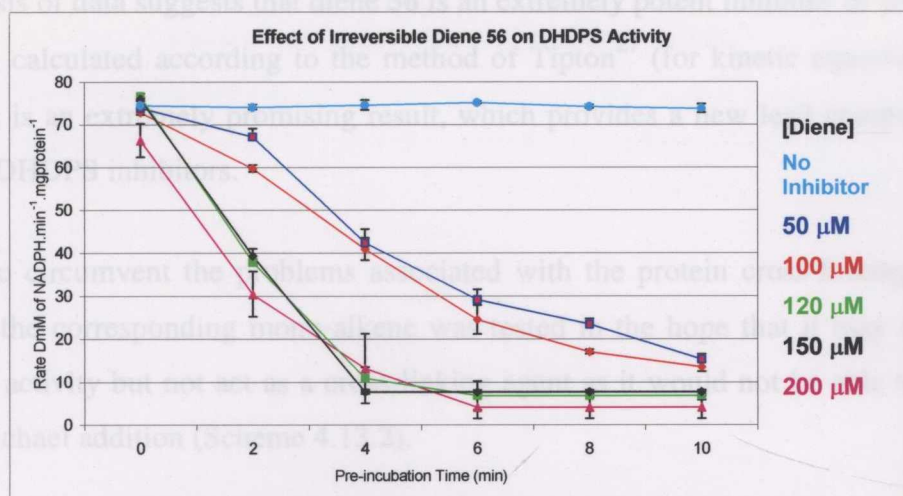


Figure 4.13.2: Effect of Diene 56 on DHDPS Activity

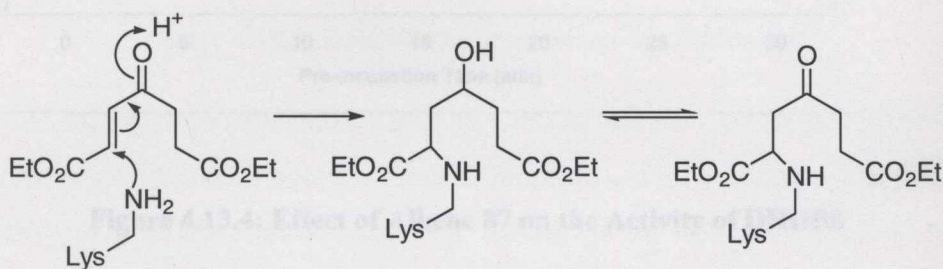
At high concentrations of diene, precipitation in the cuvette was observed. As the diene **56** can undergo two Michael additions it was predicted that protein cross-linking may be occurring. Incubating various concentrations of inhibitor **56** with DHDPS, followed by SDS-PAGE visualised by staining with Commassie brilliant blue, indicated protein cross-linking was indeed occurring (see Figure 4.13.3), resulting in precipitation of insoluble protein. This suggested that part of the inhibition may be due to non-specific binding of the inhibitor to surface lysines. However, at low concentrations of diene **56** at which the irreversible inhibition studies were performed there was no evidence of protein cross-linking, suggesting that binding to lys161 occurs preferentially, and explains the potent inhibition observed.



Figure 4.13.3: SDS-PAGE of DHDPS Incubated with Diene 56: LANE A: Sigmamarker wide molecular range, molecular weights of the bands are (from top) 205, 116, 97, 84, 66, 55, 45, 36, 29, 24, 20, 10.2 kDa; LANE B: [Diene] = 0 mM; LANE C: [Diene] = 10 mM; LANE D: [Diene] = 100 mM; LANE E: [Diene] = 5 mM; LANE F: [Diene] = 50 mM; LANE G: [Diene] = 10 mM; LANE H: [Diene] = 100 mM; LANE I: [Diene] = 5 mM; LANE J: [Diene] = 50 mM; N.B. LANES C-F incubated for 10 min and LANES G-J incubated for 30 min.

The analysis of data suggests that diene **56** is an extremely potent inhibitor of with a k_{inact} of $42 \text{ M}^{-1} \cdot \text{s}^{-1}$, calculated according to the method of Tipton²⁷ (for kinetic equations used see A.2). This is an extremely promising result, which provides a new lead compound for the design of DHDPS inhibitors.

In order to circumvent the problems associated with the protein cross-linking activity of diene **56**, the corresponding mono-alkene was tested in the hope that it may show potent inhibitory activity but not act as a cross-linking agent as it would not be able to undergo a second Michael addition (Scheme 4.13.2).



Scheme 4.13.2: Proposed Michael Addition of Alkene **87** with Lysine

Subsequent pre-incubation studies showed the alkene to be a moderate irreversible inhibitor of DHDPS. It can be seen clearly in Figure 4.13.4 that the activity was only 50% that of native DHDPS at 25 mM after fifteen minutes and that by 25 minutes the activity is only 10% that of native DHDPS. Compared with diene **56** the alkene **87** is not as potent and takes considerably more time to inhibit DHDPS.

Incubation of DHDPS with alkene **87** in buffer for 30 minutes followed by dialysis for 16 hours against Tris buffer (20 mM, pH 8.0 at 4 °C) did not show a return in activity when compared to controls, indicating that the alkene **87** does indeed act as an irreversible inhibitor. At high concentrations of alkene precipitation in the cuvette was observed as was the case with the diene **56**. However, incubating various concentrations of inhibitor **87** with DHDPS, followed by SDS-PAGE visualised by staining with Commassie brilliant blue, did not show any protein cross-linking (data not shown).

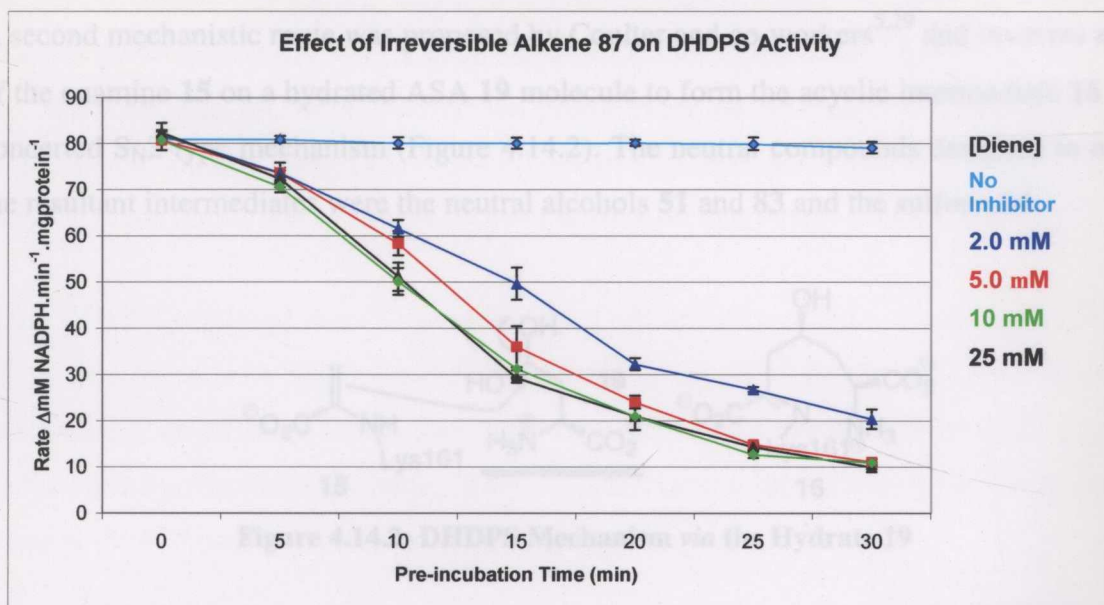


Figure 4.13.4: Effect of Alkene 87 on the Activity of DHDPS

4.14 Mechanistic Implications of DHDPS Inhibitor Studies

At the outset of this work there were two proposed mechanisms for the formation of HTHDP.

The first proposed mechanism of DHDPS involves the nucleophilic addition of the enamine **15** on ASA **8** to generate the corresponding enzyme-bound alkoxide, which must then be protonated, yielding the acyclic intermediate **16** (Figure 4.14.1). The sulfoxide compounds **53,84,85** were designed based on this mechanism, with the charge separation of the sulfoxides mimicking the charge separation as the enamine attacks the aldehyde.

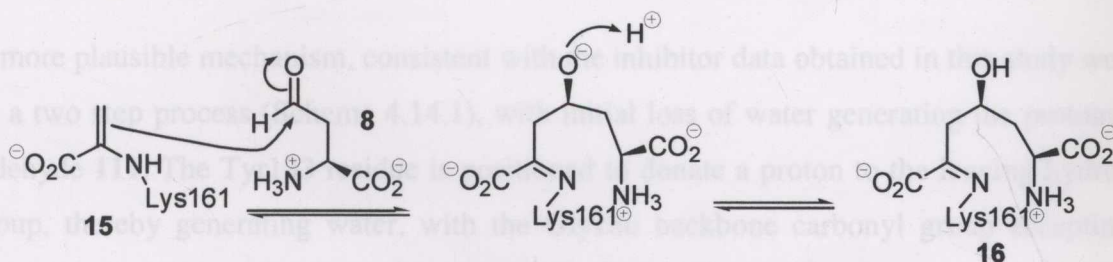


Figure 4.14.1: DHDPS Mechanism via the Aldehyde 8

A second mechanistic route was proposed by Coulter and co-workers^{5,29} and involves attack of the enamine **15** on a hydrated ASA **19** molecule to form the acyclic intermediate **16** via a concerted S_N2-type mechanism (Figure 4.14.2). The neutral compounds designed to mimic the resultant intermediates were the neutral alcohols **51** and **83** and the sulfone **54**.

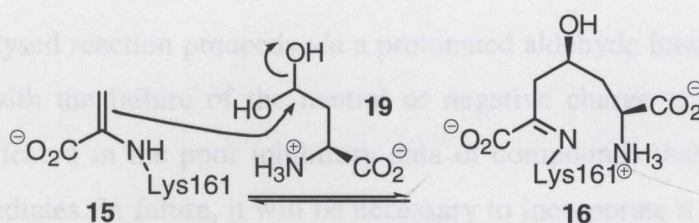


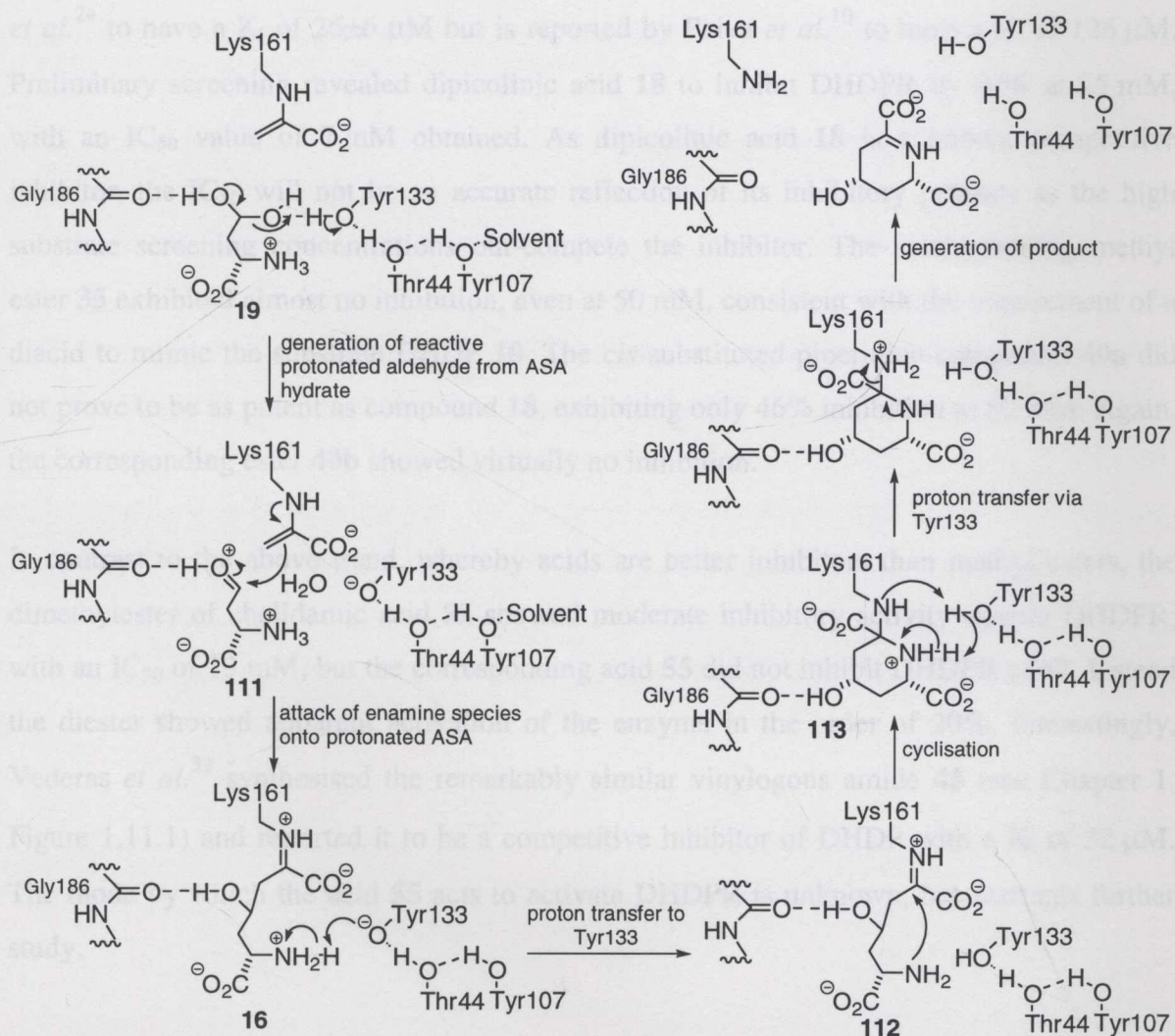
Figure 4.14.2: DHDPS Mechanism via the Hydrate **19**

The results obtained from the inhibitor studies showed that none of these compounds with a negative charge or neutral charge were potent inhibitors, with the neutral alcohols showing no inhibition of DHDPS whatsoever. The results of the inhibitor studies prompted a re-investigation into the mechanism of DHDPS. An examination of the X-ray crystallographic analysis of the *E. coli* enzyme with various inhibitors and substrate analogues bound in the active site showed the C-4 oxygen situated close to the backbone carbonyl oxygen of Gly186 and the Lys161-derived imine/enamine nitrogen.³⁰ This was previously interpreted by Blickling *et al.*³⁰ that protonation of the was via the protonated imine. Although this group is within hydrogen-bonding distance (2.8 Å), geometric and stereoelectronic factors preclude a concerted reaction in which proton transfer occurs simultaneously with C-C bond formation. Proton transfer from the protonated imine to the naked alkoxide could only occur subsequent to C-C bond formation, though it is noted in the reported crystal structure the imine proton is directed away from the C-4 oxygen atom.

A more plausible mechanism, consistent with the inhibitor data obtained in this study would be a two step process (Scheme 4.14.1), with initial loss of water generating the protonated aldehyde **111**. The Tyr133 residue is positioned to donate a proton to the leaving hydroxyl group, thereby generating water, with the Gly186 backbone carbonyl group accepting a hydrogen bond from the other hydroxyl group of the hydrate. The Thr44 residue has been shown to be essential for full activity of DHDPS, with Tyr133, Thr44 and Tyr107 proposed to be involved in a proton shuttle between the active site and solvent.³¹ An alternative interpretation is that the extensive hydrogen-bonding network of these residues stabilises

the Tyr133 anion. The second step of this process then involves attack of the enamine **15** onto the protonated ASA **111** to form the acyclic intermediate **16**. The Tyr133 anion (or proton shuttle network) then abstracts the proton from the ASA-derived ammonium group to generate a neutral amine **112**, which effects transimination/cyclisation yielding **113**. The Tyr133 is also implicated in further proton transfers between the two nitrogens.

If the DHDPS-catalysed reaction proceeds *via* a protonated aldehyde intermediate **111**, then this is consistent with the failure of the neutral or negative charge at C-4 to mimic the intermediate, as reflected in the poor inhibitory data of compounds that were designed to mimic such intermediates. In future, it will be necessary to incorporate a positively charged group at the C-4 position to mimic, the positively charge intermediate.



Scheme 4.14.1: Proposed DHDPS Mechanism *via* a Protonated Aldehyde Intermediate 111

4.15 Preliminary Compound Screening of DHDPR inhibitors

4.15.1 DHDPR Inhibitor Screen of Nitrogen Containing Heterocycles

Although the designed product-based inhibitors of DHDPS did not prove to be potent DHDPS inhibitors they were also screened as potential substrate based inhibitors of DHDPR. Preliminary screening assays were performed as for DHDPS (section 4.9), but with the assay conditions reversed so the rate-limiting step was the DHDPR-catalysed reaction.

Dipicolinic acid is a known competitive inhibitor of DHDP. It has been reported by Reddy *et al.*²⁴ to have a K_i of $26 \pm 6 \mu\text{M}$ but is reported by Paiva *et al.*¹⁰ to have a K_i of $126 \mu\text{M}$. Preliminary screening revealed dipicolinic acid **18** to inhibit DHDPR by 93% at 25 mM, with an IC_{50} value of 7 mM obtained. As dipicolinic acid **18** is a known competitive inhibitor, the IC_{50} will not be an accurate reflection of its inhibitory potency as the high substrate screening concentrations out-compete the inhibitor. The corresponding methyl ester **35** exhibited almost no inhibition, even at 50 mM, consistent with the requirement of a diacid to mimic the substrate DHDP **10**. The *cis*-substituted piperidine compound **40a** did not prove to be as potent as compound **18**, exhibiting only 46% inhibition at 50 mM. Again, the corresponding ester **40b** showed virtually no inhibition.

In contrast to the above trend, whereby acids are better inhibitors than methyl esters, the dimethylester of chelidamic acid **52** showed moderate inhibitory activity against DHDPR, with an IC_{50} of 13 mM, but the corresponding acid **55** did not inhibit DHDPR at all. Instead the diester showed apparent activation of the enzyme in the order of 20%. Interestingly, Vederas *et al.*³² synthesised the remarkably similar vinylogous amide **45** (see Chapter 1, Figure 1.11.1) and reported it to be a competitive inhibitor of DHDP with a K_i of $32 \mu\text{M}$. The mode by which the acid **55** acts to activate DHDPR is unknown, but warrants further study.

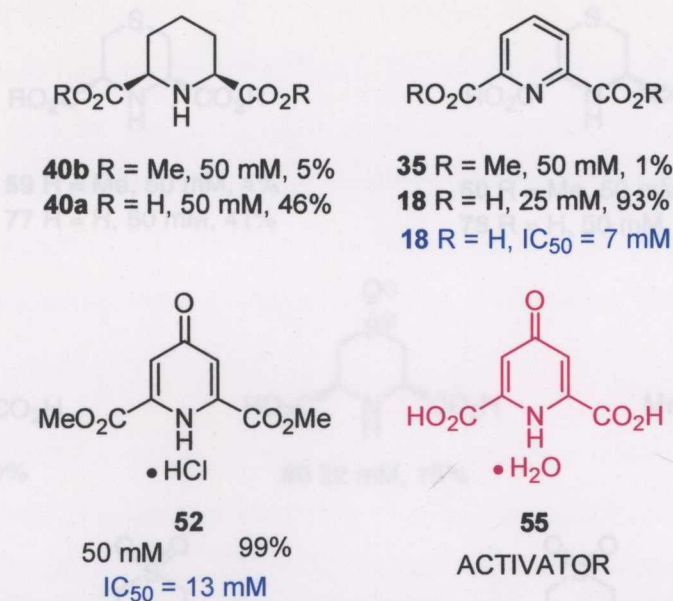


Figure 4.15.1: Nitrogen Containing Heterocyclic Inhibitors of DHDPR: Percent Inhibition of DHDPR Activity at the Stated Concentration, [DHDPR]=1.0 mM.

4.15.2 DHDPR Inhibitor Screen of Sulfur Containing Heterocycles Compounds

Diacids **77** and **78** showed more potent inhibition than the corresponding diesters **59** and **60**, respectively, although the inhibition was quite weak. The *trans*-sulfoxide **71** showed no inhibition at 50 mM. The *anti*-sulfoxide **80** showed 15% inhibition at 22 mM, more potent than the epimeric *syn*-sulfoxide **79**, which showed only 10% inhibition at 22 mM. The *trans*-sulfone diacid **82** was a significantly better inhibitor of DHDPR, compared with the corresponding diester **76**. Similarly, the *cis*-sulfone diester **54** showed very weak inhibition of only 15% at 50 mM. As per the DHDPS inhibitors, inclusion of functionality at the C-4 position did not appear to increase the inhibitory potency. In general, however, the diacids were more potent inhibitors than the corresponding esters: with one exception the diester **52**.

As for DHDPS studies (section 4.11 and 4.12), the kinetic data were fitted to mathematical models using the Enzfitter[®] computer program that simulated competitive, non-competitive, uncompetitive and mixed inhibition patterns to determine the model of best fit and subsequently the inhibition constant K_i . Lineweaver-Burk and Hanes-Haas plots were also generated using Enzfitter.

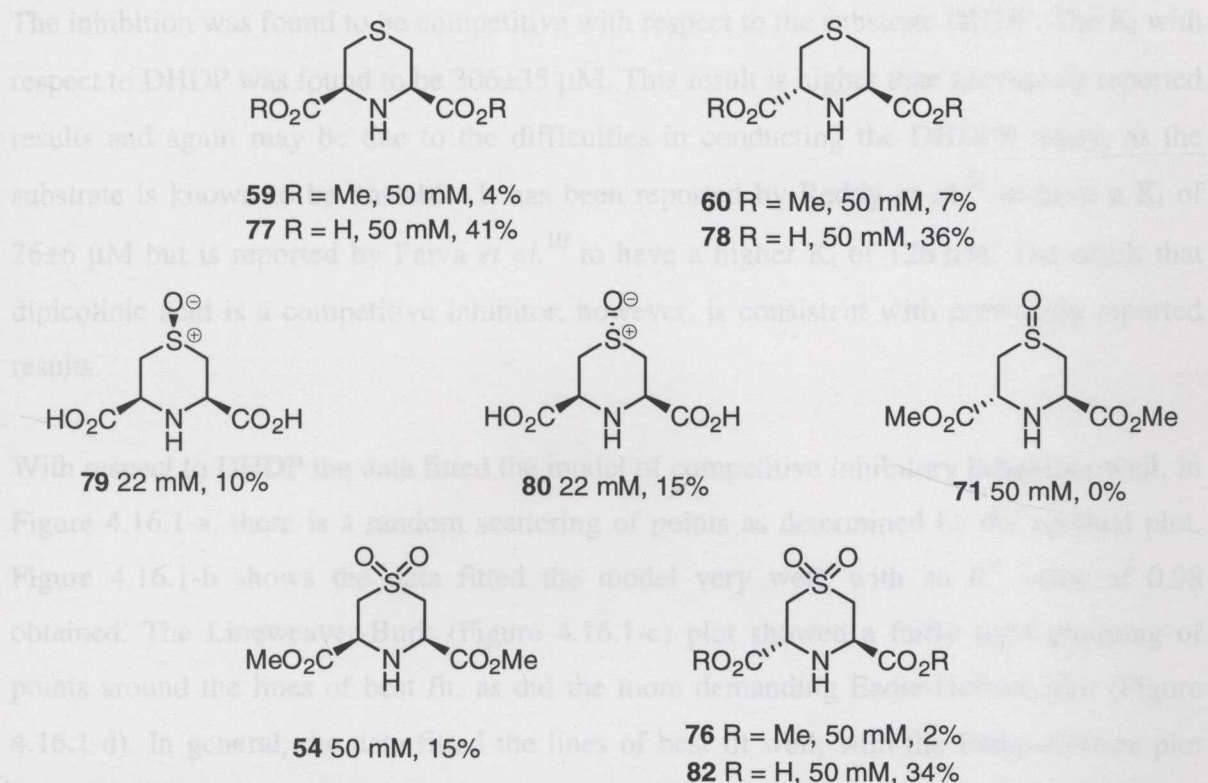


Figure 4.15.2: Sulfur Containing Heterocyclic Inhibitors of DHDPR: Percent Inhibition of DHDPR Activity at the Stated Concentration, [DHDP]=1.0 mM.

4.16 Inhibition of DHDPR by Dipicolinic Acid

Dipicolinic acid **18** is a known competitive inhibitor of DHDPR. In order to relate results obtained herein to those of other groups a detailed kinetic analysis of dipicolinic acid **18** was performed. The inhibition kinetics of dipicolinic acid **18** with respect to DHDP were run at a range of inhibitor and substrate concentrations. Dipicolinic acid **18** concentrations were varied between 0–5.0 mM with respect to DHDP. The concentration of ASA was varied between 0.07–1.0 mM, while the pyruvate concentration was held constant at 2.50 mM.

As for DHDPS studies (section 4.11 and 4.12), the kinetic data were fitted to mathematical models using the Enzfitter¹⁴ computer program that simulated competitive, non-competitive, uncompetitive and mixed inhibition patterns to determine the model of best fit and subsequently the inhibition constant K_i . Lineweaver-Burk and Eadie-Hofstee were also generated using Enzfitter.

The inhibition was found to be competitive with respect to the substrate DHDP. The K_i with respect to DHDP was found to be $306 \pm 35 \mu\text{M}$. This result is higher than previously reported results and again may be due to the difficulties in conducting the DHDPR assay, as the substrate is known to be unstable. It has been reported by Reddy *et al.*²⁴ to have a K_i of $26 \pm 6 \mu\text{M}$ but is reported by Paiva *et al.*¹⁰ to have a higher K_i of $126 \mu\text{M}$. The result that dipicolinic acid is a competitive inhibitor, however, is consistent with previously reported results.

With respect to DHDP the data fitted the model of competitive inhibitory behaviour well. In Figure 4.16.1-a, there is a random scattering of points as determined by the residual plot. Figure 4.16.1-b shows the data fitted the model very well, with an R^2 value of 0.98 obtained. The Lineweaver-Burk (Figure 4.16.1-c) plot showed a fairly tight grouping of points around the lines of best fit, as did the more demanding Eadie-Hofstee plot (Figure 4.16.1-d). In general, the data fitted the lines of best fit well, with the Eadie-Hofstee plot distinctly showing divergent lines of best fit with the x-axis, indicative of a competitive inhibitor.

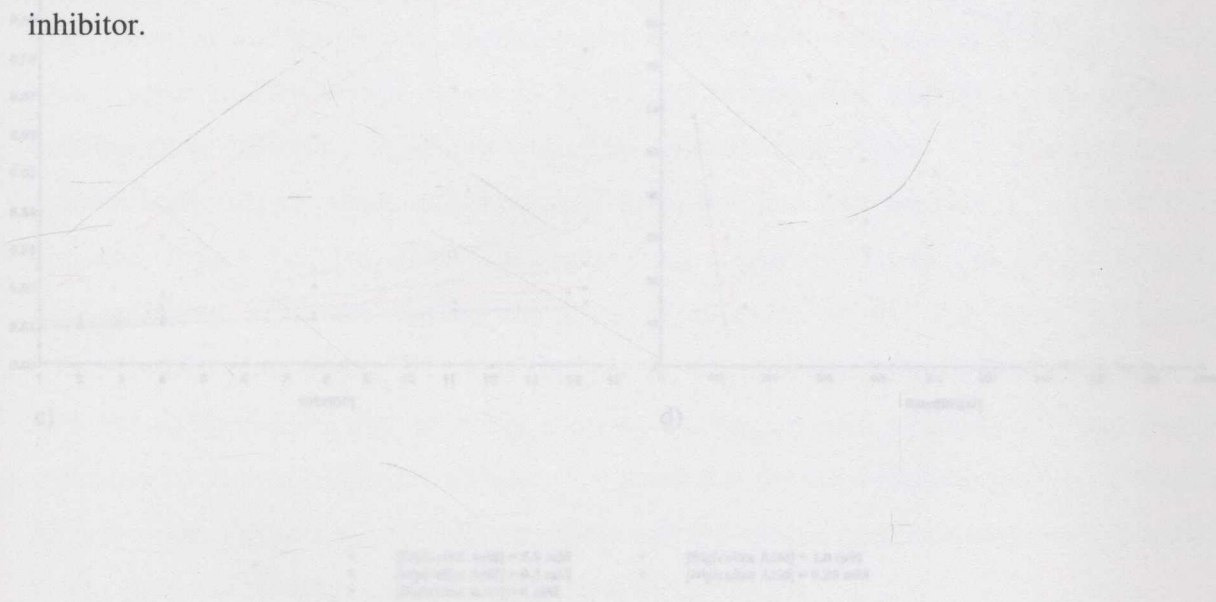


Figure 4.16.1: DHDPR Kinetics with Respect to DHDP at Different Concentrations of Dipicolinic Acid; a) Residuals Plot b) Raw Data with Fitted Model c) Lineweaver-Burk Plot ($R^2 = 0.98$, $P < 0.05$) d) Eadie-Hofstee Plot ($R^2 = 0.98$, $P < 0.05$).

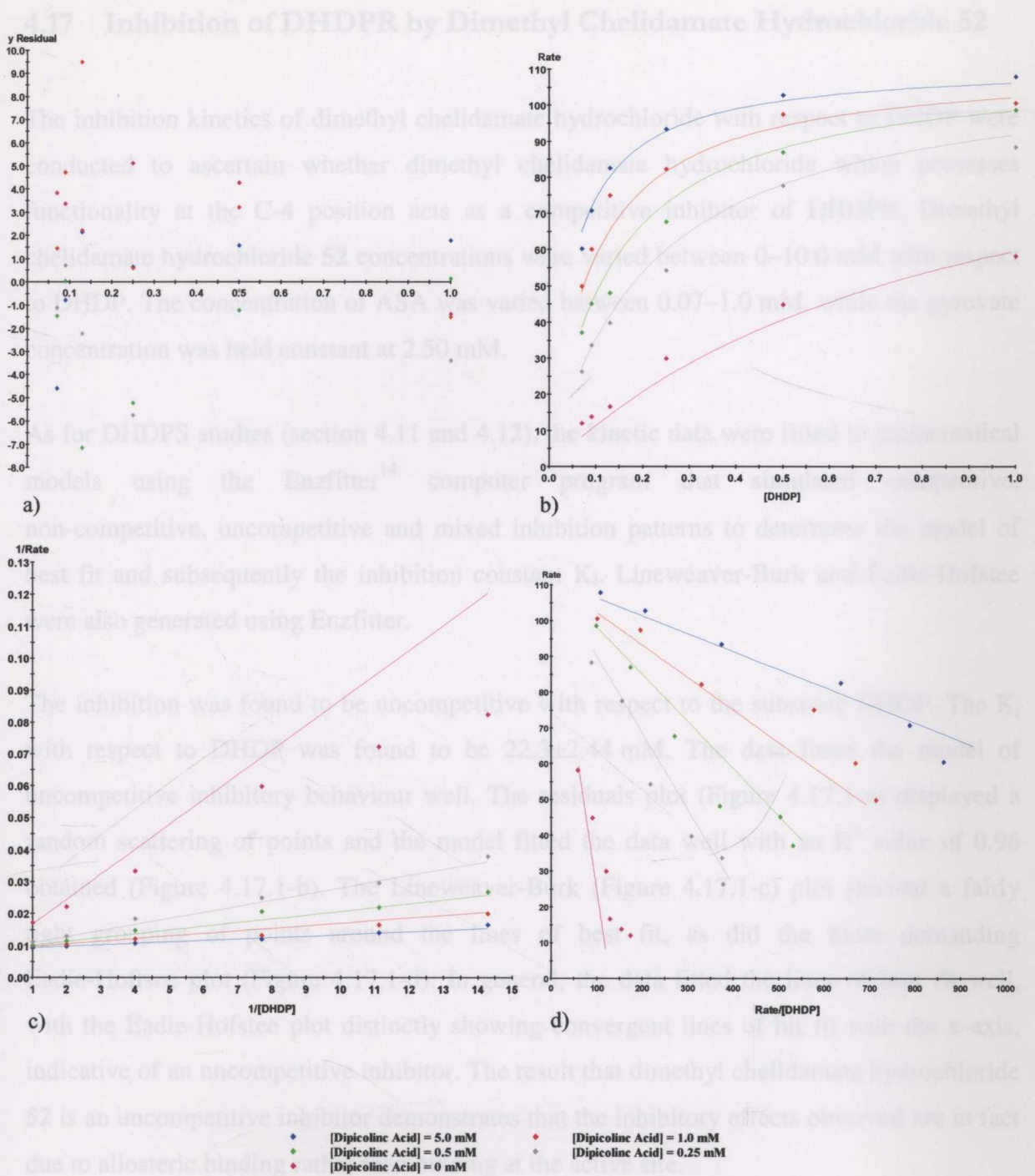


Figure 4.16.1: DHDPR Kinetics with Respect to DHDP at Different Concentrations of Dipicolinic Acid; a) Residuals Plot b) Raw Data with Fitted Model c) Lineweaver-Burk Plot ($R^2 = 0.98$, $P < 0.05$) d) Eadie-Hofstee Plot ($R^2 = 0.98$, $P < 0.05$).

4.17 Inhibition of DHDPR by Dimethyl Chelidamate Hydrochloride 52

The inhibition kinetics of dimethyl chelidamate hydrochloride with respect to DHDP were conducted to ascertain whether dimethyl chelidamate hydrochloride which possesses functionality at the C-4 position acts as a competitive inhibitor of DHDPR. Dimethyl chelidamate hydrochloride **52** concentrations were varied between 0–10.0 mM with respect to DHDP. The concentration of ASA was varied between 0.07–1.0 mM, while the pyruvate concentration was held constant at 2.50 mM.

As for DHDPS studies (section 4.11 and 4.12), the kinetic data were fitted to mathematical models using the Enzfitter¹⁴ computer program that simulated competitive, non-competitive, uncompetitive and mixed inhibition patterns to determine the model of best fit and subsequently the inhibition constant K_i . Lineweaver-Burk and Eadie-Hofstee were also generated using Enzfitter.

The inhibition was found to be uncompetitive with respect to the substrate DHDP. The K_i with respect to DHDP was found to be 22.3 ± 2.44 mM. The data fitted the model of uncompetitive inhibitory behaviour well. The residuals plot (Figure 4.17.1-a) displayed a random scattering of points and the model fitted the data well with an R^2 value of 0.96 obtained (Figure 4.17.1-b). The Lineweaver-Burk (Figure 4.17.1-c) plot showed a fairly tight grouping of points around the lines of best fit, as did the more demanding Eadie-Hofstee plot (Figure 4.17.1-d). In general, the data fitted the lines of best fit well, with the Eadie-Hofstee plot distinctly showing convergent lines of best fit with the x-axis, indicative of an uncompetitive inhibitor. The result that dimethyl chelidamate hydrochloride **52** is an uncompetitive inhibitor demonstrates that the inhibitory effects observed are in fact due to allosteric binding rather than binding at the active site.

Figure 4.17.1: DHDPR Kinetics with Respect to DHDP at Different Concentrations of Dimethyl Chelidamate Hydrochloride: a) Residuals Plot b) Raw Data with Linear Model c) Lineweaver-Burk Plot ($R^2 = 0.96$, $P < 0.05$) d) Eadie-Hofstee Plot ($R^2 = 0.96$, $P < 0.05$)

4.18 Summary

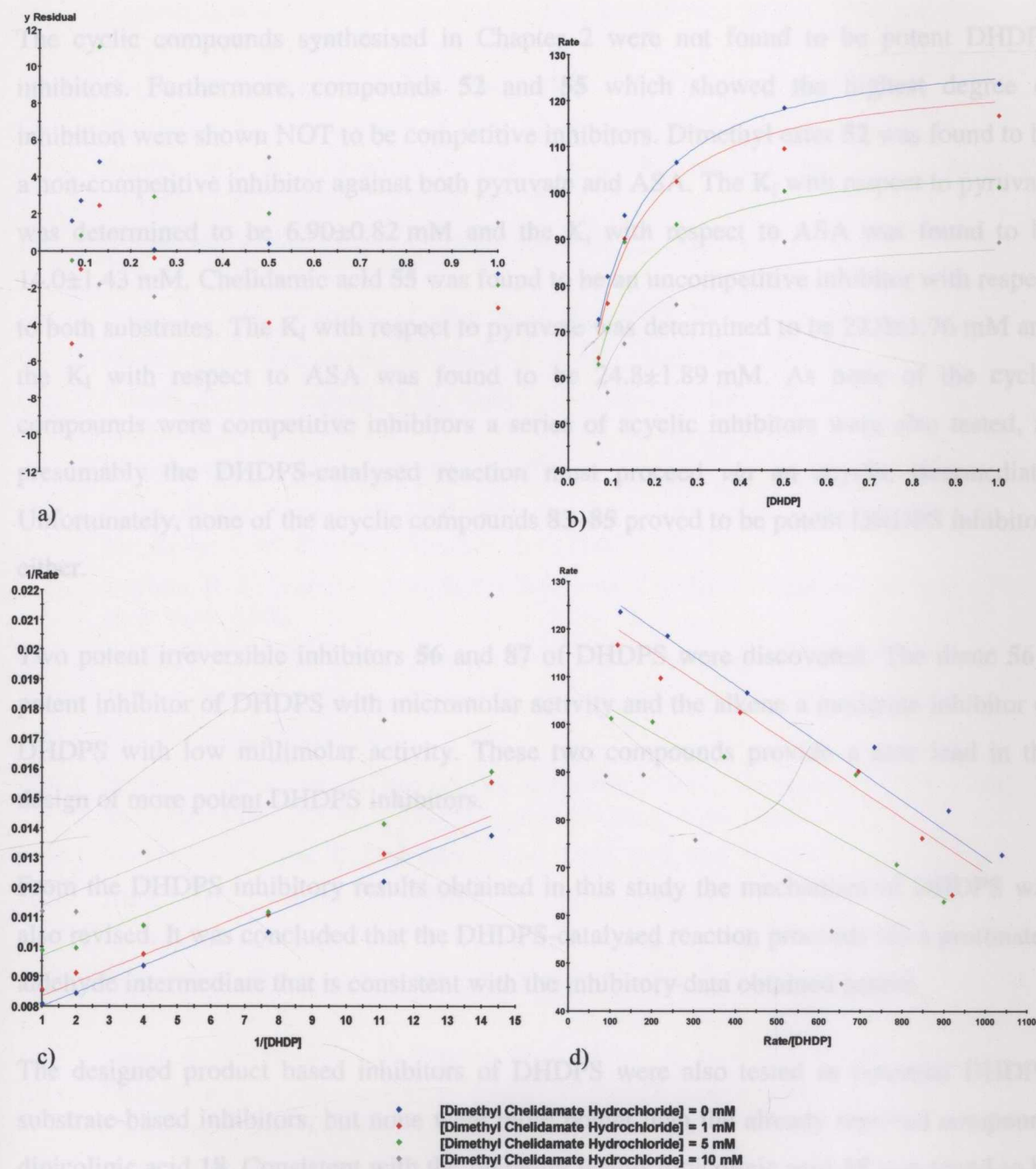


Figure 4.17.1: DHDPR Kinetics with Respect to DHDP at Different Concentrations of Dimethyl Chelidamate Hydrochloride; a) Residuals Plot b) Raw Data with Fitted Model c) Lineweaver-Burk Plot ($R^2 = 0.96$, $P < 0.05$) d) Eadie-Hofstee Plot ($R^2 = 0.96$, $P < 0.05$).

4.18 Summary

The cyclic compounds synthesised in Chapter 2 were not found to be potent DHDPS inhibitors. Furthermore, compounds **52** and **55** which showed the highest degree of inhibition were shown NOT to be competitive inhibitors. Dimethyl ester **52** was found to be a non-competitive inhibitor against both pyruvate and ASA. The K_i with respect to pyruvate was determined to be 6.90 ± 0.82 mM and the K_i with respect to ASA was found to be 14.0 ± 1.43 mM. Chelidamic acid **55** was found to be an uncompetitive inhibitor with respect to both substrates. The K_i with respect to pyruvate was determined to be 22.0 ± 1.76 mM and the K_i with respect to ASA was found to be 24.8 ± 1.89 mM. As none of the cyclic compounds were competitive inhibitors a series of acyclic inhibitors were also tested, as presumably the DHDPS-catalysed reaction must proceed *via* an acyclic intermediate. Unfortunately, none of the acyclic compounds **83–85** proved to be potent DHDPS inhibitors either.

Two potent irreversible inhibitors **56** and **87** of DHDPS were discovered. The diene **56** a potent inhibitor of DHDPS with micromolar activity and the alkene a moderate inhibitor of DHDPS with low millimolar activity. These two compounds provide a new lead in the design of more potent DHDPS inhibitors.

From the DHDPS inhibitory results obtained in this study the mechanism of DHDPS was also revised. It was concluded that the DHDPS-catalysed reaction proceeds *via* a protonated aldehyde intermediate that is consistent with the inhibitory data obtained herein.

The designed product based inhibitors of DHDPS were also tested as potential DHDPR substrate-based inhibitors, but none were more potent than the already reported compound dipicolinic acid **18**. Consistent with the literature results dipicolinic acid **18** was found to be a competitive inhibitor of DHDPR with a K_i of 306 ± 35 μ M with respect to its substrate DHDP. Dimethyl chelidamate hydrochloride **52** was found to be an uncompetitive inhibitor of DHDPR with a K_i of 22.3 ± 2.44 mM.

4.19 References

- (1) Cornish-Bowden, A. *Fundamentals of Enzyme Kinetics*; 2nd ed.; Portland Press Ltd.: Princeton, 1999.
- (2) Yugari, Y.; Gilvarg, C. *J. Biol. Chem.* **1965**, *240*, 4710.
- (3) Shedlarski, J. G.; Gilvarg, C. *J. Biol. Chem.* **1970**, *245*, 1362.
- (4) Borthwick, E. B.; Connell, S. J.; Tudor, D. W.; Robins, D. J.; Shneier, A.; Abell, C.; Coggins, J. R. *Biochem. J.* **1995**, *305*, 521.
- (5) Coulter, C. V.; Gerrard, J. A.; Kraunsoe, J. A. E.; Pratt, A. J. *Pest. Sci.* **1999**, *55*, 887.
- (6) Bugg, T. D. H.; Walsh, C. T. *Nat. Prod. Rep.* **1992**, 199.
- (7) Mirwaldt, C.; Korndorfer, I.; Huber, R. *J. Mol. Biol.* **1995**, *246*, 227.
- (8) Couper, L.; McKendrick, J. E.; Robins, D. J. *Bioorg. Med. Chem. Lett.* **1994**, *4*, 2267.
- (9) Karsten, W. *Biochemistry* **1997**, *36*, 1730.
- (10) Paiva, A. M.; Vanderwall, D. E.; Blanchard, J. S.; Kozarich, J. W.; Williamson, J. M.; Kelly, T. M. *Biochim. Biophys. Acta* **2001**, *1545*, 67.
- (11) Beynon, R. J.; Easterby, J. S. *Buffer Solutions: The Basics*; Oxford University Press: New York, 1996.
- (12) Pearce, F. G. B. Sc. Hons. Thesis, University of Canterbury, 1999.
- (13) Roberts, S. J. MSc Thesis, University of Canterbury, 2002.
- (14) Biosoft: Cambridge, 1999.
- (15) Fersht, A. *Structure and Mechanism in Protein Science: A guide to enzyme catalysis and protein folding*; W.H. Freeman and Company: New York, 1998.
- (16) Dowd, J. E.; Riggs, D. S. *J. Biol. Chem.* **1965**, *249*, 863.
- (17) Atkins, G. L.; Nimmo, I. A. *Biochem. J.* **1975**, *149*, 775.
- (18) Kumpaisal, R.; Hashimoto, T.; Yamada, Y. *Plant Physiol.* **1987**, *85*, 145.
- (19) Dereppe, C.; Bold, G.; Ghisalpa, O.; Edbert, E.; Schar, H. *Plant Physiol.* **1992**, *98*, 813.
- (20) Laber, B.; Gomis-Ruth, F.; Romao, M. J.; Huber, R. *Biochem. J.* **1992**, *288*, 691.
- (21) Dobson, R. C. J.; Gerrard, J. A.; Pearce, F. G. *Biochem. J.* **2003**, *Immediate Publication*, 28th October as manuscript BJ20031389.
- (22) Laber, B.; Gomis-Ruth, F. X.; Romao, M. J.; Huber, R. *Biochem. J.* **1992**, *288*, 691.
- (23) Eisner, U.; Kuthan, J. *Chemical Reviews* **1972**, *72*, 1.
- (24) Reddy, S. G.; Sacchettini, J. C.; Blanchard, J. S. *Biochemistry* **1995**, *34*, 3492.
- (25) Tamir, H.; Gilvarg, C. *J. Biol. Chem.* **1974**, *249*, 3034.
- (26) Kraunsoe, J. A. E. Part II Thesis, Oxford University, 1992.
- (27) Tipton, K. F. In *Enzymology*; Engel, P. C., Ed.; BIOS Scientific Publishers: Oxford, 1996, p 115.
- (28) Engel, P. C. *Enzymology*; BIOS Scientific Publishers: Oxford, 1966.
- (29) Coulter, C. V.; Gerrard, J. A.; Kraunsoe, J. A. E.; Moore, D. J.; Pratt, A. J. *Tetrahedron* **1996**, *52*, 7127.

-
- (30) Blickling, S.; Renner, C.; Laber, B.; Pohlenz, H.; Holak, T. A.; Huber, R. *Biochemistry* **1997**, *36*, 24.
- (31) Dobson, R. C. J. PhD Thesis, University of Canterbury, 2003.
- (32) Caplan, J. F.; Renjian, Z.; Blanchard, J. S.; Vederas, J. C. *Org. Lett.* **2000**, *24*, 3857.

5.1 General Procedures for Synthesis

Chemicals were purchased from Sigma-Aldrich (Sydney, Australia), Precious Metals (Melbourne, Australia) or Nova-2

Plotting points were determined using a Ketchikan bearing ring and we used

EXPERIMENTAL

CHAPTER 5

5.1 General Procedures for Synthesis

Chemicals were purchased from Sigma-Aldrich (Sydney, Australia), Strem (Melbourne, Australia), Precious Metals (Melbourne, Australia) or Nova-gen (Sydney, Australia).

Melting points were determined using a Reichert heating stage and are uncorrected.

Infrared absorption spectra were obtained using a Perkin Elmer 1600 series FTIR, Shimadzu FTIR-8400S or Bio-Rad FTS-7 spectrometer as a thin film between sodium chloride plates or potassium bromide discs.

Optical rotations were obtained using a POLAAR 2001 Polarimeter at 589 nm in the indicated solvent and concentration (g/100 mL) at 22 °C.

¹H Nuclear magnetic resonance spectra were recorded using a Bruker AC200B, Bruker Avance DPX 300 or a Bruker AMX 400 spectrometer and are reported as parts per million (ppm) downfield shift from appropriate internal reference or residual solvent peak. The ¹H n.m.r. data are reported as chemical shift (δ_{H}), relative integral, multiplicity (s = singlet, br = broad, d = doublet, t = triplet, app = apparent), coupling constant (J = Hz) and assignment. ¹³C Nuclear magnetic resonance spectra were recorded using a Bruker AC 200B or Bruker AMX 400 spectrometer. The ¹³C n.m.r. data are expressed as parts per million downfield shift (δ_{C}) from tetramethylsilane as internal reference.

Low resolution electron impact (EI) mass spectra were recorded on a Finnigan PolarisQ ion trap mass spectrometer using electron impact ionisation mode at 40 or 70 eV. Low resolution electrospray ionisation spectra were recorded on a Finnigan LCQ. High resolution electron impact mass spectra were recorded on a VG Autospec mass spectrometer operating at 70 eV (Australian National University, Canberra). High resolution electrospray mass spectra were recorded on a Bruker ApexII Fourier Transform Ion Cyclotron Resonance mass spectrometer, 7.0 T magnet; fitted with an off-axis Analytica electrospray source (University of NSW, Sydney).

Elemental analyses were performed at the Campbell Microanalytical Laboratory, University of Otago, Dunedin, New Zealand.

X-ray crystal structure determination of **71** was performed using a Bruker SMART 1000 CCD diffractometer.

Analytical thin layer chromatography was performed using precoated aluminium backed silica gel plates (Merck Kieselgel 60 F254). Compounds were visualised by ultra-violet fluorescence or by staining with phosphomolybdic acid, ninhydrin or potassium permanganate. Flash chromatography was carried out using Merck Kieselgel 60 (230–400 mesh) with the indicated solvents. Solvent compositions are mixed %v/v as specified.

Preparative HPLC was carried out using a Waters 600 Multisolvant Delivery Pump, Waters 712 WISP (Waters Intelligent Sample Processor), UV200 Spectra Physics UV/VIS monitor (λ 210 nm). The column used was a Beckmann/Altex Ultrasphere ODS 5 μ (250 \times 10 mm ID).

Solvents and reagents were purified according to the method of Perrin and Amarego.¹

5.2.2 *o*-2-*o*-6-Bis(methoxycarbonyl)- α -4-hydroxycyclohexanone and

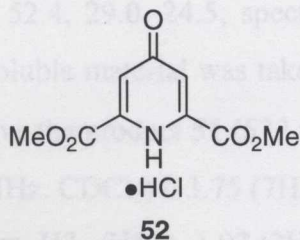
meso-2,5-Bis(methoxycarbonyl)- α -4-hydroxycyclohexanone



To a suspension of dimethyl chelidamate hydrochloride 52 (2.09 g, 8.61 mmol) in water was added Rh/Alumina powder Degussa type (100 mg), and the mixture hydrogenated on a Parr hydrogenator at 45 psi for 8 h at 60 °C. The solution was filtered through celite and the solvent removed *in vacuo* to give an off-white solid. The crude product was dissolved in brine (40 mL), and Na_2CO_3 (1.31 g, 12.4 mmol) and ethyl acetate were added and the mixture stirred for 10 min. The aqueous phase was saturated with NaCl and extracted with ethyl acetate (12 \times 30 mL). The combined organic fractions were dried (MgSO_4) and concentrated *in vacuo* to yield a white solid (1.97 g). The mixture was suspended in hexane

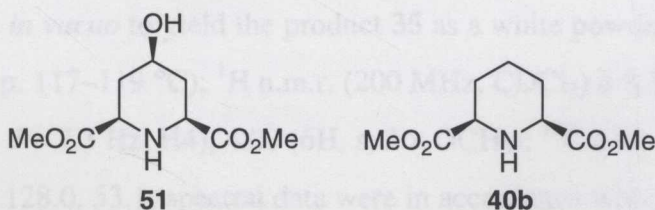
5.2 Synthesis of Cyclic Inhibitors

5.2.1 Dimethyl chelidamate hydrochloride^{2,3} **52**



To a stirred suspension of chelidamic acid **55** (4.00 g, 19.9 mmol) in methanol (76 mL) was added 2,2-dimethoxypropane (28.2 mL, 229 mmol) and concentrated hydrochloric acid (906 μ L, 29.8 mmol). The mixture was refluxed for 4 h under a CaCl_2 drying tube, allowed to cool to room temperature and stirred for 3 days. The solvent was removed *in vacuo* to yield the product **52** as an off-white solid (4.75 g, 98%), m.p. 126–128 $^\circ\text{C}$ (lit.³ m.p. 169.5–171.0 $^\circ\text{C}$); ^1H n.m.r. (200 MHz, CD_3OD) δ 7.82 (2H, s), 4.06 (6H, s, OCH_3); ^{13}C (100 MHz, CDCl_3) δ 170.9, 164.5, 148.4, 117.1, 54.3; spectral data were in accordance with literature values.³

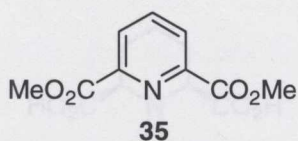
5.2.2 *c*-2-*c*-6-Bis(methoxycarbonyl)-*r*-4-hydroxypiperidine^{2,3} **51** and *meso*-2,6-Bis(methoxycarbonyl)piperidine³ **40b**



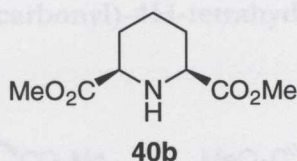
To a suspension of dimethyl chelidamate hydrochloride **52** (2.09 g, 8.61 mmol) in water was added Rh/Alumina powder Degussa type (100 mg), and the mixture hydrogenated on a Parr hydrogenator at 45 psi for 8 h at 60 $^\circ\text{C}$. The solution was filtered through celite and the solvent removed *in vacuo* to give an off-white solid. The crude product was dissolved in brine (40 mL), and Na_2CO_3 (1.31 g, 12.4 mmol) and ethyl acetate were added and the mixture stirred for 10 min. The aqueous phase was saturated with NaCl and extracted with ethyl acetate (12 \times 30 mL). The combined organic fractions were dried (MgSO_4) and concentrated *in vacuo* to yield a white solid (1.97 g). The mixture was suspended in hexane

(10 mL) and refluxed for 30 min. After hot filtration through a Buchner funnel, the filtrate was evaporated to give the product **40b** as a white solid (281 mg, 16%), m.p. 91–92 °C (lit.³ m.p. 91.5–92.5); ¹H n.m.r. (200 MHz, CDCl₃) δ 3.74 (6H, s, 2 × OCH₃), 3.39 (2H, dd, *J* = 1.9, 10.3 Hz, H₂/H₆), 2.36 (1H, br s, NH), 1.98 (3H, m), 1.37–1.48 (3H, m); ¹³C n.m.r. (75 MHz, CDCl₃) δ 173.3, 58.8, 52.4, 29.0, 24.5; spectral data were in accordance with literature values.³ The hexane insoluble material was taken up in a minimum of chloroform and precipitated with hexane to give the product **51** (572 mg, 31%), m.p. 138–139 (lit.³ m.p. 139.0–140.0 °C) ¹H n.m.r. (200 MHz, CDCl₃) δ 3.75 (7H, m, 2 × OMe, H₄), 3.40 (2H, dd, *J* = 2.2, 11.9 Hz, H₂/H₆), 2.32 (2H, m, H_{3_{eq}}/H_{5_{eq}}), 1.97 (2H, br s, OH, NH), 1.35 (2H, m); ¹³C n.m.r. (100 MHz, CDCl₃) δ 172.1, 68.0, 56.6, 52.5, 37.6; spectral data were in accordance with literature values.³

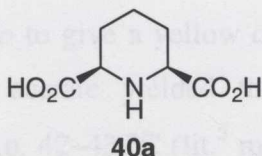
5.2.3 Dimethyl dipicolinate⁴ **35**



To a stirred solution of dipicolinic acid **18** (4.0 g, 23.9 mmol) in methanol (40 mL) at 0 °C was added thionyl chloride (1.8 mL). The resulting mixture was stirred at room temperature for 2 days. The reaction mixture was diluted with saturated NaHCO₃ (200 mL) and extracted with CH₂Cl₂ (4 × 100 mL). The combined organic layers were dried (MgSO₄) and the solvent removed *in vacuo* to yield the product **35** as a white powder (2.35 g, 74%), m.p. 117–118 °C (lit.⁴ m.p. 117–119 °C); ¹H n.m.r. (200 MHz, CDCl₃) δ 8.33 (2H, d, *J* = 7.9 Hz, H₃/H₅), 8.06 (1H, t, *J* = 7.3 Hz, H₄), 4.00 (6H, s, 2 × OCH₃); ¹³C n.m.r. (75 MHz, CDCl₃) δ 165.0, 148.2, 138.3, 128.0, 53.1; spectral data were in accordance with literature values.⁴

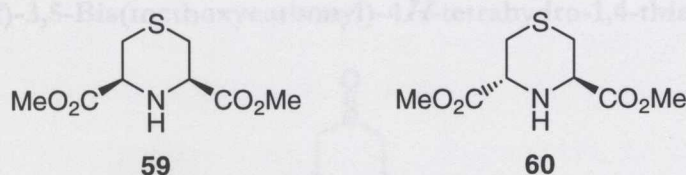
5.2.4 *meso*-2,6-Bis(methoxycarbonyl)piperidine^{2,3} **40b**

To a stirred solution of dimethyl dipicolinate **35** (1.00 g, 5.07 mmol) in chloroform (30 mL) was added PtO₂ (100 mg, 10 mol%) and the mixture stirred under an atmosphere of hydrogen at room temperature for 48 h. The reaction mixture was filtered through celite and concentrated *in vacuo* to yield the product **40b** as a white solid (538 mg, 53%) m.p. 90–92 °C (lit.³ m.p. 91.5–92.5 °C); spectral data were in accordance with earlier reported values.³

5.2.5 2,6-Piperidine dicarboxylate⁴ **40a**

To a stirred suspension of dipicolinic acid **18** (1.5 g, 8.98 mmol) in glacial acetic acid (50 mL) was added PtO₂ (150 mg, 10 mol%) and the mixture stirred under an atmosphere of hydrogen at room temperature for 48 h. The reaction mixture was filtered through celite and acidified with concentrated hydrochloric acid (5 mL). The precipitate was isolated by filtration to yield the product **40a** as a white powder (1.2 g, 77%); m.p. > 275 °C (decomp.) (lit.⁴ m.p. 290–295 °C). ¹H n.m.r. (200 MHz, D₂O) δ 3.82–3.90 (2H, m, H2/H6), 2.23–2.30 (2H, m, H3/H5), 2.03 (1H, m), 1.50–1.70 (3H, m); ¹³C n.m.r. (50 MHz, D₂O) δ 171.7, 57.5, 25.6, 22.4; spectral data were in accordance with literature values.⁴

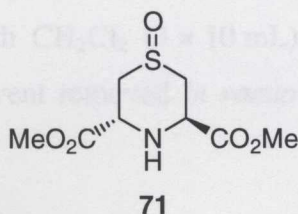
5.2.6 *meso*-3,5-Bis(methoxycarbonyl)-4H-tetrahydro-1,4-thiazane⁵ **59** and
(3*R*,5*R*)-3,5-Bis(methoxycarbonyl)-4H-tetrahydro-1,4-thiazane⁵ **60**



To a stirred solution of methyl 2,3-dibromopropionate **61** (515 μL , 4.06 mmol) in dry ethanol (8.5 mL) at 0 °C was added dry triethylamine (566 μL , 4.06 mmol) and the mixture stirred at 0 °C for 30 min. A solution of L-cysteine methyl ester hydrochloride **62** (698 mg, 4.06 mmol) and dry triethylamine (1.13 mL, 8.13 mmol) in dry ethanol (20 mL) was added *via* a cannula. The resulting mixture was stirred for 7 h at 70 °C, then concentrated *in vacuo*. The off-white solid was dissolved in water (20 mL) and extracted into ethyl acetate (3 \times 20 mL). The combined organic layers were washed with water (2 \times 20 mL), dried (MgSO_4) and concentrated *in vacuo* to give a yellow oil. Column chromatography eluting with 20% dichloromethane/ethyl acetate yielded the *meso*-thiazane **59** as a yellow crystalline solid (314 mg, 35%), m.p. 42–43 °C (lit.⁵ m.p. 43–44 °C). ^1H n.m.r. (400 MHz, CDCl_3) δ 3.61 (6H, s, 2 \times OCH_3), 3.55 (2H, dd, $J = 2.3, 10.8$ Hz, H3/H5), 2.62 (2H, dd, $J = 2.3, 13.8$ Hz, $\text{H}_{2\text{eq}}/\text{H}_{6\text{eq}}$), 2.51 (3H, m, NH and $\text{H}_{2\text{ax}}/\text{H}_{6\text{ax}}$); ^{13}C n.m.r. (100 MHz, CDCl_3) δ 171.2, 59.8, 52.7, 29.2; spectral data were in accordance with literature values.⁵ Further elution with 20% dichloromethane/ethyl acetate yielded the (*R,R*)-thiazane **60** also as a yellow crystalline solid (375 mg, 42%), m.p. 58–59 °C (lit.⁵ m.p. 60 °C). ^1H n.m.r. (400 MHz, CDCl_3) δ 3.96 (2H, dd, $J = 3.5, 6.8$ Hz, H3/H5), 3.72 (6H, s, 2 \times OCH_3), 2.86 (2H, dd, $J = 13.5, 3.5$ Hz, H2/H6), 2.79 (2H, dd, $J = 13.5, 6.8$ Hz, H2/H6), 2.63 (1H, br s, NH); ^{13}C n.m.r. (100 MHz, CDCl_3) δ 172.5, 55.9, 52.9, 29.3; spectral data were in accordance with literature values.⁵

5.3 Oxidation of Sulfides

5.3.1 (3*R*,5*R*)-3,5-Bis(methoxycarbonyl)-4*H*-tetrahydro-1,4-thiazane-1-oxide 71



Method A - Oxidation with sodium periodate

To a stirred solution of (*R,R*)-thiazane **60** (46 mg, 210 μ mol) in methanol (0.5 mL) was added a solution of NaIO₄ (45 mg, 210 μ mol) in water (0.5 mL), which resulted in an exothermic reaction and immediate precipitation of a white solid. The reaction was left to stand for 48 h. The mixture was diluted with water (10 mL) and extracted with CH₂Cl₂ (9 \times 10 mL). The combined organic fractions were dried (MgSO₄) and the solvent removed *in vacuo* to yield the sulfoxide **71** as a white solid. Purification by column chromatography eluting with ethyl acetate afforded sulfoxide **71** as a white crystalline solid (49 mg, 80%), m.p. 149–151 °C; Found C 40.7, H 5.6, N 6.0, C₈H₁₃NO₅S requires C 40.8, H 5.6, N 6.0%; ¹H n.m.r. (400 MHz, CDCl₃) δ 4.66 (1H, dd, *J* = 2.4, 10.8 Hz, H_{5ax}), 3.98 (1H, dd, *J* = 3.8, 5.2 Hz, H_{3eq}), 3.80 (3H, s, OCH₃), 3.79 (3H, s, OCH₃), 3.53 (1H, ddd, *J* = 2.4, 3.8, 13.8 Hz, H_{2eq}), 3.29 (1H, dt, *J* = 2.4, 13.4 Hz, H_{6eq}), 2.94 (1H, dd, *J* = 5.2, 13.8 Hz, H_{2ax}), 2.82 (1H, dd, *J* = 10.8, 13.4 Hz, H_{6ax}); ¹³C n.m.r. (100 MHz, CDCl₃) δ 172.4, 172.0, 53.5, 50.8, 47.7, 46.1; IR ν_{\max} (NaCl)/cm⁻¹ 3347, 1728, 1232, 1031; MS *m/z* (EI) 235 (M⁺, 73%), 176 (M-CO₂Me, 100%).

Method B-Oxidation with meta-chloroperbenzoic acid

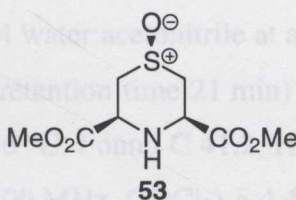
To a stirred solution of the (*R,R*)-thiazane **60** (121 mg, 0.552 mmol) in dichloromethane (1.5 mL) was added *meta*-chloroperbenzoic (*m*-CPBA) acid (190 mg, 1.14 mmol) and the reaction mixture stirred at room temperature overnight. The reaction mixture was concentrated *in vacuo*. Column chromatography eluting with 10% methanol/dichloromethane yielded the sulfoxide **71** (108 mg, 77%).

Method C - Oxidation with hydrogen peroxide

To a stirred solution of (*R,R*)-thiazane **60** (61 mg, 0.278 mmol) in acetonitrile (1.5 mL) was added hydrogen peroxide (30% aqueous) (8 μ L, 0.278 mmol) and the reaction mixture was stirred at room temperature overnight. The mixture was concentrated *in vacuo*, dissolved in water (10 mL) and extracted with CH₂Cl₂ (3 \times 10 mL). The combined organic fractions were dried (MgSO₄) and the solvent removed *in vacuo* to yield the sulfoxide **71** (50 mg, 78%).

Method D - Oxidation with wet bromine

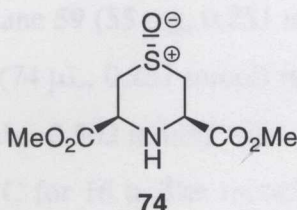
To a stirred solution of (*R,R*)-thiazane **60** (70 mg, 0.319 mmol) in dichloromethane (1.5 mL) was added a solution of NaHCO₃ (81 mg, 0.959 mmol) in water (1.5 mL) and the mixture cooled to 0 °C. Bromine in CCl₄ (0.28 M) (1.15 mL, 0.319 mmol) was added at 0 °C and the mixture stirred overnight at room temperature. The product was extracted into CH₂Cl₂ (5 \times 10 mL) and the combined organic layers washed with NaHCO₃ (1 \times 10 mL) and Na₂S₂O₃ (1 \times 10 mL), dried (MgSO₄) and the solvent removed *in vacuo* to yield the sulfoxide **71** (45 mg, 60%).

5.3.2 c-3,c-5-Bis(methoxycarbonyl)-4H-tetrahydro-1,4-thiazane-r-1-oxide 53

To a stirred solution of *meso*-thiazane **59** (31 mg, 0.141 mmol) in dichloromethane (1 mL) was added a solution of NaHCO₃ (12 mg, 0.141 mmol) in water (1 mL). Bromine in CCl₄ (0.28 M) (510 μ L, 0.141 mmol) was added dropwise and the mixture stirred at room temperature for 30 min. The mixture was diluted with saturated NaHCO₃ (10 mL) and extracted into CH₂Cl₂ (4 \times 10 mL) and dried (MgSO₄). The combined organic layers were concentrated *in vacuo* to give a 10:1 mixture of the sulfoxides **53** and **74** as a yellow oil in 61% yield. The *syn*-sulfoxide **53** was purified by preparative HPLC using a C₁₈ reverse-phase column (5 μ , 250 \times 10 mm ID) eluting with 96:4 water:acetonitrile at a flow rate of 2 mL \cdot min⁻¹. Fractions containing the *syn*-sulfoxide **53** (retention time 24 min) were collected and freeze-dried to give a white solid, m.p. 70–71 °C; ¹H n.m.r. (400 MHz, CDCl₃) δ 3.84 (6H, s, OCH₃), 3.78 (2H, br d, *J* = 11.9 Hz, H_{2eq}/H_{6eq}), 3.67 (2H, br dd, *J* =

3.6, 12.1 Hz, H3/H5), 2.75 (1H, br t, $J = 3.6$ Hz, NH), 2.65 (2H, app t, $J = 12.0$ Hz, H2_{ax}/H6_{ax}); ¹³C n.m.r. (50 MHz, CDCl₃) δ 169.9, 54.8, 53.7, 53.2; IR ν_{\max} (NaCl)/cm⁻¹ 2915, 1741, 1222, 1044. MS m/z (EI) 235 (M⁺, 8%), 176 (M-CO₂Me, 100%). HRMS m/z 235.0496; C₈H₁₃NO₅S requires 235.0514.

5.3.3 *t*-3,*t*-5-Bis(methoxycarbonyl)-tetrahydro-1,4-thiazane-*r*-1-oxide 74

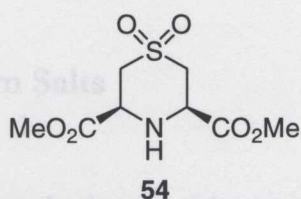


Method A - Oxidation with Sodium Periodate

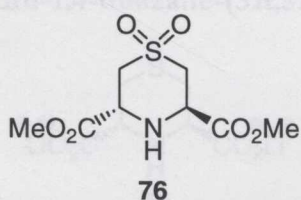
To a stirred solution of *meso*-thiazane **59** (203 mg, 0.926 mmol) in methanol (2 mL) was added a solution of sodium periodate (198 mg, 0.926 mmol) in water (1 mL). The resulting mixture was left to stir at room temperature overnight. The reaction was diluted with water (10 mL), and the product extracted into CH₂Cl₂ (4 × 10 mL). The combined organic fractions were dried (MgSO₄) and the solvent removed *in vacuo* to give a 1:5 mixture of the *syn*-sulfoxide **53** and the *anti*-sulfoxide **74** as a yellow oil (172 mg, 80%). The *anti*-sulfoxide **74** was purified by preparative HPLC using a C₁₈ reverse-phase column (5μ, 250 × 10 mm ID) eluting with 96:4 water:acetonitrile at a flow rate of 2 mL.min⁻¹. Fractions containing the *anti*-sulfoxide **74** (retention time 21 min) were collected and freeze-dried to give an off-white solid, m.p. 95–96 °C; Found C 41.2, H 5.6, N 5.9, C₈H₁₃NO₅S requires C 40.8, H 5.6, N 6.0%; ¹H n.m.r. (300 MHz, CDCl₃) δ 4.41 (2H, br d, $J = 11.7$ Hz, H3/H5), 3.81 (6H, s, OCH₃), 3.30 (2H, d, $J = 13.6$ Hz, H2_{eq}/H6_{eq}), 2.95 (1H, br s, NH), 2.52 (2H, dd, $J = 11.7, 13.6$ Hz, H2_{ax}/H6_{ax}); ¹³C n.m.r. δ (50 MHz, CDCl₃) 171.9, 49.5, 48.9, 46.9; IR ν_{\max} (NaCl)/cm⁻¹ 3307, 1738, 1229, 1044; MS m/z (EI) 235 (M⁺, 100%), 176 (M-CO₂Me, 62%).

Method B - Oxidation with meta-chloroperbenzoic acid

To a stirred solution of *meso*-thiazane **59** (84 mg, 0.383 mmol) in dichloromethane (1 mL) was added *m*-CPBA (132 mg, 0.766 mmol). The reaction mixture was stirred at room temperature overnight. The resulting solution was concentrated *in vacuo*. Purification by column chromatography eluting with 50% ethyl acetate/dichloromethane yielded a yellow oil (88 mg, 98%) as a 2:3 mixture of *syn*-sulfoxide **53** and *anti*-sulfoxide **74**.

5.3.4 *meso*-Bis(methoxycarbonyl)-4H-tetrahydro-1,4-thiazane-1,1-dioxide **54**

To a stirred solution of *meso*-thiazane **59** (55 mg, 0.251 mmol) in dichloromethane (0.5 mL) was added titanium isopropoxide (74 μ L, 0.251 mmol) and the mixture was cooled to 0 °C. Hydrogen peroxide (30%) (69 μ L, 0.502 mmol) was added and the resulting reaction mixture was left to stand at -15 °C for 16 h. The mixture was diluted with water (10 mL) and extracted with CH₂Cl₂ (4 \times 10 mL). The combined organic fractions were dried (MgSO₄) and the solvent removed *in vacuo* to yield the sulfone **54** (58 mg, 92%) as a white solid, m.p. 117–119 °C; Found C 38.2, H 5.3, N 5.6, C₈H₁₃NO₆S requires C 38.2, H 5.2, N 5.6%; ¹H n.m.r. (200 MHz, CDCl₃) δ 3.95 (2H, br d, J = 11.7 Hz, H₃/H₅), 3.82 (6H, s, OCH₃), 3.55 (2H, br d, J = 13.3 Hz, H₂_{eq}/H₆_{eq}), 3.10 (1H, br s, NH), 2.97 (2H, app t, J = 12.5 Hz, H₂_{ax}/H₆_{ax}); ¹³C n.m.r. (100 MHz, CDCl₃) δ 169.3, 56.1, 54.1, 53.6; IR ν_{max} (NaCl)/cm⁻¹ 3332, 1746, 1308, 1231, 1130; MS m/z (EI) 252 (M+H⁺, 18%), 192 (M-CO₂Me, 100%), 132 (C₄H₆SNO, 86%).

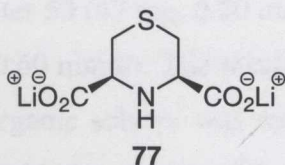
5.3.5 (3*R*,5*R*)-3,5-Bis(methoxycarbonyl)-1,4-thiazane-1,1-dioxide **76**

To a stirred solution of (*R,R*)-thiazane **59** (524 mg, 2.39 mmol) in dichloromethane (5 mL) was added titanium isopropoxide (705 μ L, 2.39 mmol) and the mixture was cooled to 0 °C. Hydrogen peroxide (30%) (822 μ L, 5.98 mmol) was added and the resulting mixture left to stand at -15 °C for 16 h. The mixture was diluted with water (10 mL) and extracted with CH₂Cl₂ (4 \times 10 mL). The combined organic fractions were dried (MgSO₄) and the solvent removed *in vacuo* to yield the sulfone **76** (444 mg, 92%) as a white solid, m.p. 104–105 °C; Found C 38.2, H 5.2, N 5.4, C₈H₁₃NO₆S requires C 38.2, H 5.2, N 5.6%; ¹H n.m.r. (400 MHz, CDCl₃) δ 4.29 (2H, t, J = 5.8 Hz, H₃/H₅), 3.77 (6H, s, OCH₃), 3.34 (4H, d, J = 5.8 Hz, H₂/H₆), 3.10 (1H, br s, NH); ¹³C n.m.r. (100 MHz, CDCl₃) δ 169.9, 53.4, 52.8, 52.4; IR

ν_{\max} (NaCl)/ cm^{-1} 3352, 1742, 1323, 1245, 1126; MS m/z (EI) 252 ($M+H^+$, 25%), 192 ($M-\text{CO}_2\text{Me}$, 100%), 132 ($\text{C}_4\text{H}_6\text{SNO}$, 84%).

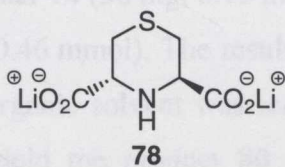
5.4 Preparation of Lithium Salts

5.4.1 Dilithium *meso*-4H-tetrahydro-1,4-thiazane-3,5-dicarboxylate **77**

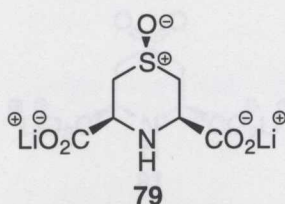


To a solution of *meso*-thiazane **59** (518 mg, 2.36 mmol) in THF/water (15 mL, 2:1) was added lithium hydroxide (169 mg, 7.09 mmol). The resulting reaction mixture was stirred at room temperature for 16 h. The organic solvent was removed under reduced pressure and the concentrate freeze-dried to yield the product **77** (492 mg, 103%, contaminated with lithium hydroxide) as a white solid; ^1H n.m.r. (300 MHz, D_2O) δ 3.33 (2H, dd, $J = 2.1$, 11.2 Hz, H3/H5), 2.69 (2H, dd, $J = 2.1$, 13.5 Hz, H2_{eq}/H6_{eq}), 2.51 (2H, app t, $J = 11.4$ Hz, H2_{ax}/H6_{ax}); ^{13}C n.m.r. (75 MHz, D_2O) δ 181.4, 64.3, 32.3; IR ν_{\max} (KBr)/ cm^{-1} 3295, 1607, 1452, 1391; MS m/z (ESI) -ve ion $[\text{M}-\text{Li}]^-$ 196 (100%); HRMS (ESI) -ive ion $[\text{M}^{2-}+\text{H}]^-$ 190.0193; $\text{C}_6\text{H}_8\text{NO}_4\text{S}$ requires 190.01802.

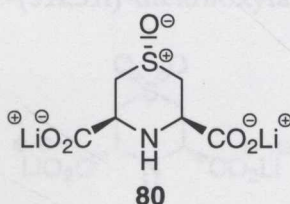
5.4.2 Dilithium 4H-tetrahydro-1,4-thiazane-(3*R*,5*R*)-dicarboxylate **78**



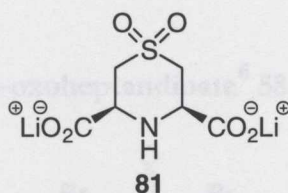
To a solution of (*R,R*)-thiazane **59** (776 mg, 3.54 mmol) in THF/water (28 mL, 3:1) was added lithium hydroxide (254 mg, 10.6 mmol). The resulting reaction mixture was stirred at room temperature for 16 h. The organic solvent was removed under reduced pressure and the concentrate freeze-dried to yield the product **78** (744 mg, 103%, contaminated with lithium hydroxide) as a white solid; ^1H n.m.r. (300 MHz, D_2O) δ 3.89 (2H, dd, $J = 3.6$, 7.0 Hz, H3/H5), 2.88 (2H, dd, $J = 3.6$, 14.1 Hz, H2/H6), 2.80 (2H, dd, $J = 7.0$, 14.1 Hz, H2/H6); ^{13}C n.m.r. (75 MHz, D_2O) δ 175.6, 57.1, 28.0; IR ν_{\max} (KBr)/ cm^{-1} 3283, 1742, 1414, 1315; MS m/z (ESI) -ve ion, $[\text{M}-\text{Li}]^-$ 196 (100%); HRMS (ESI) -ve ion ion $[\text{M}^{2-}+\text{H}]^-$ 190.0185; $\text{C}_6\text{H}_8\text{NO}_4\text{S}$ requires 190.0180.

5.4.3 Dilithium 4H-tetrahydro-1,4-thiazane- *c*-3,*c*-5-dicarboxylate-*r*-1-oxide 79

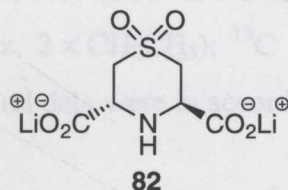
To a solution of *syn*-sulfoxide diester **53** (47 mg, 0.20 mmol) in THF/water (2 mL, 3:1) was added lithium hydroxide (14 mg, 0.60 mmol). The resulting reaction mixture was stirred at room temperature for 16 h. The organic solvent was removed under reduced pressure and the concentrate freeze-dried to yield the product **79** as a yellow solid (48 mg, 100%). ^1H n.m.r. (400 MHz, D_2O) δ 3.64 (2H, d, $J = 11.6$ Hz, $\text{H}_{2\text{eq}}/\text{H}_{6\text{eq}}$), 3.26 (2H, d, $J = 12.0$ Hz, $\text{H}_{3/\text{H}5}$), 2.37 (2H, app t, $J = 11.9$ Hz, $\text{H}_{2\text{ax}}/\text{H}_{6\text{ax}}$); ^{13}C n.m.r. (100 MHz, D_2O) δ 178.5, 58.5, 54.4; IR ν_{max} (KBr)/ cm^{-1} 3450, 1627, 1364, 1015; MS m/z (ESI) $-ve$ ion, $[\text{M-Li}]^-$ 212 (100%); HRMS (ESI) $-ve$ ion $[\text{M}^{2-}+\text{H}]^-$ 206.0124; $\text{C}_6\text{H}_8\text{NO}_5\text{S}$ requires 206.0128.

5.4.4 Dilithium tetrahydro-1,4-thiazane-*t*-3,*t*-5-dicarboxylate -*r*-1-oxide 80

To a solution of *anti*-sulfoxide diester **74** (36 mg, 0.15 mmol) in THF/water (2 mL, 3:1) was added lithium hydroxide (11 mg, 0.46 mmol). The resulting reaction mixture was stirred at room temperature for 16 h. The organic solvent was removed under reduced pressure and the concentrate freeze-dried to yield the product **80** as a yellow solid (39 mg, 108%, contaminated with lithium hydroxide). ^1H n.m.r. (400 MHz, D_2O) δ 3.67 (2H, d, $J = 12.0$ Hz, $\text{H}_{2\text{eq}}/\text{H}_{6\text{eq}}$), 3.05 (2H, d, $J = 14.5$ Hz, $\text{H}_{3/\text{H}5}$), 2.40 (2H, app t, $J = 13.3$ Hz, $\text{H}_{2\text{ax}}/\text{H}_{6\text{ax}}$); ^{13}C n.m.r. (100 MHz, D_2O) δ 178.5, 51.1, 46.2; IR ν_{max} (KBr)/ cm^{-1} 3486, 1745, 1229, 1043; MS m/z (ESI) $-ve$ ion $[\text{M-Li}]^-$ 212 (100%); HRMS (ESI) $-ve$ ion $[\text{M}^{2-}+\text{H}]^-$ 206.0131; $\text{C}_6\text{H}_8\text{NO}_5\text{S}$ requires 206.0128.

5.4.5 Dilithium *meso*-4H-tetrahydro-1,4-thiazane-3,5-dicarboxylate-1,1-dioxide **81**

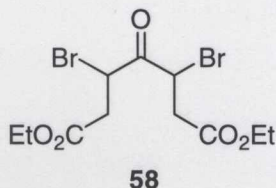
To a solution of *meso*-sulfone **54** (338 mg, 1.35 mmol) in THF/water (15 mL, 2:1) was added lithium hydroxide (129 mg, 5.40 mmol). The resulting reaction mixture was stirred at room temperature for 16 h. The organic solvent was removed under reduced pressure and the concentrate freeze-dried to yield the product **81** as a white solid (350 mg, 110%, contaminated with lithium hydroxide). ^1H n.m.r. (400 MHz, D_2O) δ 3.52 (2H, dd, $J = 2.0$, 12.1 Hz, $\text{H}_{2\text{eq}}/\text{H}_{6\text{eq}}$), 3.38 (2H, br d, $J = 12.9$ Hz, H_3/H_5), 2.93 (2H, app t, $J = 12.4$ Hz, $\text{H}_{2\text{ax}}/\text{H}_{6\text{ax}}$); ^{13}C n.m.r. (50 MHz, D_2O) δ 175.9, 58.2, 54.1; IR ν_{max} (KBr)/ cm^{-1} 3312, 1638, 1403, 1281, 1127; MS m/z (ESI) -ve ion $[\text{2M-Li}]^-$ 463 (100%); $[\text{M-Li}]^-$ 228 (55%) HRMS (ESI) -ve ion $[\text{M-Li}]^-$ 228.0172; $\text{C}_6\text{H}_7\text{LiNO}_6\text{S}$ requires 228.0159.

5.4.6 Dilithium 1,4-thiazane-(3*R*,5*R*)-dicarboxylate-1,1-dioxide **82**

To a solution of (*R,R*)-thiazane sulfone **76** (340 mg, 1.35 mmol) in THF/water (15 mL, 2:1) was added lithium hydroxide (97 mg, 4.06 mmol). The resulting reaction mixture was stirred at room temperature for 16 h. The organic solvent was removed under reduced pressure and the concentrate freeze-dried to yield the product **82** as a white solid (348 mg, 109%, contaminated with lithium hydroxide). ^1H n.m.r. (400 MHz, D_2O) δ 3.93 (2H, t, $J = 5.5$ Hz, H_3/H_5), 3.28 (4H, d, $J = 5.5$ Hz, H_2/H_6); ^{13}C n.m.r. (100 MHz, D_2O) δ 176.9, 56.0, 53.5; IR ν_{max} (KBr)/ cm^{-1} 3312, 1630, 1410, 1283, 1134; MS m/z (ESI) -ve ion $[\text{M-Li}]^-$ 228 (100%); HRMS (ESI) -ve ion $[\text{M-Li}]^-$ 228.0172; $\text{C}_6\text{H}_7\text{LiNO}_6\text{S}$ requires 228.0159.

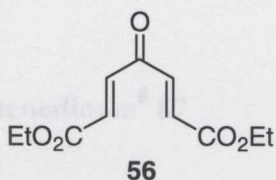
5.5 Synthesis of Acyclic Inhibitors

5.5.1 Diethyl 3,5-dibromo-4-oxoheptandioate ⁶ 58



To a stirred solution of diethyl 4-oxopimelate **57** (2.8 g, 12.2 mmol) in dry dichloromethane (55 mL) at 0 °C was added a solution of bromine (1.22 mL, 24.3 mmol) in dry dichloromethane (3 mL) over 20 min. The resulting reaction mixture was warmed to room temperature and stirred for 1 h. The reaction mixture was diluted with dichloromethane (50 mL), washed with saturated Na₂S₂O₃ (3 × 100 mL), dried (Na₂SO₄) and concentrated *in vacuo* to give a clear oil. The crude product was recrystallised from hexane at -15 °C to yield the product **58** as a white solid (3.85 g, 81%), m.p. 49–50 °C (lit.⁶ 48–49 °C); ¹H n.m.r. (200 MHz, CDCl₃) δ 5.33 (2H, dd, *J* = 6.7, 7.6 Hz, 3- and 5-H), 4.18 (4H, q, *J* = 7.2 Hz, 2 × CH₂CH₃), 3.21 (2H, dd, *J* = 7.6, 17.1 Hz, 2- and 6-H), 3.00 (2H, dd, *J* = 6.7, 17.1 Hz, 2- and 6-H'), 1.27 (6H, t, *J* = 7.2 Hz, 2 × CH₂CH₃); ¹³C n.m.r. (50 MHz, CDCl₃) δ 194.2, 169.3, 61.3, 41.5, 38.2, 14.1; spectral data were in accordance with literature values.⁶

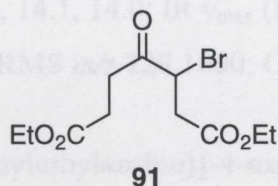
5.5.2 Diethyl (*E,E*)-4-oxohepta-2,5-dienedioate ⁶ 56



To a stirred solution of diethyl 3,5-dibromo-4-oxoheptandioate **58** (2.30 g, 5.93 mmol) in dry dichloromethane (30 mL) at 0 °C was added triethylamine (1.7 mL, 11.9 mmol). The resulting mixture was stirred at 0 °C for 45 min. The reaction mixture was diluted with dichloromethane (60 mL), washed with water (2 × 40 mL), dried (Na₂SO₄) and concentrated *in vacuo* to give a yellow solid. The crude product was recrystallised from 96% ethanol to yield the product **56** as a bright yellow needles (1.34 g, 97%), m.p. 49–50 °C (lit.⁶ 49–50 °C); ¹H n.m.r. (200 MHz, CDCl₃) δ 7.32 (2H, d, *J* = 15.9 Hz), 6.80 (2H, d, *J* = 15.9 Hz), 4.29 (4H, q, *J* = 7.1 Hz, 2 × CH₂CH₃), 1.33 (6H, t, *J* = 7.1 Hz,

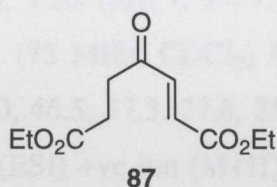
$2 \times \text{CH}_2\text{CH}_3$); ^{13}C n.m.r. (50 MHz, CDCl_3) δ 188.6, 165.4, 137.9, 133.6, 62.0, 14.5; spectral data were in accordance with literature values.⁶

5.5.3 Diethyl 3-bromo-4-oxoheptandioate⁷ **91**



To a stirred solution of diethyl 4-oxopimelate **57** (3.00 g, 13.0 mmol) in dry dichloromethane (20 mL) at 0 °C was added a solution of bromine (653 μL , 13.0 mmol) in dry dichloromethane (2 mL). The resulting reaction mixture was allowed to warm to room temperature and stirred for 30 min. The reaction mixture was diluted with dichloromethane (20 mL), washed with $\text{Na}_2\text{S}_2\text{O}_3$ (3 \times 40 mL), dried (Na_2SO_4) and concentrated *in vacuo* to give a pale yellow oil. Purification by column chromatography eluting with 30% ethyl acetate/hexane yielded the product **91** as a yellow oil (2.98, 74%). ^1H n.m.r. (200 MHz, CDCl_3) δ 4.69 (1H, t, $J = 6.3$ Hz, CHBr), 4.15 (2H, q, $J = 7.1$ Hz, OCH_2CH_3), 4.14 (2H, q, $J = 7.1$ Hz, OCH_2CH_3), 3.34–3.18 (2H, m, 2-H), 2.97–2.82 (2H, m, 5-H), 2.64 (2H, t, $J = 6.3$, 6-H), 1.27 (3H, t, $J = 7.1$ Hz, OCH_2CH_3), 1.25 (3H, t, $J = 7.1$ Hz, OCH_2CH_3); ^{13}C n.m.r. (50 MHz, CDCl_3) δ 201.6, 172.3, 170.1, 61.5, 60.8, 44.2, 38.3, 34.5, 28.2, 14.1($\times 2$); IR ν_{max} (NaCl)/ cm^{-1} 1728, 1197; MS m/z (EI) 309 ($\text{M}^{79}\text{Br}+\text{H}$, 42%), 311 ($\text{M}^{81}\text{Br}+\text{H}$, 36%), 263 ($\text{M}^{79}\text{Br}-\text{OEt}$, 100%), 265 ($\text{M}^{81}\text{Br}-\text{OEt}$, 86%); HRMS m/z 308.0257; $\text{C}_{11}\text{H}_{17}\text{BrO}_5$ requires 308.0259.

5.5.4 Diethyl 4-oxo-(*E*)-heptenedioate⁸ **87**

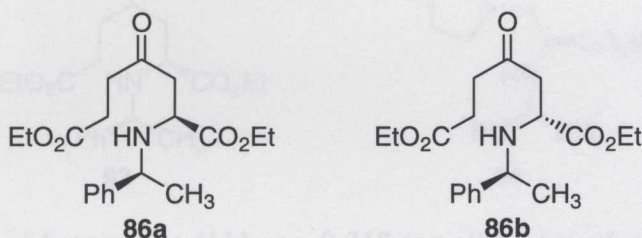


To a stirred solution of diethyl 3-bromo-4-oxopimelate **91** (2.50 g, 8.09 mmol) in dry dichloromethane (20 mL) at 0 °C was added triethylamine (1.13 mL, 8.09 mmol). The resulting reaction mixture was stirred at 0 °C for 30 min. The reaction mixture was diluted with water (20 mL), extracted with dichloromethane (3 \times 15 mL), dried (Na_2SO_4) and concentrated *in vacuo* to yield the product **87** as a yellow oil (1.65 g, 89%). ^1H n.m.r. (300

MHz, CDCl₃) δ 7.08 (1H, d, $J = 16.1$ Hz, $\underline{\text{C}}\text{H}=\text{CH}$), 6.71 (1H, d, $J = 16.1$ Hz, $\text{CH}=\underline{\text{C}}\text{H}$), 4.26 (2H, q, $J = 7.0$ Hz, OCH_2CH_3), 4.14 (2H, q, $J = 7.0$ Hz, OCH_2CH_3), 2.96 (2H, t, $J = 6.5$ Hz, $\underline{\text{C}}\text{H}_2\text{CH}_2$), 2.68 (2H, t, $J = 6.5$ Hz, $\text{CH}_2\underline{\text{C}}\text{H}_2$), 1.34 (3H, t, $J = 7.0$ Hz, $\text{OCH}_2\underline{\text{C}}\text{H}_3$), 1.27 (3H, t, $J = 7.0$ Hz, $\text{OCH}_2\underline{\text{C}}\text{H}_3$); ¹³C n.m.r. (50 MHz, CDCl₃) δ 197.7, 172.3, 165.4, 138.9, 131.2, 61.4, 60.8, 35.9, 27.8, 14.1, 14.0; IR ν_{max} (NaCl)/cm⁻¹ 1728, 1695, 1304, 1182; MS m/z (EI) 229 (M+H, 100%); HRMS m/z 228.1000; C₁₁H₁₆O₅ requires 228.0998.

5.5.4 Diethyl 2-(S)-[(1S)-phenylethylamino]-4-oxopimelate 86a and diethyl

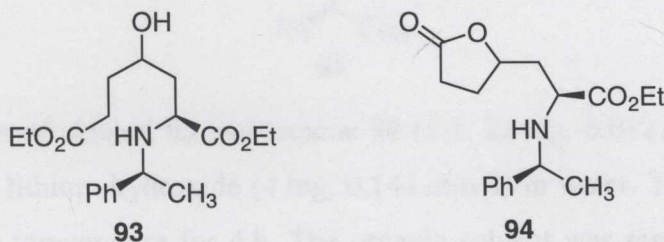
5.5.5 Diethyl 2(S)-[(1S)-phenylethylamino]-4-oxopimelate 86a and diethyl 2(R)-[(1S)-phenylethylamino]-4-oxopimelate 86b



To a stirred solution of diethyl 4-oxo-(*E*)-heptenedioate **87** (1.60 g, 7.01 mmol) in dichloromethane (20 mL) was added dropwise to a solution of (*S*)-phenylethylamine **88** (904 mL, 7.01 mmol) in dichloromethane (30 mL) at room temperature. The reaction was allowed to stir at room temperature under nitrogen for 16 h. The reaction mixture was concentrated *in vacuo* to yield a mixture of diastereomers as a yellow oil. Purification by column chromatography eluting with 30% ethyl acetate/hexane yielded a 1.2:1 mixture of **86a** and **86b** as yellow oils. **86a**: (1.02 g, 42%); $[\alpha]_{\text{D}}^{22} -52$ (c, 12.2 in CH₂Cl₂); ¹H n.m.r. (300 MHz, CDCl₃) δ 7.29 (5H, m, Ar-H), 4.36 (2H, q, $J = 7.1$ Hz, OCH_2CH_3), 4.11 (2H, q, $J = 7.1$ Hz, OCH_2CH_3), 3.84 (1H, q, $J = 6.5$ Hz, $\underline{\text{C}}\text{H}-\text{Ph}$), 3.34 (1H, t, $J = 6.3$ Hz, $\underline{\text{C}}\text{HCO}_2\text{Et}$), 2.74 (2H, d, $J = 6.3$ Hz, 3-H) 2.62–2.69 (2H, m, 6-H), 2.50–2.56 (2H, m, 5-H), 1.31 (3H, d, $J = 6.5$ Hz, $\text{CH}\underline{\text{C}}\text{H}_3$), 1.25 (3H, t, $J = 7.1$ Hz, $\text{OCH}_2\underline{\text{C}}\text{H}_3$), 1.24 (3H, m, t, $J = 7.1$ Hz, $\text{OCH}_2\underline{\text{C}}\text{H}_3$); ¹³C n.m.r. (75 MHz, CDCl₃) δ 206.2, 174.3, 172.6, 144.8, 128.4, 127.1, 127.0, 60.9, 60.6, 56.8, 55.0, 46.5, 37.3, 27.8, 25.1, 14.2, 14.1; IR ν_{max} (NaCl)/cm⁻¹ 2916, 2363, 1730, 1192; MS m/z (ESI) +ve ion $[\text{M}+\text{H}]^+$ 350 (50%), $[\text{M}+\text{Na}]^+$ 372 (42%), $[\text{2M}+\text{Na}]^+$ 721 (100%); HRMS (ESI) $[\text{M}+\text{H}]^+$ 350.1962; C₁₉H₂₈NO₅ requires 350.1962. **86b**: (965 mg, 39%); $[\alpha]_{\text{D}}^{22} -10.7$ (c, 7.29 in CH₂Cl₂); ¹H n.m.r. (300 MHz, CDCl₃) δ 7.29 (5H, m, Ar-H), 4.16–4.05 (4H, m, 2 × OCH₂CH₃), 3.78 (1H, q, $J = 6.4$ Hz, $\underline{\text{C}}\text{HPh}$), 3.70 (1H, t, $J = 6.2$ Hz, CHCO_2Et), 2.78–2.74 (4H, m, 5- and 3-H), 2.57 (2H, t, $J = 6.2$ Hz, 6-H), 1.32 (3H, d, $J = 6.4$ Hz, $\text{CH}\underline{\text{C}}\text{H}_3$), 1.25 (3H, t, $J = 7.0$ Hz, $\text{OCH}_2\underline{\text{C}}\text{H}_3$), 1.20 (3H, t,

$J = 7.0$ Hz, OCH_2CH_3); ^{13}C n.m.r. (75 MHz, CDCl_3) δ 206.3, 169.5, 169.0, 145.2, 128.4, 127.1, 126.7, 61.0, 60.6, 56.3, 55.1, 45.6, 37.8, 27.9, 23.2, 14.2, 14.1; IR ν_{max} (NaCl)/ cm^{-1} 2978, 2362, 1728, 1190; MS m/z (ESI) +ve ion $[\text{M}+\text{H}]^+$ 350 (47%), $[\text{M}+\text{Na}]^+$ 372 (42%), $[\text{2M}+\text{Na}]^+$ 721 (100%); HRMS (ESI) $[\text{M}+\text{Na}]^+$ 372.1745; $\text{C}_{19}\text{H}_{28}\text{NNaO}_5$ requires 372.1781.

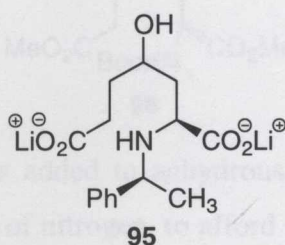
5.5.6 Diethyl 2(S)-(1(S)-phenylethylamino)-4-hydroxy-pimelate **93** and Ethyl tetrahydro-2-oxo-furan-5-[2(S)-(1(S)-phenylethylamino)]propanoate **94**



To a stirred solution of ketone **86a** (111 mg, 0.318 mmol) in dry ethanol (6 mL) was added sodium borohydride (25 mg, 0.644 mmol). The resulting solution was stirred at room temperature for 1 h. The mixture was poured onto water (20 mL) and extracted with ethyl acetate (3×20 mL). The combined organic layers were dried (Na_2SO_4) and concentrated *in vacuo* to yield a mixture of products in 1:2.8 ratio. Purification by column chromatography eluting with 30% ethyl acetate/hexane yielded the alcohol **93** as a colourless oil (25 mg, 22%) $[\alpha]_{\text{D}}^{22} - 106$ (c , 0.7 in CH_2Cl_2): ^1H n.m.r. (400 MHz, CDCl_3) δ 7.28–7.38 (5H, m, Ar-H), 4.22 (2H, m, OCH_2CH_3), 4.14 (2H, q, $J = 7.2$ Hz, OCH_2CH_3), 3.71 (1H, q, $J = 6.5$ Hz, PhCHCH_3), 3.65 (1H, m, 4-H), 3.21 (1H, dd, $J = 2.9, 11.7$ Hz, 2-H), 2.42 (2H, m, 6- CH_2), 1.68–1.75 (3H, m, 5- CH_2 and 3- CHH), 1.47 (1H, m, 3- CHH), 1.40 (3H, d, $J = 6.5$ Hz, PhCHCH_3), 1.29 (3H, t, $J = 7.0$ Hz, OCH_2CH_3), 1.26 (3H, t, $J = 7.1$ Hz, OCH_2CH_3); ^{13}C n.m.r. (100 MHz, CDCl_3) δ 128.8 ($\times 2$), 127.6, 127.0 ($\times 2$), 71.1, 61.1, 60.2, 59.3, 57.2, 39.0, 32.5, 30.1, 24.9, 14.2; IR ν_{max} (NaCl)/ cm^{-1} , 3300, 1734, 1186; MS m/z (ESI) +ve ion $[\text{M}+\text{H}]^+$ 352 (100%), $[\text{M}+\text{Na}]^+$ 374 (53%); HRMS (ESI) $[\text{M}+\text{Na}]^+$ 374.1933; $\text{C}_{19}\text{H}_{29}\text{NNaO}_5$ requires 374.1934. Further elution with 30% ethyl acetate/hexane yielded the lactone **94** also as a colourless oil (69 mg, 70%). $[\alpha]_{\text{D}}^{22} - 31.5$ (c , 3.9 in CH_2Cl_2): ^1H n.m.r. (400 MHz, CDCl_3) δ 7.25–7.36 (5H, m, Ar-H), 4.21 (1H, m, 4-H), 4.06–4.13 (3H, m, OCH_2CH_3 and PhCHCH_3), 3.45 (1H, dd, $J = 8.1$ Hz, 2-H), 2.34–2.47 (2H, m, 6- CH_2), 2.02 (1H, m, 3- CHH), 1.89 (2H, m, 5- CH_2), 1.45 (1H, m, 3- CHH) 1.39 (3H, d, $J = 6.5$ Hz, PhCHCH_3), 1.23 (3H, t, $J = 7.1$ Hz, OCH_2CH_3); ^{13}C n.m.r. (100 MHz, CDCl_3) δ 177.4,

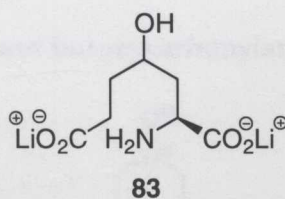
172.5, 144.8, 128.4($\times 2$), 127.3, 127.0($\times 2$), 76.5, 60.6, 58.4, 57.2, 38.0, 30.2, 29.9, 24.7, 14.1; IR ν_{\max} (NaCl)/ cm^{-1} , 3288, 1771, 1732, 1182; MS m/z (ESI) +ve ion $[\text{M}+\text{H}]^+$ 306 (100%); HRMS (ESI) $[\text{M}+\text{H}]^+$ 306.1703; $\text{C}_{17}\text{H}_{24}\text{NO}_4$ requires 306.1701.

5.5.7 Dilithium 2(*S*)-(1(*S*)-phenylethylamino)-4-hydroxy pimelate **95**



To a stirred solution of alcohol **93** and lactone **94** (1:1, 22 mg, 0.0721 mmol) in THF was added a solution of lithium hydroxide (4 mg, 0.144 mmol) in water. The resulting solution was stirred at room temperature for 4 h. The organic solvent was removed under reduced pressure and the concentrate freeze-dried to yield the product **95** (21 mg, 100%); ^1H n.m.r. (400 MHz, D_2O) δ 7.25–7.32 (5H, m, Ar-H), 3.72 (1H, m, PhCHCH_3), 3.53–3.63 (1H, m), 2.79–2.84 (1H, m), 2.04–2.11 (2H, m, 6- CH_2), 1.91–2.04 (3H, m, 5- CH_2 and 3- CHH), 1.49 (1H, m, 3- CHH), 1.26 (3H, d, $J = 6.9$ Hz, PhCHCH_3); ^{13}C n.m.r. (100 MHz, CDCl_3) δ 186.1, 186.0, 185.9, 185.2, 184.7, 184.3, 131.7($\times 2$), 131.6($\times 2$), 130.6, 130.5, 130.4($\times 2$), 130.2($\times 2$), 73.7, 72.7, 72.1, 71.5, 63.3, 61.8, 59.4, 59.3, 36.7, 35.9, 35.1, 32.3, 26.2, 26.1; MS m/z (ESI) –ve ion $[\text{M}-\text{Li}]^-$ 300 (55%), $[\text{M}^{2-}+\text{H}]^-$ 294 (100%); HRMS (ESI) $[\text{M}-\text{Li}]^-$ 300.1425; $\text{C}_{16}\text{H}_{23}\text{LiNO}_5$ requires 300.1430.

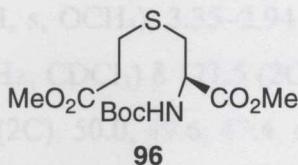
5.5.8 Dilithium (2*R*,4*RS*)-2-amino-4-hydroxy pimelate **83**



To a stirred solution of the alcohol **95** (194 mg, 0.662 mmol) in water (10 mL) was added palladium on charcoal (10 mg) and the mixture stirred under an atmosphere of hydrogen at room temperature for 48 h. The reaction mixture was filtered through celite and concentrated *in vacuo* to yield the product **83** as a white solid (125 mg, 93%). ^1H n.m.r. (300 MHz, D_2O) δ 3.69–3.3.85 (2H, br m), 2.07–2.57 (2H, m), 1.46–2.03 (4H, m); ^{13}C n.m.r. (75 MHz, CDCl_3) δ 183.4, 181.9, 179.0, 177.9, 72.1, 70.6, 68.9, 67.4, 54.7, 53.4,

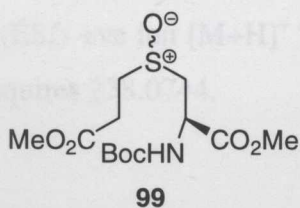
34.0, 33.8, 31.5, 30.9; MS m/z (ESI) $-ve$ ion $[M-Li]^-$ 196 (100%); HRMS (ESI) $[M-Li]^-$ 196.0802; $C_7H_{11}LiNO_5$ requires 196.0803.

5.5.9 Dimethyl (2*R*)-2-*N*-*tert*-butoxycarbonylamino-4-thiapimelate **96**



Sodium (491 mg, 10.7 mmol) was added to anhydrous methanol (75 mL) at 0 °C slowly over 30 min, under an atmosphere of nitrogen, to afford a solution of sodium methoxide. *N*-*tert*-butoxycarbonyl-L-cysteine methyl ester **98** (2.00 mL, 9.71 mmol) was added at 0 °C and the mixture warmed to room temperature. Methyl 3-bromopropionate **97** (3.18 mL, 29.1 mmol) was added and the resulting mixture refluxed for 16 h. The mixture was diluted with H₂O (50 mL) and extracted with dichloromethane (4 × 50 mL). The combined organic extracts were dried (Na₂SO₄) and concentrated *in vacuo* to give a pale yellow oil. Purification by column chromatography eluting with 10% ethyl acetate/hexane yielded the product **96** (2.61 g, 84%) as a pale yellow oil. $[\alpha]_D^{22} +12.6$ (*c*, 11.8 in CH₂Cl₂); ¹H n.m.r. (400 MHz, CDCl₃) δ 5.40 (1H, d, *J* = 8.0 Hz, NH), 4.53 (1H, dt, *J* = 8.0, 4.8 Hz, αH), 3.76 (3H, s, OCH₃), 3.68 (3H, s, OCH₃), 2.94–3.02 (2H, m, *J* = 4.8 Hz, βH), 2.78 (2H, t, *J* = 7.5 Hz, CH₂CH₂), 2.59 (2H, t, *J* = 7.5 Hz, CH₂CH₂), 1.40 (9H, s, *O**t*Bu); ¹³C n.m.r. (100 MHz, CDCl₃) δ 172.0, 171.4, 155.1, 80.2, 53.3, 52.6, 51.8, 34.6, 34.5, 28.3, 27.6; IR ν_{max} (NaCl)/cm⁻¹ 3373, 2976, 1738, 1713, 1167; MS m/z (ESI) $+ve$ ion $[M+Na]^+$ 344 (100%); HRMS (ESI) $[M+Na]^+$ 344.1136; C₁₃H₂₃NNaO₆S requires 344.1138.

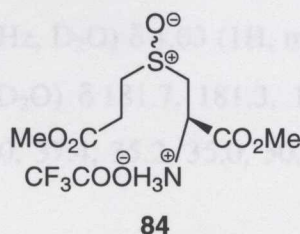
5.5.10 Dimethyl (2*R*,4*RS*)-2-*tert*-butoxycarbonylamino-4-oxo-4-thiapimelate **99**



To a stirred solution of sulfide **96** (2.18 g, 6.78 mmol) in methanol was added a solution of NaIO₄ (2.90 g, 13.6 mmol) in H₂O, which resulted in an exothermic reaction and immediate precipitation of a white solid. The reaction was left to stand for 16 h. The reaction mixture was diluted with H₂O (30 mL) and extracted with dichloromethane (5 × 30 mL). The

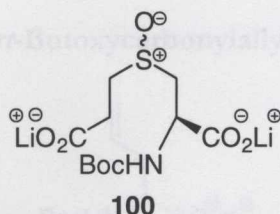
combined organic layers were dried (Na_2SO_4) and concentrated *in vacuo* to give a clear oil. Purification by column chromatography eluting with 30% dichloromethane/ethyl acetate yielded the desired product **99** (1.90 g, 83%) as a mixture of diastereomers (1:1) as a clear oil. ^1H n.m.r. (400 MHz, CDCl_3) δ 5.76 (0.5H, br s, NH), 5.70 (0.5H, br s, NH), 4.67 (1H, m), 3.77 (3H, s, OCH_3), 3.70 (3H, s, OCH_3), 3.35–2.94 (4H, m), 2.85–2.80 (2H, m), 1.41 (9H, s, OtBu); ^{13}C n.m.r. (100 MHz, CDCl_3) δ 171.5 (2C) 170.7, 170.4, 155.3, 155.1, 80.6, 80.5, 54.3, 53.5, 53.0, 52.9, 52.2 (2C), 50.0, 49.6, 47.4, 47.0, 29.6 28.2, 26.7, 26.6; IR ν_{max} (NaCl)/ cm^{-1} ; 3359, 2978, 1740, 1713, 1223, 1167, 1026; MS m/z (ESI) +ve ion $[\text{M}+\text{Na}]^+$ 360 (100%); HRMS (ESI) $[\text{M}+\text{Na}]^+$ 360.1089; $\text{C}_{13}\text{H}_{23}\text{NNaO}_7\text{S}$ requires 360.1088.

5.5.11 Dimethyl (2*R*,4*RS*)-2-amino-4-oxo-4-thiapimelate **84**



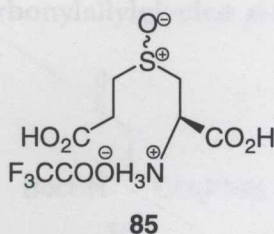
To a stirred solution of the sulfoxide diastereomers **99** (267 mg, 0.791 mmol) in dichloromethane (10 mL) was added trifluoroacetic acid (10 mL) and the resulting solution stirred for 3 h. The mixture was concentrated *in vacuo*, by co-evaporating with dichloromethane, to give a 1:1 mixture of the sulfoxide diastereomers **84** as an orange oil (278 mg, 100 %); ^1H n.m.r. (400 MHz, CDCl_3) δ 4.83 (0.5H, m, NH), 4.76 (0.5, m, NH), 3.88 (1.5H, s, OCH_3), 3.84 (1.5H, s, OCH_3), 3.72 (3H, s, OCH_3), 3.52–3.66 (2H, br m), 3.20–3.32 (2H, br m), 2.85–2.92 (2H, br m); ^{13}C n.m.r. (100 MHz, CDCl_3) δ 171.7, 171.6, 167.2, 167.1, 161.2 (q, $J = 40$ Hz, CF coupling), 114.0 (q, $J = 286$ Hz, CF coupling), 54.3, 54.2, 53.4, 52.6, 50.4, 49.6, 48.8, 48.0, 47.8, 47.0, 26.7, 26.6; IR ν_{max} (NaCl)/ cm^{-1} ; 3412, 1734, 1684, 1201, 1018; MS m/z (ESI) +ve ion $[\text{M}+\text{H}]^+$ 238 (100%); HRMS (ESI) +ve ion $[\text{M}+\text{H}]^+$ 238.0739; $\text{C}_8\text{H}_{16}\text{NO}_5\text{S}$ requires 238.0744.

5.5.12 Dilithium (2*R*,4*RS*)-2-*tert*-butoxycarbonylamino-1,6-dicarboxylate-4-oxo-4-thiapimelate **100**



To a stirred solution of sulfoxide **99** (592 mg, 1.76 mmol) in THF (10 mL) was added a solution of lithium hydroxide (84 mg, 3.51 mmol) in water (5 mL). The resulting reaction mixture was stirred at room temperature for 1 h. The organic solvent was removed under reduced pressure and the concentrate freeze-dried to yield the product **100** as a white solid (400 mg, 75%). ^1H n.m.r. (200 MHz, D_2O) δ 4.03 (1H, m), 2.23–2.99 (6H, br m), 1.26 (9H, s, *tert*Bu); ^{13}C n.m.r. (50 MHz, D_2O) δ 181.7, 181.3, 178.3, 176.1, 159.0, 158.0, 143.3, 127.1, 81.8, 81.6, 57.8, 55.8, 38.0, 37.4, 35.2, 35.0, 30.7, 30.2, 28.2, 28.1; MS m/z (ESI) +ve ion $[\text{M}+\text{Na}]$ 337 (100%).

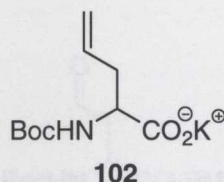
5.5.13 (2*R*,4*RS*)-2-amino-1,6-dicarboxylate-4-oxo-4-thiapimelate trifluoroacetate **85**



To a stirred suspension of sulfoxide **100** (608 mg, 1.80 mmol) in dichloromethane (15 mL) was added trifluoroacetic acid (15 mL). The reaction mixture was stirred at room temperature for 1.5 h. The reaction mixture was concentrated *in vacuo*, diluted with water (10 mL) and washed with ethyl acetate (3×10 mL). The aqueous layer was concentrated under reduced pressure to yield the product **85** as a yellow oil (651 mg, 108%). ^1H n.m.r. (400 MHz, D_2O) δ 4.24 (1H, m), 2.52–2.79 (6H, m); IR ν_{max} (NaCl)/ cm^{-1} 3419, 1703, 1661, 1204, 1143; MS m/z (ESI) +ve ion $[2\text{M}-\text{Li}+\text{H}]^+$ 437 (100%).

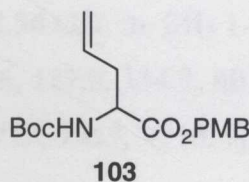
5.6 Synthesis of Aspartate β -Semialdehyde Trifluoroacetate salt

5.6.1 Potassium (*R,S*)-*N*-*tert*-Butoxycarbonylallylglycinate⁹ **102**



To a solution of (*R,S*)-allyl glycine **101** (5.00 g, 43.4 mmol) in a two-phase mixture of water/THF (1:1, 100 mL) was added KHCO_3 (4.35 g, 43.4 mmol) and di-*tert*-butyldicarbonate (12.2 g, 43.4 mmol). The mixture was stirred at room temperature for 3 days. The resulting solution was freeze-dried to give the product **102** a white solid which was used without further purification (11.2 g, 96%). ^1H n.m.r. (200 MHz, D_2O) δ 5.60 (1H, m, γH), 4.94–5.03 (2H, m, δH), 3.79 (1H, br s, NH), 2.09–2.43 (3H, m, αH , βH), 1.27 (9H, s, *t*Bu); ^{13}C n.m.r. (100 MHz, D_2O) δ 182.2, 160.2, 137.0, 121.0, 83.8, 59.6, 39.5, 30.8; spectral data were in accordance with literature values.⁹

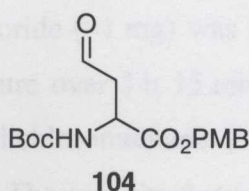
5.6.2 (*R,S*)-*N*-*tert*-Butoxycarbonylallylglycine *p*-methoxybenzyl ester⁹ **103**



To a solution of the potassium salt of (*R,S*)-*N*-*tert*-butoxycarbonylallylglycine **102** (11.2 g, 44.1 mmol) in dry DMF (100 mL) was added *p*-methoxybenzyl chloride (9.3 mL, 66.2 mmol) at room temperature. The resulting mixture was stirred at room temperature for 3 days, then diluted with water (100 mL) and extracted with ethyl acetate (5 \times 50 mL). The combined organic fractions were washed with water (3 \times 100 mL), dried (MgSO_4) and concentrated *in vacuo* to give a clear oil. Purification by column chromatography eluting with 20% ethyl acetate/hexane yielded the product **103** as a clear oil (13.0 g, 92%). ^1H n.m.r. (200 MHz, CDCl_3) δ 7.28, (2H, m, Ar-H), 6.88 (2H, m, Ar-H), 5.63 (1H, m, γH), 5.02–5.18 (3H, m, $\text{CH}_2\text{-Ar}$ and δH), 4.39 (1H, m, αH), 3.81 (3H, s, OCH_3), 2.44–2.54 (2H, m, βH), 1.43 (9H, s, *t*Bu); ^{13}C n.m.r. (50 MHz, CDCl_3) δ 171.1, 159.7, 132.2, 131.9, 129.2,

119.0, 114.0, 79.9, 69.5, 55.2, 52.9, 36.6, 28.2; IR ν_{\max} (NaCl)/ cm^{-1} 3368, 3077, 2977, 1715, 1613, 1515; spectral data were in accordance with literature values.⁹

5.6.3 (*R,S*)-*N*-*tert*-Butoxycarbonylaspatic acid β -semialdehyde *p*-methoxybenzyl ester⁹ **104**



Method A – Potassium osmate dihydrate

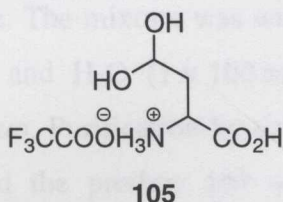
To a stirred solution of (*R,S*)-*N*-*tert*-butoxycarbonylallylglycine *p*-methoxybenzyl ester **103** (4.13 g, 12.8 mmol) in acetone/water (218 mL, 2:1) was added sodium periodate (5.49 g, 25.7 mmol), followed by potassium osmate dihydrate (\approx 47 mg, 1 mmol%). The resulting mixture was stirred for 3 days at room temperature. The reaction mixture was diluted with organic layers were dried (MgSO_4) and concentrated *in vacuo* to give a clear oil. Purification by column chromatography eluting with 20% hexane/ether yielded the product **104** as a clear oil (2.58 g, 60%). ^1H n.m.r. (200 MHz, CDCl_3) δ 9.74 (1H, s, γH), 7.30 (2H, m, Ar-H), 6.92 (4H, m, Ar-H), 5.42 (1H, br d, $J = 8.0$ Hz, NH), 5.15 (2H, s, $\text{CH}_2\text{-Ar}$), 4.65 (1H, m, αH), 3.84 (3H, s, OCH_3), 2.56 (2H, m, βH) 1.45 (9H, s, *t*Bu); ^{13}C n.m.r. (75 MHz, CDCl_3) δ 199.7, 171.3, 160.2, 130.6, 127.6, 114.2, 80.7, 68.0, 55.7, 49.2, 48.1, 46.4, 28.6; IR ν_{\max} (NaCl)/ cm^{-1} 3384, 2975, 1717, 1613, 1516; spectral data were in accordance with literature values.⁹

Method B – Osmium tetroxide

To a stirred solution of (*R,S*)-*N*-*tert*-butoxy-carbonylallylglycine *p*-methoxybenzyl ester **103** (198 mg, 0.615 mmol) in water/dioxane (15 mL, 1:2) was added a solution of osmium tetroxide in water (0.039M, 300 μL , 1.5 mmol%). The mixture was stirred for 1 h until a black colour appeared. Sodium periodate (397 mg, 1.85 mmol) was then added and the resultant solution stirred for 16 h. The reaction mixture was diluted with $\text{Na}_2\text{S}_2\text{O}_3$ (20 mL) and extracted into ethyl acetate (3×20 mL). The combined organic layers were dried (MgSO_4) and concentrated *in vacuo* to give a clear oil. Purification by column chromatography eluting with 20% hexane/ether yielded the product **104** as a clear oil (100 mg, 48%).

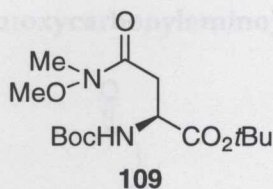
Method C – $RuCl_3 \cdot H_2O$

To a stirred solution of sodium periodate (235 mg, 1.01 mmol) in water (3 mL) was added acetonitrile/carbon tetrachloride (2 mL, 1:1). A solution of (*R,S*)-*N*-*tert*-butoxycarbonylallylglycine *p*-methoxybenzyl ester **103** (118 mg, 0.367 mmol) in acetonitrile/carbon tetrachloride (2 mL, 1:1) was added dropwise and the reaction mixture cooled to $-15\text{ }^\circ\text{C}$. Ruthenium trichloride (≈ 1 mg) was added and the resulting mixture was allowed to warm to room temperature over 1 h 15 min. The reaction mixture was filtered through celite and washed with dichloromethane (4×10 mL), diluted with water and extracted into CH_2Cl_2 (3×10 mL). The combined organic layers were dried ($MgSO_4$) and concentrated *in vacuo* to give a clear oil. Purification by column chromatography eluting with 20% hexane/ether yielded the product **104** as a clear oil (34 mg, 60%). Further elution gave the starting material (14 mg, 35%) as a clear oil.

5.6.4 (*R,S*)-Aspartic acid β -semialdehyde hydrate trifluoroacetate⁹ **105**

To a stirred solution of (*R,S*)-*N*-*tert*-butoxycarbonylaspartic acid β -semialdehyde *p*-methoxybenzyl ester **104** (500 mg, 1.49 mmol) in dry dichloromethane (9.8 mL) was added trifluoroacetic acid (9.8 mL). The resulting mixture was stirred at room temperature for 2 h. The reaction mixture was concentrated *in vacuo* to give a brown residue. The crude product was dissolved in water (20 mL) and washed with ethyl acetate (3×20 mL). The aqueous layer was freeze-dried to yield the product **105** as a pale yellow solid (231 mg, 66%). 1H n.m.r. (300 MHz, D_2O) δ 5.14 (1H, m, γH), 3.98 (1H, dd, $J = 4.0, 7.7$ Hz, αH), 2.13–1.86 (2H, m, βH); ^{13}C n.m.r. (75 MHz, $CDCl_3$) δ 163.5, 163.0, 88.4, 50.9, 38.0, 36.9; spectral data in accordance with literature values.⁹

5.6.5 *N*-*tert*-Butoxycarbonyl-L-aspartic acid 1-(*tert*-butyl ester) 4-*N*-methoxy-*N*-methylamide^{10,11} **109**



Method A - BOP.PF₆

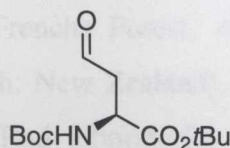
To a stirred solution of *N*-*tert*-butoxycarbonyl-L-aspartic acid 1-(*tert*-butyl ester) **108** (2.0 g, 7.63 mmol) in dichloromethane (70 mL) was added triethylamine (1.1 mL, 7.63 mmol) followed by (benzotriazol-1-yloxy) tris (dimethylamino) phosphonium hexafluorophosphate (BOP.PF₆) (3.2 g, 7.63 mmol) and the reaction mixture was stirred for 5 min. To the resultant solution was added *N,O*-dimethylhydroxyamine hydrochloride (745 mg, 7.63 mmol) followed by triethylamine (1.1 mL, 7.63 mmol). The reaction mixture was then stirred for 2 h at room temperature. The mixture was washed with HCl (2 M, 1 × 100 mL), saturated NaHCO₃ (1 × 100 mL) and H₂O (1 × 100 mL). The organic layer was dried (Na₂SO₄) and concentrated *in vacuo*. Purification by column chromatography eluting with 50% ethyl acetate/hexane yielded the product **109** as a colourless oil (2.16 g, 95%). ¹H n.m.r. (400 MHz, d₆-DMSO) δ 6.97 (1H, d, *J* = 8.3 Hz, NH), 4.25 (1H, m, αH), 3.65 (3H, s, OCH₃), 3.08 (3H, s, NCH₃), 2.74–2.78 (2H, m, βH), 1.37 (18H, s, 2 × *t*Bu); ¹³C n.m.r. (100 MHz, d₆-DMSO) δ 171.1, 170.3, 155.2, 80.4, 78.4, 60.9, 50.3, 33.4, 30.9, 28.4, 28.0; IR ν_{max} (NaCl)/cm⁻¹ 3430, 2977, 1717, 1662, 1496; ¹H n.m.r. spectral data were in accordance with literature values.¹⁰

Method B - PyBOP

To a stirred solution of *N*-*tert*-butoxycarbonyl-L-aspartic acid 1-(*tert*-butyl ester) **108** (2.51 g, 8.71 mmol) in dichloromethane (70 mL) was added triethylamine (1.4 mL, 8.71 mmol) followed by (benzotriazol-1-yloxy) tris-pyrrolidinophosphonium hexafluorophosphate (PyBOP) (5.00 g, 9.58 mmol) and the reaction mixture stirred for 5 min. To the resultant solution was added *N,O*-dimethylhydroxyamine hydrochloride (935 mg, 9.58 mmol) followed by triethylamine (1.4 mL, 9.58 mmol). The reaction mixture was then stirred for 2 h at room temperature. The mixture was washed with HCl (1 M, 1 × 100 mL), saturated NaHCO₃ (1 × 100 mL) and H₂O (1 × 100 mL). The organic layer was dried (Na₂SO₄) and concentrated *in vacuo*. Purification by column chromatography

eluting with 50% ethyl acetate/hexane yielded the product **109** as a colourless oil (2.61 g, 90%).

5.6.6 *tert*-Butyl (*S*)-2-(*tert*-butoxycarbonylamino)-4-oxo-butanoate^{10,11} **110**



110

To a stirred solution of *N*-*tert*-butoxycarbonyl-L-aspartic acid 1-(*tert*-butyl ester) *N*-methoxy-*N*-methylester **109** (2.10 g, 6.34 mmol) in THF (90 mL) at $-78\text{ }^{\circ}\text{C}$ was added dropwise over 20 min DIBAL in hexane (1 M, 12.0 mL, 12.0 mmol) and the reaction mixture stirred for 2 h. The reaction mixture was diluted with saturated NaHSO_4 (100 mL) and extracted with ether ($3 \times 100\text{ mL}$). The combined organic layers were washed with H_2O ($1 \times 100\text{ mL}$), HCl (2 M, $1 \times 100\text{ mL}$), saturated NaHCO_3 ($1 \times 100\text{ mL}$), dried (Na_2SO_4) and concentrated *in vacuo*. Purification by column chromatography eluting with 50% ethyl acetate/hexane yielded the product **110** as a colourless oil (1.48 g, 86%). ^1H n.m.r. (400 MHz, d_6 -DMSO) δ 9.60 (1H, s, CHO), 7.21 (1H, d, $J = 7.68\text{ Hz}$, NH), 4.34 (1H, m, αH), 2.64–2.81 (2H, m, βH), 1.54 (18H, s, $2 \times t\text{Bu}$); ^{13}C n.m.r. (100 MHz, d_6 -DMSO) δ 200.2, 170.5, 155.2, 80.8, 78.3, 49.0, 44.3, 28.1, 27.5; IR ν_{max} (NaCl)/ cm^{-1} 3374, 2978, 1718, 1508, 1368; ^1H n.m.r. spectral data were in accordance with literature values.¹⁰

5.7 General Procedures for Enzymology and Kinetics

Chemicals were purchased from Sigma-Aldrich (Castle Hill, Australia); media for bacterial cultures were purchased from Invitrogen (Christchurch, New Zealand). SDS-PAGE gels were purchased from Gradipore (Frenchs Forest, Australia). Restriction enzymes were purchased from Roche (Christchurch, New Zealand). Bio-Rad protein assay kit and DNA ladders were purchased from Bio-Rad laboratories (Auckland, New Zealand). Column chromatography media were purchased from Amersham Pharmacia Biotech (Auckland, New Zealand) as HiTrap pre-packed columns or as a loose gel, which was packed in Pharmacia XK26 columns.

pH measurements were made using either a standard meter fitted with a Russell Combination (Tris compatible) electrode type no. TR/CMAW711/TB or a Denver UltraBASIC pH/mV meter with a pH/ATC KCl electrode type no. 300729.1.

Centrifugation was performed in an Eppendorf centrifuge 5430, on a small scale (< 1.5 mL) at up to 15,000 rpm using a 16F24-11 rotor and on large scale (< 50 mL) at up to 5250 rpm using a 16A4-44 rotor at 4 °C. Large volumes 50–200 mL were centrifuged using a Heraeus Sepatech 20RS centrifuge at 4 °C.

Columns were run using a Gilson Minipuls M312 peristaltic pumps with Gilson Modess 740 systems control software on a Digital Venturis 466PC and a Gilson FC 203B fraction collector.

Polyacrylamide gel electrophoresis (PAGE) was routinely run on a Bio-Rad mini PROTEAN[®] III Gel electrophoresis unit SE 400, using a Bio-Rad 300 power pac. Agarose gel electrophoresis was run on a Hoefer HE33 Mini Horizontal Submarine Unit, using a Bio-Rad 300 power pac unit. Agarose gels were visualised on a T2210 UV transilluminator (302 nm).

Ultra-Violet (UV) spectroscopy was performed on a Hewlett-Packard 8452A diode array spectrophotometer with a recirculating water bath attached for temperature control. All cuvettes used were 1 cm path length plastic cuvettes from Sarstedt Inc. (North Carolina, USA).

5.8 Bacterial Cultures

All *E. coli* cultures were grown under sterile conditions. All media and equipment were autoclaved at 121 °C for 20 min, or purchased sterile. Solutions were made up in sterile deionised water. During the transfer of cultures, all equipment was flamed and surfaces sterilised with ethanol.

5.8.1 Media

The following media were used for culturing *E. coli* XL-1 Blue pJG001 and *E. coli* XL-1 Blue pJK001.

Luria-Bertani¹² (LB broth)	LB broth	20 g/L
LB Agar	LB broth	20 g/L
	Agar	15 g/L

5.8.2 Antibiotics

Stock solutions of antibiotics were stored at -20 °C. The following final concentrations were used for selection.

Ampicillin	100 µg/mL
Tetracycline	20 µg/mL

5.9 Bacterial Strains

Strains of *E. coli* were available that had been transformed with high copy number pBluescript plasmids. *E. coli* XL-1 Blue pJG001 contained a plasmid that had the *ampR* (β -lactamase) and *dapA* (DHDPS) gene.¹³ *E. coli* XL-1 Blue pJK001 contained a plasmid that had the *ampR* (β -lactamase) and *dapB* (DHDPR) genes.¹⁴ This provided a simple and convenient means of over-expression. The plasmids had been introduced into *E. coli* XL-1 Blue using the calcium chloride method and successful transformants were identified by conferred ampicillin resistance.¹⁵

5.9.1 Preparation of Glycerol Freezes

A 1.0 mL aliquot of an overnight culture was added to 0.25 mL of sterile 80% glycerol (propan 1,2,3-triol) in deionised water in a screw top Eppendorf. The tube was gently vortexed before being flash frozen in liquid nitrogen ($-196\text{ }^{\circ}\text{C}$) for long term storage at $-80\text{ }^{\circ}\text{C}$.

5.9.2 Plate Preparation

Plates were poured using aseptic technique into sterile petri dishes. 25–30 mL of media per plate was adequate for overnight growth on LB media. Any bubbles formed were removed by quickly flaming the surface before the agar had hardened. The plates were allowed to set overnight before being used. The plates could be stored for three weeks if kept at $4\text{ }^{\circ}\text{C}$.

5.9.3 Incubation of Colonies

Agar plates were streaked with *E. coli* XL-1 Blue (from glycerol freeze, an overnight culture, or a single colony on an agar plate of not more than 3 days old stored at $4\text{ }^{\circ}\text{C}$) using a flamed sterile nichrome wire; the concentration was successively decreased across the plate to allow for selection of a single colony. The plates were incubated, inverted, overnight at $37\text{ }^{\circ}\text{C}$. Individual colonies were selected with a wire loop and used to inoculate 3 mL of liquid medium. These starter cultures were grown for approximately 8–10 h in an orbital incubator ($37\text{ }^{\circ}\text{C}$, 180 rpm) and subsequently used to inoculate larger quantities of media.

5.9.4 Standard Plasmid Preparation by Alkaline Lysis¹²

The following solutions were used in the plasmid preparation.

Solution I (4 °C)	50 mM glucose
	25 mM Tris.HCl pH 8.0
	10 mM EDTA pH 8.0
Solution II (r.t.)	0.2 M NaOH
	1% SDS
Solution III (4°C)	60 mL, 5 M potassium acetate
	1.5 mL glacial acetic acid
	28.5 mL H ₂ O

An *E. coli* XL-1 Blue pJG001 or *E. coli* XL-1 Blue pJK001 glycerol freeze was streaked out on LB agar containing standard concentrations of ampicillin and tetracycline, and incubated overnight at 37 °C. A single colony was selected and used to inoculate 3 mL of LB broth containing standard concentrations of ampicillin and tetracycline, and incubated overnight at 37 °C (180 rpm).

A 1.5 mL aliquot of overnight culture was transferred to an Eppendorf tube and centrifuged (13 000 rpm, 10 min); the supernatant was carefully removed by aspiration. The cell pellet was resuspended in 100 µL of ice cold solution I, gently vortexed and chilled on ice for 10 min. 200 µL of freshly prepared solution II was then added slowly and mixed by gentle rotation and chilled on ice for 5 min. 150 µL of ice-cold solution III was added and gently mixed until the viscosity decreased and a white precipitate formed, which was chilled on ice for 20 min and centrifuged (10,000 rpm, 15 min). The supernatant was carefully transferred to a fresh tube and the double-stranded DNA precipitated with 2 volumes of 100% ethanol at 4 °C. After standing for 2 min, the solution was centrifuged (13,000 rpm, 4 °C, 10 min) and the supernatant removed, leaving the dried DNA pellet.

The pellet was rinsed with 3 mL of 70% ethanol and dried again. Finally, the DNA was resuspended in 50 µL sterile Tris.HCl (10 mmol), EDTA (1 mmol).

5.9.5 Restriction Digests

Restriction digests were typically performed in 15 μL volumes. *Hind* III and *Eco*R I were used individually for single digests of 2 μL of plasmid DNA and in combination for a double digest of 2.0 μL plasmid DNA. Restriction digests were carried out using 1.5 μL of 10 \times restriction buffer, 0.2 μL of each required restriction enzyme and made up to 15 μL with sterile H_2O , and the digests were incubated at the appropriate temperature for 1 h.

Double digest of pJG001 with *Hind* III and *Eco*R I

11.1 μL H_2O

2.0 μL DNA solution from standard plasmid preparation

1.5 μL buffer

0.2 μL *Eco*R I

0.2 μL *Hind* III

15 μL Total

Incubated for 1 h at 37 $^\circ\text{C}$. 4.0 μL loading buffer was added and mixed immediately prior to running of the DNA gel.

5.9.6 Agarose Gel Electrophoresis¹²

1% Agarose gel	0.3 g agarose
	30 mL of 0.5 TBE buffer
1 × TBE buffer	54 mM Tris.borate
	1 mM EDTA pH 8.0
Loading dye	30% glycerol
	0.25% bromophenol blue
	0.25% xylene cyanol
	RNAse, final concentration of 10 mg/mL

Restriction fragments were mapped on a 1% (w/v) agarose gel against a one kb ladder. A 1% agarose solution (0.3 g agarose in 30 mL 1 × TBE buffer) was heated and allowed to cool slightly ($\approx 50^\circ\text{C}$) before being poured into a gel casting tray and the well comb inserted. The gel was allowed to set (≈ 30 min) before the comb was removed. The casting tray was then transferred into a gel tank containing electrophoresis 1 × TBE buffer. The gel was loaded with DNA samples (10 μL) mixed with 3 μL Bio-Rad nucleic acid loading buffer and 1 μL of 10 $\text{mg}\cdot\text{mL}^{-1}$ RNAse. A DNA ladder was also loaded; 6 μL of the one kb ladder. The gel was run at 80 V for 1.5 h until the bromophenol blue band was nearing the end of the gel. The gel was stained with ethidium bromide (0.5 $\mu\text{g}\cdot\text{mL}^{-1}$) for 30 min. The stained DNA fragments were visualised on an UV transilluminator with a wavelength of 302 nm. The gel was then photographed under UV light.

Samples were diluted to an appropriate concentration and mixed with an equal volume of treatment buffer, centrifuged to mix, and heated in boiling water for 3 min. 40 μL of the mixture was loaded onto the wells of a 4-20% pre-cast gradient gel from GenSipore, a marker was also added. The gel was electrophoresised at 4 $^\circ\text{C}$ at constant voltage (150 V) for approximately 1.5 h until the bromophenol blue had run to the bottom of the resolving gel. The gel was stained for 30-60 min in Coomassie brilliant blue, and then washed with destain.

5.9.7 Sodium Dodecyl Sulfate Polyacrylamide Gel Electrophoresis (SDS-PAGE)¹⁶

The following stock solutions were used for conducting SDS-PAGE electrophoresis.

Electrophoresis tank buffer	6.0 g Tris.HCl
	28.8 g glycine
	20 mL 10% SDS
	Made up to 2 L with H ₂ O
Coomassie brilliant blue stain	1.0 g Coomassie brilliant blue
	500 mL MeOH
	100 mL glacial acetic acid
	Made up 1 L with H ₂ O
Destain	50 mL MeOH
	100 mL glacial acetic acid
	850 mL H ₂ O
Sample treatment buffer (2x)	125 μ L of 1 M Tris.HCl pH 8.0
	2 mL 10% (w/v) SDS
	1 mL glycerol
	500 μ L 2-mercaptoethanol
	125 μ L 1% (w/v) bromophenol blue
	750 μ L H ₂ O
	Stored at -20 °C

Samples were diluted to an approximate concentration and mixed with an equal volume of treatment buffer, centrifuged to mix, and heated in boiling water for 3 min. 40 μ L of the mixture was loaded onto the wells of a 4–20% pre-cast gradient gel from Gradipore, a marker was also added. The gel was electrophoresised at 4 °C at constant voltage (150 V) for approximately 1.5 h until the bromophenol blue had run to the bottom of the resolving gel. The gel was stained for 30–60 min in Coomassie brilliant blue, and then washed with destain.

5.9.8 Preparation of Dialysis Tubing

Dialysis tubing (cellulose membrane molecular weight cut-off >12 000 kDa) was run under cold water for 2 h then boiled for 10 min in a 2% (w/v) solution of sodium bicarbonate and 0.05% (w/v) EDTA. Care was taken to ensure the tubing remained submerged at all times. The tubing was then boiled for further 10 min in deionised water, and the same procedure repeated. The solution was cooled and the tubing stored in 0.1% (w/v) sodium azide for up to three months.

Small scale dialysis < 150 μ l were performed using Slide-A-Lyzer mini dialysis cups (from Pierce, molecular weight cut-off > 7000 kDa) according to the manufacturers instructions.

5.10 Isolation and Purification of DHDPS (modified from^{13,17})

5.10.1 DHDPS Overexpression

An *E. coli* XL-1 Blue pJG001 glycerol freeze was streaked out on LB agar containing the standard concentrations of ampicillin and tetracycline and grown overnight at 37 °C. A single colony was selected and used to inoculate 3 mL of LB broth containing the standard concentrations of ampicillin and tetracycline, and incubated overnight at 37 °C. A 750 μ L aliquot of overnight culture was used to inoculate 750 mL of LB broth containing standard concentrations of ampicillin and tetracycline, and incubated overnight at 37 °C. The cells were then chilled on ice for 30 min, and harvested by centrifugation (5000 rpm, 4 °C, 10 min).

The cells were resuspended in 20 mM Tris.HCl pH 8.0 at 4 °C (equivalent to the volume of supernatant removed). The cell suspension was centrifuged (5000 rpm, 4 °C, 10 min), the supernatant was discarded and the cell pellet resuspended in 20 mM Tris.HCl pH 8.0 at 4 °C (equivalent to the volume of supernatant removed).

To obtain the crude enzyme extract, the cells were flash-frozen in liquid nitrogen and thawed overnight on ice at 4 °C over seven consecutive nights. The supernatant was collected by centrifugation (5000 rpm, 4 °C, 10 min).

5.10.2 DHDPS Purification

The crude extract was loaded onto a Q-Sepharose ion exchange column that had been pre-equilibrated with three bed volumes of 20 mM Tris.HCl pH 8.0 at 4 °C. The column was then washed with five bed volumes of the start buffer 20 mM Tris.HCl pH 8.0 at 4 °C. DHDPS was eluted with a 0 to 1.0 M NaCl salt gradient in 20 mM Tris.HCl pH 8.0 at 4 °C. The column was washed with three bed volumes of regeneration buffer 1 M NaCl in 20 mM Tris.HCl pH 8.0 at 4 °C. The eluted fractions were tested for DHDPS activity using the *o*-aminobenzaldehyde assay and the active fractions were pooled together.

The pooled fractions were transferred to 12 kDa molecular weight cut-off Sigma dialysis tubing prepared according to the manufacturer's instructions.

Dialysis Buffer (1 L)	20 mM Tris.HCl pH 8.0 at 4 °C	2.24 g
	1 mM EDTA	372 mg
	1 mM 2-mercaptoethanol	14 μ L
	1% ammonium sulphate	1 g

After being dialysed against 50 volumes of dialysis buffer overnight, the dialysed sample was loaded onto a Phenyl Sepharose column which had been pre-equilibrated with three bed volumes of 20 mM Tris.HCl pH 8.0 at 4 °C. The column was then washed with five bed volumes of the start buffer 0.5 M $(\text{NH}_4)_2\text{SO}_4$ pH 8.0 at 4 °C. DHDPS was eluted with a 0.5 to 0 M $(\text{NH}_4)_2\text{SO}_4$ gradient in 20 mM Tris.HCl pH 8.0 at 4 °C. The column was washed with three bed volumes of regeneration buffer 0.5 M $(\text{NH}_4)_2\text{SO}_4$ in 20 mM Tris.HCl pH 8.0 at 4 °C. The eluted fractions were tested for DHDPS activity using the *o*-aminobenzaldehyde assay.

Following a second dialysis against 50 volumes of dialysis buffer, the pooled fractions were loaded onto a 2 mL Hi-Trap Q Sepharose column pre-equilibrated with ten bed volumes of start buffer 20 mM Tris.HCl pH 8.0 at 4 °C. The column was then washed with five bed volumes of the start buffer 20 mM Tris.HCl pH 8.0 at 4 °C. DHDPS was eluted with a 0 to 1.0 M NaCl salt gradient in 20 mM Tris.HCl pH 8.0 at 4 °C. The column was washed with three bed volumes of regeneration buffer 1 M NaCl in 20 mM Tris.HCl pH 8.0 at 4 °C. The fractions were assayed for DHDPS activity using the *o*-aminobenzaldehyde assay and the active fractions were pooled.

The pooled fractions were dialysed a third time against 50 volumes of dialysis buffer and loaded onto a 2 mL Hi-Trap Q Sepharose column pre-equilibrated with ten bed volumes of start buffer 20 mM Tris.HCl pH 8.0 at 4 °C. The column was then washed with five bed volumes of the start buffer 20 mM Tris.HCl pH 8.0 at 4 °C. DHDPS was eluted with a 0 to 1.0 M NaCl salt gradient in 20 mM Tris.HCl pH 8.0 at 4 °C. The column was washed with three bed volumes of regeneration buffer 1 M NaCl in 20 mM Tris.HCl pH 8.0 at 4 °C. The fractions were assayed for DHDPS activity using the *o*-aminobenzaldehyde assay and active fractions were pooled together and stored in 1 mL aliquots at -20 °C.

5.10.3 The *o*-Aminobenzaldehyde Assay for Qualitative Assessment of the Presence of DHDPS Activity.

Buffer (200 mM Tris.HCl, pH 8.0 at 4 °C, 80 mM pyruvate)	150 μ L
<i>o</i> -Aminobenzaldehyde (50 mg.mL ⁻¹ in ethanol)	3 μ L
Test solution	9 μ L
(<i>R/S</i>)-ASA (10 mM) (added last)	6 μ L

The mixture was incubated at 30 °C for 30 min, and the reaction was quenched by adding 10% (w/v) trichloroacetic acid (150 μ L). A deep purple colour indicated the presence of DHDPS activity, while a yellow colour indicated the absence of DHDPS. Controls lacking (*R/S*)-ASA and enzyme solutions were also included, as well as a positive control containing fully characterised DHDPS.

After each purification step, 1 mL was taken to determine specific activities of the enzyme and purification.

5.11 Isolation and Purification of DHDPR¹⁴

5.11.1 DHDPR Overexpression

An *E. coli* XL⁻¹ Blue pJK001 glycerol freeze was streaked out on LB agar containing the standard concentrations of ampicillin and tetracycline and grown overnight at 37 °C. A single colony was selected and used to inoculate 3 mL of LB broth containing the standard concentrations of ampicillin and tetracycline, and incubated overnight at 37 °C. A 750 µL aliquot of overnight culture was used to inoculate 750 mL of LB broth containing standard concentrations of ampicillin and tetracycline, and incubated overnight a 37 °C. The cells were chilled on ice for 30 min, and then harvested by centrifugation (5000 rpm, 4 °C, 10 min).

The cells were resuspended in 20 mM Tris.HCl pH 8.0 at 4 °C. The cell suspension was centrifuged (5000 rpm, 4 °C, 10 min), the supernatant was discarded and the cell pellet resuspended in an equal volume of 20 mM Tris.HCl pH 8.0 at 4 °C.

To obtain the crude extract, the cells were ultrasonicated for 5 min in 3 second bursts, with 10 seconds between bursts. The supernatant was collected by centrifugation (5000 rpm, 4 °C, 10 min).

5.11.2 DHDPR Purification^{14,15}

The crude extract was heat shocked in 1 mL aliquots at 70 °C for two min, followed immediately by cooling on ice. The precipitated proteins were removed by centrifugation (5000 rpm, 4 °C, 10 min) and the supernatant was collected.

The crude sample was loaded onto the Q-Sepharose ion exchange column that had been pre-equilibrated with three bed volumes of 20 mM Tris.HCl pH 8.0 at 4 °C. The column was then washed with five bed volumes of the start buffer 20 mM Tris.HCl pH 8.0 at 4 °C. DHDPR was eluted with a 0 to 1.0 M NaCl salt gradient (over 3 h) in 20 mM Tris.HCl pH 8.0 at 4 °C. The column was washed with three bed volumes of regeneration buffer 1 M NaCl in 20 mM Tris.HCl pH 8.0 at 4 °C. The eluted fractions were tested for DHDPR activity using the coupled assay and the active fractions were pooled together.

Active fractions were pooled and transferred to 12 kDa molecular weight cut-off Sigma dialysis tubing, prepared according to the manufacturer's instructions, and dialysed overnight and against 50 × dialysis buffer.

Dialysis Buffer (1 L)	20 mM Tris.HCl pH 8.0 at 4 °C	2.24 g
	1 mM EDTA	372 mg
	1 mM 2-mercaptoethanol	14 µL
	1% ammonium sulphate	1 g

The dialysed sample was loaded onto a 1 mL (2 ×) High-Trap nucleotide affinity column that had been pre-equilibrated with three bed volumes of 20 mM Tris.HCl pH 8.0 at 4 °C. The column was washed with five bed volumes of the start buffer 20 mM Tris.HCl pH 8.0 at 4 °C. DHDPR was eluted with a 0 to 1.0 M NaCl salt gradient (over 2 min) in 20 mM Tris.HCl pH 8.0 at 4 °C. The column was washed with three bed volumes of regeneration buffer 1 M NaCl in 20 mM Tris.HCl pH 8.0 at 4 °C. The eluted fractions were tested for DHDPR activity using the coupled assay and the active fractions were pooled and dialysed against 50 × dialysis buffer overnight. The dialysed sample was stored in 1 mL aliquots at -20 °C.

5.11.3 The Qualitative Coupled Assay to Test Fractions for DHDPR Activity^{14,15}

Buffer (200 mM HEPES, pH 8.0 at 4 °C)	500 μ L
H ₂ O	270 μ L
Pyruvate (100 mM)	50 μ L
NADPH (5.4 mM)	30 μ L
DHDPS (in excess)	50 μ L
Test solution	50 μ L
(<i>R/S</i>)-ASA (added last)	<u>50 μL</u>
Total Volume	1 mL

All components except the test solution were added to the cuvette and incubated at 30 °C for 3–5 min. The test solution was added with quick mixing using the pipette tip. The change in absorbance at 340 nm was recorded over 120 seconds, blanked against H₂O. Controls containing no ASA, and controls lacking DHDPS were also carried out. A positive control containing fully characterised DHDPR was also carried out.

After each purification step of DHDPR, 1 mL was taken to determine specific activities of the enzyme and purification.

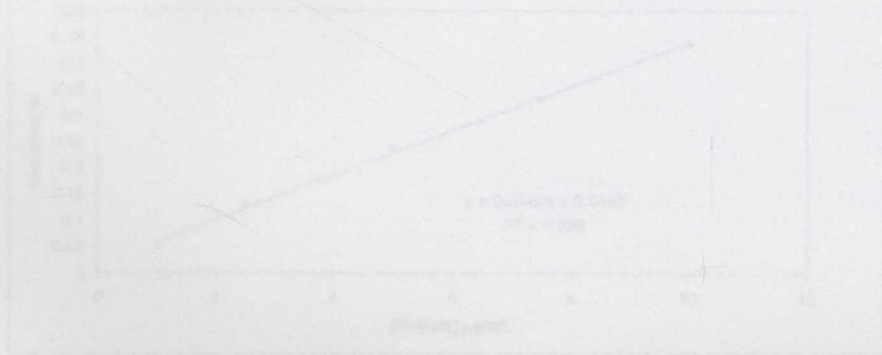


Figure 5.11.1: Typical Standard Curve Obtained Using Bradford's Assay

DHDPS and DHDPR purification samples of unknown protein concentration were diluted with water until the addition of 80 μ L of diluted unknown sample gave an absorbance reading at 595 nm in the range obtained by the standards. Protein concentration was then obtained from the BSA standard curve of known concentrations. Each measurement was performed at least in duplicate.

5.11.4 Enzyme Purity

Enzyme purity was evaluated by monitoring sample homogeneity as judged by SDS-PAGE stained with Coomassie brilliant blue and changes in specific activity.

5.11.5 Bradford Assay (determination of protein concentration)^{18,19}

Five dilutions of a protein standard bovine serum albumin (BSA) ranging from 10 $\mu\text{g/mL}$ to 1.0 $\mu\text{g/mL}$ were required. These dilutions gave absorbance readings at 595 nm between 0.1 and 1.0.

Assay

BSA/unknown solution	80 μL
H ₂ O	720 μL
Bio-Rad Bradford dye reagent concentrate	200 μL

Samples were incubated at room temperature for exactly 6 min before measuring absorbance at 595 nm, blanked against a solution containing 800 μL dH₂O and 200 μL Bio-Rad solution. This data enabled the preparation of a standard curve.

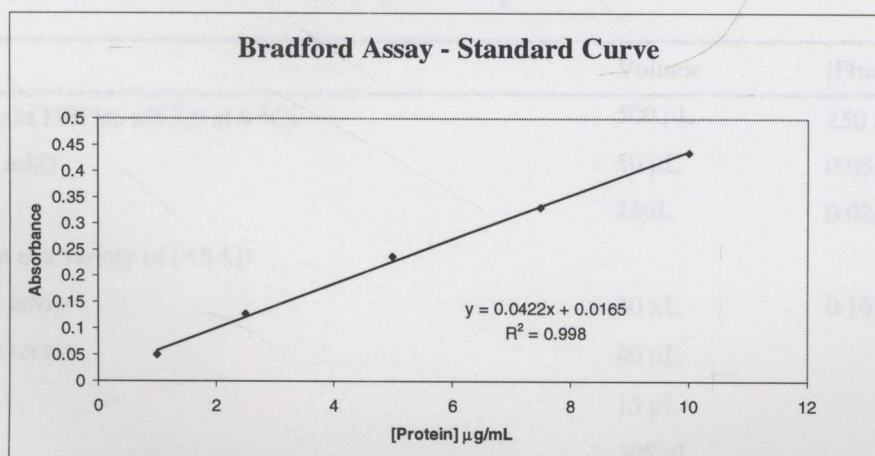


Figure 5.11.1: Typical Standard Curve Obtained Using Bradfords Assay

DHDPS and DHDPR purification samples of unknown protein concentration were diluted with water until the addition of 80 μL of diluted unknown sample gave an absorbance reading at 595 nm in the range obtained by the standards. Protein concentrations were then obtained from the BSA standard curve of known concentrations. Each measurement was performed at least in duplicate.

5.12 Enzyme kinetics of DHDPS^{13,20,21}

5.12.1 Kinetics of DHDPS with Respect to (*S*)-ASA

ASSAY	Volume	[Final]
Buffer (500 mM HEPES pH 8.0 at 4 °C)	500 μ L	250 mM
Pyruvate (20 mM) (held constant at a variety of [pyruvate])	50 μ L	0.05–2.0 mM
(<i>S</i>)-ASA	20 μ L	0.02–0.80 mM
NADPH (5.4 mM)	30 μ L	0.162 mM
DHDPR (in excess)	80 μ L	
DHDPS	15 μ L	
H ₂ O	305 μ L	
Total	1 mL	

The reaction was initiated in the cuvette by the addition of freshly prepared (*S*)-ASA, mixed by inversion of the cuvette. ΔA_{340} nm was measured over 120 sec at 30 °C, blanked against H₂O. Measurements were made in at least duplicate for each concentration of the varied substrate.

Pyruvate and (*S*)-ASA concentrations were determined by using the equation $A = \epsilon \times l \times C$ ($\epsilon_{\text{NADPH}} = 6220 \text{ M}^{-1}\text{cm}^{-1}$). It is assumed the number of moles of NADPH consumed equals the number of moles of pyruvate or (*S*)-ASA.

5.12.2 Kinetics of DHDPS with Respect to Pyruvate

ASSAY	Volume	[Final]
Buffer (500 mM HEPES pH 8.0 at 4 °C)	500 μ L	250 mM
Pyruvate (20 mM)	50 μ L	0.05–2.0 mM
(<i>S</i>)-ASA (held constant at a variety of [ASA])	20 μ L	0.02–0.80 mM
NADPH (5.4 mM)	30 μ L	0.162 mM
DHDPR (in excess)	80 μ L	
DHDPS	15 μ L	
H ₂ O	305 μ L	
Total	1 mL	

The reaction was initiated in the cuvette by the addition of freshly prepared (*S*)-ASA, mixed by inversion of the cuvette. ΔA_{340} nm was measured over 120 sec at 30 °C, blanked against H₂O. Measurements were made in at least duplicate for each concentration of the varied substrate.

Pyruvate and (*S*)-ASA concentrations were determined by using the equation $A = \epsilon \times l \times C$ ($\epsilon_{\text{NADPH}} = 6220 \text{ M}^{-1}\text{cm}^{-1}$). It is assumed the number of moles of NADPH consumed equals the number of moles of pyruvate or (*S*)-ASA.

5.13 Enzyme kinetics of DHDPR^{14,15,21}

5.13.1 Kinetics of DHDPR with Respect to DHDP

ASSAY	Volume	[Final]
Buffer (500 mM HEPES pH 8.0 at 4 °C)	500 μ L	250 mM
Pyruvate (50 mM)	50 μ L	2.5 mM
(S)-ASA (held constant at a variety of [ASA])	20 μ L	0.07–1.0 mM
NADPH	30 μ L	0.04–0.12 mM
DHDPR	15 μ L	
DHDPS (in excess)	20 μ L	
H ₂ O	365 μ L	
Total	1 mL	

The reaction was initiated in the cuvette by the addition of freshly prepared DHDPR, mixed by inversion of the cuvette. ΔA_{340} nm was measured over 120 sec at 30 °C, blanked against H₂O. Measurements were made in at least duplicate for each concentration of the varied substrate.

Pyruvate and (S)-ASA concentrations were determined by using the equation $A = \epsilon \times l \times C$ ($\epsilon_{\text{NADPH}} = 6220 \text{ M}^{-1}\text{cm}^{-1}$). It is assumed the number of moles of NADPH consumed equals the number of moles of pyruvate or (S)-ASA.

5.13.2 Kinetics of DHDPR with Respect to the Cofactor NADPH

ASSAY	Volume	[Final]
Buffer (500 mM HEPES pH 8.0 at 4 °C)	500 μ L	250 mM
Pyruvate (50 mM)	50 μ L	2.5 mM
(S)-ASA	20 μ L	0.07–1.0 mM
NADPH (held constant at a variety of [NADPH])	30 μ L	0.04–0.12 mM
DHDPR	15 μ L	
DHDPS (in excess)	20 μ L	
H ₂ O	365 μ L	
Total	1 mL	

The reaction was initiated in the cuvette by the addition of freshly prepared (S)-ASA, mixed by inversion of the cuvette. ΔA_{340} nm was measured over 120 sec at 30 °C, blanked against H₂O. Measurements were made in at least duplicate for each concentration of the varied substrate.

Pyruvate and (S)-ASA concentrations were determined by using the equation $A = \epsilon \times l \times C$ ($\epsilon_{\text{NADPH}} = 6220 \text{ M}^{-1}\text{cm}^{-1}$). It is assumed the number of moles of NADPH consumed equals the number of moles of pyruvate or (S)-ASA.

5.14 Irreversible Inhibition Studies of 56 and 87 with Respect to DHDPS

ASSAY	Volume	[Final]
Buffer (500 mM HEPES pH 8.0 at 4 °C)	500 μ L	250 mM
Pyruvate (20 mM)	50 μ L	1.0 mM
(S)-ASA	20 μ L	1.0 mM
NADPH (5.4mM)	30 μ L	0.162 mM
DHDPR (in excess)	50 μ L	
DHDPS	15 μ L	
Inhibitor	10 μ L	
H ₂ O	355 μ L	
Total	1 mL	

A solution of buffer (600 μ L), DHDPS (120 μ L) and inhibitor (80 μ L) were added together and incubated at 30 °C. 100 μ l aliquots were taken at specified intervals (beginning at time x and ending at time y) and added to a solution containing buffer (420 μ L), NADPH (30 μ L), DHDPR (50 μ L) and H₂O (355 μ L and incubated for 3 min.

The reaction was initiated in the cuvette by the addition of freshly prepared (S)-ASA, mixed by inversion of the cuvette. ΔA_{340} nm was measured over 120 sec at 30 °C, blanked against H₂O. Measurements were made in at least duplicate for each concentration of inhibitor.

5.15.2 Inhibitional Screening Assay for DHDPS

ASSAY	Volume	[Final]
Buffer (500 mM HEPES pH 8.0 at 4 °C)	500 μ L	250 mM
Pyruvate (20 mM)	50 μ L	1.0 mM
(S)-ASA	20 μ L	1.0 mM
NADPH (5.4 mM)	30 μ L	0.162 mM
DHDPR	50 μ L	
DHDPS (in excess)	15 μ L	
Inhibitor	100 μ L	
H ₂ O	235 μ L	
Total	1 mL	

The reaction was initiated in the cuvette by the addition of freshly prepared (S)-ASA, mixed by inversion of the cuvette. ΔA_{340} nm was measured over 120 sec at 30 °C, blanked against H₂O. Measurements were made in at least duplicate for each concentration of inhibitor.

Pyruvate and (S)-ASA concentrations were determined by using the equation $A = \epsilon \cdot c \cdot l$ ($\epsilon = 1.2 \times 10^4$ L mol⁻¹ cm⁻¹). It is assumed the number of moles of NADPH consumed equals the number of moles of pyruvate or (S)-ASA.

5.15 Inhibition of DHDPS and DHDPR by HTHDP 17 Mimics²¹

5.15.1 Inhibition Screening Assay for DHDPS

ASSAY	Volume	[Final]
Buffer (500 mM HEPES pH 8.0 at 4 °C)	500 μ L	250 mM
Pyruvate (20 mM)	50 μ L	1.0 mM
(S)-ASA	20 μ L	1.0 mM
NADPH (5.4 mM)	30 μ L	0.162 mM
DHDPR (in excess)	50 μ L	
DHDPS	15 μ L	
Inhibitor	100 μ L	Varies
H ₂ O	235 μ L	Varies
Total	1 mL	

The reaction was initiated in the cuvette by the addition of freshly prepared (S)-ASA, mixed by inversion of the cuvette. ΔA_{340} nm was measured over 120 sec at 30 °C, blanked against H₂O. Measurements were made in at least duplicate for each concentration of inhibitor.

Pyruvate and (S)-ASA concentrations were determined by using the equation $A = \epsilon \times l \times C$ ($\epsilon_{\text{NADPH}} = 6220 \text{ M}^{-1} \text{cm}^{-1}$). It is assumed the number of moles of NADPH consumed equals the number of moles of pyruvate or (S)-ASA.

5.15.2 Inhibition Screening Assay for DHDPR

ASSAY	Volume	[Final]
Buffer (500 mM HEPES pH 8.0 at 4 °C)	500 μ L	250 mM
Pyruvate (20 mM)	50 μ L	1.0 mM
(S)-ASA	20 μ L	1.0 mM
NADPH (5.4 mM)	30 μ L	0.162 mM
DHDPR	50 μ L	
DHDPS (in excess)	15 μ L	
Inhibitor	100 μ L	Varies
H ₂ O	235 μ L	
Total	1 mL	

The reaction was initiated in the cuvette by the addition of freshly prepared (S)-ASA, mixed by inversion of the cuvette. ΔA_{340} nm was measured over 120 sec at 30 °C, blanked against H₂O. Measurements were made in at least duplicate for each concentration of inhibitor.

Pyruvate and (S)-ASA concentrations were determined by using the equation $A = \epsilon \times l \times C$ ($\epsilon_{\text{NADPH}} = 6220 \text{ M}^{-1} \text{cm}^{-1}$). It is assumed the number of moles of NADPH consumed equals the number of moles of pyruvate or (S)-ASA.

5.16 Inhibition Kinetics of DHDPS by HTHDP 17 Mimics²¹

5.16.1 Kinetics of Inhibitor with Respect to (S)-ASA

ASSAY	Volume	[Final]
Buffer (500 mM HEPES pH 8.0 at 4 °C)	500 μ L	250 mM
Pyruvate (50 mM) (held constant at a variety of [pyruvate])	50 μ L	2.5 mM
(S)-ASA	20 μ L	0.04–1.5 mM
NADPH (5.4 mM)	30 μ L	0.162 mM
DHDPR (in excess)	80 μ L	
DHDPS	15 μ L	
Inhibitor	100 μ L	Varies
H ₂ O	205 μ L	
Total	1 mL	

The reaction was initiated in the cuvette by the addition of freshly prepared (S)-ASA, mixed by inversion of the cuvette. ΔA_{340} nm was measured over 120 sec at 30 °C, blanked against H₂O. Measurements were made in at least duplicate for each concentration of the varied substrate.

Pyruvate and (S)-ASA concentrations were determined by using the equation $A = \epsilon \times l \times C$ ($\epsilon_{\text{NADPH}} = 6220 \text{ M}^{-1}\text{cm}^{-1}$). It is assumed the number of moles of NADPH consumed equals the number of moles of pyruvate or (S)-ASA.

5.16.2 Kinetics of Inhibitor with Respect to Pyruvate

ASSAY	Volume	[Final]
Buffer (500 mM HEPES pH 8.0 at 4 °C)	500 μ L	250 mM
Pyruvate (20 mM) (held constant at a variety of [ASA])	50 μ L	0.05–2.0 mM
(S)-ASA	20 μ L	1.5 mM
NADPH (5.4 mM)	30 μ L	0.162 mM
DHDPR (in excess)	80 μ L	
DHDPS	15 μ L	
Inhibitor	100 μ L	
H ₂ O	205 μ L	Varies
Total	1 mL	

The reaction was initiated in the cuvette by the addition of freshly prepared (S)-ASA, mixed by inversion of the cuvette. ΔA_{340} nm was measured over 120 sec at 30 °C, blanked against H₂O. Measurements were made in at least duplicate for each concentration of the varied substrate.

Pyruvate and (S)-ASA concentrations were determined by using the equation $A = \epsilon \times l \times C$ ($\epsilon_{\text{NADPH}} = 6220 \text{ M}^{-1}\text{cm}^{-1}$). It is assumed the number of moles of NADPH consumed equals the number of moles of pyruvate or (S)-ASA.

5.17 Inhibition kinetics of DHDPR by HTHDP 17 Mimics²¹

5.17.1 Kinetics of Inhibition with Respect to DHDP

ASSAY	Volume	[Final]
Buffer (500 mM HEPES pH 8.0 at 4 °C)	500 μ L	250 mM
Pyruvate (50 mM)	50 μ L	2.5 mM
(S)-ASA (held constant at a variety of [ASA])	20 μ L	0.07–1.0 mM
NADPH	30 μ L	0.04–0.12 mM
DHDPR	15 μ L	
DHDPS (in excess)	20 μ L	
Inhibitor	100 μ L	Varies
H ₂ O	265 μ L	
Total	1 mL	

The reaction was initiated in the cuvette by the addition of freshly prepared DHDPR, mixed by inversion of the cuvette. ΔA_{340} nm was measured over 120 sec at 30 °C, blanked against H₂O. Measurements were made in at least duplicate for each concentration of the varied substrate.

Pyruvate and (S)-ASA concentrations were determined by using the equation $A = \epsilon \times l \times C$ ($\epsilon_{\text{NADPH}} = 6220 \text{ M}^{-1}\text{cm}^{-1}$). It is assumed the number of moles of NADPH consumed equals the number of moles of pyruvate or (S)-ASA.

(15) Coulter, C. V. PhD, University of Canterbury, 1997.

(16) Payne, S. E. D. Phil. Thesis, University of Canterbury, 1998.

(17) Mirwaldt, C.; Kornacker, V.; Huber, R. *J. Mol. Biol.* 1995, 246, 227.

(18) Bradford 'Bio-Rad Protein Assay Instruction Manual', 1976.

(19) Bradford, M. M. *Anal. Biochem.* 1976, 72, 248.

(20) Pearce, F. G. B.Sc. Honors Thesis, University of Canterbury, 1999.

(21) Roberts, S. J. MSc Thesis, University of Canterbury, 2002.

5.18 References

- (1) Perrin, D. D.; Amarego, W. L. F. *Purification of Laboratory Chemicals*; 3rd ed.; Pergamon Press: Australia, 1988.
- (2) Hermann, K.; Drieding, S. A. *Helv. Chem. Acta* **1975**, *58*, 1805.
- (3) Chênevert, R.; Dickman, M. J. *Org. Chem.* **1996**, *61*, 3332.
- (4) Chrystal, E. J. T.; Couper, L.; Robins, D. J. *Tetrahedron* **1995**, *51*, 10241.
- (5) Paradisi, M. P.; Zecchini, G. P.; Torrini, I.; Lucente, G. J. *Heterocyclic Chem.* **1990**, *27*, 1661.
- (6) Lemaire-Audoire, S.; Vogel, P. *Tetrahedron Asymmetry* **1999**, *10*, 1283.
- (7) Maillard, J.; Delaunay, P.; Langlois, M.; Portevin, B.; Legeai, J.; Manuel, C. *Eur. J. Med. Chem.* **1984**, *19*, 451.
- (8) Tadeusz, L.; Andrej, P.; Krzystof, M. *Chemia Stosowana* **1978**, *22*, 111.
- (9) Tudor, D. W.; Lewis, T.; Robins, D. J. *Synthesis* **1993**, 1061.
- (10) Wernic, D.; DiMaio, J.; Adams, J. J. *Org. Chem.* **1989**, *54*, 4224.
- (11) Roberts, S. J.; Morris, J. C.; Dobson, R. C. J.; Gerrard, J. A. *Bioorg. Med. Chem. Lett.* **2003**, *13*, 265.
- (12) Sambrook, J.; Fritsch, E. F.; Maniatis, T. *Molecular cloning: A laboratory approach.*; Oxford University Press: New York, 1989.
- (13) Gerrard, J. A. D. Phil. Thesis, Oxford University, 1992.
- (14) Kraunsoe, J. A. E. Part II Thesis, Oxford University, 1992.
- (15) Coulter, C. V. PhD, University of Canterbury, 1997.
- (16) Fayle, S. E. D. Phil. Thesis, University of Canterbury, 1998.
- (17) Mirwaldt, C.; Korndorfer, I.; Huber, R. *J. Mol. Biol.* **1995**, *246*, 227.
- (18) Bradford "Bio-Rad Protein Assay, Instruction Manual", 1976.
- (19) Bradford, M. M. *Anal. Biochem.* **1976**, *72*, 248.
- (20) Pearce, F. G. B.Sc. Hons. Thesis, University of Canterbury, 1999.
- (21) Roberts, S. J. MSc Thesis, University of Canterbury, 2002.

A.1 Crystallographic Data for Compound 71

A colourless blade-like crystal was attached with Exton Parafilm N, to a short length of fibre supported on a thin piece of copper wire inserted in a copper mounting pin. The crystal was cooled in a nitrogen gas stream from an Oxford Cryosystems Cryostream. A Bruker SMART 1000 CCD diffractometer employing graphite monochromated MoK α radiation, generated from a sealed tube was used for the data collection. Cell

APPENDIX

parameters were $a = 9.2817(15)$ Å, $b = 10.5236(17)$ Å, $c = 10.5688(17)$ Å, $V = 1032.3(3)$ Å³. Data were collected at 170(3) Kelvin with ω scans to 56.52° 2θ . The data integration and reduction were undertaken with SAINT and XPREP¹, and subsequent computations were carried out with the *teXsan*,² WinGX,³ and XTAL⁴ graphical user interfaces. The intensities of 203 standard reflections recollected at the end of the experiment did not change significantly during the data collection. A Gaussian absorption correction⁵ was applied to the data.

The structure was solved in the space group $P2_12_12_1$ (#19) by direct methods with SIR97,⁶ and extended and refined with SHELXL-97.⁷ The non-hydrogen atoms in the asymmetric unit were modelled with anisotropic displacement parameters. In general a riding atom model was used for the hydrogen atoms, with the exception of H(1N) which was located and modelled with an isotropic displacement parameter. An ORTEP⁸ depiction of the molecule with 50% displacement ellipsoids is provided in Figure 2.5.3. The absolute structure was established with the Flack parameter⁹⁻¹² refining to 0.00(5).

Formula of the Refinement Model	$C_9H_{17}NO_5S$
Model Molecular Weight	255.25
Crystal System	orthorhombic
Space Group	$P2_12_12_1$ (#19)
a	9.2817(15) Å
b	10.5236(17) Å
c	10.5688(17) Å
V	1032.3(3) Å ³
ρ_c	1.514 g cm ⁻³
Z	4
Crystal Size	0.630 x 0.328 x 0.113 mm
Crystal Colour	colourless
Crystal Habit	blade
Temperature	150(2) Kelvin
λ (MoK α)	0.71073 Å
μ (MoK α)	0.315 mm ⁻¹

A.1 Crystallographic Data for Compound 71

A colourless blade-like crystal was attached with Exxon Paratone N, to a short length of fibre supported on a thin piece of copper wire inserted in a copper mounting pin. The crystal was quenched in a cold nitrogen gas stream from an Oxford Cryosystems Cryostream. A Bruker SMART 1000 CCD diffractometer employing graphite monochromated MoK α radiation generated from a sealed tube was used for the data collection. Cell constants were obtained from a least squares refinement against 959 reflections located between 5.46 and 55.97° 2 θ . Data were collected at 150(2) Kelvin with ω scans to 56.52° 2 θ . The data integration and reduction were undertaken with SAINT and XPREP¹, and subsequent computations were carried out with the teXsan,² WinGX,³ and XTAL⁴ graphical user interfaces. The intensities of 203 standard reflections recollected at the end of the experiment did not change significantly during the data collection. A Gaussian absorption correction^{1,5} was applied to the data.

The structure was solved in the space group $P2_12_12_1$ (#19) by direct methods with SIR97,⁶ and extended and refined with SHELXL-97.⁷ The non-hydrogen atoms in the asymmetric unit were modelled with anisotropic displacement parameters. In general a riding atom model was used for the hydrogen atoms, with the exception of H(1N) which was located and modelled with an isotropic displacement parameter. An ORTEP⁸ depiction of the molecule with 50% displacement ellipsoids is provided in Figure 2.3.3. The absolute structure was established with the Flack parameter⁹⁻¹² refining to 0.00(5).

Formula of the Refinement Model	C ₈ H ₁₃ NO ₅ S
Model Molecular Weight	235.25
Crystal System	orthorhombic
Space Group	$P2_12_12_1$ (#19)
<i>a</i>	9.2817(15) Å
<i>b</i>	10.5236(17) Å
<i>c</i>	10.5688(17) Å
<i>V</i>	1032.3(3) Å ³
<i>D_c</i>	1.514 g cm ⁻³
<i>Z</i>	4
Crystal Size	0.630x0.328x0.113 mm
Crystal Colour	colourless
Crystal Habit	blade
Temperature	150(2) Kelvin
λ (MoK α)	0.71073 Å
μ (MoK α)	0.315 mm ⁻¹

$T(\text{Gaussian})_{\text{min,max}}$	0.840, 0.965
$2\theta_{\text{max}}$	56.52°
hkl range	-12 12, -13 13, -14 14
N	10067
N_{ind}	2450($R_{\text{merge}} 0.0260$)
N_{obs}	2411($I > 2\sigma(I)$)
N_{var}	142
Residuals* $R1(F)$, $wR2(F^2)$	0.0219, 0.0546
GoF(all)	1.293
Residual Extrema	-0.194, 0.229 e ⁻ Å ⁻³

* $R1 = \sum ||F_o| - |F_c|| / \sum |F_o|$ for $F_o > 2\sigma(F_o)$; $wR2 = (\sum w(F_o^2 - F_c^2)^2 / \sum (wF_c^2)^2)^{1/2}$ all reflections

$w = 1 / [\sigma^2(F_o^2) + (0.020P)^2 + 0.20P]$ where $P = (F_o^2 + 2F_c^2) / 3$

Table 1. Non-Hydrogen Atom Coordinates, Isotropic Thermal Parameters and Occupancies

atom	x	y	z	$U_{eq}(\text{\AA}^2)$	Occ
S(1)	0.39880(3)	0.65011(3)	0.59135(3)	0.01989(8)	1
O(1)	0.24089(10)	0.64163(10)	0.62266(8)	0.0249(2)	1
O(2)	0.17210(10)	0.38639(9)	0.45270(10)	0.0249(2)	1
O(3)	0.08943(10)	0.54324(9)	0.32759(9)	0.02298(19)	1
O(4)	0.27278(11)	0.97259(9)	0.35374(9)	0.0258(2)	1
O(5)	0.31416(12)	0.87156(9)	0.16976(9)	0.0304(2)	1
N(1)	0.36477(11)	0.64472(12)	0.29374(10)	0.0202(2)	1
C(1)	0.43590(14)	0.52213(13)	0.48303(13)	0.0218(3)	1
C(2)	0.34638(13)	0.52490(12)	0.36135(13)	0.0199(3)	1
C(3)	0.31361(14)	0.75396(12)	0.36631(12)	0.0182(2)	1
C(4)	0.41426(15)	0.77723(12)	0.47769(11)	0.0204(3)	1
C(5)	0.18703(14)	0.48950(12)	0.37962(12)	0.0198(2)	1
C(6)	0.02487(15)	0.34126(15)	0.46652(14)	0.0285(3)	1
C(7)	0.30262(13)	0.87076(12)	0.28304(12)	0.0205(3)	1
C(8)	0.25217(17)	1.09227(14)	0.28707(15)	0.0307(3)	1

Table 2. Hydrogen Atom Coordinates, Isotropic Thermal Parameters and Occupancies

atom	x	y	z	$U_{eq}(\text{Å}^2)$	Occ
H(1N)	0.3200(16)	0.6403(15)	0.2221(15)	0.021(4)	1
H(1A)	0.5393	0.5249	0.4601	0.026	1
H(1B)	0.4181	0.4405	0.5269	0.026	1
H(2)	0.3880	0.4578	0.3052	0.024	1
H(3)	0.2155	0.7339	0.4000	0.022	1
H(4A)	0.3896	0.8590	0.5186	0.025	1
H(4B)	0.5149	0.7827	0.4471	0.025	1
H(6A)	-0.0359	0.4103	0.4986	0.043	1
H(6B)	0.0228	0.2700	0.5262	0.043	1
H(6C)	-0.0115	0.3131	0.3841	0.043	1
H(8A)	0.3399	1.1135	0.2400	0.046	1
H(8B)	0.2314	1.1598	0.3483	0.046	1
H(8C)	0.1713	1.0841	0.2280	0.046	1

Table 3. Anisotropic Thermal Parameters (\AA^2)

atom	U(1,1)	U(2,2)	U(3,3)	U(1,2)	U(1,3)	U(2,3)
S(1)	0.02173(14)	0.02141(14)	0.01654(13)	-0.00039(12)	-0.00157(11)	0.00073(12)
O(1)	0.0233(4)	0.0274(5)	0.0242(4)	0.0024(4)	0.0049(4)	0.0037(4)
O(2)	0.0248(5)	0.0207(5)	0.0291(5)	-0.0028(4)	-0.0017(4)	0.0023(4)
O(3)	0.0209(4)	0.0220(4)	0.0260(5)	0.0006(4)	-0.0019(4)	-0.0011(4)
O(4)	0.0318(5)	0.0208(5)	0.0247(5)	0.0031(4)	-0.0005(4)	0.0020(4)
O(5)	0.0413(6)	0.0301(5)	0.0199(5)	-0.0020(5)	0.0020(4)	0.0047(4)
N(1)	0.0216(5)	0.0232(5)	0.0158(5)	0.0000(4)	0.0012(4)	-0.0018(4)
C(1)	0.0194(6)	0.0217(6)	0.0243(6)	0.0040(5)	-0.0016(5)	-0.0023(5)
C(2)	0.0184(6)	0.0199(6)	0.0213(6)	0.0017(5)	0.0009(5)	-0.0027(5)
C(3)	0.0178(5)	0.0202(6)	0.0167(6)	-0.0017(5)	0.0008(5)	-0.0004(5)
C(4)	0.0244(6)	0.0193(6)	0.0176(6)	-0.0039(5)	-0.0016(5)	0.0005(4)
C(5)	0.0216(6)	0.0176(5)	0.0202(6)	-0.0001(5)	0.0007(5)	-0.0051(5)
C(6)	0.0264(7)	0.0254(7)	0.0338(7)	-0.0049(6)	0.0007(6)	0.0039(6)
C(7)	0.0155(5)	0.0234(6)	0.0226(6)	-0.0029(5)	-0.0004(4)	0.0023(5)
C(8)	0.0316(7)	0.0227(7)	0.0377(8)	0.0030(6)	-0.0043(6)	0.0072(6)

Table 4. Non Hydrogen Bond Lengths (Å)

Atom	atom	Distance	atom	atom	Distance
S(1)	O(1)	1.5052(10)	S(1)	C(1)	1.8008(14)
S(1)	C(4)	1.8036(13)	O(2)	C(5)	1.3390(16)
O(2)	C(6)	1.4541(16)	O(3)	C(5)	1.2012(16)
O(4)	C(7)	1.3354(16)	O(4)	C(8)	1.4558(16)
O(5)	C(7)	1.2020(16)	N(1)	C(2)	1.4593(17)
N(1)	C(3)	1.4613(16)	C(1)	C(2)	1.5314(19)
C(2)	C(5)	1.5375(18)	C(3)	C(7)	1.5152(17)
C(3)	C(4)	1.5226(17)			

Symmetry Operators

- (1) x, y, z (2) $-x+1/2, -y, z+1/2$ (3) $-x, y+1/2, -z+1/2$
 (4) $x+1/2, -y+1/2, -z$

Table 5. Non Hydrogen Bond Angles (°)

atom	atom	atom	angle
O(1)	S(1)	C(1)	106.36(6)
O(1)	S(1)	C(4)	105.54(6)
C(1)	S(1)	C(4)	96.67(6)
C(5)	O(2)	C(6)	114.83(10)
C(7)	O(4)	C(8)	116.79(11)
C(2)	N(1)	C(3)	112.63(10)
C(2)	C(1)	S(1)	114.58(9)
N(1)	C(2)	C(1)	111.36(10)
N(1)	C(2)	C(5)	112.54(10)
C(1)	C(2)	C(5)	114.32(11)
N(1)	C(3)	C(7)	110.81(10)
N(1)	C(3)	C(4)	109.45(11)
C(7)	C(3)	C(4)	111.09(10)
C(3)	C(4)	S(1)	110.29(9)
O(3)	C(5)	O(2)	124.58(12)
O(3)	C(5)	C(2)	123.64(12)
O(2)	C(5)	C(2)	111.61(11)
O(5)	C(7)	O(4)	124.76(12)
O(5)	C(7)	C(3)	125.32(12)
O(4)	C(7)	C(3)	109.87(10)

Symmetry Operators

- (1) x, y, z (2) $-x+1/2, -y, z+1/2$ (3) $-x, y+1/2, -z+1/2$
 (4) $x+1/2, -y+1/2, -z$

Table 6. Torsion Angles (°)

atom	atom	atom	atom	angle	Distance
O(1)	S(1)	C(1)	C(2)	58.21(11)	0.9900
C(4)	S(1)	C(1)	C(2)	-50.17(11)	1.0000
C(3)	N(1)	C(2)	C(1)	-63.05(13)	0.9900
C(3)	N(1)	C(2)	C(5)	66.83(13)	0.9900
S(1)	C(1)	C(2)	N(1)	56.78(13)	0.9900
S(1)	C(1)	C(2)	C(5)	-72.16(13)	0.9900
C(2)	N(1)	C(3)	C(7)	-167.03(10)	
C(2)	N(1)	C(3)	C(4)	70.12(13)	
N(1)	C(3)	C(4)	S(1)	-68.54(12)	
C(7)	C(3)	C(4)	S(1)	168.78(9)	
O(1)	S(1)	C(4)	C(3)	-54.10(10)	
C(1)	S(1)	C(4)	C(3)	54.97(10)	
C(6)	O(2)	C(5)	O(3)	-0.16(18)	
C(6)	O(2)	C(5)	C(2)	-175.55(11)	
N(1)	C(2)	C(5)	O(3)	10.87(18)	
C(1)	C(2)	C(5)	O(3)	139.22(13)	
N(1)	C(2)	C(5)	O(2)	-173.69(10)	
C(1)	C(2)	C(5)	O(2)	-45.35(15)	
C(8)	O(4)	C(7)	O(5)	0.42(19)	
C(8)	O(4)	C(7)	C(3)	-177.31(11)	
N(1)	C(3)	C(7)	O(5)	9.78(18)	
C(4)	C(3)	C(7)	O(5)	131.67(14)	
N(1)	C(3)	C(7)	O(4)	-172.51(10)	
C(4)	C(3)	C(7)	O(4)	-50.61(14)	

Symmetry Operators

- (1) x, y, z (2) $-x+1/2, -y, z+1/2$ (3) $-x, y+1/2, -z+1/2$
 (4) $x+1/2, -y+1/2, -z$

Table 7. Hydrogen Bond Lengths (Å)

atom	atom	Distance	atom	atom	Distance
N(1)	H(1N)	0.865(16)	C(1)	H(1A)	0.9900
C(1)	H(1B)	0.9900	C(2)	H(2)	1.0000
C(3)	H(3)	1.0000	C(4)	H(4A)	0.9900
C(4)	H(4B)	0.9900	C(6)	H(6A)	0.9800
C(6)	H(6B)	0.9800	C(6)	H(6C)	0.9800
C(8)	H(8A)	0.9800	C(8)	H(8B)	0.9800
C(8)	H(8C)	0.9800			

Symmetry Operators

- (1) x, y, z (2) $-x+1/2, -y, z+1/2$ (3) $-x, y+1/2, -z+1/2$
 (4) $x+1/2, -y+1/2, -z$

Table 8. Hydrogen Bond Angles (°)

atom	atom	atom	angle
C(2)	N(1)	H(1N)	109.0(11)
C(3)	N(1)	H(1N)	110.2(11)
C(2)	C(1)	H(1A)	108.6
S(1)	C(1)	H(1A)	108.6
C(2)	C(1)	H(1B)	108.6
S(1)	C(1)	H(1B)	108.6
H(1A)	C(1)	H(1B)	107.6
N(1)	C(2)	H(2)	106.0
C(1)	C(2)	H(2)	106.0
C(5)	C(2)	H(2)	106.0
N(1)	C(3)	H(3)	108.5
C(7)	C(3)	H(3)	108.5
C(4)	C(3)	H(3)	108.5
C(3)	C(4)	H(4A)	109.6
S(1)	C(4)	H(4A)	109.6
C(3)	C(4)	H(4B)	109.6
S(1)	C(4)	H(4B)	109.6
H(4A)	C(4)	H(4B)	108.1
O(2)	C(6)	H(6A)	109.5
O(2)	C(6)	H(6B)	109.5
H(6A)	C(6)	H(6B)	109.5
O(2)	C(6)	H(6C)	109.5
H(6A)	C(6)	H(6C)	109.5
H(6B)	C(6)	H(6C)	109.5
O(4)	C(8)	H(8A)	109.5
O(4)	C(8)	H(8B)	109.5
H(8A)	C(8)	H(8B)	109.5
O(4)	C(8)	H(8C)	109.5
H(8A)	C(8)	H(8C)	109.5
H(8B)	C(8)	H(8C)	109.5

Symmetry Operators

(1) x, y, z (2) $-x+1/2, -y, z+1/2$ (3) $-x, y+1/2, -z+1/2$ (4) $x+1/2, -y+1/2, -z$

A.2 Kinetic Equations¹³

Reversible Inhibition

s and i represent the concentrations of substrate and inhibitor respectively. K_s , K'_s and K_i and K'_i are the dissociation constants.¹⁴

Competitive Inhibition

$$v = \frac{V \cdot s}{s + K_m(1 + i/K_i)} = \frac{V}{1 + \frac{K_m}{s} \left(1 + \frac{i}{K_i}\right)}$$

Non-Competitive Inhibition

$$v = \frac{V \cdot s}{(1 + i/K_i)(K_s + s)} = \frac{V}{\left(1 + \frac{K_s}{s}\right) \left(1 + \frac{i}{K_i}\right)}$$

Uncompetitive Inhibition

$$v = \frac{V \cdot s}{\frac{K_m}{(1 + i/K_i)} + s} = \frac{V}{1 + \frac{i}{K_i} + \frac{K_m}{s}}$$

Mixed Inhibition

$$v = \frac{V \cdot s / (1 + i/K'_i)}{s + K_s \frac{(1 + i/K_i)}{(1 + i/K'_i)}} = \frac{V}{(1 + i/K_i) + (1 + K_s/s)(1 + i/K_i)}$$

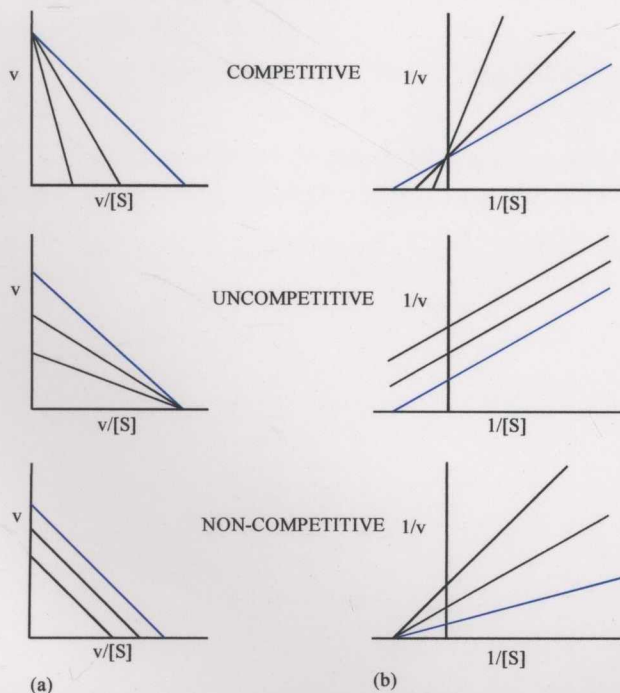


Figure A.2.1: (a) Eadie-Hofstee and (b) Lineweaver-Burk plots of different types of inhibition. The blue line in each plots shows the reaction in the absence of inhibitor; the black lines are for the reaction in the presence of an inhibitor.¹⁵

Irreversible Inhibition¹⁶

A_0 and A are the enzyme activities at times zero and t , respectively. It is assumed that $i \gg e$

$$\frac{dei}{dt} = k.i$$

$$\ln \frac{A}{A_0} = -k.i.t = k'.t$$

where $k' = k.i$

- (4) Drenth, J. *Acta Crystallogr., Sect. A* 1958, 14, 41.
- (5) Cuppen, P., *Acta Crystallogr., Sect. A* 1960, 16, 100.
- (6) Shotton, A., North, D. C., *Acta Crystallogr., Sect. A* 1961, 17, 100.
- (7) Shotton, A., *Acta Crystallogr., Sect. A* 1962, 18, 100.
- (8) Shotton, A., *Acta Crystallogr., Sect. A* 1963, 19, 100.
- (9) Johnson, C. K. Oak Ridge National Laboratory, Oak Ridge, Tennessee, 1976.
- (10) Flack, H. D. *Acta Crystallogr., Sect. A* 1983, 39, 876.
- (11) Bernardinelli, G.; Flack, H. D. *Acta Crystallogr., Sect. A* 1985, 41, 500.
- (12) Flack, H. D.; Bernardinelli, G. *Acta Cryst.* 1999, A55, 908.
- (13) Flack, H. D.; Bernardinelli, G. *J. Appl. Cryst.* 2000, 33, 1143.
- (14) Cogoli-Berthel, A. *Fundamentals of Enzyme Kinetics* 2nd ed., Portland Press Ltd, London, 1990.
- (15) Dixon, K. F. *Enzymes*, 3rd ed., Ed: P. D. Boyer, Academic Press, New York, 1970, p. 415.
- (16) Dixon, K. F. *Enzymes*, 3rd ed., Ed: P. D. Boyer, Academic Press, New York, 1970, p. 415.

A.3 References

- (1) Bruker, SMART, SAINT and XPREP. Area detector control and data integration and reduction software. Bruker Analytical X-ray Instruments Inc.: Madison, Wisconsin, USA, 1995.
- (2) Molecular Structure Corporation; MSC: 3200 Research Forest Drive, The Woodlands, TX 77381, 1997-1998.
- (3) WinGX, Farrugia, L. J. *J. Appl. Cryst.* **1999**, *32*, 837.
- (4) Hall, S. R.; du Boulay, D. J.; Olthof-Hazekamp, R. Eds Xtal3.6 System, University of Western Australia, 1999.
- (5) Coppens, P.; Leiserowitz, L.; Rabinovich, D. *Acta Cryst.* **1965**, *18*, 1035.
- (6) Altomare, A.; Burla, M. C.; Camalli, M.; Cascarano, G. L.; Giacovazzo, C.; Guagliardi, A.; Moliterni, A. G. G.; Polidori, G.; Spagna, R. J. *J. Appl. Cryst.* **1999**, *32*, 115.
- (7) Sheldrick, G. M.; SHELX 97 Programs for Crystal Structure Analysis. University of Göttingen. Institut für Anorganische Chemie der Universität, Tammanstrasse 4, D-3400 Göttingen, Germany, 1998.
- (8) Johnson, C. K. Oak Ridge National Laboratory, Oak Ridge, Tennessee, 1976.
- (9) Flack, H. D. *Acta Crystallogr., Sect A* **1983**, *39*, 876.
- (10) Bernardinelli, G.; Flack, H. D. *Acta Crystallogr., Sect A* **1985**, *41*, 500.
- (11) Flack, H. D.; Bernardinelli, G. *Acta Cryst.* **1999**, *A55*, 908.
- (12) Flack, H. D.; Bernardinelli, G. *J. Appl. Cryst.* **2000**, *33*, 1143.
- (13) Cornish-Bowden, A. *Fundamentals of Enzyme Kinetics*; 2nd ed.; Portland Press Ltd.: Princeton, 1999.
- (14) Tipton, K. F. In *Enzymology*; Engel, P. C., Ed.; BIOS Scientific Publishers: Oxford, 1996, p 115.
- (15) Fersht, A. *Structure and Mechanism in Protein Science: A guide to enzyme catalysis and protein folding*; W.H. Freeman and Company: New York, 1998.
- (16) Tipton, K. F. In *Enzymology*; Engel, P. C., Ed.; BIOS Scientific Publishers: Oxford, 1996, p 156.